A Forest Monitoring System for Tanzania: Mapping Change and Extent

Elikana Maige John

A thesis submitted in fulfillment of the requirements for the degree of Doctor of Philosophy

January 5, 2023

Aberystwyth University

Supervisors: Dr Pete Bunting and Dr Andrew Hardy

Declaration and Statements

Declaration

This work has not previously been accepted in substance for any degree and is not being concurrently submitted in candidature for any degree.

Signed .... Date: .....05.01.2023.....

Statement 1

This thesis is the result of my own investigations except where otherwise stated. Where correction services have been used, the extent and nature of the correction are clearly marked in footnote(s). Other sources are acknowledged by footnotes and giving explicit references. A bibliography is appended.

Signed .... Date: .....05.01.2023.....

Statement 2

I hereby give consent for my thesis, if accepted, to be available for photocopying and for inter-library loan, and for the title and summary to be made available to outside organisations.

Signed .... Date: .....05.01.2023.....

Acknowledgements

I am very grateful to those who have contributed and supported me during my doctoral study at Aberystwyth University. Without any of them, this research work would not have been possible.

First and foremost, I wish to place on records my heartfelt and sincere thanks to my supervisors for providing me with an opportunity to complete my PhD thesis. I appreciate Dr Pete Bunting for the contributions, time and ideas to make my work productive and stimulating. Your valuable suggestions, comments, and guidance encouraged me to learn more day by day. What I, however, know for sure is that I am profoundly and forever grateful to you. You were a critical force that got me to the finishing line.

I am incredibly thankful to Dr Andrew Hardy; you have been a tremendous mentor and guidance for me. Your friendly advice, suggestions and encouragement on my research allowed me to grow as a research scholar. Thank you for your valuable time, cooperation, and generosity has been the most profitable experience for me.

I want to take this opportunity to thank the Commonwealth Scholarship Commission in the UK (CSC) for its special funding for my academic struggle at Aberystwyth University. I am very honoured to be the recipient of their grant. This thesis would not have been possible without that support.

I have loved every moment and feel privileged to work with my PhD colleagues in the Earth Observation and Ecosystem Dynamics Research Group (EOED), thanked for their manifold supports and many joyful moments throughout the past three years.

I wish to express my sincere credits to my wife and our children for patient, love, care and encouragement. Your support was tremendous in me getting through the many hurdles of the PhD process. You encouraged me, given me much-needed self-care. Finally, I want to express my honest and sincere thankfulness to my parents and siblings for their prayers.

Abstract

Tropical forests provide essential ecosystem services related to human livelihoods. However, the distribution and condition of tropical forests are under significant pressure, causing shrinkage and risking biodiversity loss. Tanzania is undergoing substantial forest cover changes, but monitoring is limited, partly due to a lack of remote sensing knowledge, tools, and methods. This study has demonstrated a comprehensive approach for creating a national-scale forest monitoring system using Earth Observation data to inform decision-making, policy formulation, and combat biodiversity loss. A Maximum Entropy model was used to predict forest change under different climate change scenarios (RCP 4.5 and RCP 8.5 for 2055 and 2085). This analysis identified that these landscapes will experience increased isolation and reduced connectivity. For example, upland forests, essential refugia of species, and endemism were predicted to almost halve in extent by 2085. A national forest baseline was created for 2018 through the application of Landsat 8 imagery. The classification was developed using the extreme gradient boosting (XGBoost) machine-learning algorithm and achieved an accuracy of 89% and identified 46% of the country's area is covered with forest. Of those forested areas, 45% were found within nationally protected areas. Using a novel methodology where habitat suitability analysis was used to constrain the classification, the forest baseline was classified into forest types, with an overall accuracy of 85%. Woodlands (open and closed) were found to make up 79% of Tanzania's forests. To map changes in forest extent, an automated system for downloading and processing Landsat 8 imagery was used along with the XGBoost classifiers trained to define the national forest extent. The Landsat 8 scenes were individually downloaded and processed and the identified changes were summarised on an annual basis. Forest losses identified for 2019 were found to total 157,204 hectares, with an overall accuracy of 82%. Forest loss within Tanzania has already triggered ecological problems and alterations in ecosystem types and species loss. Therefore, the importance of a forest monitoring system, such as the one presented in this study, will enhance conservation programmes and support efforts to save the last remnants of Tanzania's pristine forests.

List of publications

Peer-reviewed paper

John, E., Bunting, P., Hardy, A., Roberts, O., Giliba, R., Silayo, D. S., 2020. Modelling the impact of climate change on Tanzanian forests. *Diversity and Distributions* 26:1663-1686. https://doi.org/10.1111/ddi.13152

John, E., Bunting, P., Hardy, A.; Silayo, D.S., Masunga, E., 2021. A Forest Monitoring System for Tanzania. *Remote Sensing,* 13, 3081. https://doi.org/10.3390/rs13163081

§§§§

Table of Contents

List of Figures

List of Tables

Chapter 1

Tropical Forests

1.1 Introduction

Tropical forests remain the core of the global biosphere and the hub of several earth systems and cultural frameworks. The biome comprises an intricate and wide variety of macro and micro-scale habitat variability, which influences animals, plants, hydrology, soil quality, and seasonality encountered by diverse human communities worldwide (Roberts, 2019). Globally, tropical forest habitats are dynamic, with the mosaics of expansion (e.g., woody encroachment), contraction at the expense of another habitat (e.g., succession), or even complete disappearance (e.g., deforestation) (Venter et al., 2018). For example, across Africa, it is common for landscapes to consist of a mixture of forest, woodland, and grassland mosaics. Therefore, there is no generally agreed universal definition of tropical forests.

Therefore, the descriptions of eco-regions are based on the climates they occur, the composition of plants and animals they inhabit, and the complex nature of

interactions among different components that make tropical forest ecosystems. Tropical forests characterised by varied structural and physiognomic types ranging from evergreen forest, seasonally dry deciduous forest, savanna, and thorn scrub to grassland and semi-desert vegetation exists (Torello-Raventos et al., 2013).

The diverse nature of tropical forests has been recognised as providing many essential ecosystem services, benefiting the human population (Willis et al., 2013). However, the extent and distribution of tropical forests have significantly reduced over the last century, primarily due to human disturbance and deforestation (Malhi et al., 2013). This is of international concern, as in addition to anthropogenic change, climate-induced change is increasing the risk of biodiversity loss across the tropics (Lambin et al., 2003).

1.2 Distribution and Environment

Tropical forests are confined to the equator mainly between the Tropic of Cancer and Capricorn at latitude 23.5°N and 23.5°S (Grace et al., 2014; Moore, 2008; Corlett, 2014) (Figure 1.1), the majority in the Neotropical region (South America) with an area of about 4 x 10^6 km^2, Asia covering about 2.5 x 10^6 km^2 and Africa with an area of about 1.8 x 10^6 km^2 (Thomas and Baltzer, 2001). The total coverage of tropical forests is approximately 10% of the entire world's land area (Corlett, 2014). However, it is crucial in terms of global biogeochemical and water cycles and forms the most abundant terrestrial reservoir of biological variety (Mayaux et al., 2005).

The tropical regions receive high solar energy levels and a longer vegetation growing

period supported by a pattern of warm air circulation and relatively wet seasons. Rainfall varies between the years driven by Intertropical Convergence Zone (ITCZ), including El Niño cycles resulting in seasonal variability. Temperatures decrease with altitude, decreasing at about 0.6°C for every 100 m up-slope. Tropical forests exist with an annual rainfall of roughly above 800 mm and a mean temperature of above 7°C, where drier areas support savanna, grassland, or desert, and colder regions have treeless alpine vegetation, especially on high mountains. Similarly, tropical forests grow on a vast range of soil types, from intensely fertile soils in volcanic areas and river floodplains to infertile peat and sand where adequate nutrient recycling is present (Corlett, 2014).

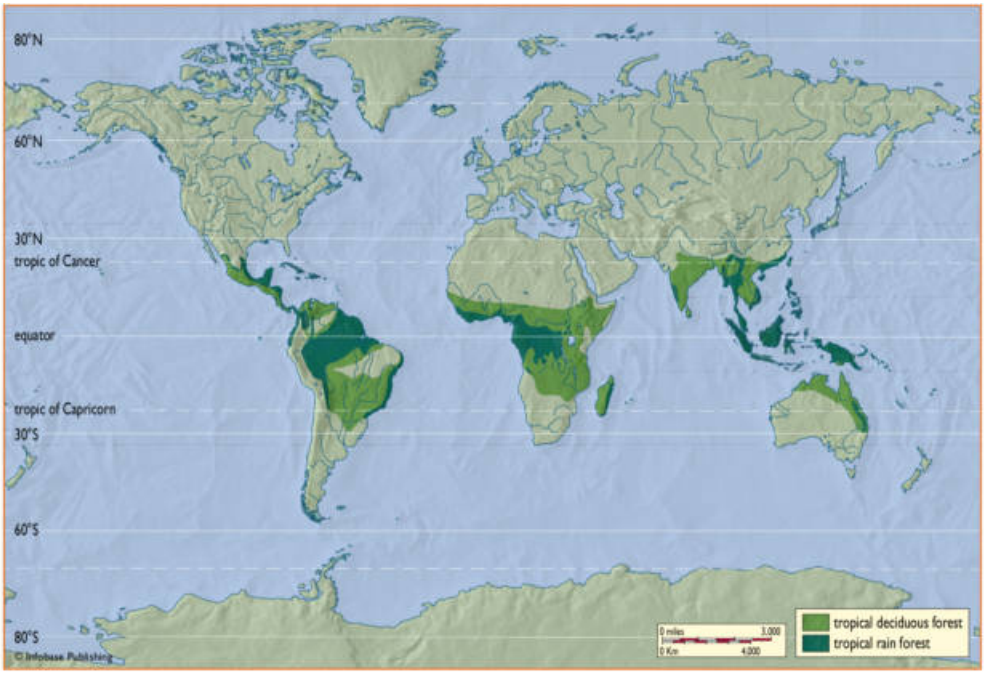

Figure 1.1: The global location of the tropical forests. Sourced from Moore (2008)

1.3 Why are Tropical Forests Important?

The importance of tropical forests is well recognised as they form the most distinct and complex biome on Earth, with unique and distinct biological organisms of high economic value and many human livelihoods dependent on these ecosystems (Potapov et al., 2012; Bazzaz, 1998). About two-thirds of global biodiversity is found in tropical forests (Gardner et al., 2009) and 50% of well-known plant species are located in tropical forests (Mayaux et al., 2005; Duveiller et al., 2008). They also play a significant role in the global carbon cycle, absorb an enormous amount of incoming solar radiation, and, consequently, have very low solar radiation reflectivity (albedo). Hence, tropical forests have been recognised globally in different Multilateral Environmental Agreements (MEA) such as the Convention on Biological Diversity (CBD) and the United Nations Framework Convention on Climate Change (UNFCCC) (Duveiller et al., 2008). However, they are decreasing at all levels, mainly conversion to other land use (Figure 1.2) that is expected to increase (Wright and Muller-Landau, 2006), intensifying the net flux of carbon dioxide into the atmosphere (Fearnside, 2000; Cramer et al., 2004).

The tropical forests are changing globally (Figure 1.4) due to a diverse array of drivers (Figure 1.2). The situation is particularly critical in tropical dry forests and woodlands, with a suitable climate for many arable crops with natural land clearing and burning (Malhi et al., 2014). Preventing these anthropogenic changes is a significant challenge to overcome from a political and social point of view. These issues are relevant at multiple scales, with both local and global issues to be tackled. However, the application of Earth Observation data can help to address issues of inadequate information (Malhi et al., 2014). The Food and Agriculture

Organisation of the United Nations (UN-FAO) has been a pioneer in conducting global forest resources assessment since 1947, at an interval of five to ten years (Olander et al., 2008). These have been a primary source of information on tropical forest extent and loss around the global (Hansen et al., 2010).

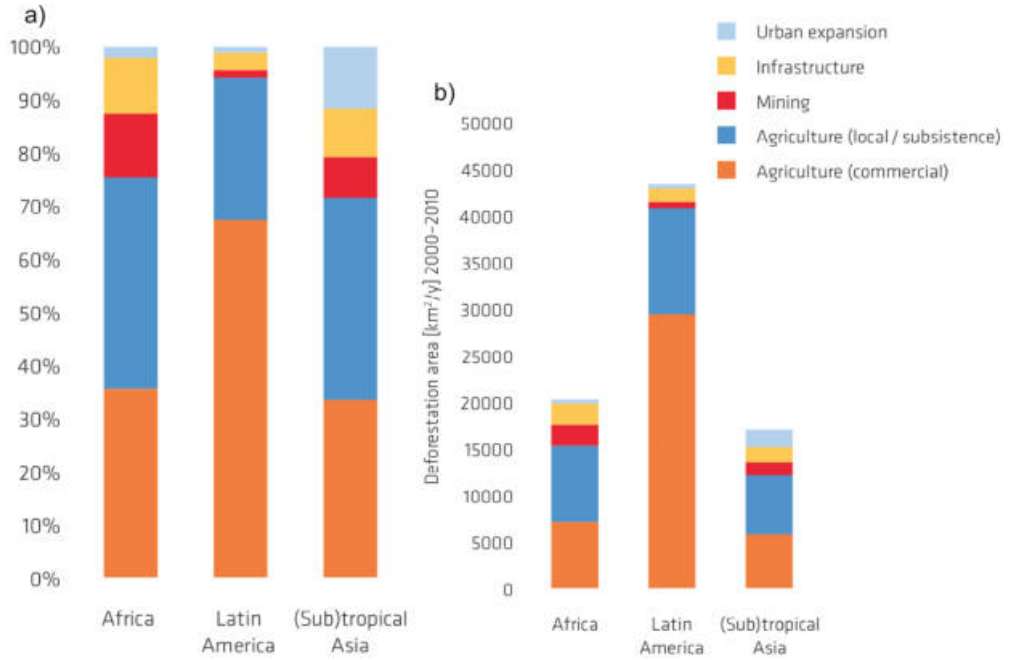

Figure 1.2: a)The proportion of deforestation drivers and b) Area proportion of deforestation drivers. Estimates of the magnitude of deforestation drivers as recorded by 46 countries: a)sum of country data weighted by net forest area change by country b) weighted by net forest area change by country for the period 2000 – 2010. Sourced from Hosonuma et al. (2012)

The FAO tropical forest data are valuable and have been widely used. However, the quality is often questionable, as reporting methods and accuracy vary from one country to another (Meyer and Turner, 1992), alongside variation in tropical forest definitions (DeFries et al., 2002). For example, a declining trend in deforestation for tropical regions was reported by FRA for the 1980s to 1990s, while the opposite trend was reported from satellite-based studies (DeFries et al., 2002).

Therefore, the provision of satellite-based data is referred back to the 1970s (Figure 1.3) with more missions to be launched over the coming years (Reiche et al., 2016) will support in investigating changes in tropical forest areas with broad geographic coverage. However, the vast majority of the research on tropical forest monitoring to date is heavily biased toward particular areas, especially the South American forests (Malhi et al., 2014) whilst Africa, apart from the Congo Basin, has been severely understudied. For example, for the period from 1995 – 2003, about two-thirds of studies focused on the Amazon Basin, 18% focused on central Africa and 17% on Southeast Asia (Fuller, 2006). Therefore, expanding tropical forest monitoring beyond these areas is required to capitalise on Earth Observation data availability with extensive area coverage. Perhaps most importantly, attempts to combine societal constraints while contributing to an increase in scientific knowledge and provide up-to-date and appropriate maps of the tropical forest status.

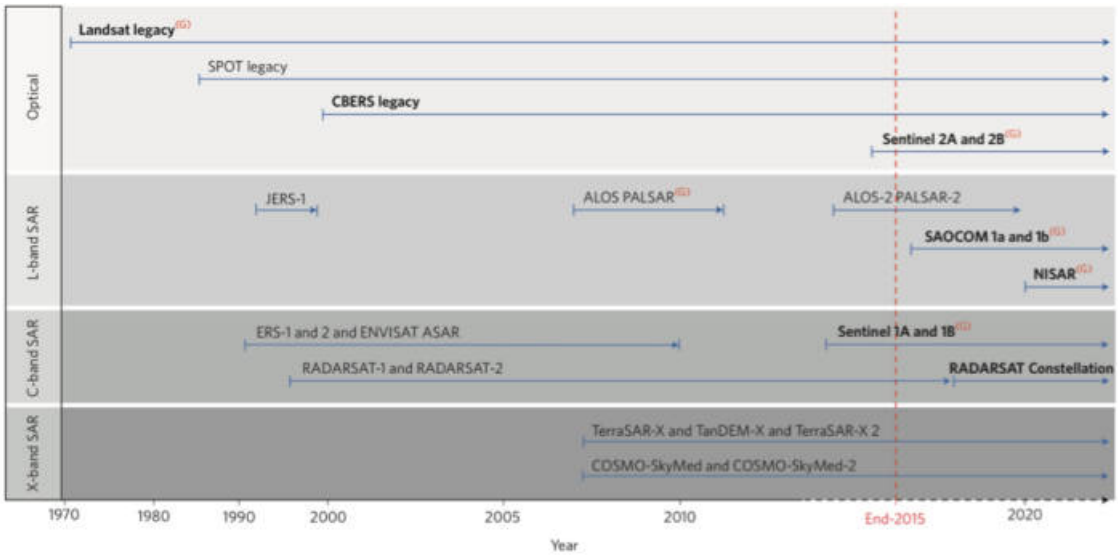

Figure 1.3: Historical, current, and future optical and synthetic aperture radar (SAR) missions. The access of data in bold is in the free-of-charge missions and the missions with restricted data policy access in mid-2015. The expected missions to continue with data acquisition are in red (G). Sourced from Reiche et al. (2016)

1.3.1 Tropical Forest Conversion

Before modern agriculture and industrialisation, tropical forests were largely pristine natural environments (Roberts et al., 2017). Human activities entrenched in changes of social and economic systems and referred to as the agent and causes of tropical forest loss (Meyer and Turner, 1992; Myers, 1993; Geist and Lambin, 2002) (Figure 1.2). The term agent is confined to individuals, corporations, government agencies, or development projects that clear the forests, while causes are the motive forces in clearing forests (Tejaswi, 2007). In the tropics, especially in developing countries, small-scale farming for subsistence or cash crops, rural population expansion, and local population growth or immigration into hinterland forest areas accelerate forest conversion. Similarly, an increase in capital investments induces

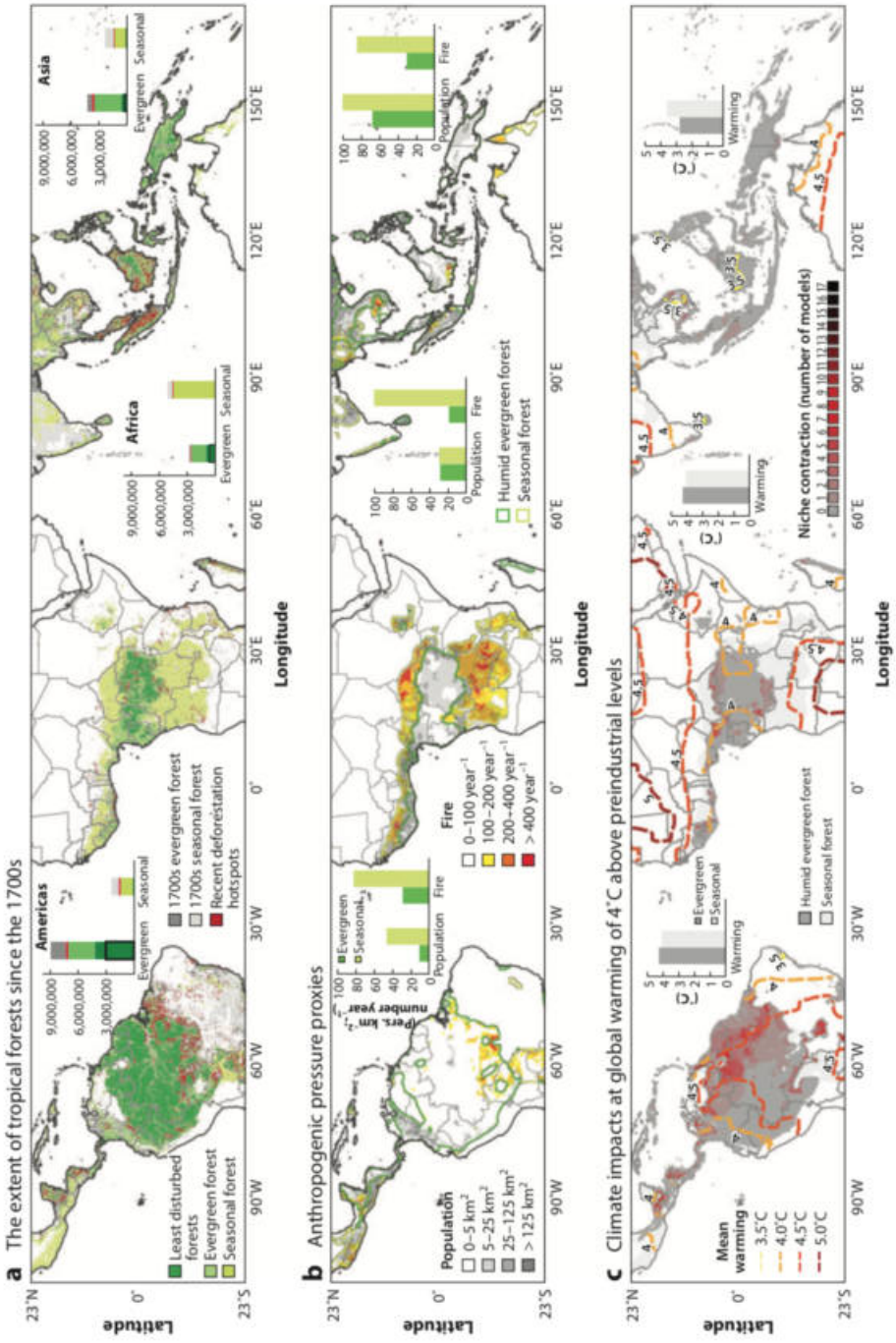

Figure 1.4: Changes in tropical forests in geological time. Sourced from Malhi et al. (2014)

the development of infrastructures such as road construction, fossil-fuel, minerals extraction, and hydro-electric dams at the expense of removing the forests (Malhi et al., 2014). Therefore, anthropogenic changes influence tropical forests on both spatial and temporal scales, resulting in significant short-term and gradual long-term change (Coppin and Bauer, 1996).

The decrease/loss of forest cover is simply deforestation, which implies a shift from forests into other land covers (forest to non-forest) formations without the revival of forests by natural or artificial reforestation within a human planning horizon (Achard et al., 2010; Palo, 1999), i.e., tree cover falls below the minimum crown cover resulting in carbon stock reduction (DeFries et al., 2007).

1.3.2 Impact of Tropical Forest Loss

The loss of tropical forests has been of international concern (Fisher, 2012), and affects erosion, increase in run-off and flooding, increase in CO_2 concentration, climate change, and biodiversity loss (Lambin et al., 2003; Mas, 1999; Godoy et al., 2012; Bazzaz, 1998). Therefore, the removal of tropical forests will increase the albedo, reducing evapotranspiration, and decrease water cycling between the land and the atmosphere (Bazzaz, 1998) resulting in reductions in local, regional, and continental rainfall. It impacts the terrestrial life, marine environment, and even the atmospheric condition as carbon dioxide is released into the atmosphere and hence changes the global climate (Houghton, 2012; Sitch et al., 2015; Le Quéré et al., 2009). The impacts, coupled with the change in the hydrological regime (water quality and water flows), increase soil erosion and sediment deposits. Consequently, adverse changes in tropical forest conditions impact millions of people

in the regional, global environment, and biodiversity distribution (De Wasseige et al., 2014). It will continue to be a significant problem in tropical countries in the next 20–30 years as anticipated by Craglia et al. (2012), and will increase water scarcity, affect air quality, and public health, with economic losses and social consequences (Barbier and Burgess, 2001; Busch and Engelmann, 2015). The deforestation in tropics has been reported widely as an important part of reducing scientific doubts about the estimates of greenhouse gas emissions (Achard et al., 2002). This demonstrates the need for more conservation of tropical forests, including reducing threats from (Figure 1.2). Table 1.1 summarises some studies on the impacts of tropical deforestation.

Table 1.1: Summary of studies on the impact of tropical deforestation

Areas	**References**
Biological diversity loss	(Myers et al., 2000; Bradshaw et al., 2009; Pandit et al., 2007)
Increase atmospheric concentration of Carbon dioxide (carbon sink)	(Houghton, 2003a; Costa and Foley, 2000)
Climate change at local and region	(Nobre et al., 1991; Malhi et al., 2008; Lawrence and Vandecar, 2015)
Impact on livelihoods of people depending on the tropical forests	(Brown et al., 2014; Culas, 2007)

1.3.3 Climate Change and Tropical Forest Loss

Climate change impacts pose a significant threat to tropical forests and biodiversity, including alterations in ecosystem types and species loss. For example, climate change may induce prolonged droughts, intense fires, plant stress, and tree mortality (Nobre et al., 2016). It will also increase mixed forest, savanna, and grassland, and expansion of savanna, grasslands, and desert ecosystems. Similarly,

rainfall variations have impacted tropical forests as changes in phenological time affected pollination and seed dispersal and narrowed biological diversity (Bazzaz, 1998).

The loss of tropical forests contributes about 20 – 30% of the world's greenhouse gas emissions (Figure 1.5), through CO_2 (Achard et al., 2007; Goetz et al., 2009). Different studies have reported carbon emissions caused by tropical forests loss (Harris et al., 2012). However, uncertainties in emissions results are also highly associated with land-use change fluxes (Achard et al., 2010; Houghton, 2003b). For example, Harris et al. (2012) reported tropical deforestation accounts for about 0.80GtC (8.0%) of all emissions, Grace et al. (2014) reported about 0.90GtC (8.49%) of all emissions, and Houghton (2003b), reported about 0.81GtC, accounting for about 7.44% of emissions. Nevertheless, these figures identify tropical forest losses as contributing to climate change, something which needs to change if global warming is to be restricted to just 2°C (Houghton et al., 2015). However, there is increasing evidence of climate action of limiting global warming to 1.5textsuperscript∘C (Rogelj et al., 2018), through protecting and expanding forest ecosystems that store carbon and minimise emissions from land use.

The effect of future climatic conditions necessitates monitoring tropical forests, and policy responses are required. However, there is limited availability of the data and methods required, especially in sub-Saharan Africa enabling policy action (Mitchard, 2018). Under the Kyoto Protocol and during the first commitment period 2008 – 2012, committed to reducing CO_2 emissions and other GHGs at below 5 % compared to 1990 levels. It is to be achieved by conserving tropical forests and enhancing carbon stored in the forests by monitoring. The use of freely available Earth Observation data is an important part of that. The changes

in carbon stocks can be quantified based on the activities related to afforestation, reforestation programs, and regeneration (Patenaude et al., 2005) as the necessary mechanism of the United Nations Framework Convention on Climate Change (UNFCCC) (Achard et al., 2010).

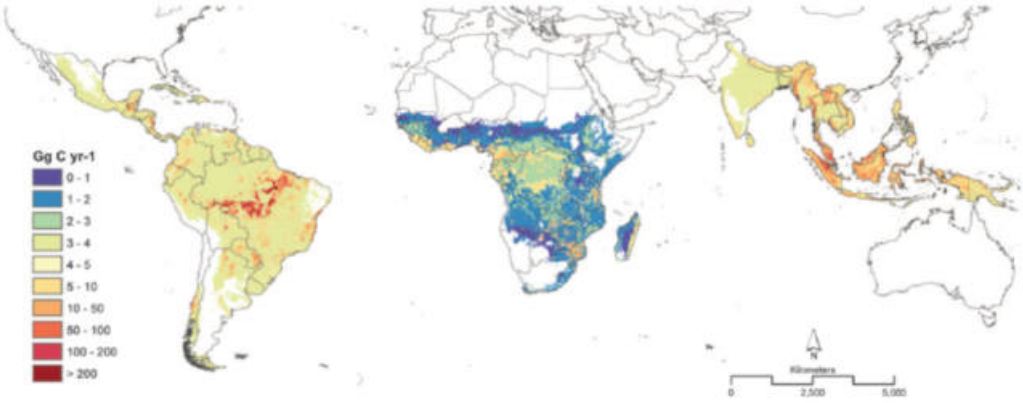

Figure 1.5: The extent of carbon emissions from tropical deforestation between 2000 and 2005. Sourced from Harris et al. (2012)

1.3.4 Institutions and Policies on Tropical Forest Monitoring

The loss of tropical forests has a global impact. International agency organisations are putting efforts together to halt the problem through international cooperation agreements. For example, the adoption of conventions such as the Paris Agreement in 2015 under the United Nations Framework Convention on Climate Change (UNFCC). The UNFCCC has been exploring possible ways of reducing greenhouse gas (GHG) emissions resulting from tropical deforestation (DeFries et al., 2007). It is achieved by assessing forest cover extent and loss; valuable for forest resource management, conservation, and monitoring (Potapov et al., 2012). The information on

tropical forest loss is necessary for developing strategies and assessing programs' proficiency in sustainable forest use, conservation, and Reducing Emissions from Deforestation and Degradation (REDD+) initiatives (Shapiro et al., 2015; Huntingford et al., 2013). The REDD+ creates the financial value of carbon stored in forests due to the focus on curbing tropical deforestation (Brown et al., 2014). The efforts to reduce tropical deforestation caused by the conversion of forests to cropland, pasture, or other land use are the most significant steps in reducing carbon emissions from tropical forests.

The declaration on tropical forest conservation efforts includes the XIV World Forest Congress in 2015, Durban, South Africa, on enhancing new technologies for forest monitoring and improving decision-making. A mechanism such as carbon credit can be used to reduce deforestation in tropical countries. It is an alternative economic support approach to reduce rates of tropical deforestation (DeFries et al., 2002; Fearnside, 2003).

The necessity of accurate information on the extent, losses, and causes of tropical deforestation is a yardstick for policy and decision-makers. Recent international agreements such as the 2030 Agenda on Sustainable Development require Earth Observation data to achieve Sustainable Development Goals (SDGs) for enhancing life on land (goal 15) and its targets. However, Culas (2007), argued that there should be a synergy between institutional factors and export marketing policies on forest products in curbing tropical deforestation.

1.4 African Tropical Forests

Africa is home to some of the most magnificent tropical forests in the world after the Amazon basin. About 20% – 23% of the total area is covered by forests and recognised for high biodiversity levels; significant hotspot areas include the Congo basin of Central Africa, the Upper Guinea forest of West Africa, and the Eastern Arc Mountains in East Africa (Eva et al., 2006; Gondo, 2012). The African tropical forests provide livelihoods for more than 60 million people dwelling within or in the vicinity of the forests for food, medicinal products, fuel, fibers, non-timber forest products, and gratifying societal and cultural purposes (De Wasseige et al., 2014).

This dependency has increased the dynamic state of these forests and hence increased the decline in forest cover. The decline in forest cover is associated with changes in policies that fail to prevent illegal activities in forests, correlated with the absence of defined tenure that has increased over-utilisation. Moreover, political instability, civil conflicts, and logistics linked with poor infrastructure increased forest loss in Africa (Malhi et al., 2013). For instance, about 44% of forest cover decreased in three countries of Sudan, Zambia, and the Democratic Republic of Congo from 1990 to 2000 (Nair and Tieguhong, 2004).

Likewise, pressures on savanna woodlands in Southern and East Africa have intensified due to social pressures from increasing conflict over the use of forest resources (FAO, 2016). However, the lack of national capacity on reporting deforestation in many African countries remains a barrier. Similarly, the rates of deforestation and patterns are uncertain as deforestation often occurs on small scales by subsistence

farmers (Malhi et al., 2013) (Figure 1.2). Therefore, knowledge about the extent of forest area in Africa is essential, as is the availability of medium to high-resolution images such as those acquired from Landsat and Sentinel-1/-2 archives. These data will support both management and monitoring for the commitment of the REDD+ process, which requires a continuing process of Measurements, Reporting, and Verification (MRV) in monitoring deforestation or regrowth of African forests at national scales (De Wasseige et al., 2014).

1.4.1 Vegetation Types in Africa

The categorisation of African vegetation as defined in 1903 and modification of classification progressed in the early 1980s' to 16 vegetation types. The main classes: are forest, woodland, bushland and thicket, shrubland, grassland, wooded grassland, desert, Afroalpine vegetation, scrub woodland, mangrove, herbaceous fresh-water swamp, and aquatic vegetation, saline and brackish swamp, bamboo and anthropic landscapes (White, 1983).

The development of remote sensing techniques and images has improved the classification of vegetation types in Africa (Mayaux et al., 2004), merging some classes and expanding others to obtain the main forest categories. For instance, commonly used sub-classes of the forest include montane forest, sub-montane forest, closed deciduous forest, swamp forest, and mangrove. Savanna woodlands expanded to deciduous woodland, deciduous shrubland with sparse trees, open deciduous shrubland, and grassland with scattered trees and thickets (Figure 1.6).

The forest classifications have also applied physiognomy characteristics like height, canopy cover, density, thorniness, deciduousness, and leaf type to separate bushes

and grasses from forests. For example, canopy cover for shrubs is classified as closed and open, and deciduous and evergreen forests are split into needle-leaf and broadleaf subclasses (Ardö, 2015).

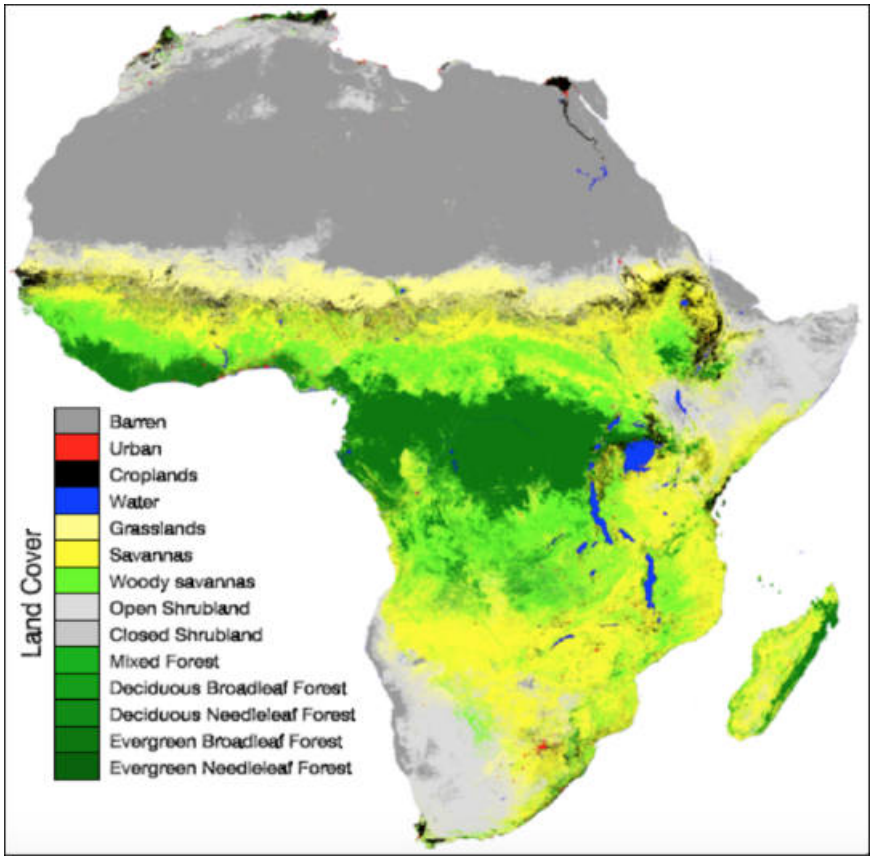

Figure 1.6: Land cover map of Africa derived from MODIS depicting the distribution of different vegetation types. Adapted from Ardö (2015)

1.4.2 Forest

The forests in Africa are sub-categorised based on the amount of rainfall, temperature, and altitude. Most of the forests in Africa remain evergreen or semi-evergreen throughout the year with monthly mean temperatures not less than 25°C, and the mean annual precipitation of above 1500 mm except in the western part of Mada-

gascar, which is drier and where deciduous forests grow. The forests are composed of three storeys layers and, are usually dominated by the middle strata, reaching about 20 – 40 m high. The upper tree strata reach a height of 40 to 60 m and are often characterised by emergents (Sayer, 1992). Therefore, forest types include montane forest, sub-montane forest, closed evergreen lowland forest, closed deciduous forest, swamp forest, and mangrove forest.

1.4.2.1 Montane forest

Montane forests are found at a high altitude between 1000 and 2500 m above sea level and characterised by the presence of clouds. Both montane grasslands to alpine deserts exist and receive more rain than lowland forests and are frequently abundant in epiphytes. However, the height of the trees decreases with increasing altitude. Therefore, they are recognised for the provision of hydrological services and the protection of biodiversity. Montane forests occur on the disconnected highlands spreading from West Africa and Sudan in the North through the Albertine Rift and the Eastern Arc Mountains, Mt. Kilimanjaro, Mt. Kenya, and Mt. Elgon in Uganda to the Southern Africa highlands. Montane forests are fragile ecosystems susceptible to anthropogenic activities and climate change, increasing vulnerability and leading to extensive habitat fragmentation (Foster, 2001; Soh et al., 2019).

1.4.2.2 Sub-montane forest

The sub-montane forests occur in very restricted localities representing an intermediary between lowland forests and montane forests and occur at elevations of

900 – 1500 m. The canopy can reach a height of around 15 to 20 m with occasional emergent trees and may also contain shrubs. However, the sub-montane forests are less well known with biological parameters related to lowland and montane forests and are subjected to similar stresses related to climatic and anthropogenic. Sub-montane forests occur in isolated and fragmented endemic-rich forests of East Africa on the Eastern Arc Mountains of Kenya and Tanzania (East Usambara Mountains) and patches from Somalia to Mozambique, West Africa in Cameroon, the central Guinea-Congolian forests, and the unique forest ecosystem in Madagascar (Sayer, 1992; Malhi et al., 2013).

1.4.2.3 Closed evergreen lowland forest

The closed evergreen lowland forests are unique with a combination of different ecological, climatic, and human interactions. Well-drained soils characterise them, and the upper canopy may reach more than 5 m of height and a canopy cover of higher than 70% at an altitude up to 900 m above mean sea level (Bartholome and Belward, 2005). They occur mainly in two regions of Central Africa in the Congo basin with the upper stratum of 35–45 m and fewer seasonal variations. Mixtures of closed semi-deciduous forests are also found in West Africa in the upper layer up to 70% mixed with evergreen class (Mayaux et al., 2004).

1.4.2.4 Closed deciduous forest

Closed deciduous forests are characterised by shedding off their leaves during the dry season and sprouting new leaves during the rainy season. They exist in lowland areas of high water tables like riverine or riverbanks. Closed deciduous forests have

broad leaves and a close canopy above 40%. They may attain a height of greater than 5 m, occurring in Uganda, Kenya, Tanzania, Ethiopia, Cameroon Equatorial Guinea, and Madagascar (White, 1983; Sayer, 1992).

1.4.2.5 Swamp forest

Swamp forests are defined based on location, habitat, opposing forest structure, and physiognomy and occur permanently or periodically influenced by freshwater. The Congolian swamp forest is the most extensive in Africa, with a flat area between 350 and 400 m in elevation (Dargie et al., 2017). The structure of swamp forests and species composition is influenced by flooding frequencies and the soil drainage conditions with high nutrients due to the decomposition of accumulated materials, which support plants' growth (Thomas and Baltzer, 2001). These properties generate sub-types of the forest like riparian forests and periodically inundated forests with the upper layer reaching 45 m high (White, 1983).

1.4.2.6 Mangrove forest

Mangroves occur on the seashores and river estuaries between high and low watermarks, are permanently influenced by saltwater, usually grow in distinct zones, and are only rarely mixed. Albeit the zonation depends upon the tide, the more proximal the species extends to the mangrove's outer edge, with extended and closer stands in saltwater. In Africa, by 2005, about 3.2 million hectares of coastal land were covered with mangrove forests (Osorio et al., 2016) with 17 mangrove species, where eight species are found in the west and central Africa while nine species are novel to the coast of East Africa. The distribution extends along the

Atlantic coast from Mauritania, Senegal in the Saloum Delta, Guinea Bissau, and Central Africa from Liberia to Angola and along the Indian Ocean from Somalia to South Africa. The mangrove forest attains a greater than 30% of the canopy cover (Ajonina et al., 2008).

1.4.3 African savanna

Savanna is a vast landscape in Africa covering about 15.1 million km^2 with grasses, an open tree canopy, and a short wet season, which prevents this ecosystem from being a closed forest (Campbell et al., 1996). The dry season is associated with lightning-induced or human-set fires and restricts vegetation growth (Scholes and Archer, 1997). Savanna vegetation grows in dry climatic conditions where the temperature ranges from 23–28°C, low precipitation, and frequent seasonal drought. It characterises the savanna ecosystem as drought resistance (xerophytic), and the existence of common fire has induced savanna plants to adapt to fire incidences (phyrophytic) (Skarpe, 1992; Marchant, 2010).

Table 1.2 summarises the adaptation features of the savanna woodlands. In many parts of Africa (East and Southern Africa), savanna woodlands have been known locally as miombo woodlands (Huntley, 1982; Frost et al., 1986; Campbell et al., 1996), which describes trees in the genus of *Brachystegia*, *Jubernardia* and *Isoberlinia* (Malmer, 2007; Campbell et al., 1996). It is estimated that savanna woodlands may attain a height between 4–11 m and a canopy cover between 14–65% for fine-leafed savanna and deciduous savanna (Scholes et al., 2004).

Southern and Central Africa are recognised with vast savanna woodlands (miombo woodlands), extending from Angola, Zambia, Tanzania, Malawi, Mozambique,

South Africa, Namibia, Zimbabwe, and parts of the Democratic Republic of Congo (Campbell et al., 2007; Malmer, 2007) (Figure 1.7). African savannas are subjected to intensive agriculture and pasture by supporting the livelihood of many communities (Mitchard and Flintrop, 2013). For instance, 2.7 million km^2 of the savanna area in Central and Southern Africa (Campbell et al., 2007) support about 60 million people as a source of wood or charcoal that provides energy for 40 million people in urban areas (De Wasseige et al., 2014). The savanna biome is further categorised based on seasonal cycles as deciduous, deciduous shrubland with sparse trees, open deciduous shrubland, thickets, and grassland with scattered trees (Chidumayo, 2001).

Table 1.2: General adaptation features of savanna woodland

Structure	**Explanation**
Deciduous	Trees usually lose leaves during the dry period to reduce evapotranspiration
Leaves	Small leaves, waxy and often thorn-like and sunken stomata to reduce moisture loss
Bark	Thick and or resinous which protect the vascular system in the dry season and fire incidence
Roots	Most trees are deep-rooted to reach the water table and wide root network to increase the surface area for water absorption
Spacing	Open spacing about 80 stems per ha, which also reduces competition for scarce water and nutrients
Water storage	Semi-succulent trees like baobab which store water in the trunk
Dormancy	Most of the trees become dormant for the duration of the dry period which during this period trees shed leaves

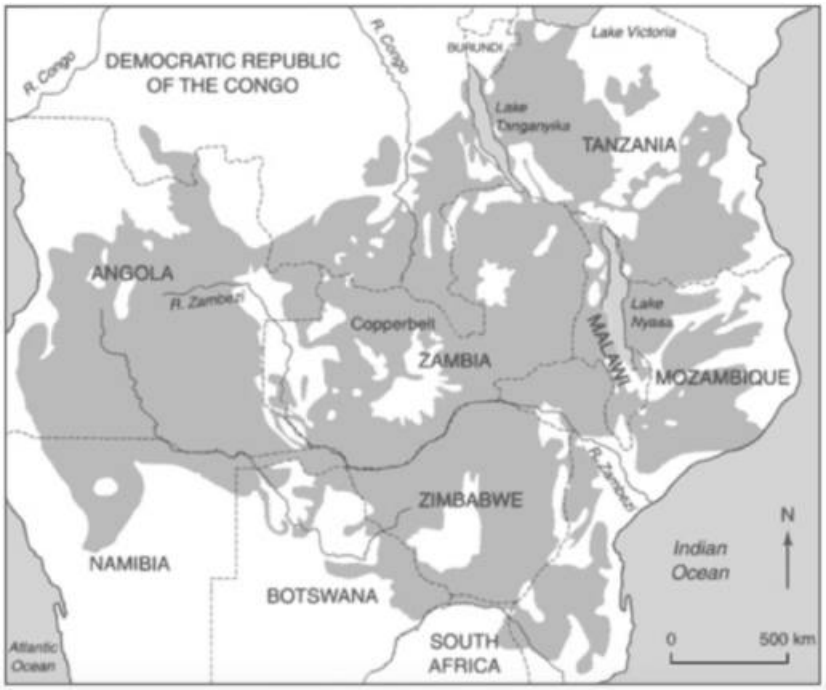

Figure 1.7: The distribution of savanna woodlands (miombo) in Africa. Sourced from Malmer (2007)

1.4.3.1 Deciduous woodland

A form of savanna forest with an open canopy of about 15 – 40% and height higher than 5 m and sometimes with discontinues, fewer shrubs lose their leaves in the dry season. They occur mainly in East and Central Africa in Tanzania, Madagascar, Botswana, Zambia, and Lesotho (Jin et al., 2013).

1.4.3.2 Deciduous shrubland with sparse trees

This form a mosaic of shrubs less than 5 m tall with scattered trees of about 50 – 70%, which appear emergent and less localised, and a layer of perennial grasses reaching 20 – 50% (Chidumayo et al., 2011).

1.4.3.3 Open deciduous shrubland

An open stand of bushes, usually 0.5 to 5 m tall, with canopy cover greater than 25%. Bushes typically cover 50 – 70% of the area, while grasses cover the remaining 20 – 50%. Open deciduous shrublands are present in most of Africa's dry regions with shallow soils, for example, Karoo shrubland in Namibia (Burke, 2001).

1.4.3.4 Thickets

Thickets consist of dense evergreen or deciduous shrubs without grass or other breaks in the canopy. Thickets grow and interlock, making an impassable community, and typically grow up to 5 m tall but may also reach 8 – 11 m in height. In Africa, significant areas of thicket are present in Tanzania, Zambia, South Africa, and Ethiopia.

1.4.3.5 Grassland with sparse trees

The grassland of the savanna is more extensive and with a continuous layer of grasses. Grasses and other herbs cover the ground; either without woody plants or woody covers $< 10\%$ of the land. They are found in central Madagascar, on the Kalahari sands in western Zambia and eastern Angola, and part of west Uganda with a mixture of thickets (Sayer, 1992).

1.5 Forests in Tanzania

Tanzania is endowed with a tremendous diversity of forests, with an estimated 48.1 million ha of forest, representing 55% of the total country land area (88.3 million ha) (MNRT, 2015), placing among the top 36 global biodiversity hot spots (Myers et al., 2000) (Figure 1.8). Management of forest resources in Tanzania is by the central government at about 34.5%, local government authorities at about 6.5%, under village management (village land) at about 45.7%, private forest land at about 7.3% and 5.7% on general-use land (MNRT, 2015).

The importance of forest resources is well-known, ranging from ecosystem services for wood and non-wood forest products (NWFPs) supporting people's livelihood and the country's economy, contributing about 4% of the gross domestic product (GDP) (Green Advocates International, Inc., 2014). The wood products range from firewood, charcoal, and round to sawn wood, with 92% of energy in Tanzania coming from wood (fuelwood) (Malimbwi et al., 2016; URT, 2001). Ecosystem services include watershed protection for power generation and irrigation, soil conservation, biodiversity preservation, climatic amelioration, and ecotourism. Climate change mitigation is increasingly important for forests, most notably through REDD, forest conservation, sustainable management of forests, and enhancement of forest carbon stocks (REDD+) initiatives (Mustalahti et al., 2012).

Despite the importance and diverse nature of forests, Tanzania is placed among the countries with the most extensive forest cover loss (Hansen et al., 2013), mainly induced by human activities. Generally, forest encroachment, shifting cultivation, and wildfires are common. For instance, it has been estimated that between 1990

and 2010, the loss of forest cover was about 403,350 ha per year (FAO, 2010), inline with Tanzania forest reference emission levels, reported a loss of about 469,420 ha per year (URT, 2017). Efforts to halt the loss of forests are in place, but deforestation continues to occur at an alarming rate that contributes significantly to the ongoing loss of biodiversity. Limited capacity for forest monitoring has also compromised these efforts. The government has relied on estimates based on either global-scale studies or small-area local studies. These data are an essential source of information. However, they lack uniformity and completeness in terms of time and coverage (Brink and Eva, 2009).

The increased invasion and shifting cultivation in protected and unprotected forests are speedily decreasing the natural forest cover and forest biodiversity (URT, 2001). A declining trend in forest cover threatens people's survival and, therefore, is an issue of profound concern and utmost priority for forest monitoring to support policy-makers for sustainable forest management in Tanzania.

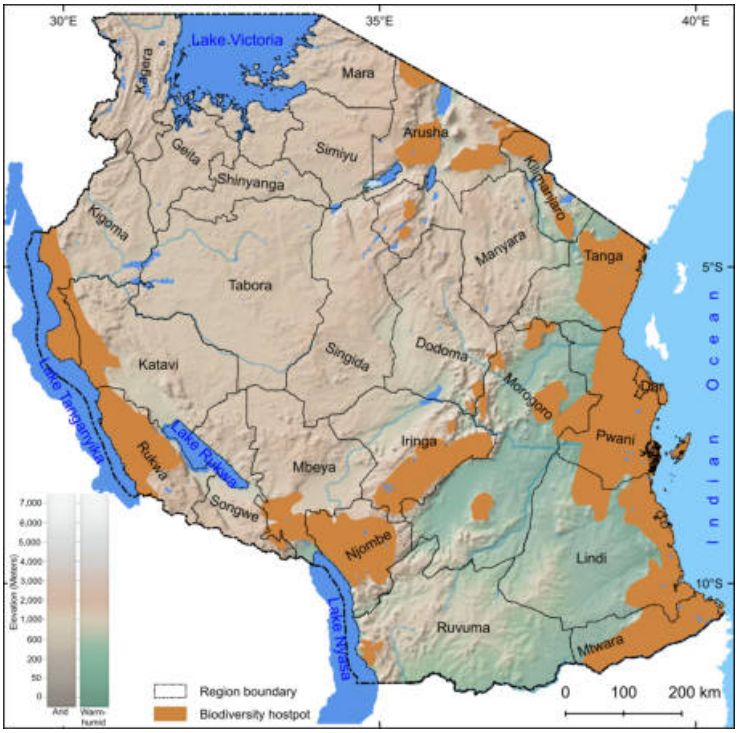

Figure 1.8: Biodiversity hotspots in Tanzania. Created using Natural Earth data and biodiversity hotspots layer sourced from Hoffman et al. (2016)

1.5.1 Forest Types and Distribution

Natural forests are significant categories of vegetation in Tanzania. They contain over 10,000 plant species, hundreds of which are endemic and about 2,261 plant species endangered, whereby 1,456 species are likely threatened and 805 species are potentially threatened (Stévart et al., 2019). Natural forests include woodlands categorised as closed and open and forests classified as montane in mountainous areas, and lowland, and mangrove forests along the coast of the Indian ocean.

The woodlands are found in the country's western, central, and southern parts, with a closed canopy, especially along Lake Tanganyika and parts of the north with

Accacia-Commiphora woodland (Burgess et al., 2004). The distribution of forests and woodlands varies, whereby woodlands occupy about 50.6% of the country area, forests approximately 3.5%, and around 45.9% occupied by other land covers (Malimbwi et al., 2016).

1.5.1.1 Forests

The forests occur in continuous stands of trees that reach up to 50 m in height and are rich in species. Disturbances are also present. Altitude is the determinant of forest distribution where precipitation and nutrient recycling is high. Three canopy layers may exist in tall forests: emergent, middle, and lower and characterised further by the presence of lianas, climbers, creepers, and epiphytes, mostly ferns (Vesa et al., 2010). Three subtypes of forests exist, including montane, lowland, and mangroves.

1.5.1.2 Montane Forest

Montane forests are categorised based on altitude and rainfall per year, as either humid montane or dry montane forests. The moist montane forests are found around 1400 to 1850 m above sea level, with rainfall ranging from 1200 mm to above 2000 mm per year (Robertson, 2002). Humid montane forests exist in two layers, whereby the upper layer consists of trees reaching a height of about 15 – 30 m and sub-emergent trees about 5 -10 m in height with a herbaceous layer of the forest floor. They occur along the west Usambara Mountains and on Mt. Kilimanjaro. The dry montane forests are found up to 1200 m elevation with rainfall between 850 and 1300 mm per year. The rainless period persists for up to 5 months and the

mean tree height range from 10 to 20 m occasionally reaching 45 m. They occur on the Eastern part of Mount Meru, Mount Hanang, Poroto, Mount Rungwe, and the Livingstone Mountains (Mugasha et al., 2004) (Figure 1.9a).

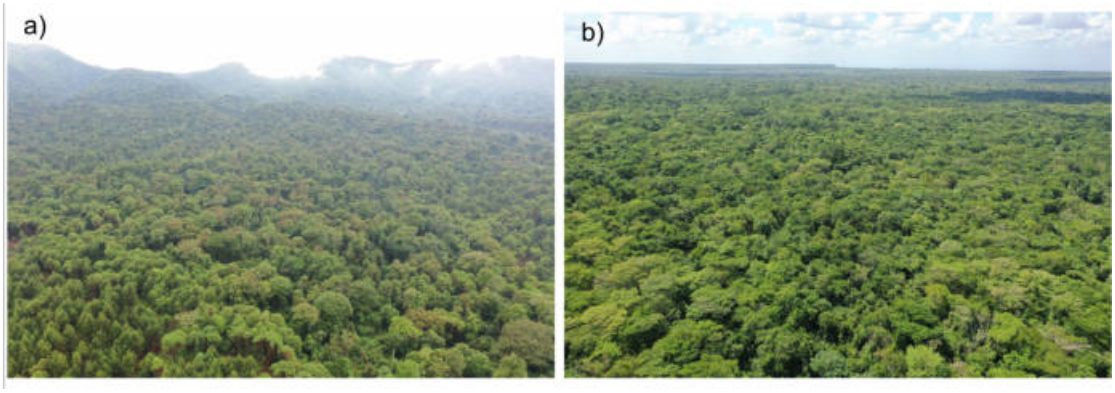

Figure 1.9: a) Montane b) Lowland forest in Tanzania based on drone capture at the height of about 60 m at a) Mount Rungwe Nature Forest Reserve (Mbeya) and b) Rondo Nature Forest Reserve (Lindi), October 2018

1.5.1.3 Lowland Forest

The lowland forests are found near the coast of the Indian Ocean and in smaller areas consisting of mosaics with woodlands and montane forests (Figure 1.9b). For instance, the lower part of the Eastern Arc Mountains with altitudes ranging from 540 – 810 m above sea level, and rainfall amount varies from 1000 -1500 mm per year. The mean tree height in the lowland forest ranges from 15 to 20 m, with emergent trees reaching 35 m (Burgess et al., 2010; Robertson, 2002). Lowland forests are associated with bamboo and occur on the South of Iringa to the Lindi region, up to 615 m of altitude. According to MNRT (2015), lowland forests are estimated to cover an area of about 1.7 million ha.

1.5.1.4 Mangrove Forest

The mangrove forests grow on the upper part of the intertidal zone of the delta's sheltered shores, alongside the river estuaries and creeks with silt and clay soil at an altitude of about 25 m above sea level (Burgess et al., 2010) (Figure 1.10). The height of mangrove forests ranges from shrubs to tall trees, which reach about 2 m to 30 m and above (Mugasha, 1996). Mangrove forests extend from Tanga in the north to Mtwara region in the south, where the Ruvuma river forms an estuary near the Mozambique border. The largest area of mangroves occurs in the Rufiji River delta, but mangroves are also present in the Wami and Ruvu River deltas.

Figure 1.10: Mangrove forest in Tanzania based on drone capture at the height of about 60 m at Nyamisati- Rufiji delta, October 2018

1.5.1.5 Woodland

The savanna woodlands (miombo woodlands) cover the largest area of natural vegetation in Tanzania, about 90% of the total forest cover (URT, 1998). Miombo woodlands are generally dominated by the tree species of *Brachystegia, Julbernadia* and *Isobernia* (Backéus et al., 2006; Campbell et al., 2007; White, 1983). They exist in three layers; the first layer with canopy trees of 14–20 m in height, the second layer has trees with a height of 8–12 m (Mugasha, 1996) and the third consists of trees of 1–2 m high (Campbell et al., 1996). The canopy cover determines the type of savanna woodlands as closed (Figure 1.11a) or open (Figure 1.11b).

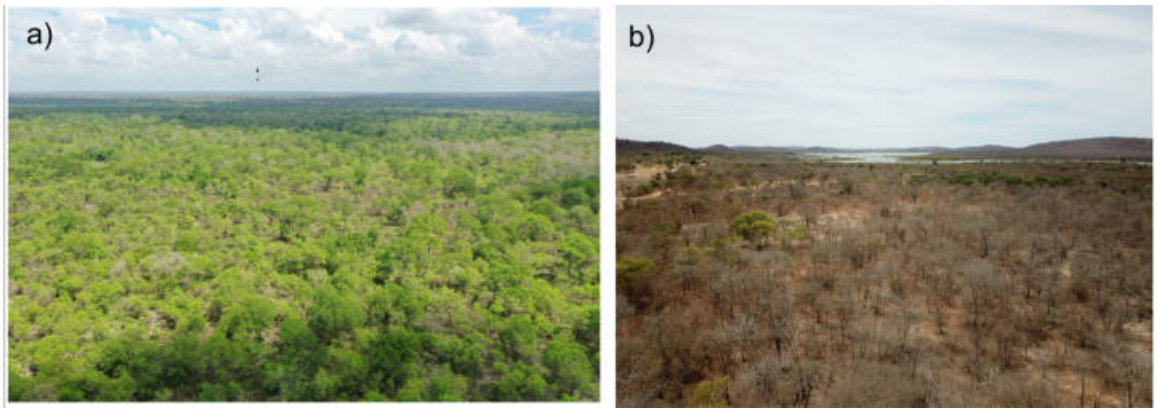

Figure 1.11: a) Closed b) Open woodland in Tanzania based on drone capture at the height of about 60 m at a) Ngulakula forest reserve (Rufiji), October 2018 and b) Igombe river forest reserve (Tabora), October 2019

1.5.1.6 Closed woodland

Closed woodlands (Figure 1.11a) are characterised by a crown cover of greater than 40% and the availability of perennial C4-grasses. This ecosystem has regular fire occurrences from May to November before the rainy season. Humans rather than natural fires cause most fires (Mugasha et al., 2004).

1.5.1.7 Open woodland

Open woodlands (Figure 1.11b) share similar characteristics as closed woodland, with the main difference being canopy cover, where open woodlands have a crown cover of about 10 – 40%.

1.5.1.8 Thicket

Thicket woodlands are characterised by impenetrable woody density and a height of less than 5 m and a crown cover of 5 to 10% and are found in central Tanzania (Itigi thickets) (Figure 7.17).

Figure 1.12: Thicket woodland in Tanzania based on drone capture at the height of about 60 m at Itigi-Manyoni, October 2019

1.6 Motivation of Study

For a developing country such as the United Republic of Tanzania, forests are a significant resource at multiple levels. Despite the value of forests, changes

in use patterns pose a noticeable threat to forest resource sustainability in both socio-economic and ecological functioning. It has increased the scarcity of forest resources, further aggravated by the continuing high deforestation rate and associated with a change in climatic conditions experienced in many parts of Tanzania. Therefore, the need for data and information on the state of Tanzania's forest resources is of increasing importance. Yet, Tanzania's forest resource status and trends are mostly unknown, with current data being fragmented and outdated (Vesa et al., 2010).

The lack of institutional capacity has largely constrained data reliability on Tanzanian forest resources with inadequate national-wide coverage in forest monitoring using an Earth Observation (EO) based system. The application of an EO-based system, especially using freely accessible satellite data and advanced remote sensing methods, can provide a cost-effective and timely approach to achieving systematic wall-to-wall information about forest monitoring in Tanzania. This information is required to support the national policy processes for the enhancement of sustainable forest management (SFM) while at the same time addressing the issues of REDD+ and Green House Gas (GHG) as international reporting obligations and the 2030 Agenda for Sustainable Development Goals (SDGs) through combating deforestation (Anderson et al., 2017).

1.7 Study Aim and Objectives

This study aims to create the basis for a long-term national forest monitoring system for Tanzania. Such a system needs to help the country bridge the information gap and knowledge concerning remote sensing in forest monitoring over a national

level. It further serves as a strategy for reducing the dependence on traditional forest surveys in Tanzania, which are expensive, time-consuming, and spatially limited. Every update needs 2 to 5 years to cover the country. Similarly, the field inventory data are acquired using sample plots and typically grouped to the forest stand level with a shortfall in the forest types' spatial variability.

To achieve this aim, the study will focus on the following research questions:

i. What is the distribution of the different forest types in Tanzania?

ii. How the forest types will be impacted by future climate change?

iii. What is Tanzania's current (baseline) spatial extent of forest cover?

iv. How can forest extent change be mapped as part of an on-going monitoring system?

In achieving the stated research questions, this study sought to achieve the following objectives:

i. To map the distribution of major forest (including woodland) types in Tanzania using Earth observation data;

ii. To assess the impacts of future climate change on forests in the mainland of the United Republic of Tanzania (hereafter referred to as Tanzania);

iii. To develop a method for establishing the current (baseline) spatial extent of forest cover in Tanzania;

iv. To develop a method for detecting changes in forest extent as a part of an on-going monitoring system.

1.8 Outline of the thesis

This thesis consists of nine chapters:

Chapter 1 provides a detailed review of the general background to the study of tropical forests, specifically in terms of their distributions and changes. The chapter concludes with the research significance and outlines the research aim questions, and objectives.

Chapter 2 provides background to the study, reviewing habitat suitability modelling and future climate change impacts for different forest types and their implications for forest conservation decisions. The chapter reviews different remote sensing and spatial analysis methods and constraints of remote sensing data from various sources for tropical forest monitoring.

Chapter 3 describes mainland Tanzania in terms of geographical location, climatic conditions, and vegetation cover. The study area was used to develop the methods for mapping forest extent and monitoring change.

Chapter 4 presents an overview of the datasets used in the study and their preprocessing, and analysis. The forest inventory data used to assess the accuracy of the land cover and change maps are described. The Free/Libre and Open-Source software (FLOSS) used in this study is also outlined.

Chapter 5 describes the pilot area (the Rufiji catchment) for a subnational study and the methodology for generating a new forest baseline (forest/non-forest) and forest type classification. The chapter provides an understanding of data volume and constraints associated with storage and processing times.

Chapter 6 presents an approach for spatial climate change modelling relevant to Tanzanian forests for assessing the present and simulating future climate change scenarios on diverse forest types. This provides an overview of the implications for changes in the distribution of the forest types in the globally significant tropical ecosystems of Tanzania.

Chapter 7 presents the methodology for generating forest baseline and forest types maps for Tanzania provides the findings and discusses these and the implications for forest management in Tanzania.

Chapter 8 describes a forest change analysis and monitoring method based on the forest baseline developed in Chapter 7 over Tanzania, provides the outputs discusses these in relation to current and future forest management

Chapter 9 presents the main conclusions of the research, discussing the key findings, research questions, research limitations, future outlook for mapping and monitoring tropical a, and contributions to operational forest monitoring systems.

Chapter 2

Background

Critical actions are required to support tropical forest conservation through effective monitoring, especially from anthropogenic and climate change impacts as forest habitat destruction continues unabated around the tropics. Essential measures include predicting forest habitat and forest mapping and associated changes. To do this, we need to take advantage of key technologies such as Earth Observation data, computational power, and machine learning.

2.1 Forest Habitat Suitability Modelling

Tropical forests are essential components of climate change mitigation strategies, such as REDD+ under the UNFCCC (Romijn et al., 2012). However, the changing climate induces a threat to tropical forest ecosystem habitats as changes in precipitation regimes and temperature increase pests, diseases, and fire and storm incidences. Yet, there is little information on these threats to the forests, especially

in the sub-Saharan region (Chidumayo et al., 2011), impacting human livelihoods that depend on forest-related services and exacerbating poverty. The situation induces increased deforestation and degradation of the remaining suitable forest habitats (Thomson et al., 2010). Therefore, information on the relationship between forest habitats and climate change will support national forest management and design monitoring methods to protect the remaining tropical forests.

Efforts to protect and enhance critical forest habitats while mitigating climate change effects on species diversity and distribution need supportive information for informed policy decisions, spatial planning, and conservation practices based on reliable habitat suitability and underlying environmental factors (Guisan et al., 2013).

The application of habitat suitability models (HSMs) or species distribution models is a useful tool for forest monitoring and supports improving tree species' ecological knowledge (Guisan et al., 2013) for informing landscape-scale decisions (Bellamy et al., 2020; Seidl et al., 2017) and climate change.

2.1.1 Predictive Forest Habitat Distribution Modelling

HSMs are categorised as static and probabilistic. They are static and probabilistic because they statistically relate the distributions of populations, species, communities, or biodiversity to their present environment. The static distribution models act as equilibrium – or at least pseudo-equilibrium - between the environment and observed species patterns. The probability of the mode is important because it predicts the occurrences of species conditional on the environmental covariates (Guisan and Zimmermann, 2000).

The predictive model's functionality and selection are based on the species occurrence record and the predictor variables (Elith et al., 2006). Therefore, the growth in computational power, machine learning, and Earth Observation data (Guisan et al., 2017) has increased the use and application of predictive models for forest habitat suitability analysis and future climate change predictions.

The predictive models include the envelope approach that focuses on the geographical (Burgman and Fox, 2003) and environmental (Busby, 1991) distribution of species or population. A regression-based model that relies on robust statistical theories (e.g., Guisan et al., 2002) for example, Generalized Linear Models (GLMs), Generalized Adaptive Models (GAMs) (Antúnez et al., 2017) and Multivariate Adaptive Regression Splines (MARS) (Elith and Leathwick, 2007) and the other predictive models are based on Boosting and Bagging approaches. These include Random Forest (RF) (Valavi et al., 2020) and Boosted Regression Tree (BRT) (Elith et al., 2008).

The Maximum Entropy (MaxEnt) (Phillips et al., 2004) approach has been widely applied in predicting species and distribution modelling (Elith et al., 2011). For example, modelling habitat suitability of *Dipterocarpus alatus* trees in Central Thailand (Kamyo and Asanok, 2020), climate change impacts on the distribution of *Euscaphis japonica* trees in China (Zhang et al., 2020), a shift in the range for Brachystegia (miombo) woodland as evidence from climate change in Southern Africa (Pienaar et al., 2015), and prediction of debts in coastal forests extinction in South Africa using habitat suitability models (Olivier et al., 2013).

2.1.2 HSM for forest conservation decision

HSMs are increasingly applied to address forest dynamics simulation, associating habitat requirements (Edenius and Mikusiński, 2006) with climate projection scenario analysis (Van Vuuren et al., 2011a) for more practical planning tools in forest management. They can also be used to support the mitigation of future climate impacts on forests, hence serving biodiversity and human livelihood. It will support identifying suitable forest habitats for restoration and conservation, which can contribute to increasing forest cover and maintaining important forest matrices and the connectivity of forest fragments. Therefore, HSM can be applied to establish the habitat suitability for different forest types (e.g., in Tanzania) to support regional and global efforts on restoring degraded and deforested landscapes (Seidl et al., 2017). They can also be used to support the prediction of climate change impacts on forests, including those identified in the Fifth Assessment Report (AR5) of the United Nations Intergovernmental Panel on Climate Change (IPCC) on the climate and associated with Representative Concentration Pathways (RCPs) scenarios (Van Vuuren et al., 2011a). This is required for reducing emissions from deforestation and forest degradation (REDD+) as proposed by the United Nations Framework Convention on Climate Change (UNFCCC) (Romijn et al., 2012).

2.2 Forest mapping

The application of remote sensing appears to make significant contributions to monitoring the remaining tropical forests. Importantly, remote sensing comprises

a collection of information on physical, chemical, and biological systems about the Earth's physical planet (Achard et al., 2010). It is, therefore, applied in monitoring by assessing the past, and current status, and changes for both natural and human-made environments. The availability of satellite data since the 1970s (Figure 1.3), with reasonable ground resolution (Coppin and Bauer, 1996; Huang et al., 2009), (for example 30 m for Landsat) provides timely information related to tropical forest areas and associated changes over time with extensive area coverage (Franklin, 2001).

The repeated coverage at short intervals (e.g., 1-16 days) with imagery consistently available helps to improve the detection, identification, and mapping of forests, with this need for monitoring and reporting (Nelson et al., 2022; Borlaf-Mena et al., 2021; Mas, 1999; Coppin and Bauer, 1996). Earth observation data allow measurements of all forest areas at a relatively low cost, regardless of remoteness and access. The process of monitoring tropical forests has effectively improved with more reliable results as remotely sensed data are combined with ground measurements (DeFries et al., 2007).

The mapping and monitoring of tropical forests using different satellite data sources have received increased attention from governments, non-government, academic, and private sectors (Fuller, 2006; Keenan et al., 2015). EO also supports the UNFCCC by contributing spatial estimates of GHG emissions associated with deforestation, especially in tropical regions (Achard et al., 2010). The state of tropical forests and their dynamics, derived through monitoring, are essential inputs to sustainable forest management policies. It is necessary for forest ecosystem management implementation, which requires accurate and up-to-date mapping data (Coppin and Bauer, 1996).

Remote sensing operational systems have supplemented or complemented the traditional approach of forest cover survey from field samples, which is no longer the most efficient means to map forest cover at regular intervals over large areas (Fuller, 2006). Remotely sensed data have contributed to the increased speed, cost efficiency, precision, and timeliness associated with inventories and made it possible to generate maps of forest characteristics with different spatial resolutions and accuracies than before (Lister et al., 2020; Crowley and Cardille, 2020; McRoberts and Tomppo, 2007).

2.3 Remote Sensing Data for Tropical Forest Monitoring

Remote sensing data are collected and classified based on platform carriers and sources of energy. The platform is a vehicle that carries the sensor, for example, satellites, aircraft, or balloons, and the sensors receive electromagnetic radiation and convert it into a signal that is recorded and displayed as numerical data in the form of an image. The wavelengths of energy used by different types of sensors are used to categorise sensors specifically as optical or radar instruments. Optical and radar satellites operate in varying portions of the electromagnetic spectrum and can be used to capture information on forests (Lynch et al., 2013).

2.3.1 Optical Data

Optical remote sensing offers extensive data applied in tropical forest mapping and monitoring due to its broad area coverage, repetitiveness, and cost-effectiveness.

The sun is the energy source for optical sensors where the energy is reflected from the Earth's surface and the resulting information for vegetation is generated based on the surface of the canopy and little information under the canopy. The relevant wavelength regions are from the visible to near and middle infrared of the electromagnetic spectrum at about 0.4 to 2.5 μm (Horning et al., 2010). The high spatial resolution optical data relevant for large-scale forest monitoring varies from 3 (e.g., PlanetScope) to 30 m (Landsat)

The capability of optical sensors in vegetation mapping is related to sensitivity to greenness (Tong et al., 2019), fractional tree cover (Putzenlechner et al., 2022), tree density (Gomes et al., 2018), forest type, and vegetation density (Lynch et al., 2013). These characteristics have made it possible to estimate foliar chemical content (foliar chemistry), which is linked to the biogeochemical status of the forest ecosystem. This supports determining changes in plant species composition (Girard et al., 2020) and forest stress monitoring (e.g., damage due to fire, climate/weather-related hazards including drought events, floods, and extreme temperatures as part of climate change and disturbances (David et al., 2022)). The presence of insects and disease can also alter the foliage with this also causing structural changes (e.g., in crown form or branching pattern of trees) as can human activities such as elective or high-intensity logging or thinning (Mitchell et al., 2017).

In contrast, coarse resolution ($>$ 100 m) includes Moderate Resolution Imaging Spectroradiometer (MODIS), National Ocean and Atmospheric Administration (NOAA, and Advanced Very High-Resolution Radiometry (AVHRR). These have been useful in biomass mapping and estimation at a national, regional, and global scale (Kumar et al., 2015). AVHRR data have been used for mapping global

vegetation, whilst MODIS data and derived measures (e.g., indices) have been used to generate a quantitative measure of vegetation such as Gross Primary Production (GPP), the fraction of Absorbed Photosynthetically Active Radiation (fAPAR), and Leaf Area Index (LAI) (Fensholt et al., 2006). Table 2.1 summarises that some of the studies utilised optical data to monitor different types of tropical forests.

Table 2.1: Some studies utilised optical data in mapping tropical forests

References	Location	Data type	Brief description
(Kim et al., 2015)	Humid tropical forest (34 countries)	Landsat images- 30 m	Estimation of forest area and associated change from 1990 – 2010 (Wall to wall mapping)
(Hansen et al., 2010)	Global forest cover loss	MODIS images- 500 m	Mapping of tropical forests (wall to wall mapping)
(Hansen et al., 2013)	Global forest cover change	Landsat images- 30 m	Mapping of tropical forests (wall to wall mapping)
(Achard et al., 2014)	Humid tropic tropical forest	Landsat images- 30 m	Estimation of deforestation and forest regrowth based on samples

Limitation of optical sensors: Atmospheric conditions frequently prevent observations from optical data (e.g., because of clouds or haze) or compromise the signal due to atmospheric scattering and absorption, especially during the wet season. This reduces the number of satellite passes suitable for monitoring the tropical forest, as only cloud-free scenes can be processed. To obtain all-weather capacity, active radar systems, which penetrate clouds, have capabilities that are advantageous in comparison to optical data, especially in the tropics where cloud cover is frequent (Lu and Weng, 2007; Rosenqvist et al., 2000).

2.3.2 Radio Detection and Ranging (Radar) Data

Radar operates in the microwave part of the electromagnetic spectrum (EMS). It is sensitive to different vegetation properties such as leaf area index (LAI), and other parameters related to forest structure such as height and volume. The radar's energy can penetrate the tree canopy (wavelength dependent) capturing information on the leaves, branches, and trunks (Lynch et al., 2013). The radar system collects data related to the backscattering process whereby reflected signals generate data on the image. It involves scattering and absorption of energy when hitting the tree canopy, and the radar measures the strength of the backscatter. The signals emitted from radar (transmitting antenna) occur at both horizontal (H) and vertical (V) polarization.

In radar, the polarization (plane) of the electromagnetic radiation waves is recorded as horizontally (H) or vertically (V) transmitted and received (i.e., HH, VV, or VH; (Horning et al., 2010)). Radar systems operate in the microwave portion of the EMS, and are therefore able to penetrate clouds and haze (including from smoke) and are therefore well suited for use in the tropics where clouds are persistent and fires are also commonplace (De Grandi et al., 2000; Siegert et al., 2001).

Forest monitoring using Synthetic Aperture Radar (SAR) data is an increasingly promising remote sensing approach for mapping forest disturbances in the tropics because of the ability to operate in all weather conditions of the day or night (Hirschmugl et al., 2020). Spaceborne radar currently operates at X-band, C-band, and L-band. For example, TanDEM-X Interferometric data have been used in forest height mapping such as Chen et al. (2019) in Northwest Canada. The height estimates provided R^2 values of 0.78 and 0.88, mean errors (ME) of 1.66 m and 1.90

m, and root-mean-square errors (RMSE) of 2.7 m and 2.9 m, respectively, when compared to independent height estimates derived from field plots and airborne LiDAR. Similarly, Sentinel-1 time series have been used for estimating boreal forest height mapping in Central Finland with an accuracy of 28.3% rRMSE for pixel-level predictions, and 18.0% rRMSE on stand level (Ge et al., 2022).

The release of the Japanese Earth Resources Satellite (JERS SAR), Advanced Land Observing Satellite-2 (ALOS-2), Phased-Array L-band Synthetic Aperture Radar – 2 (PALSAR-2) mosaics at 25 m resolution by the Japan Aerospace Exploration Agency (JAXA) significantly increased access to radar data and studies related to forest monitoring with SAR. Similarly, ALOS PALSAR mosaics were used to produce the first SAR-based annual for 2007–2010 global maps of forest and non-forest cover, from which forest losses and gain maps were also generated (Shimada et al., 2014). Forest disturbance monitoring using different SAR sensors has also been demonstrated using Sentinel-1 C-band and TerraSAR-X data (e.g., in the Republic of Congo) (Hirschmugl et al., 2020).

The estimation of forest parameters such as tree height, DBH, etc. have been achieved with lower frequency (L and P band) Synthetic Aperture Radar (SAR) (Santos et al., 2003). Radar data, for example, TerraSAR-X have been used in mapping deforestation in the tropical rainforest of Ecuador with an accuracy of about 81% in the classification of forest and non-forest (Delgado-Aguilar et al., 2017). However, C-band SAR data is less suited for forest disturbance assessment and above-grove biomass estimation than L-band SAR due to its shorter wavelength, which limits the penetration into the canopy (Hirschmugl et al., 2020).

Limitation of radar data: Radar remote sensing provides a solution in ar-

eas of persistent clouds. However, radar images have constraints of speckle noise, which may result in low classification accuracy (Maghsoudi et al., 2012). These require more processing techniques; for example, the temporal reduction filter (Lopes et al., 1990; Quegan and Yu, 2001). Topography also causes geometric and radiometric distortions, particularly in mountainous areas (Joshi et al., 2016).

2.3.3 Light Detection and Ranging (LiDAR)

LiDAR is an active remote sensing technique; similar to radar, but the difference is that the laser operates in the visible or near-infrared part of the electromagnetic spectrum (Hudak et al., 2002). It works by transmitting the laser light's pulse toward the ground and measuring the time for the return pulse. Therefore, the information is collected based on the distances between the sensor and the object on the ground. It is determined by the return time for each pulse back to the sensor (Lillesand et al., 2015; Lim et al., 2003). In vegetation mapping, the incident pulse of energy usually reflects off the canopy, including branches, leaves, and the ground surfaces (Dubayah and Drake, 2000).

Forest parameters that can be measured with an airborne LiDAR system include canopy height, subcanopy height, topography, and the vertical distribution of the intercepted surface between the canopy top and the ground (Dubayah and Drake, 2000). These parameters enable estimation of tree basal area (Means et al., 1999), wood volume (Wang et al., 2008), aboveground biomass (Lu et al., 2012) and LAI (Lefsky et al., 1999).

Further application of the airborne LiDAR system is for identifying historical forest disturbances, such as selective logging and recovery in tropical forests. For exam-

ple, Kent et al. (2015), analyzed canopy gaps in an area of 16 km^2, and about 10.2% of canopy gap fraction were found in logged areas as related to 5.6% in unlogged areas. Similar monitoring of selective logging on the western Amazonia between 2010 and 2011, indicated a decrease in the canopy from 22.8% to 18.7% (Andersen et al., 2014).

Airborne LiDAR data have also been combined with other airborne data (Carnegie Airborne Observatory (CAO) hyperspectral data) in mapping tree species composition of savanna woodlands in South Africa with an overall accuracy of 79% (Cho et al., 2012). Similarly, Castillo et al. (2012) used LiDAR remote sensing to map the growth distribution (succession stages) of secondary forest in the dry tropical forests of Costa Rica based on changes in vertical structure (height) and obtained an accuracy of r^2 equal to 0.69. The derived information from LiDAR is increasing and supporting decision-makers in the forestry discipline (Hudak et al., 2009; Roberts et al., 2020). Although both types of sensors present different advantages in monitoring tropical forests, this thesis focuses on utilising optical sensors, as data are extensively available and free to download.

Limitation of LiDAR: The limitation is associated with a high cost for commercial airborne LiDAR for a small area of coverage (Bohak et al., 2020).

2.4 Information Extraction from Remote Sensing Data

The development and availability of different remote sensing techniques are increasing opportunities to observe, monitor, and study Earth's surface, atmosphere, and

environment (Miyoshi et al., 2020). To optimally exploit remote sensing data, it is important to consider pre-processing, information extraction, and interpretation requirements and processes that allow the generation of useful information relevant to address user needs. With an optical system, information is collected in the green, red, infrared, near-infrared, and shortwave infrared of the EMR spectrum (Brolly et al., 2021), and classification from such data typically involves assigning each pixel value in the image to a predefined class that represents a specific feature/objects on the ground (Sivanpillai et al., 2005). This enhances the capacity to then assess, monitor, and predict the dynamics of land covers and the influence of both human activities and natural events and processes on environments (Brolly et al., 2021).

The identification of features on an image is either by visual or automated techniques. Visual interpretation has been the traditional method for extracting information, with this informed by the known characteristics of objects discerned from aerial photographs or satellite imagery (Sowmya et al., 2017). In this approach, a human interpreter uses various parameters of object recognition and interprets objects/phenomena and their spatial and spectral patterns based on tone, shape, size, pattern, texture, and shadow (Horning et al., 2010). However, in computing technology and storage, visual analysis has instead been replaced with sophisticated image classification algorithms (Sarker, 2021; Barmpoutis et al., 2020). These include the application of artificial intelligence (AI), particularly machine learning (ML) and deep learning (DL), which have become widespread in research and incorporated into different applications, including text mining, spam detection, video recommendation, image classification, and multimedia concept retrieval (Sarker, 2021). AI algorithms exist to effectively build data-driven systems for classification

analysis, regression, data clustering, feature engineering, dimensionality reduction, association rule learning, or reinforcement learning techniques (Alzubaidi et al., 2021). Such approaches have also improved forest mapping and monitoring over larger forest areas; such as in Africa (e.g., using DL)(Waldeland et al., 2022).

2.4.1 Image Classification

Image classification converts the continuous pixel values measured by the instrument to a set of categories, with thematic meaning to the end user. The entire image classification process involves: a) defining the classification system, b) selecting data from different sensors, c) collecting reference data, and finally, d) conducting an accuracy assessment (Jensen et al., 2005; Lu and Weng, 2007). Important factors to consider during the selection of the image classification approach include the spatial resolution of the remotely sensed data, data sources, and accessibility of software for image classification. It is important to identify the optimal approach for the problem being tackled as there isn't a single 'best' classification approach for all problems (Hubert-Moy et al., 2001; Horning et al., 2010).

The method of extracting information from remotely sensed data includes per-pixel (Wu et al., 2021; You et al., 2019; Foody et al., 1996; Vieira et al., 2003), sub-pixel (Wang et al., 2020; Qi et al., 2019; Lu et al., 2003) or object-level or a combination (hybrid) of this (Deepan and Sudha, 2020; Zhang et al., 2020; Lu and Weng, 2007). Classification algorithms have evolved alongside the advancement in computing power available. These classification techniques include neural networks, decision trees, and support vector machine (Zagajewski et al., 2021; Jozdani et al., 2019; Blaschke, 2010; Franklin and Wulder, 2002; Rogan et al., 2008; Lu and Weng,

2007) which are based on statistical assumptions (e.g., either parametric or non-parametric).

2.4.1.1 Parametric classifiers

Parametric classifiers are based on the assumption that the data have Gaussian distribution by creating parameters for the mean vector and covariance matrix (Hubert-Moy et al., 2001; Lu and Weng, 2007; Kamavisdar et al., 2013; Cortijo and De La Blanca, 1997). It assumes a normal distribution for each class in an image. Example of parametric classifiers includes a Maximum Likelihood algorithm, Bayesian, Multivariate Gaussian, Naive Bayes, Decision Tree, Support Vector Machine, Classification Tree, discriminant analysis, and Minimal Distance Classifier (Sahoo and Kumar, 2012).

Maximum likelihood classifier (MLC): The maximum likelihood classifier is possibly used to be the most extensively applied technique for classifying remote sensing data. It relies on statistical assumptions of a normal distribution of class signatures (Huang et al., 2002). The image classes are pre-defined with adequate training samples, referred to as signatures (Lu and Weng, 2007). MLC presumes each pixel has a probability of belonging to a particular class. Therefore, each pixel is assigned to a class based on the highest level of probability. The MLC is limited by the distribution of the training data set, which may not be statistically distinguishable in feature space (Schowengerdt, 2006; Ahmad and Quegan, 2012). Consequently, the final thematic map appears to have a mixture of isolated labeled pixels in other classes which increases the classification error. It may occur when there is an overlap within the training samples for a given category (Cortijo and De La Blanca, 1997).

MLC has been applied to classify tropical forests for tree species mapping and forest types (Erinjery et al., 2018; Laurin et al., 2016). The comparison of MLC with other techniques found it can provide robust results for both optical and radar data. For instance, in an analysis of hyperspectral data, three classification techniques were compared (MLC, ANN, and decision tree classifier), ML performed better with an accuracy of 86% (Kuching, 2007). Table 2.2 summarises some of the accuracy results for MLC techniques in different types of tropical forests.

Table 2.2: Example of MLC application in tropical forest mapping

Vegetation type	**Sensor type**	**Accuracy** (%)	**Reference**
Tropical forest	Landsat TM	94.84	(Foody et al., 1996)
Tropical forest	Airborne Image	86	(Kuching, 2007)
Tropical forest	ASTER	88.50	(Baatuuwie and Van Leeuwen, 2011)
Tropical forest	Landsat image	90.94	(Tottrup, 2004)
Mixed forest	SAR image	59.4	(Waske and Braun, 2009)
Rain forest	Hyperspectral image	88	(Clark et al., 2005)
Tropical land cover	Landsat TM	97	(Ahmad and Quegan, 2012)
Montane Tropical forest	Landsat TM	87	(Helmer et al., 2000)
Tropical forest	Landsat TM and PALSAR	91.1	(Laurin et al., 2013)
Species mapping	Sentinel-2	90.73	(Laurin et al., 2016)

Discriminant analysis (DA) algorithm: DA is also a statistical parametric technique, which depends on the average sample and the covariance matrix calculated from the training sample. The estimated covariance matrix is calculated by the regularisation process using two parameters of quadratic, ML classifier, and linear classification (variance matrix) to reduce cross-validation error (Cortijo and De La Blanca, 1997). It minimises intra-class variance and maximises inter-class variances (Hubert-Moy et al., 2001). However, this method also suffers from similar limitations as the ML classifier as the sample average and covariance matrix

are not robust in features separation (Herwindiati et al., 2014).

Parametric classifiers are limited to fixed decision boundaries of the training samples. When the training samples are not aligned with the decision boundaries, misclassified pixels are produced and a noisy classification often results from (Cortijo and De La Blanca, 1997; Hubert-Moy et al., 2001). The application of non-parametric techniques is considered robust in reducing noisy classifications and in the tree species classification of the tree species (Table 2.3).

Table 2.3: Summary results of DA techniques in tropical forest mapping

Vegetation type	**Sensor type**	**Accuracy** (%)	**Reference**
Tropical rain forest	Landsat TM	86	(Thessler et al., 2008)
Tropical tree species	Aerial photography, CASI and HyMap	87	(Lucas et al., 2008)
Rain forest-species	Hyperspectral image	87	(Clark et al., 2005)
Tropical forest	Landsat image	90.94	(Tottrup, 2004)
Mixed forest	SAR image	59.4	(Waske and Braun, 2009)
Rain forest	Hyperspectral image	88	(Clark et al., 2005)
Tropical forest	Landsat TM	92.20	(Foody and Hill, 1996)

2.4.1.2 Non-parametric classifiers

The non-parametric classifiers (machine learning algorithms) have few underlying assumptions of data distribution like normality or normalised mean and variance have been demonstrated as providing more reliable classification than parametric classifiers (Foody, 1995). The application of non-parametric classifiers in remote sensing-based applications has increased over the past decade (Thanh Noi and Kappas, 2018).

The growth of open-source machine learning/deep learning with the application of artificial intelligence provides systems provide the ability to learn and improve

classification outputs without being explicitly programmed. The availability of machine learning libraries supports the classification process, including Scikit-Learn, TensorFlow, and Keras. Example of machine learning classifiers includes Support Vector Machines (SVMs), Artificial Neural Networks (ANNs), k-Nearest Neighbor (k-NN), Random Forest (RF), Extremely Randomized Tree classifier (ERT), Extreme Gradient boosting (XGBoost), and Light Gradient Boosting (LGBM). Therefore, this study will mainly focus on the application of machine learning classifiers (non-parametric classifiers).

Support Vector Machines (SVM): SVM is a machine learning algorithm (Huang et al., 2002) that works by building a hyperplane concerning the maximum gap of the training samples used for classification. It subsequently classifies the features into one of the defined classes (e.g., land covers) (Qian et al., 2015). The most significant distance in the hyperplane of the adjacent training sample of the given class results in a good separation. When the margin is more extensive, it lowers the generalisation error of the classifier (Kamavisdar et al., 2013). For example, when two classes cannot be separated linearly, the method looks for the hyperplane that maximises the margin and minimises the proportional quantity of the misclassification errors (Pal, 2005). SVM is useful for classification due to its ability to work with limited training samples (Mountrakis et al., 2011). The application of SVMs in vegetation mapping with different types of remote sensing data is well documented (see Huang et al., 2008; Su et al., 2009; Keramitsoglou et al., 2006; Knorn et al., 2009).

A comparison of classification methods will focus on the accuracy of the results. For instance, Thanh Noi and Kappas (2018), compared three non-parametric classifiers; RF, k-NN and SVM for land cover classification using Sentinel-2 images

and SVM outweigh the other two techniques with marginal differences; SVM had 95.29%, followed by RF with 94.59% and k-NN with 94.10%. Whilst Qian et al. (2015) obtained 92.6% for SVM, decision tree (DT) 88.4% and k-NN with 86.8%. Similarly, Kaszta et al. (2016) compared four classifiers; k-NN, ML, RF, and SVM on a seasonal separation of African savanna woodland classification using Worldview-2 image and the results indicate the accuracy of 83% and 77% for SVM on pixel and object-based classification respectively, followed by RF for 82% and 75%, k-NN had 80% and 73% and ML had 78% and 72% respectively (Kaszta et al., 2016).

Table 2.4 presents significant SVM findings in forest mapping using different sensors. SVMs indicate high-accuracy classification results, but a disadvantage of this technique is that it depends on quite a lot of hyper-parameters, which need to be optimised (Pal, 2005).

Table 2.4: Summary results of SVM techniques in tropical forest mapping

Vegetation type	**Sensor type**	**Accuracy** (%)	**Reference**
Natural tropical forest	ALOS PALSAR	86	(Longépé et al., 2011)
Rain forest	Landsat TM	84.30	(Sesnie et al., 2010)
Tropical vegetation	Radar data	99	(Lardeux et al., 2009)
Mapping tree species	WorldView-2	77	(Omer et al., 2015)
Tropical rainforest	Synthetic Aperture Radar (SAR)	63.30	(Pouteau and Stoll, 2012)

Artificial Neural Networks (ANNs): This classifier is made of layers, and each layer constitutes neurons. The neurons are comprised of at least three arranged layers; an input layer, one or more hidden layers, and an output layer. The neuron in the input layer informs of the individual pixels' multispectral reflectance values, such as texture, surface roughness, terrain elevation, slope, and aspect. The hidden layer helps simulate the non-linear arrangement of the input data, and the output layer represents the final thematic map cover class (Jensen et al., 2005).

The advantages of ANNs have been discussed in comparison with other techniques (Mas and Flores, 2008). For some applications, ANNs have demonstrated an improved classification accuracy with the ability to adapt or learn from the previous results and update the classification more objectively, based on the ability to learn intricate patterns (Lek and Guégan, 1999). The classifier also can combine multi-source data from different sensors and auxiliary data like elevation, slope (Carpenter et al., 1997; Benediktsson et al., 1990), and more using less training dataset (Paola and Schowengerdt, 1995).

These advantages extend the application of ANNs in land cover classification, unmixing and retrieving biophysical features of cover, change detection, data fusion, object recognition, and prediction (Mas and Flores, 2008). Pal (2005) compared three classification techniques of ML, ANNs, and SVMs based on the number of bands and training dataset and the results ranked ANNs the second; SVMs (93.6%), ANNs (88.4%), ML (85.8%). In a comparison of mapping tropical coast forests in Thailand using ASTER images, ANNs showed an accuracy of 94.99% as compared to 94.15% for SVM and 93.9% for ML (Szuster et al., 2011). Olthof et al. (2004), used ANNs to map storm damage impacts on deciduous forests using Landsat data and produced an overall accuracy of 94%. However, the method is computationally complex which reduces its accessibility for those classifying remote sensing data (Thanh Noi and Kappas, 2018). Table 2.5 summarises the application of ANN in different types of tropical forests.

Table 2.5: Summary results of ANN techniques in tropical forest mapping

Vegetation type	**Sensor type**	**Accuracy** (%)	**Reference**
Tropical forest	SPOT HRV	95	(Kimes et al., 1999)
Tropical forest	Landsat ETM+	r = 0.82	(Ingram et al., 2005)
Species mapping	Landsat TM	83	(Foody and Cutler, 2006)
Forest cover mapping	PALSAR and MODIS	89	(Dong et al., 2012)
Forest biomass prediction	Landsat TM	r > 0.71	(Foody et al., 2003)

k-Nearest Neighbor (k-NN): k-NN is the most well-known and extensively used non-parametric classifier. It works by searching the k nearest neighbors of a majority sample to classify in a given training data sets. The majority votes of its neighboring object classify the feature in an image through euclidean distance evaluation, and the most populated class (pixel) is assigned to the selected neighbors. Sometimes is referred to as the nearest neighbor when the value of k is equal to one (Cortijo and De La Blanca, 1997). The value of k had a significant role in the performance of classification accuracy, as the tuning parameter of the k-NN classifier (Qian et al., 2015). The essential parameters in k-NN are the distance metric, defined by the relative position of the feature on the image. The k value depends on the nearest neighbors and the size of the geographical radius of the searching a neighbor pixel occurrence (Tomppo and Halme, 2004; Haapanen et al., 2004).

The critical part is the selection of the k value in achieving the desirable classification results (Franco-Lopez et al., 2001; McRoberts and Tomppo, 2007). The large value of k reduces the *"salt and pepper"* effect that is common to many classification outputs. However, boundaries between classes are less separated, while a small k value increases misclassification results (Lu et al., 2014). k-NN is widely applied in the multi-source estimation of forest inventories with the use of satellite data and field measurements (Tomppo and Halme, 2004; Koukal et al., 2007;

Haapanen et al., 2004).

The main advantages of the k-NN method include easy application, as there are no statistical assumptions (Thessler et al., 2008), the potential of combining different data from other sources (Franco-Lopez et al., 2001), and the ability to produce both statistics for arbitrary area units as well as wall to wall maps (Tomppo and Halme, 2004). However, the disadvantages of k-NN require extensive training datasets to train accurately, which can also result in a classifier that is slow to apply. Working with comprehensive training data set has been a drawback of the k-NN classifier in terms of computation and handling (Hubert-Moy et al., 2001). Moreover, the rule is negatively affected by wrongly labeled training samples as errors are propagated (Cortijo and De La Blanca, 1997). Applications of k-NN on tropical forest mapping are summarised in Table 2.6.

Table 2.6: Previous studies applied the kNN method in tropical forest mapping

Vegetation type	**Sensor type**	**Accuracy** (%)	**Reference**
Land cover mapping	Sentinel-2	95	(Thanh Noi and Kappas, 2018)
Forest/non-forest classification	Landsat TM and ETM+	r = 0.82	(Haapanen et al., 2004)
Tropical rain forest	Landsat TM and SRTM	83	(Thessler et al., 2008)
Tropical forest-	Landsat TM and PALSAR	89	(Lu et al., 2014)

Random Forest (RF): RF is a machine learning classifier, as a tree-based classifier (Rodriguez-Galiano et al., 2012), assuming that each tree depends on the values of a random vector sampled independently and with the same distribution for all trees in the forest (Breiman, 2001). RF classifier works by selecting randomly subsets of the training samples and variables, which produce several decision trees (Belgiu and Drăguţ, 2016).

The advantages of RF include determining each variable's importance and hence

increasing classification accuracy (Rodriguez-Galiano et al., 2012; Cutler et al., 2007). The benefits of RF are outlined in Chutia et al. (2016). The variables are ranked based on their weight in explaining the dependent variables. Non-linear relationships of nonparametric and categorical data are also handled. It reduces the challenge of spatial autocorrelation, which bias parametric linear models (Segal, 2004).

RF classifier is gaining popularity in remote sensing classification due to its accuracy of classification outputs (Pal, 2005; Belgiu and Drăguţ, 2016). The approach is being increasingly applied in mapping conditions of forest health (Wang et al., 2015) and mapping tree canopy cover and biomass (Karlson et al., 2015). Pelletier et al. (2016), assessed the robustness of RF in mapping land cover in the south of France combining Landsat 8, sentinel-2, and SPOT-5 sensors and with an overall accuracy of 83.3% compared to 77.1% from SVM. The bootstrap aggregation technique of the RF classifier makes the classifier less sensitive to noise (Chan and Paelinckx, 2008; Rodriguez-Galiano et al., 2012). However, the method is sensitive to the sampling design (Belgiu and Drăguţ, 2016). Table 2.7 summarises some RF technique applications in different types of tropical forests.

Extreme Gradient Boosting (XGBoost) and Light Gradient Boosting (LGBM):

The XGBoost is a machine learning classifier algorithm that can be applied for both regression and classification tasks and has been designed to work with large and complicated datasets (Chen and Guestrin, 2016; Ke et al., 2017). XGBoost is a parallelized (Figure 2.1) and optimized version of the gradient boosting algorithm (Al Daoud, 2019). Parallelizing the whole boosting process vastly improves the training time. Instead of training the best model on the data (like in traditional

Table 2.7: Past studies utilised the RF approach in a tropical forest mapping

Vegetation type	**Location**	**Sensor type**	**Accuracy** (%)	**Reference**
Tropical forest deforestation	Latin America and Caribbean	MODIS	84.6	(Aide et al., 2013)
Forest/non-forest mapping	Australia	Landsat TM	96	(Mellor et al., 2013)
Mapping forest health	Asia	IKONOS	97.1	(Wang et al., 2015)
Land cover change mapping	South Africa	Landsat ETM+	74	(Wessels et al., 2016)
Forest habitat fragmentation	Brazil	Landsat 8	88	(Reynolds et al., 2016)
Wetland forest	Ethiopia	Landsat, PALSAR and Topographic	94.4	(Dubeau et al., 2017)
Forest deforestation estimation	Madagascar	Landsat	83.3	(Grinand et al., 2013)

methods), this algorithm has the capability of handling thousands of models on various subsets of the training dataset and then voting for the best-performing model (Chen and He, 2022).

Therefore, XGBoost is a scalable tree-boosting approach that has demonstrated good results across a wide range of applications in numerous analysis and machine learning competitions (Mitchell and Frank, 2017). The XGBoost method focuses on building several models sequentially, whereby each new model tries to fix the deficiencies in the previous model. Also, it is useful and robust for noise reduction and mapping uneven class distribution, particularly in steep and inaccessible areas with difficult field data collection (Zhang et al., 2019). Additionally, XGBoost is also supporting parallel and complicated computing on both central processing units (CPUs) and graphics processing units (GPUs), which increases training and prediction speed (Mitchell and Frank, 2017).

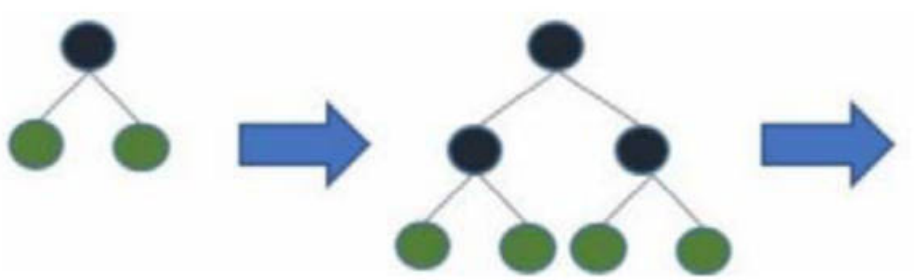

Figure 2.1: XGBoost level-wise tree growth. Sourced from Al Daoud (2019)

LightGMB is one such algorithm that depends on decision trees (Figure 2.2) and is used in predicting the accuracy to attain the desired results (Al Daoud, 2019). It is a gradient-boosting framework and powerful algorithm that uses a tree-based learning methodology (McCarty et al., 2020). The computation speed is very fast for this algorithm, hence the name “light”. LGMB can also process a large

volume of data and requires a lesser amount of memory. The LGBM performs a classification by using the features it selects.

The main difference with XGBoost is that the decision trees in LGBM split the tree leaf with the best fit whereas other boosting algorithms split the tree depth-wise or level-wise rather than leaf-wise. So when growing on the same leaf in LGBM, the leaf-wise algorithm can reduce more loss than the level-wise algorithm and hence results in much better accuracy which can rarely be achieved by any of the existing boosting algorithms(Al Daoud, 2019).

Hence, LightGBM focuses on selecting the most useful feature for the decision tree's growth and does not require feature selection before model training. It can use the assessment of feature importance, especially regarding complex datasets (Shi et al., 2019). Also is robust to overfitting as trees are grown sequentially by altering the weight of the training data distribution to reduce function loss (Ustuner and Balik Sanli, 2019).

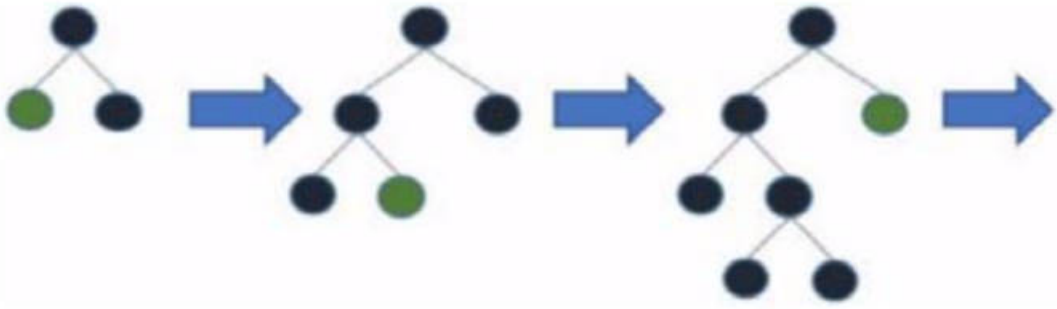

Figure 2.2: LightGBM level-wise tree growth. Sourced from Al Daoud (2019)

2.4.2 Analysis of tropical forest cover change detection

Forest cover change detection entails applying multi-temporal data sets to differentiate areas of forest between dates of imaging (Singh, 1989; Coppin and Bauer, 1994; Lillesand et al., 2015). Well-timed and precise change detection of forest resources is enormously vital for understanding relationships and interactions between human or natural phenomena for better decision-making (Lu et al., 2004). The forest change detection process depends mainly on the temporal factors (when and how long the changes occurred) (Hussain et al., 2013; Coppin et al., 2004).

Forest disturbances may arise in the short term due to fire or forest insects and in the long term such as human-induced changes, for example, conversion from forest to other land covers or exploitation of the forest resource (Coppin et al., 2004). This necessitates an appropriate timing for the image acquisitions. For disturbances that occur over a short period, image acquisitions are required at a temporal high frequency. However, where changes are presented for a long period then the frequency of observations becomes critical (Lunetta et al., 2004), but identifying the date on which a change occurs is important. For instance, to identify the date of a deforestation event a high temporal frequency of images is required, whilst for assessing trends in forest growth, extended time series covering multiple years are required (Franklin, 2001). The main aspects considered for change detection include detecting the changes, identifying the nature of changes, measuring the extent of changes, and assessing the spatial pattern of change (Macleod and Congalton, 1998). Forest change detection studies with remotely sensed data have used various methodologies in the tropical environment (Mas, 1999).

The robust quantitative estimates of forest cover change is a necessary step in the process of managing tropical forests and is essential for supporting decision-making processes and interventions focused on sustainable forest management. It is an important way of understanding the extent of forest cover loss and gains over time (Ygorra et al., 2021). The expansion of agriculture into forest land, timber logging, charcoal production, and firewood harvesting are the major drivers of deforestation in the tropics (De Alban et al., 2018). Changes in forest cover can alter the supply of the ecosystem and influence the biological processes, hydrological fluxes, and regional climate leading to greenhouse gas emissions affecting the well-being of nature and humanity (Negassa et al., 2020).

Therefore, it is important to have a good understanding of all processes leading to tropical forest cover change, such as deforestation, degradation, afforestation, and regeneration. Earth Observation data are critical in providing a systematic and temporally resolved assessment of those changes. The current availability of long-term Landsat sensor data and the launch of Sentinel-1A/1B and -2A/2B are fostering the development of new approaches to better characterize temporal changes in forests (De Bem et al., 2020). Furthermore, advances in high performance and cloud computing, machine learning, and high-quality temporal datasets (e.g., Landsat collection 1), as well as the development of datacube formats, are increasingly facilitating the analysis of forest cover change and the temporal dynamics of forest biophysical parameters (Bouvet et al., 2018; Berninger et al., 2018).

Table 2.8 summarises some of the tropical forest cover change based on satellite data (Kim et al., 2015) and (Figure 2.3) presents annual deforestation rates in some tropical hotspots of Amazon, Congo Basin, and South East Asia (Rosa et al.,

2016).

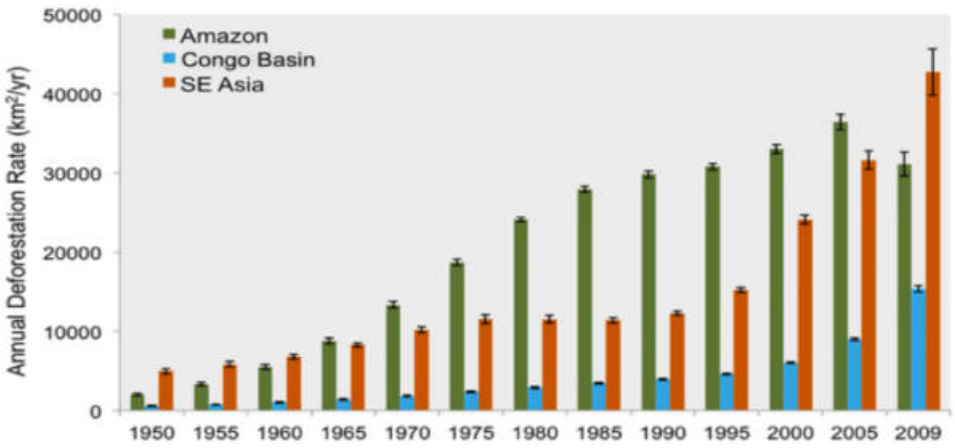

Figure 2.3: Tropical annual deforestation rates based on 100 model replicates at five years' interval. Sourced from Rosa et al. (2016)

Table 2.8: Satellite-based estimates of tropical forest cover change (1000 ha/yr) for the 1990s and 2000s

Area	1990s	2000s	ΔRate	Method	Data	Reference
Tropics	-5648	-9111	61.3%	Sampling	Landsat	(FAO and JRC, 2012)
Tropics	-6000	-7000	16.7%	Sampling	Landsat	(FAO and JRC, 2014)
Humid tropics	-5800	-		Sampling	AVHRR	(Achard et al., 2002)
Tropics	-6050	-5930	-2%	Sampling	Landsat	(Achard et al., 2014)
Humid tropics	-3960	-3170	-20%	Sampling	Landsat	(DeFries et al., 2002)
Tropics	-5563	-	-	Wall-to-wall	AVHRR	(Hansen et al., 2008)
Humid tropics	-	-5400 (gross loss)	-	Sampling	Landsat	(Hansen et al., 2013)
Humid tropics	-4040	-6535	61.8%	Wall-to-wall	Landsat	(Kim et al., 2015)

2.4.2.1 Change Detection Methods

Different change detection methods have been applied in detecting forest disturbances (e.g., Huang et al., 2010; Jin and Sader, 2005; Hansen et al., 2008; Kennedy et al., 2009; Lunetta et al., 2006). These methods are grouped into two categories of variation in the analysis of classification results between two dates and analysis of radiometric differences between dates (Zhan et al., 2000; Singh, 1989).

2.4.2.1.1 Map-to-Map Change: This type of technique, commonly known as post-classification or delta classification, discriminates between two imaging dates. Each image between the two periods is registered and classified independently (Lillesand et al., 2015; Coppin et al., 2004). The explicit knowledge of the baseline classification and the change transition benefits this technique (Tewkesbury et al., 2015). It has the advantage of providing more useful information on initial and final land cover classes in the form of a complete matrix of change direction (Fan et al., 2008; Coppin et al., 2004). However, the final change thematic map entirely depends on the accuracy of each independently classified image, whereby the error in the initial classification is likely to be taken to the last change detection process.

Forest-type change mapping over a large geographic area is still challenging, due to complex forest-type compositions, spectral similarity among various forest types, poor quality images with clouds or cloud shadows, and difficulties in managing and processing a large amount of data (Li et al., 2022) compared to forest/non-forest change mapping whereby only two classes are considered

Therefore, to achieve change detection with post-classification, a high level of spatial registration accuracy of the two images is a pre-requisite (Singh, 1989; Mas, 1999; Lillesand et al., 2015). Hence, accurate spatial registration will eliminate misclassified pixels in either of the two dates labeled as change (Zhan et al., 2000).

2.4.2.1.2 Image-to-Image: Each pixel in an image is subjected to arithmetic operations to generate changes over time. There are several types of image-to-image change detection methods.

Image differencing: Arithmetic operation of subtracting digital image value from another digital image of the same area but acquired at different dates, i.e., time t_1 and time t_2. A pixel-by-pixel comparison produces a third image with numerical values different from the original images. The two images need to be perfectly co-registered before differencing. However, in practice, exact image registration and perfect radiometric corrections are never obtained for multidate images. Residual differences in radiance not caused by land cover changes are still present in images due to structural and functional images not having the same signal intensity in the same areas (Théau, 2022).

The challenge then of this technique is to identify threshold values of change and no-change in the resulting images. The standard deviation measure is often used as a reference value to select these thresholds (Li et al., 2019). Different normalization, histogram matching, and standardization approaches are used on multidate images to reduce the scale and scene-dependent effects on differencing results. The image differencing method is usually applied to single bands but can be also applied to processed data such as multidate vegetation indices or principal components (Théau, 2022).

The result pixels with values at or near zero have similar spectral values and have no change, and the areas of radiance change will have positive or negative values over the two epochs (Campbell and Wynne, 2007; Jensen et al., 2005; Coppin et al., 2004; Macleod and Congalton, 1998; Lillesand et al., 2015). This technique can identify pixels that have changed in brightness value between the two periods (Jensen et al., 2005). A comparison with other change detection methods found superior results with image differencing compared to post-classification (Macleod and Congalton, 1998).

Image rationing: Image rationing is also a pixel-to-pixel computation by the ratio of the images from two different times t_1 and time t_2. The pixels of no change will have one value, and changed pixels will have higher or lower values. This technique had the advantage of normalising sun angle and shadows for the images (Lillesand et al., 2015). However, the method also needs to have perfect co-registration of the two images before rationing, and the selection of the threshold value for change no-change remains critical (Singh, 1989).

Change Vector Analysis (CVA): CVA is a multivariate method that generates output information based on change vector direction and multispectral change of magnitude between the two images dates. The spectral change vector represents the type of change, and the vector direction indicates or discriminates transitions occurrence (Nackaerts et al., 2005; Johnson and Kasischke, 1998; Flores and Yool, 2007; Bruzzone and Serpico, 1997). Identification of change and no-change pixels is determined by setting a threshold value through stages of this iterative process until the optimal amount of the magnitude of change is obtained (Chen et al., 2003). However, features like deep water are available to select the threshold value for unchanged pixels and record their scope from the change vector image (Jensen et al., 2005).

For example, a change in the intensity value (brightness) from one image to another, which relates to a change in color, is the spectral direction of change used in showing vegetation changes. It is relatively straightforward to differentiate forest from bare soil (i.e., deforestation). If the first image has forest cover and the second image appears to be barren soil, the intensity will be different as the soil will be brighter in most spectral bands and the forest will be darker. Hence, the directional change in color will be observed and distinguished between a kind of

changes (Horning et al., 2010). Therefore, CVA is applied as a change detection technique in forest monitoring (Silva et al., 2003) but also suffers a similar challenge in identifying change transitions.

Image transformation: Typically involves the separation of features on the two images of the same area acquired at different times (Singh, 1989). This transformation is based on first-order (linear) or high-order statistics (nonlinear) operators such as variance, correlation, etc. The most common transformation methods are principal component analysis (PCA), Multivariate Alteration Detection (MAD), Iteratively Reweighted Multivariate Alteration Detection (IR-MAD), Covariance Equalization (CE), and the Cross-Covariance (CRC) (Minu and Shetty, 2015). The PCA is commonly used, with this being a linear transformation that defines a new, orthogonal coordinate system such that the data can be represented without correlation. The transformation is found from the original data's eigenvectors of the covariance matrix. Each pixel is transformed by vector multiplication of its original vector and the eigenvectors, resulting in coordinates in the new space. The transformed data is re-arranged back into two images corresponding to the first and second principal components. The first component images contain no-change pixels whereas the second component images contain change information between the different dates (Lillesand et al., 2015).

Tasselled cap (TC) is a linear transformation consisting of a set of parameters, called TC coefficients, to convert the original set of bands to a new set of uncorrelated bands through a weighted sum of the first ones (Zanchetta and Bitelli, 2017). The original m-band space is transformed into a new n-dimensional set of axes (with $n \leq m$) with different coordinates for the image pixels. The new axes often referred to as "features" have a physical meaning in terms of surface char-

acteristics and are not image-dependent. Therefore, TC transformation is used to enhance the contrast between forest, cleared areas, and regrowth, where images are stacked into a composite multi-date and used in a principal components (PC) transformation to identify change components. In addition, consecutive TC image pairs can be differenced and stacked into a composite multi-date differenced image (Guild et al., 2004).

TC provides an analytical way to detect and compare changes in vegetation, soil, and manmade features over short- and long-term periods and is used to enhance the contrast in the image to differentiate the area of change, such as deforestation, and regrowth (Zanchetta et al., 2015). TC reduces the Landsat images' spectral redundancy for visible and infrared bands and generates vegetation indices of brightness, greenness, and wetness (Schowengerdt, 2006). An example of the TC technique application includes a change detection in deforestation and land conversion in Brazil (Guild et al., 2004). See Mas (1999) for a detailed comparison of different change detection methods in monitoring land cover changes.

2.4.2.1.3 Map-to-Image method: The map-to-image change detection (Bunting et al., 2018; Thomas et al., 2018), as opposed to the widely used image-to-image and map-to-map methods (Walter, 2004; Dingle Robertson and King, 2011; Bruzzone and Prieto, 2002), aims to avoid the particular classification errors that are common with post-classification comparison procedures from the individual classification (Desclée et al., 2006) while maintaining the classification context which is not possible using an image-to-image approach. Therefore, with the map-to-image approach, a baseline map with well-defined classes is used to detect changes from a second independent image.

The map-to-image method works by assuming a known spectral from the optical data response distribution (e.g., normal) for the classes of interest (i.e., forest/non-forest), and change features are identified as features that do not fit the expected distribution will reside within the tail (i.e., not near the mean). Therefore, the normality is assessed using skewness (asymmetry) and kurtosis (peakedness) of the distribution (Thomas et al., 2018) following the number of observations (images) acquired over a given period and location. A key advantage of this method is that it uses the earlier map and aims to update the current map to generate the next map rather than create a new one while also requiring only a limited number of parameters for deriving changes.

2.5 African Forests Monitoring System

African forests play a crucial role in the global carbon cycle but are deteriorating due to deforestation, witnessing overexploitation to meet the demand for natural resources across the region. According to Achard et al. (2002), estimates of forest cover change analysis in Africa using remote sensing started in the late 1990s through the UN FAO Remote Sensing Survey of the Global Forest Resource Assessment and the TREE-2 project of the Joint Research Centre (JRC).

The UN FAO reported a deforestation rate of 0.34% per year between 1990 and 2000 and TREES, reported a deforestation rate of 0.36% per year (Mayaux et al., 2005). An example of the forest cover change analysis in African tropical forests focused on the Congo basin of Central Africa (Table 2.9). However, intimate knowledge of forest cover change in other parts of the region is crucial to improve forest governance and strengthening forest monitoring.

Table 2.9: Example of studies on deforestation in the African region based on remote sensing data

Author	Location	Data	Brief description
(Brinkmann et al., 2014)	Madagascar	Landsat	Deforestation mapping
(Zhuravleva et al., 2013)	DR-Congo	Landsat	Forest degradation
(Potapov et al., 2012)	DR-Congo	Landsat ETM+	Forest cover loss
(Hansen et al., 2008)	Congo Basin	MODIS and Landsat	Forest cover change
(Duveiller et al., 2008)	Central Africa	Landsat TM and ETM	Deforestation mapping

2.6 Forest Monitoring from Space in Tanzania

Tanzania has been relying on field surveys to assess forest area estimates. The surveys are based on a sampling design, as the practicalities and cost of mapping, the whole country are prohibitive. Hence, extensive forest areas remain under-sampled due to their inaccessibility. The application of remotely sensed data in forest mapping and monitoring allows for a reduction in the use of field samples and improves forest extent estimates (Næsset et al., 2016). In Tanzania, remotely sensed data is limited in forest mapping and monitoring. However, forest mapping has a long history in Tanzania from aerial photographs centered on designating types of forests for logging purposes and general land cover. For instance, in 1984, a Southern African Development Community (SADC) produced a woody biomass map, which was used to estimate forest extent in Tanzania (MNRT, 2015).

In 1995 and 1996, two projects implemented another design for natural resource mapping in Tanzania through Hunting Technical Services (HTS) and the Africover project under the United Nations Food and Agricultural Organization (FAO). The HTS land cover map was produced with the interpretation of scale-controlled Landsat TM and *Système pour l'Observation de la Terre* (SPOT) images cap-

tured between May 1994 and July 1996. The land cover map was produced with six vegetation classes (MNRT, 2015). The Africover land cover map was generated through visual interpretation of Landsat and SPOT images acquired between February 1995 and June 1998 (Wang et al., 2005).

The most recent land use and cover were delivered through the National Forest Resources Monitoring and Assessment (NAFORMA) project (2009-2014). Landsat images acquired between June 2008 and June 2009 were utilised in the classification process and the map was applied in linear extrapolation and comparison of the 1984 SADC map and 1995 HTS map for estimating forest cover change in Tanzania (MNRT, 2015).

Despite previous studies having used satellites based on forest mapping (Reiche et al., 2016) few studies have assessed area coverage and trend of forest cover in Tanzania (Table 2.10). Most of the studies concentrated on protected areas, hotspots (high biodiversity), i.e., the Eastern Arc Mountains, mangroves, and other coastal forests (Godoy et al., 2012; Green et al., 2013; Mayes et al., 2015; Kashaigili et al., 2013). It indicates that forests outside the areas with less importance (general-use land) remain unmonitored. Therefore, this shows a lack of a comprehensive monitoring system for the extent and condition of forests in Tanzania. However, both previous estimates of forest extent change in Tanzania show a decrease in forest cover at the expense of other land uses (Table 2.10) (URT, 2014a).

Table 2.10: Example of deforestation studies based on remotely sensed data in Tanzania

Author	Location	Data	Description
(Mayes et al., 2015)	Western Tanzania (Tabora)	Landsat 5 and 8	Loss of forest cover ≈ 7%
(Kashaigili et al., 2013)	Coastal of Tanzania	Landsat 3 and 4	Forest reserves (Pugu and Kazimzumbwi), rates loss ≈ 4.5- 25.3%
(Godoy et al., 2012)	Coastal of Tanzania	Landsat 5 and 7	A decrease in deforestation rates ≈ 1.0% - 0.4% /year from 2000 to 2007
(Green et al., 2013)	Eastern Arc mountains forests	Landsat 4, 5 and 7	Loss 5% of green forest and ≈ 43% of Miombo woodland

A new global deforestation analysis based on satellite estimated forest loss trend in Tanzania from 2001 - 2019 (Hansen et al., 2013) presented by Global Forest Watch[1] indicated average deforestation of 132,056 ha per year for 19 years as summarised on Table 2.11. Given this enduring condition, there is a pressing need to provide up-to-date and appropriate estimates of the status of forests in Tanzania, to evaluate the impact of past and current changes on the functioning, survival, and use of this knowledge, to improve the understanding and forecast the consequences for future applications (Huang et al., 2009).

[1] https://www.globalforestwatch.org/

Table 2.11: Tree cover loss trend in Tanzania (2001 - 2019) and corresponding above-ground biomass. Sourced from Hansen et al. (2013) version 1.7 for 2019

Year	Tree cover loss (ha)	Aboveground biomass loss (Mg)	Aboveground CO_2 emissions (Mg)
2001	82,214	12,671,096	23,230,343
2002	85,081	1,208,008	22,146,827
2003	84,068	11,395,125	20,891,063
2004	66,892	8,835,618	16,198,632
2005	91,583	12,196,269	22,359,826
2006	85,296	10,618,161	19,466,629
2007	121,685	16,250,075	29,791,803
2008	164,251	20,845,152	38,216,111
2009	143,354	18,208,623	33,382,479
2010	138,486	18,561,346	34,029,135
2011	137,805	18,464,285	33,851,189
2012	154,433	20,232,335	37,092,613
2013	181,510	22,715,834	41,645,695
2014	198,228	25,207,949	46,214,579
2015	111,961	14,120,429	25,887,453
2016	152,854	19,537,038	35,817,902
2017	194,876	24,763,073	45,398,966
2018	171,708	21,547,702	39,504,120
2019	142,773	18,298,897	33,547,978

2.7 Challenges of Monitoring Tanzanian Forests from Space

Limited access to remote sensing data, exceptionally high resolution for verification, and technical infrastructure (hardware, software, and internet access) have restricted the ability to regularly monitor the forests of Tanzania (DeFries et al., 2007; Pettorelli et al., 2014), specifically at a national scale. It is linked with the high price of proprietary software in processing the remotely sensed data, reflected in the budget deficit (Horning et al., 2010). Clouds and shadow contaminations from optical sensors (Huang et al., 2009; Tucker and Townshend, 2000) remain a significant issue in mapping and monitoring forests. Clouds restrict when two images are needed for mapping forest change over the same season (Ju and Roy,

2008). Seasonality fluctuation in the tropics has also hindered forest mapping, especially in separating non-forested vegetation (Walker, 2016).

However, the advances in technology in spaceborne radar imagery, which operates at microwave frequencies, provide an alternative solution for mapping tropical forests, as these data are unaffected by clouds and other atmospheric conditions, including the new Sentinel satellite constellation that provides both optical and radar data at high resolution and temporal frequency (Shimizu et al., 2019).

Therefore, integrating radar and optical sensors for future applications could circumvent the problem of clouds (Reiche et al., 2013). The availability of free, open-source software has bridged the gap related to processing and analysing large data sets (Pettorelli et al., 2014; Bunting et al., 2014). Similarly, increased computer storage and processing technology capacities have made it feasible in mapping forest cover over large areas (Walker, 2016).

Chapter 3

Study Area Description

3.1 Geographical Location

The study focused on the United Republic of Tanzania mainland, located in East Africa between latitudes 10^0 00' and 11^0 45' South of the Equator and longitudes 29^0 15' and 41^0 00' East of the Greenwich (Figure 3.1). The country occupies 945,100 km^2 with the highest point in Africa, Mount Kilimanjaro rising 5,950 meters above sea level. Except along the coast, most of Tanzania lies above 200 m, and much of the country is higher than 1000 m above sea level and bordered by eight countries (Figure 3.1).

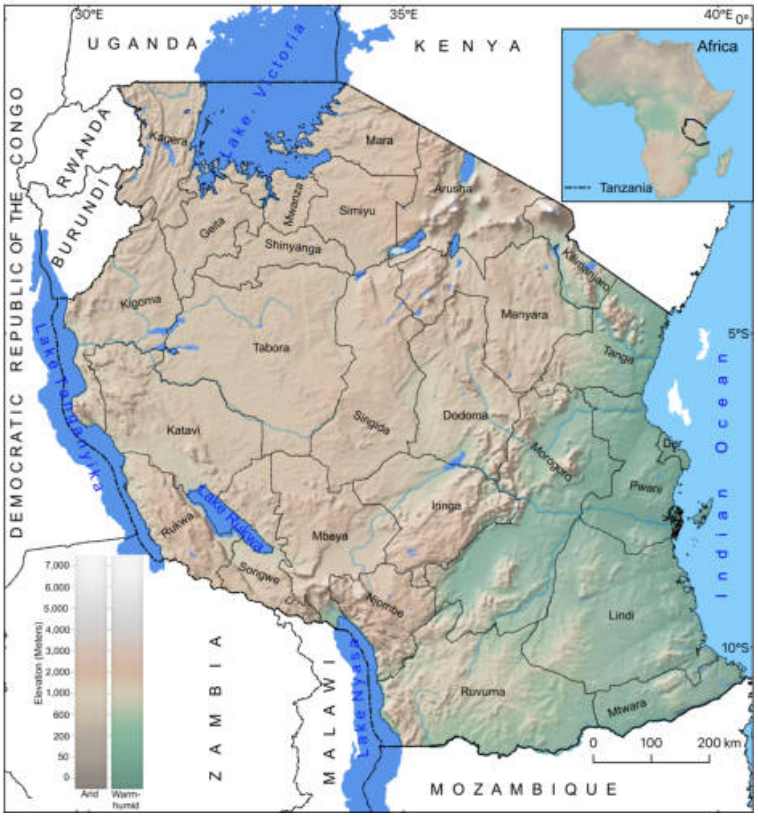

Figure 3.1: Map of the study area with regions labelled. Created using Natural Earth data in QGIS

3.2 Climate conditions

The climate of Tanzania is mostly classified into Tropical Savannah (Aw) based on Köppen Climate Classification (Spinoni et al., 2015) with alternating dry and wet seasons (Figure 3.2)[1]. However, the climate is mainly influenced by the changes in elevation. Therefore, four microclimate zones exist:

1. **Lowland Coastal Zone** - depicts an area with an elevation that ranges between 0 and 1000 m above sea level and is frequently moist with rainfall

[1] https://commons.wikimedia.org/wiki

ranging from 1000 mm to 1800 mm per year.

2. **Highlands Zone** - includes the North-Eastern Highlands and the Southern Highlands. As catchment areas, these are usually receiving high rainfall of up to 2000 mm per year.

3. **Plateau Zone** - Areas located around Lake Victoria and along the west, mainly dry areas with an average rainfall of around 600 mm.

4. **Semi-Arid Zone** - comprises the country's central regions and, on average, gets less than 600 mm per year.

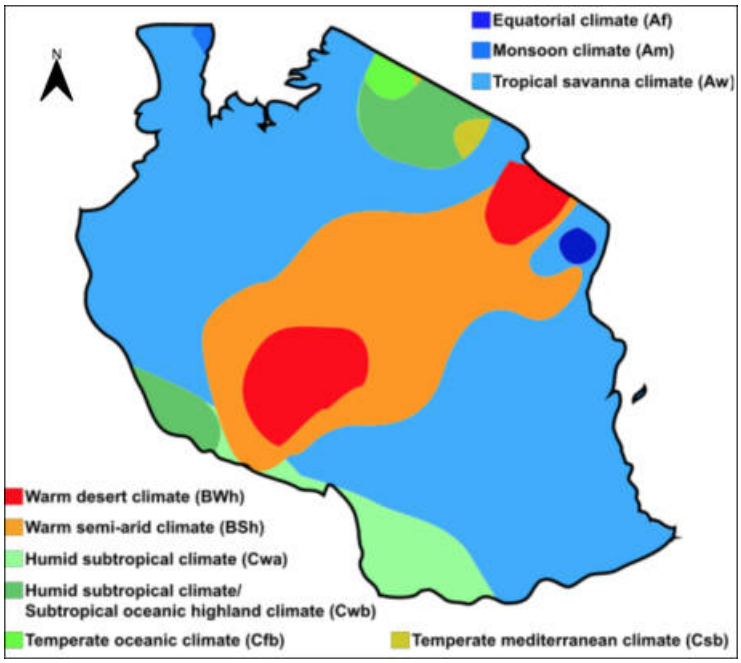

Figure 3.2: Köppen Climate Classification of Tanzania. Sourced from Wikimedia commons

Generally, the country receives bimodal rainfall linked with the southward and northward movement of the Inter-Tropical Convergence Zone (ITCZ), ranging below 400 mm and a maximum of over 2000 mm per year (Hardy et al., 2013). The

long dry season occurs from May to October, with a rainfall period from November to April. The rain season along the coast and the areas around Mount Kilimanjaro occur from March to May, with short rains between October and December. In the western part of the country, around Lake Victoria, rainfall is adequately distributed throughout the year, with the peak period between March and May. The maximum mean temperature ranges from 26.6^0C in the southwestern to 33.1^0C in the northeastern for September to March while the mean minimum temperature occurs in July with a range of 5.3^0C in the southwestern parts and 18.3^0C in the coastal areas (National Bureau of Statistics, 2017). Figure 3.3 summarises the average monthly temperature and rainfall in Tanzania over 25 years (World Bank Group and others, 2019).

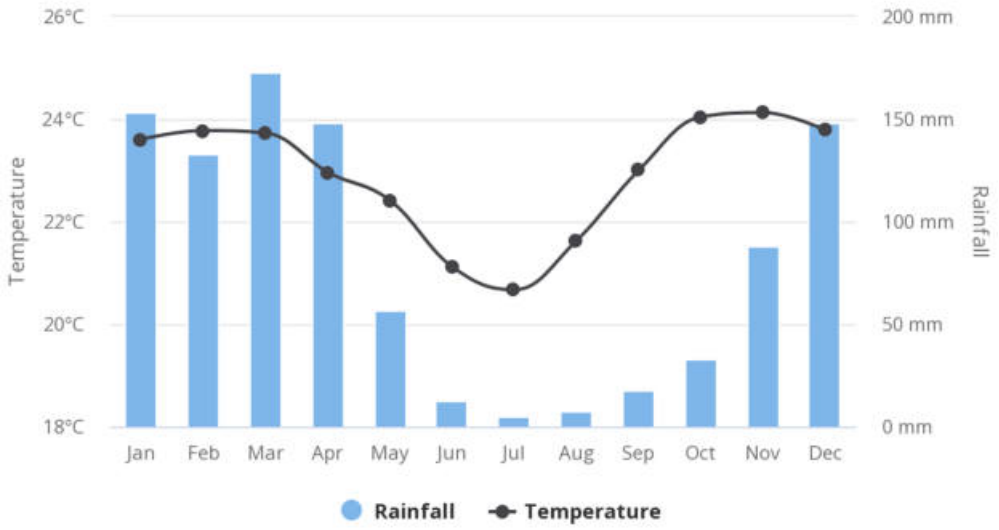

Figure 3.3: Tanzania average monthly temperature and rainfall for 1991-2016. Sourced from World Bank Group and others (2019)

3.3 Soil and Geology

Tanzania has 19 dominant soil types, according to the World Reference Base for Soil Resources (WRB). The most predominant soil type is Cambisols covering about 35.64% of the country area. This type of soil is characterized by slight or moderate weathering of parent materials and the absence of substantial portions of illuviated clay, organic matter, and aluminum or iron compounds. It supports various forest types, especially on the steep slopes of highlands. Other dominant kinds of soils are Acrisols (8.67%), Leptisols (8.11%), Luvisols (7.26%), Ferrasols 6.32%), Vertisols (5.02%) and Lixisols (4.95%) (Mlingano Agricultural Research Institute, 2006).

The Great Rift Valley is one of the most distinctive geological features, caused by faulting throughout eastern Africa and associated with volcanic activity in the country's north-eastern regions. Two branches of the Rift Valley run through Tanzania. The western part holds Lakes Tanganyika, Rukwa, and Nyasa, while the eastern section ends in northern Tanzania and includes Lakes Natron, Manyara, and Eyasi (Chorowicz, 2005).

3.4 Drainage

Tanzania has an abundance of inland water with several lakes and rivers (Figure 3.4). Inland water occupies about 20% of the total land area. wetlands occupy 10% of the country area of which 5.5% are international Ramsar sites, freshwater lakes (6.1%), and rivers and their catchment areas. There are over 2,810 rivers and

streams (permanent and seasonal), 2,325 springs, 440 lakes and dams, and 22,379 deep boreholes (URT, 2014a).

There are about 115 wetlands ecosystems, the most significant of which include Kilombero, Malagarasi-Muyovosi, Rufiji-Mafia, Lake Natron, and Ihefu. In terms of their distribution, 60% extend over village land while the remaining 40% are located on public and protected land (URT, 2014b). Lake Tanganyika forms the deepest and longest freshwater lake in Africa and the second globally, which runs along the western border of Burundi, DRC, and Zambia. Lake Victoria is the world's second-largest lake and drains into the Nile River. The country also has many large rivers, including Rufiji, Kagera, Mara, Ruaha, Pangani, Ruvuma, and Malagarasi, flowing into nine drainage basins (Figure 3.4, Table 3.1).

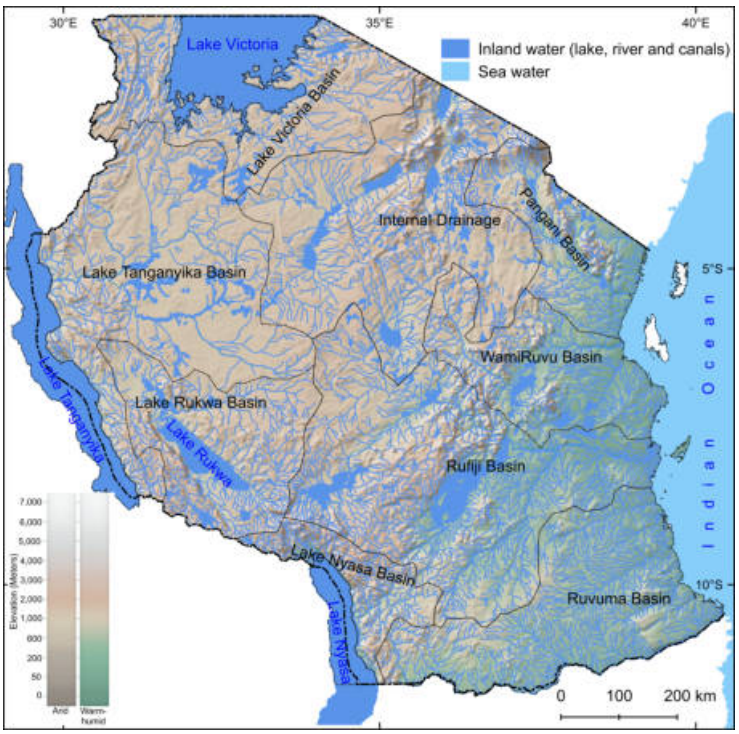

Figure 3.4: Tanzania drainage system. Created using Natural Earth and DIVA-GIS data in QGIS

However, water resources have become a national concern since the mid-1990s due to new agriculture opportunities, increasing the demand for irrigation and hydropower. The increase in water scarcity and the long dry season have contributed to water-use conflicts, growing in many cities and rural areas. Similarly, there is a lack of information on water quantity and quality and an inadequate framework for tackling cross-sectoral water issues, resulting in a lack of sustainable water resource management (URT, 2014b).

Table 3.1: Water basins in Tanzania

Basin	Catchment area (km^2)	Drainage basin
Pangani	55,176.82	Indian Ocean
Wami/Ruvu	66,867.18	Indian Ocean
Rufiji	182,708.10	Indian Ocean
Ruvuma	102,743.38	Indian Ocean
Lake Nyasa	34,266.09	Indian Ocean
Lake Rukwa	77,808.92	Endorheic basin
Lake Tanganyika	167,732.23	Atlantic Ocean
Lake Victoria	114,508.14	Mediterranean Sea
Internal drainage	143,67.76	Endorheic basin

3.5 Vegetation description

Tanzania is endowed with various vegetation types (Figures 3.5–3.6 and Figure 3.7). The relative appearance distinguishes between vegetation types and subtypes in terms of stature, stratification, canopy closure, and relative composition. The vegetation composition resulted in three primary layers of trees, shrubs/bushes, and grasses/herbs. Five types of vegetation are distinguished in Tanzania, divided into four forest types, two woodland types, three bushland types, thicket, and thicket with emergent trees and grassland (Table 3.2).

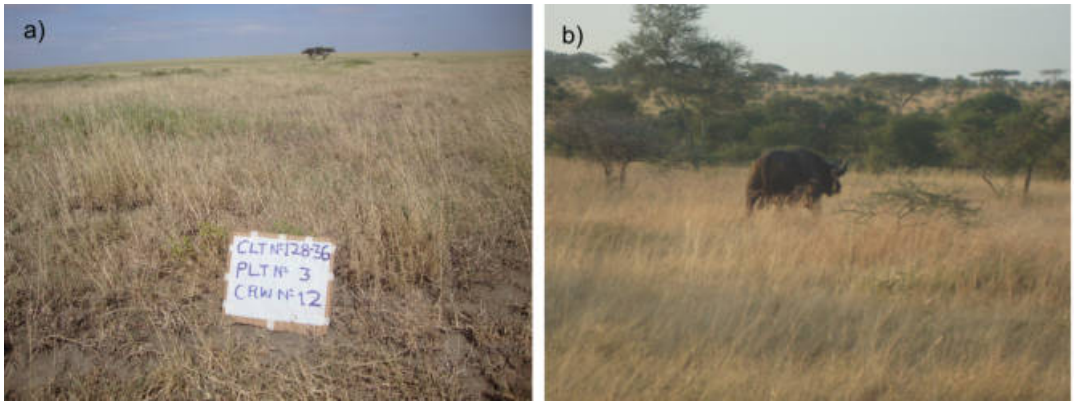

Figure 3.5: a) Open grassland and b) Wooded grassland. Credit: NAFORMA 2012

The unmixed grassland (Figure 3.5a) is often limited to the plains of the Serengeti, Masai Steppe, to alpine areas of the Southern Highlands; only exposure and edaphic conditions prevent the natural development of trees apart from grasses or herbs. However, most of the grassland vegetation occurs as subtypes combined with either a limited wooded or bushed component (Figure 3.5b) and (Figure 3.6b). Bushland is predominantly comprised of woody plants, which are multi-stemmed from a single root base. The other type of vegetation constitutes agriculture crops, including agroforestry systems, wooded crops, herbaceous crops, and grain crops (Vesa et al., 2010) (Figure 3.7).

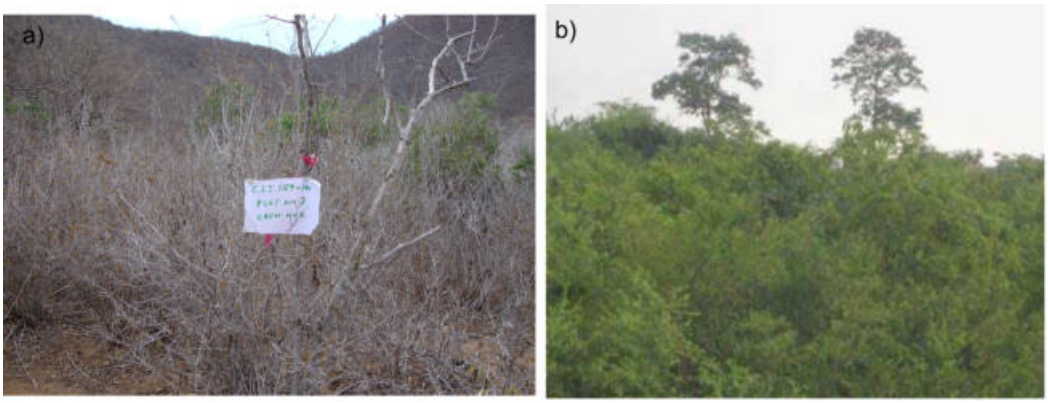

Figure 3.6: a) Dense bushland and b) bushland with emergent trees. Credit: NAFORMA 2012

The conversion of natural vegetation to other land uses resulted in different vegetation categories whereby the physiognomy varies widely following the importance of the tree and crop components. This occurs in the agroforestry system, woodland, bushland and grassland with scattered crops. The agroforestry systems contain permanent tree crops (timber and fruit) mixed with permanent and annual crops (banana, yam, beans, coffee, etc.) (Figure 3.7a-b).

Figure 3.7: Agroforestry system a) tree crops and b) mixture of tree crops and other trees. Credit: NAFORMA 2012

Table 3.2: Potential vegetation types in Tanzania

Primary-class	**Sub-class**	**Main uses**
Forest	Montane	Catchment forests
	Lowland	Groundwater forests, some coastal forests
	Mangrove	Productive ecosystems for both utilization and conservation
	Plantation	Timber and fuelwood production
Woodland	Closed	Both closed and open are used for beekeeping, hunting, recreation, grazing, conservation, timber production
	Open	
Thicket	Emergent trees	Beekeeping, hunting, recreation, grazing, conservation
Bushland	Dense	Grazing
	Open	Hunting, recreation, grazing
	Emergent trees	Grazing
Grassland	Open	Both used for hunting, recreation, grazing, wildlife
	Wooded	
	Bushed	

3.5.1 Forest regeneration

The capacity of forests to recover (regenerate) from natural and anthropogenic disturbances remains the key to sustainable forests' existence. Forests in Tanzania regenerate quickly following wood harvesting (logging), fire, floods, prolonged drought, or clearing from shifting cultivation. Once vegetation has been cleared and the land abandoned, regeneration often occurs. Still, the speed of forest regeneration depends on the severity of disturbances and methods used in a clearing, the sources available for regeneration (vegetative shoots), and site history (type, frequency, and intensity of stress or disturbance) (Mugasha et al., 2004).

For example, natural regeneration in woodlands depending on species may require four to five years (Mugasha et al., 2004). However, some species may attain a

height of up to 3 m within one year after harvest with no further disturbances (Sangeda and Maleko, 2018). Studies indicate that lowland forest areas abandoned from cultivation recover between 11-31 years, compared to the montane forest with recovery between $<$ 6 to 10 years (Mwampamba and Schwartz, 2011).

3.6 Administrative and Demographic

Administratively, Tanzania is divided into 26 regions (Figure 3.8), with 162 districts. Tanzania's population has increased more than five times, from 10.05 million in 1960 to about 59.7 million in 2020 (Figure 3.9). The average annual intercensal growth rate is 2.7, according to the 2012 Population and Housing Census (PHC). However, Tanzania's total population is projected to reach about 130 million by 2050, nearly threefold of the current level (URT, 2018).

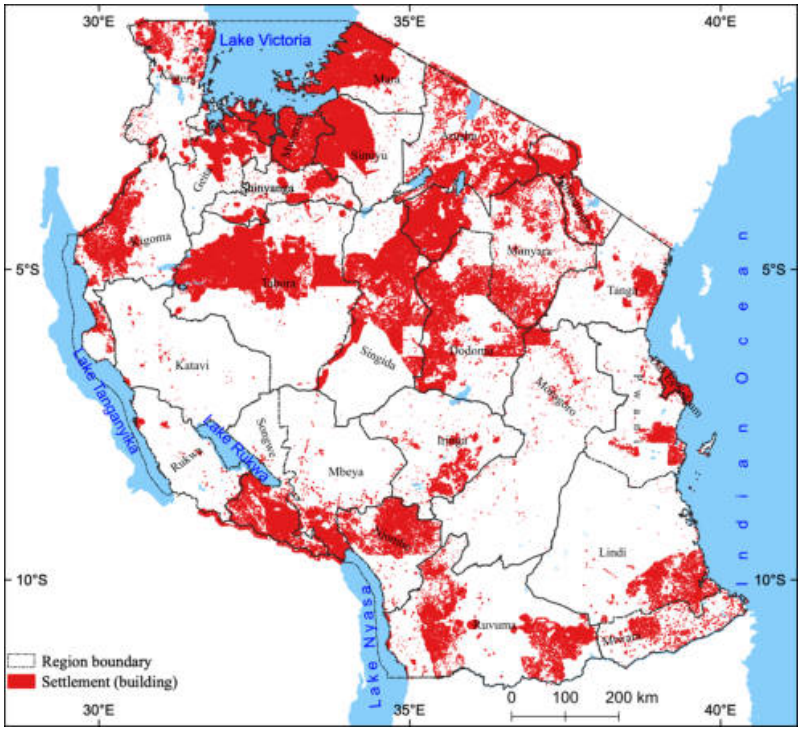

Figure 3.8: Tanzania settlement areas by 2020. Created using Humanitarian Data Exchange (HDX) based Open Street Map Export (HDX, 2020)

The current urban population is expected to grow from 22 million in 2020 (35% of the total) to over 70 million (53%) by 2050, increasing migration to urban areas (World Bank, 2019). The growth of new urban settlements progressing emerging, and existing cities and towns are quickly expanding (Figure 3.8). For example, according to the United Nations (2019), Dar es Salaam is expected to become a megacity by 2030, with a population predicted to surpass 10 million people.

Nevertheless, due to the high population increase, the number of people in rural areas is anticipated to rise from 33 to 65 million people over the same period (World Bank, 2019). An intensification of pressures on and conflicts surrounding natural resources is expected.

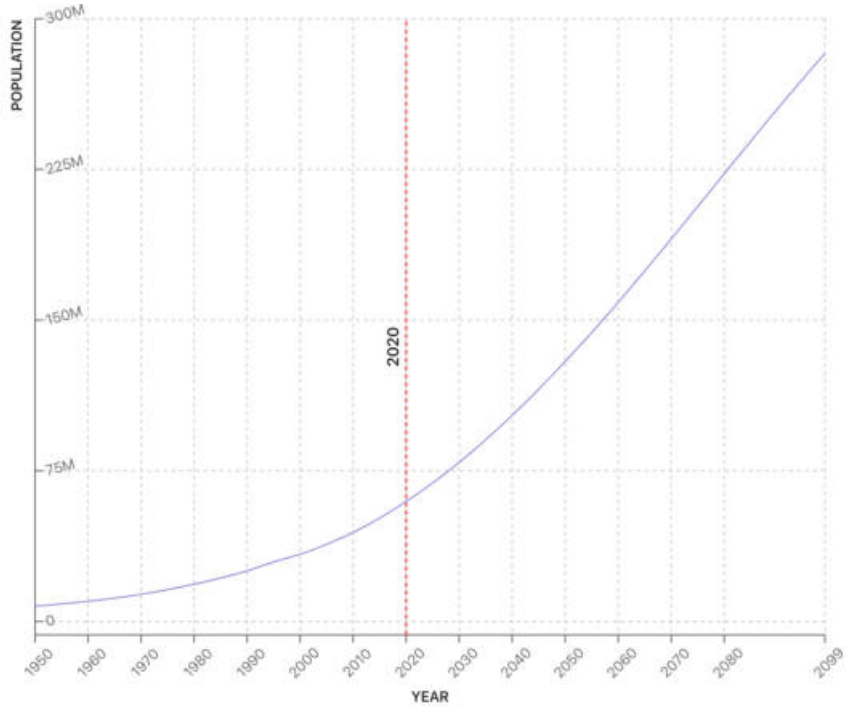

Figure 3.9: Tanzania population trend from 1950 projected to 2020. Sourced from United Nations, 2019 World Population Prospects

3.7 Economy and land cover

Tanzania has a mixed economy in which agriculture represents a key role (Figure 3.10) (Bergius et al., 2020). Around 70% of the population live in rural areas and depend on natural resources for food, fuel, and fodder. Only about 17% of rural dwellers have access to electricity, and approximately 85% of Tanzania's power requirements are supported by biomass such as charcoal and firewood, predominantly for cooking and heating (International Renewable Energy Agency, 2017).

Agriculture includes crop production, animal husbandry, forestry, and fishing.

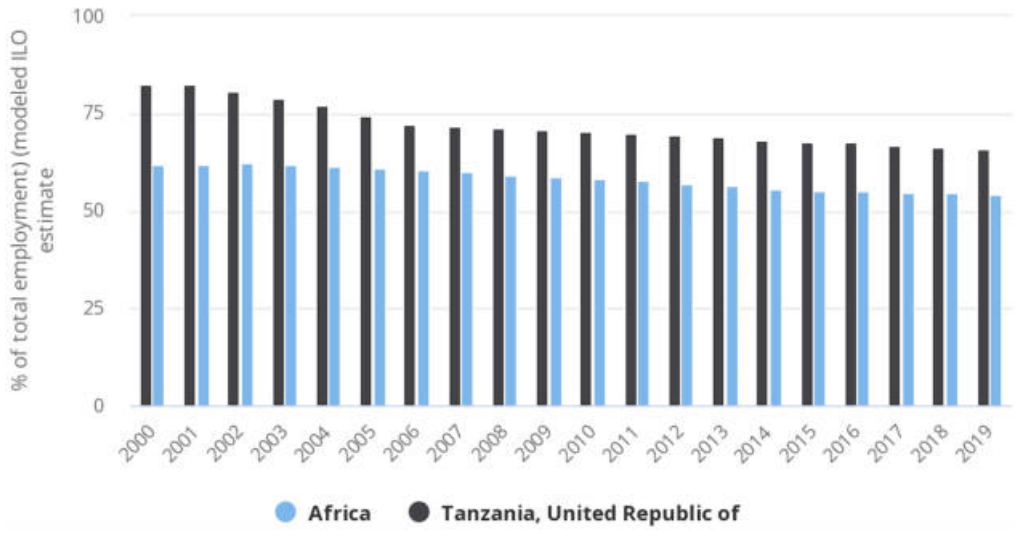

Figure 3.10: Employment in agriculture (% of total employment in Tanzania). Sourced from World Bank Group and others (2019)

About 44 million hectares of arable land (approximately 45% of total land area) (Figure 3.11), out of which only 24% is under crop production (World Bank, 2019). The cultivated land consists of roughly 80% traditional subsistence farming systems with considerable diversity of crops grown and field size. Therefore, agriculture is the most vital economic sector, employing more than two-thirds of the country's workforce and sustaining more than three-quarters of Tanzanians' livelihoods (Bergius et al., 2020).

However, poor land use and watershed management practices have led to the degradation of forests and watercourses, endangering the natural resource base upon which Tanzania's economy and the poor depend. Increasingly, natural catastrophes such as droughts and El Niño climatic crises have influenced agricultural productivity, power generation, and transportation. This has had detrimental impacts on the economy. Despite the overall gradual growth in sub-Saharan Africa, Tanzania's GDP has grown at an average annual rate of 6.6% in real terms over

the past decade (World Bank, 2019).

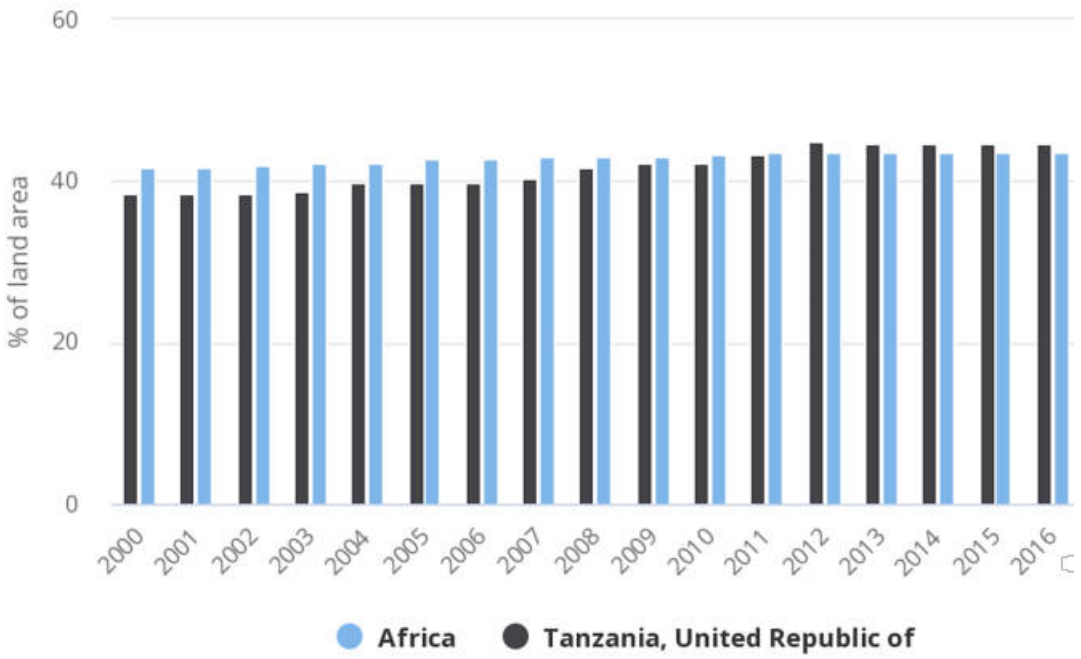

Figure 3.11: Tanzania agriculture land (% of land area). Sourced from World Bank Group and others (2019)

The most recent statistics on land cover types were presented in the National Forest Monitoring and Assessment (NAFORMA) of Tanzania (MNRT, 2015). However, global land cover products also exist since the year 2015 (Figure 3.12) through Land Cover Climate Change Initiative (CCI) under the European Space Agency (ESA) CCI projects (Santoro et al., 2017). More than 60% of Tanzania's land is covered with forest/woodland/bushland/grassland (Table 3.3). The cultivated land accounts for about 20%, but a small percentage infringed in forest/woodland/bushland and a greater extent in grasslands.

Table 3.3: Land cover types in Tanzania (MNRT, 2015)

Land cover	Area (ha)	%
Forest		
Montane	995,300	1.1
Lowland	1,656,500	1.9
Mangrove	158,100	0.2
Plantation	554,500	0.6
Woodland		
Closed woodland woodland	8,729,000	9.9
Open woodland	35,997,300	40.8
Woodland with scattered crops	2,530,000	2.9
Bushland		
Thicket	971,900	1.1
Dense bushland	2,012,400	2.3
Bushland with emergent trees	309,400	0.4
Thicket with emergent trees	308,300	0.4
Open bushland	2,843,500	3.2
Bushland with scattered crops	1,162,700	1.3
Grassland		
Wooded grassland	4,712,300	5.3
Bushed grassland	438,900	0.5
Open grassland	3,091,100	3.5
Grassland with scattered crops	596,600	0.7
Cultivated land		
Agro-forestry system	1,373,000	1.6
Wooded crops	1,521,100	1.7
Herbaceous crops	5,045,400	5.7
Mixed tree cropping	154,700	0.2
Grain crops	9,866,700	11.2
Open land		
Bare soil	161,100	0.2
Salt crusts	18,300	0.0
Rock outcrops	73,100	0.1
Water		
Inland waters	154,700	0.2
Swamp	1,007,900	1.1
Rock outcrops	73,100	0.1
Others		
Unspecified (e.g., built-up areas)	1,892,700	2.1

3.8 Forests and Wildlife conservation

The protection of forests and wildlife areas in Tanzania represents about one-third of the country's total land area and is one of the world's highest ratios (World Bank, 2019).

3.8.1 Forest resources

The forest areas act as a carbon sink, absorbing emissions generated in the country and beyond, making a net sink of GHGs. Economically, forests' contribution to the national GDP is estimated to be between 2.3% and 10% of the country's total GDP. However, the subsidy is underestimated as the actual consumption of wood fuels, bee products, catchment, environmental values, and other forest products remains unrecorded, especially in rural areas (URT, 2014b).

In Tanzania, 'Forest' is defined as an area of land with at least 0.5 ha, with a minimum tree crown cover of 10% or with existing tree species planted or naturally having the potential of attaining more the 10% crown cover, and with trees which have the potential or have reached a minimum height of 3 m at maturity *in-situ* (URT, 2017).

Forests link and support other sectors. For example, forests stabilize stream flows and reduce disasters such as landslides, erosion, and floods in steep topography areas and high precipitation. Forests also have an essential function in the supply of irrigation water for lowland farming and fish production. Forest management categorises forests either by vegetation cover, usage (e.g., production), and legal status. Production forest is an area of land covered by forest, reserved or used

principally for sustainable production of timber and other forest produce.

In contrast, protection for forests is provided by forest reserves or used chiefly for protecting watersheds, soil, and biodiversity protection. The productive forest area comprised 60.3% of the total forest area, and about 39.7% of the forest area accounted for protected forest areas, and most are catchment areas and natural reserves. Furthermore, concerning legal status, approximately 23.3% of the forest area is within wildlife-protected regions (National Bureau of Statistics, 2017).

3.8.2 Wildlife sector

The wildlife sector has an essential contribution to the national economy through tourism, photographic scenery, wild animal hunting, and licensing of trophy sales. The protection of wildlife areas is under the National Parks, Game Reserves, and Game controlled areas. These areas are both home to wild animals with various activities, organization, and protection statuses.

National parks in Tanzania cover a total area of 57,424 km^2. Ruaha is the biggest national park with an area of about 20,300 km^2 (35.4%) of the total area of national parks. Serengeti is the next largest national park with an area of 14,763 km^2 about 25.7% of the total area of Tanzania's national parks. Saanane is the smallest national park covering about 50 km^2 (URT, 2014b).

Game reserves are wildlife-protected areas declared for conservation. However, consumptive and non-consumptive wildlife utilization is allowed with permits. There are a total of 28 game reserves covering an area of about 117,755.4 km^2. Selous is the largest game reserve covering an area of 50,000 km^2 with approximately 42.5% of the total area under game reserves. The remaining game reserves

individually constitute less than 10% of the general game reserve area. There are a total of 42 game-controlled areas covering 55,565.02 km^2. Kilombero is a dominant game-controlled area covering 6,500 km^2, equivalent to 11.7% of the total game-controlled areas (National Bureau of Statistics, 2017).

The linked impacts of climate change, and anthropogenic factors, including encroachment, land fragmentation, deforestation, and degradation of natural habitats, affect the existence of wildlife ecosystems. Such changes in natural habitats may change wildlife distribution patterns and are compounded by climate change, and such circumstances may raise conflict for resources. Among migratory species, which use a network of sites, may constrain their ability to adapt to changes (URT, 2014b).

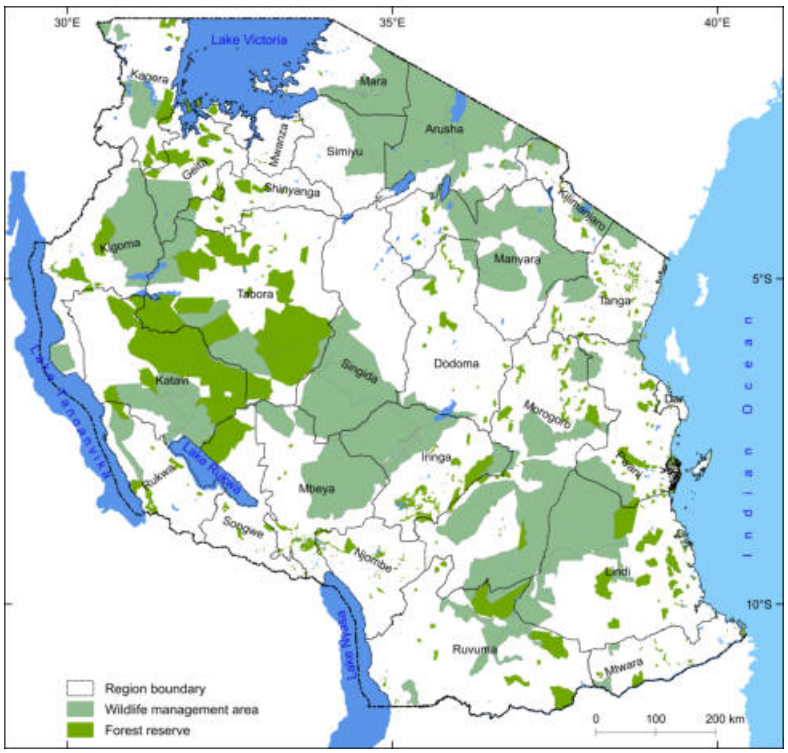

Figure 3.13: Protected areas in Tanzania

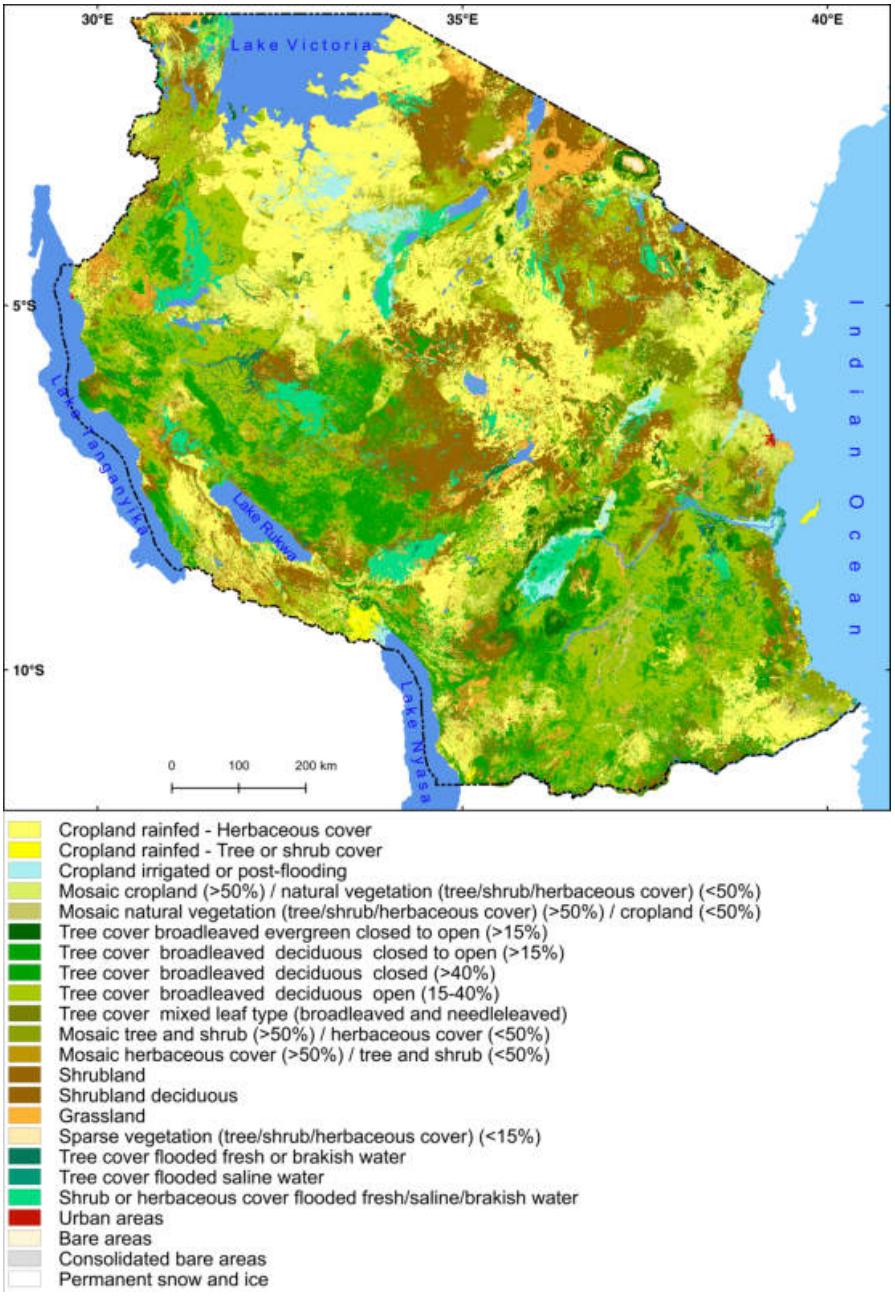

Figure 3.12: Tanzania land cover for the year 2015 from ESA CCI (Santoro et al., 2017). Legend modified for only present land covers in Tanzania.

Chapter 4

Datasets and Software

The study integrated data from different sources and Free/ Libre and Open-Source Software (FLOSS) to monitor and analyse the extent of forests in Tanzania. The data were sourced from Landsat 8 Satellite Sensor, environmental data, PlanetScope images provided by Planet Labs, fieldwork survey, using a drone and hand-held Global Positing System (GPS), and forest inventory data from the National Forest Inventory (NFI).

4.1 Remotely Sensed Data

The satellite-based imagery provides data spanning over 40 years. Landsat delivers the most extensive and most advanced experience of medium spatial resolution satellite imagery (Roy et al., 2014). Medium-resolution satellite data establishes a great wealth of data required to map and monitor forest cover and cover change at a global, national and local scale.

However, persistent cloud cover and low data availability in the tropics (Mitchard et al., 2011; Duveiller et al., 2008), created excessive gaps in the Landsat archives (Broich et al., 2011) and tree phenological variations have remained a challenge in mapping tropical forests. Therefore, images were selected from the dry season (June to November) to minimise cloud contamination and discrepancies in reflectance caused by seasonal vegetation fluxes and sun angle changes (Coppin and Bauer, 1996). However, before the final image acquisition, it was necessary to evaluate the year's optimal time for separating forest phenological changes from other vegetative classes based on yearly seasonality (Table 4.1).

Table 4.1: A summary of clear-sky image availability in Tanzania based on seasonality

Month	**Seasonality**	**Cloud Free observations**	**Remarks**
January - March	Wet season	3 - 6	Cloudy and low number of clear-sky images
April - June	Wet to dry season	6 - 11	Moderate number of clear-sky images
July - September	Dry season	> 11	High number of clear-sky images
September - December	Dry to rain onset	11 - 6	High to moderate number of clear-sky images

The structure and composition of tropical forests are highly variable and complex (Marselis et al., 2018; Bhavsar et al., 2017; Mayes et al., 2015). It has been associated with seasonal patterns (plant phenology) as when leaf flush, senescence, and leaf abscission occurs (Samanta et al., 2012). Understanding these behaviors supports the discrimination of different forest compositions and types in the tropics under different seasons (wet or dry) (Table 4.1). The application of satellite measurements has made it possible to examine these changes. For example, an increase in near-infrared (NIR) reflectance is observed during the dry season (more light) and a decrease during the wet season (less light) (Samanta et al., 2012). Therefore, the reflectance properties of vegetation change from one season to another.

For this study, images were selected from the dry season. However, it was not possible to identify the optimal month for separating forests from other vegetation covers like grasses, bushes, crops, etc. Therefore, the Normalised Difference Vegetation Index (NDVI; equation 4.1) was used as a radiometric measure of photosynthetic active radiation absorption of the canopy chlorophyll in observing vegetation growth and variation through the growing seasons.

$$NDVI = \frac{NIR - RED}{NIR + RED} \tag{4.1}$$

During the peak of the green season, the spectral response of deciduous and evergreen forests, agriculture, and shrubs are almost similar at 30 m resolution, with high NDVI values. Hence, throughout the rainy season, it is hard to separate forests from other vegetation during the rainy season due to having similar spectral signatures, which may cause over-estimating forests' extent. Therefore, during dryer months, leafless deciduous vegetation is classified as bright or dark soil (low NDVI response and high reflectivity on IR bands), reaching the highest separability compared to evergreen vegetation.

Therefore, the zonal statistic available in the Remote Sensing and GIS Software Library (RSGISLib) was used to extract the monthly NDVI value for each vegetation type from the images. Polygons were used as regions of interest and as input to perform the pixel-in analysis, by averaging the pixels in the polygon (equation 4.2)(Bunting et al., 2014).

$$\overline{X} = \sum X_i K | \sum K' \tag{4.2}$$

Where K denotes the percentage of the pixel that intersect the polygon and if K

= 1 means the polygon is entirely contained in the pixel. Extracted pixel values for all pixels within a polygon were exported as a comma-separated values (CSV) file and used for further analysis (NDVI plots for different vegetation types for June to November).

4.1.1 Landsat 8 Satellite Sensor

The Landsat Data Continuity Mission (LDCM) launched Landsat 8 on February 11, 2013, with two improved sensor payloads, the Operational Land Imager (OLI) and the Thermal Infrared Sensor (TIRS) (Irons et al., 2012). The OLI sensor was added with two reflective bands of a short-wavelength blue band (0.43 - 0.45 μm), which is intended to improve the sensitivity to chlorophyll and other suspended materials in coastal areas and enhance atmospheric aerosol properties. The other is a new short-wavelength infrared (1.36 - 1.39 μm) that can be used for cirrus cloud detection because of strong absorption by water vapor (Roy et al., 2014; Sun et al., 2017).

Landsat 8 captures a 185 km swath with an approximate final scene size of 185 km x 180 km and is defined in the second Worldwide Reference System (WRS-2) with 30 m spatial resolution (Figure 4.1). It provides repetitive and synoptic observations with a temporal resolution of every 16 days, making it suitable for forest mapping and monitoring. Landsat 8 uses pushbroom sensors with long and linear arrays of detectors, improving data quality (signal/noise ratio) and radiometric resolution (12 bits), higher than the preceding Landsat TM and ETM+ with 8 bits.

Landsat 8 data from OLI and TIRS sensors are radiometrically corrected, co-registered, and corrected for terrain distortion (Irons et al., 2012), and therefore,

reduce the uncertainty during applications (Roy et al., 2014). Approximately 700 Landsat 8 scenes are acquired per day, compared to about 450 image scenes from Landsat 7 (Ihlen, 2019). This has increased the availability of images to minimise the problem of clouds, especially in the tropics. Therefore, Landsat 8 data were used to establish the forest baseline and subsequent forest changes for this study.

Similarly, the development of the Copernicus Programme by the European Space Agency (ESA) and the European Union (EU) has contributed and increased to the effective monitoring of tropical forests by producing Sentinel-2 multispectral products. Sentinel-2 satellites are the second constellation of the ESA Sentinel missions and carry multispectral scanners onboard. The current adoption and application of Sentinel-2 can be attributed to the higher spatial resolution of 10 m in the visible through to the near-infrared bands which are higher than many other medium spatial resolution images, the high temporal resolution of 5 days, and the availability of the red-edge bands providing opportunities for multiple applications (Immitzer et al., 2016). Sentinel-2 offers improved data compared to other low to medium-spatial resolution satellite images (e.g., Landsat), especially in temporal and spatial resolution. Note that the 13 bands for Sentinel-2 images have spatial resolutions ranging from 10 to 60 m (Drusch et al., 2012).

However, for this study, at a country scale, Sentinel-2 images were not used because of an excessive data volume requiring more processing and classification time, and short temporal coverage (from 2015) (Lima et al., 2019) compared to Landsat mission (Reiche et al., 2016). Though the methods developed are transferable to Sentinel-2 and are expected for future forest monitoring in Tanzania, considering short revisit cycles that can support detecting forest changes including near to

when they occur.

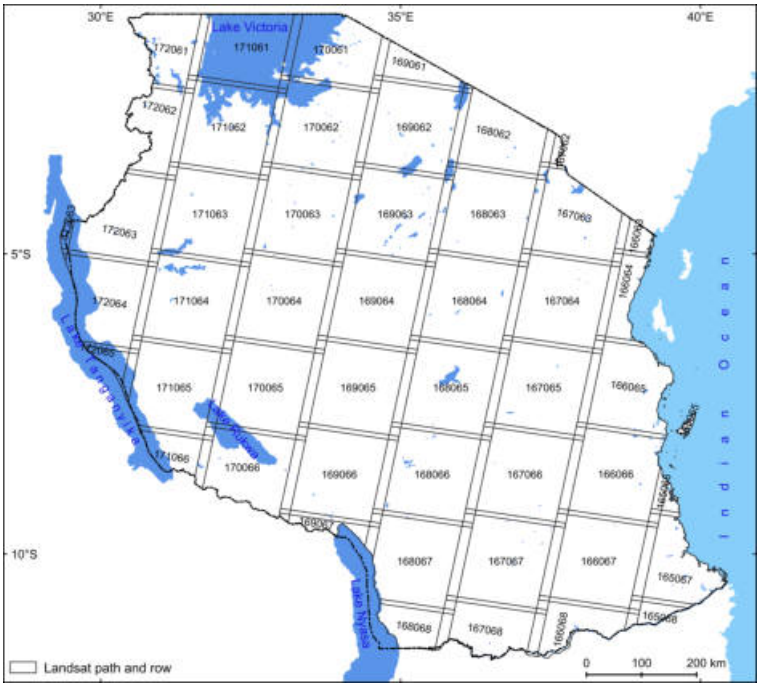

Figure 4.1: Tanzania Landsat paths and rows in WRS-2

4.1.2 PlanetScope Imagery

The PlanetScope[1] data were collected to support the accuracy assessment of the classification results from the Landsat 8 imagery. The PlanetScope constellation can image the entire land surface every day with a capacity of collecting 150 million km^2 (Lemajic et al., 2018) and comprises around 200 satellite micro-satellites (Doves) imaging at 3 m spatial resolution (Baloloy et al., 2018). The satellites serve in two different orbits; the International Space Station (ISS) and the Sun Synchronous Orbit (SSO). The SSO is typical to many earth-observing satellites that set equator crossing time and acquire images only in descending orbit. The

[1] https://www.planet.com/

ISS was used during the demonstration phase where PlanetScope CubeSats were launched into an orbit with a 52-degree inclination at approximately 420 km altitude (Kääb et al., 2019). PlanetScope data acquired from 2016 and in early 2017 were the result of this launch, but thereafter ground-based launches were used to introduce near-polar sun-synchronous orbits. Coverage during this demonstration period (i.e., 2016 to 2017) was more sporadic and included gaps (Frazier and Hemingway, 2021).

The SSO satellites cross the equator at 9:30-11:30, acquiring images of an area at almost the same time in every revisit (Guyana Forestry Commission and others, 2011). The scenes were acquired in four spectral bands of Red, Green, Blue, and Near-Infrared (NIR), and an Analytical Ortho Tile product (level (3A) was selected as multiple orthorectified scenes merged in a single strip and provided sufficient details (spatial resolution of 3 m) to validate results from medium resolution (30 m) of Landsat 8.

4.2 Environmental Data

Forest mapping and monitoring through remote sensing requires data processing from images acquired by sensors on satellites and other platforms, to extract information about targets/features on the Earth's surface or processes of interest at a given time (Arenas-Castro et al., 2019). One of the significant advantages of remote sensing is the ability to access, in some cases, an extensive open database (e.g., for Landsat). This allows for the analysis of images obtained for different points in time, which can be used to analyse changes in the surface (Giuliani et al., 2020). Therefore, this study used a combination of data such as environmental

variables that were applied during image pre-preprocessing (e.g., Digital Elevation Model) and assessing forest types, habitat suitability, and subsequent future climate change impact. The environmental variables selected included those relating to climate, terrain, and soil characteristics. The environmental variables were acquired from the KITE dataset (AFRICLIM)[2] (Platts et al., 2015). The Shuttle Radar Topography Mission (SRTM) 1-arc second elevation data, were obtained from USGS Earth Explorer. Soil characteristic variables were derived from World Soil Information (ISRIC)[3] (Hengl et al., 2015).

4.3 Field Data Collection using drones

The best period of discrimination in most of the forest cover areas in Tanzania is during the dry season (late June to mid-October). The dry season indicates a period of lower water availability that limit the growth of shrubs, herbaceous plants, and grasses. It enables the separation of forests from other vegetation with remotely sensed data. It is challenging to separate forests from other green understories in the rainy season due to similarities in their spectral reflectance. Therefore, field data were collected between September - October 2018 and 2019.

Field data collection is vital for accurately interpreting the results of the satellite image analysis (Congalton and Green, 2019), through verification, evaluation, or to assess the results of classified outputs. Field data can provide reliable data to guide the analytical process, such as creating training samples to support classification. Also, contribute information on real-time data modelling for the spectral response

[2] https://webfiles.york.ac.uk/KITE/AfriClim/ByCountry/Tanzania/
[3] https://www.isric.org

of landscape features (Lillesand et al., 2004), including different forest types, tree species, and land uses.

Two kinds of information were collected, including flying a drone at a height of approximately 60 m and GPS records for the areas visited. The other information recorded includes forest type, land use, land cover, and any associated forest disturbances. The field samples for accuracy assessment were chosen to focus on areas of the thematic map that were visually inspected and found to be less separated the pixels in terms of forest/non-forest and forest type. As a result, areas, where different forest categories occur in mosaics with mixed pixels (e.g., open and closed woodlands, lowland forests) or in close proximity to each other, were considered (e.g., montane and upland tropical forests). Tanzania has a vast area of forest categories (MNRT, 2015), and it was not possible to cover all places with the limited time available in the field and with a drone flight time of about 25 minutes per flight.

4.4 Forest Inventory Data

The forest inventory data were acquired from the National Forest Resources Monitoring and Assessment (NAFORMA) based on a total of about 32,660 plots collected from May 2010 to June 2013, including about 19,382 plots covering forested areas. The forest inventory included information on biophysical parameters (number of stems per ha, basal area per ha, volume per ha, biomass per ha, land use, vegetation type, soil type, regeneration (number and species of seedlings), forest management, disturbances, species, and ownership. Plots consisted of 1, 5, 10, and 15 m radius concentric nested circular subplots, collected over a series of

study clusters – L-shaped transects, consisting of six to ten plots with 250 m spacing between plots. The study clusters were distributed based on a double sampling for the stratification approach (Tomppo et al., 2014). Forest inventory data are usually collected on a much finer scale, which allows modelling the distribution of tree species on a much finer scale and accuracy assessments. Therefore, the forest inventory data were used for establishing the habitat suitability of forest types in Tanzania and subsequent future climate change impact prediction (Chapter 6) and accuracy assessment for forest types classification (Chapters 5 and 7).

The habitat suitability for the forest types was established using the dominant tree species from the forest inventory data. These data contain information that links forest-habitat relationships for different forest ecological sites. The species were selected as proxy indicators of habitat types for different existing forest types in Tanzania. The presence-only records were chosen based on abundance from the plot measurements for each forest type. The selection included both percentage frequency (occurrence) and abundance (proportional of individuals). This implies that only the most frequent and abundant species from each forest type were selected for establishing the habitat suitability of forest types in Tanzania.

The sampling design for the inventory data captures the forest condition under all forest types. At every location, the L-shaped cluster was established with five sampling plots for each arm located at 250 m distances from one another (both arms of the L had equal length) (Figure 4.2). The sampling plot locations were established using a held-hand global positioning system (GPS) and presented in a local projection. The study clusters from the inventory were distributed based on a double sampling for stratification (Tomppo et al., 2014).

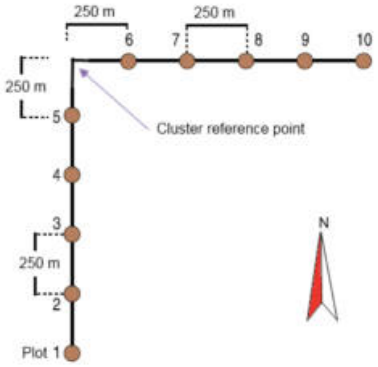

Figure 4.2: Cluster design for ground truth dataset collection. Sourced from Vesa et al. (2010)

4.5 Free/Libre Open Source Software (FLOSS)

The FLOSS promotes collaboration and contributions from different parties in software production and innovation processes in generating an innovative capability in software technology that offers mature, capable, and reliable software to contribute to the creation of this infrastructure (Yildirim and Ansal, 2011). FLOSS creates a unique opportunity for developing countries such as Tanzania, to reduce reliance on commercial software and to create spatial data infrastructures (SDI) where resources for system development and maintenance are scarce (Brovelli et al., 2017). FLOSS appears as a solution to the question of intellectual property, which limits the application of remote sensing as neither copyright nor patents can bring an acceptable balance between innovation incentives and knowledge sharing (Zimmermann and Jullien, 2007). The introduction of FLOSS induced a revolution in the field of remote sensing, supporting collaboration, with practical knowledge and the exchange of ideas and information in a significant way

(Kganyago and Mhangara, 2019; Ciolli et al., 2017).

Therefore, the application of FLOSS in geospatial data and analysis (Bunting et al., 2014), aims at sustainability in the current and future forest monitoring for supporting the development of early warning systems for forest change in Tanzania. Hence, FLOSS gave a long-term solution to software costs (de Klerk and Buchanan, 2017) and was applied to this study.

4.5.1 Remote Sensing and GIS Software Library (RSGISLib)

The Remote Sensing and GIS Software Library (RSGISLib)[4] (Bunting et al., 2014) is a collection of tools for processing and analysing remote sensing and GIS datasets. The tools are accessible through a Python binding with over 300 functions in a scriptable manner for data analysis and batch processing. RSGISLib contains a comprehensive set of modules including; image calibration, classification, image calculations, image filtering, image morphology, image registration, image utilities, raster GIS, image segmentation, vector utilities, zonal statistics, etc. RSGISLib can interact with other open-source software, for example, a combination of RSGISLib and GDAL support vegetation index calculations derived from Landsat 8 and Sentinel-2 images, including the Normalized Difference Vegetation Index (NDVI) and Normalized Difference Water band Index (NDWI) for informing on the photosynthetic activity or water content of different vegetation cover types.

The ability of RSGISLib to support extensive dataset analysis and large area cov-

[4] https://www.rsgislib.org

erage were important aspects of this study with an extensive area coverage of about 945,100 km^2. RSGISLib can be used on standard computers and High-performance computing (HPC) with the ability to process data and execute intricate calculations at high speeds. The capability of RSGISLib has been applied to large-scale mapping, including the global mangrove Mapping extent (Bunting et al., 2018), Mapping mangrove extent and change with worldwide coverage (Thomas et al., 2018). Therefore, the RSGISLib was deemed to be well-suited for this national-scale study.

4.5.2 Python

Python[5] is a high-level scripting language and flexible in processing and automation of processes with the ability to support various programming models, including object-oriented, functional programming, and procedural styles making clear and understandable syntax. Therefore, it has an extensive standard library, fully utilised in bindings of RSGISLib (Bunting et al., 2014). This study employed Python language from image acquisition through Google cloud services[6] to pre-processing and analysis of the final results.

4.5.3 Geospatial Data Abstraction Library (GDAL)

Geospatial Data Abstraction Library (GDAL[7]) provides a library for reading and writing raster and vector geospatial data formats. It also supports access to user and geographic metadata information. GDAL also provides a set of tools that

[5] https://www.python.org
[6] https://cloud.google.com/storage/docs/public-datasets
[7] https://gdal.org

are valuable to access information from the header file (e.g., satellite image) with useful command-line utilities for data translation and processing (Clewley et al., 2014; Zhao et al., 2011). It provides functions to open raster files and retrieve their meta-data as well as their image data; supports building image pyramids, statistics, and an attribute raster attribute table (RAT) (Clewley et al., 2014) and reading and converting HDF5 image file format into standard GIS format (Bunting and Gillingham, 2013; Zhao et al., 2011).

4.5.4 Scikit-learn

The Scikit-learn[8] is an open-source, popular machine-learning library available from within Python (Pedregosa et al., 2011). It offers dozens of built-in machine learning algorithms and models that support supervised, and unsupervised learning and various tools for model fitting, data preprocessing, model selection, and evaluation (Garreta and Moncecchi, 2013). The library is built upon the Scientific Python set of libraries (Table 4.2).

Table 4.2: Some examples of Scikit-learn Libraries

Library	**Application**
NumPy	For base n-dimensional array package
SciPy	For scientific computing
Matplotlib	For 2D/3D plotting
IPython	For an enhanced interactive console
Sympy	For symbolic mathematics symbols
Pandas	For data structures and analysis

Scikit-learn provides implementations for many popular machine learning classi-

[8] https://scikit-learn.org/stable/

fication algorithms such as Support Vector Machines, Neural Networks, Random Forests, K-Nearest Neighbors, Decision Trees, K-Means, and Principal Component Analysis. Therefore, many of the machine learning classifications implemented in this study use the Scikit-learn module alongside RSGISLib for applying the model to the image data.

4.5.5 Extreme Gradient Boosting (XGBoost)

Selection of a classification model is a critical stage that intends to optimise classification by minimising error and improving classification accuracy, processing time, and managing large dataset (Britto Jr et al., 2014). XGBoost, is a novel machine learning algorithm, as a decision tree-based ensemble technique for structured or tabular data (Li et al., 2020). XGBoost is a flexible and highly scalable tree structure enhancement model that can handle sparse data, greatly improve algorithm speed, reduce computational memory in very large-scale data training, and can reduce the degree of model overfitting (Chen and Guestrin, 2016; Li et al., 2019).

4.5.5.1 Why XGBoost was selected

XGBoost was selected over other algorithms because of the following attributes:-

System Optimization

i. Parallelization: XGBoost algorithm uses successive tree building in a parallelized application. It is made possible because of the exchangeable nature of loops used for building base learners; the outer loop computes the leaf nodes of a tree and the second inner loop calculates the features. Therefore, to improve

run time, the order of loops is interchanged utilising initialization through a global scan of all instances and sorting using parallel threads. This switch improves algorithmic performance by offsetting any parallelization overheads in computation.

ii. Tree Pruning: XGBoost uses the 'max_depth' parameter and starts pruning trees backward. This 'depth-first' approach improves computational performance significantly.

iii. Hardware Optimization: The algorithm has been designed to make efficient use of hardware resources. This is accomplished by cache allocating internal buffers in each thread to store gradient statistics. Further enhancements such as 'out-of-core' computing optimize available disk space while handling big data frames that do not fit into memory (Chen et al., 2019).

Algorithmic Enhancements

i. Regularization: It penalizes more complex models through regularization to prevent overfitting.

ii. Sparsity Awareness: XGBoost naturally admits sparse features for inputs by automatically 'learning' the best missing value depending on training loss and handles different types of sparsity patterns in the data more efficiently.

iii. Weighted Quantile Sketch: XGBoost employs the distributed weighted Quantile Sketch algorithm to effectively find the optimal split points among weighted datasets.

iv. Cross-validation: The algorithm comes with a built-in cross-validation method at each iteration, taking away the need to explicitly program this search and

to specify the exact number of boosting iterations required in a single run (Hanif, 2019).

Therefore, XGBoost is gaining popularity in data mining and is increasingly utilised by data scientists and has provided leading-edge outcomes in different fields, notably the financial area, such as business forecast risk assessment (Carmona et al., 2019), crops mapping (Ustuner and Balik Sanli, 2019), physical activity classification in health monitoring (Rahman et al., 2020), but remains relatively not fully utilised in forestry (Li et al., 2019). In this study, XGBoost was implemented in the python interface (Brownlee, 2018) for both forest baseline classification for forest/non-forest, forest types classification, and forest change analysis to support forest monitoring in Tanzania.

4.5.6 TuiView

TuiView[9] is an open-source viewer for remote sensing data initially designed to view raster data and support display vector data (Clewley et al., 2014). Python is the scripting language used in TuiView through the PyQt library for the GUI elements and GDAL to view images. It contains much functionality for viewing and manipulating Raster Attribute Tables (RAT), required in the object-based classification within RSGISLib and capable of handling extensive datasets and generating overviews (Clewley et al., 2014). TuiView also allows querying and plotting of raster values and display of raster attribute tables and highlighting rows for queried pixels and creating new attribute table columns and updating of columns (Bunting, 2017). In this study, TuiView supported the prompt and

[9] http://tuiview.org/

efficient visualisation of large files and executed simple queries.

4.5.7 Quantum GIS (QGIS)

Quantum GIS (QGIS) is an Open Source Geographic Information System that is released under the GNU Public License (GPL) (Sherman et al., 2004). QGIS integrates with Python scripting language in the automation of GIS tasks. Since its inception in 2002, several versions of QGIS exist free for download. Therefore, the software provides useful GIS tools in spatial analysis, geoprocessing, geometry, and data management tasks. QGIS also links (expendable) to support various formats such as basic ESRI shapefiles and image formats like KEA (Bunting and Gillingham, 2013) also able to link with Web Map Service (WMS) and Web Feature Service (WFS). The tasks implemented through QGIS for this study included data creation (vector data), editing, and map composition.

4.5.8 KEA file format

The KEA is an image file format that supports the full implementation of the GDAL data model within an HDF5 file. The file format was accessed through a software library libKEA and GDAL. The format has comparable performance to existing formats and can help compress large raster files into small sizes using zlib without losing image information (Bunting and Gillingham, 2013). The KEA file format enabled the compression of large remotely sensed datasets for this study for both storage and analysis.

4.5.9 Raster Input and Output (I/O) simplification (RIOS)

The Raster Input and Output (I/O) simplification (RIOS[10]) is an assemblage of python modules that make it easy to write raster processing code in Python (Gillingham and Flood, 2013). Raster data comes in many file formats with some of them, even multilayer files. Managing large datasets that exceed the capacity of the main memory is often the bottleneck in the computation. Therefore, RIOS reads an image into memory in a block and converts it from one format to another, and saves newly created objects, types, and amounts of stored information (e.g., object size, range of values). It handles the opening of the existing image and creating the new image and checking the alignment of projections, raster grid, stepping through the raster in small blocks, and reading and writing Raster Attribute Tables (Clewley et al., 2014; Bunting, 2017). RIOS supported the analysis of large datasets for this study in small blocks without hindering computational memory.

4.5.10 Atmospheric and Radiometric Correction of Satellite Imagery (ARCSI) software

Utilising optical imagery requires specialised algorithms and dedicated tools, especially for the analysis of large datasets. Pre-processing is an indispensable step for producing analysis-ready data (ARD) products. ARCSI[11] aims to address pre-processing challenges by providing an automatic architecture for retrieving the atmospheric correction parameters to generate ARD data (Bunting et al., 2018).

[10] http://www.rioshome.org
[11] https://arcsi.remotesensing.info

The analysis's main task is to employ an atmospheric correction for using the 6S radiative transfer model (Vermote et al., 1997), accessed through the python interface Py6S (Wilson, 2013). The software provides a fully automated processing chain for the pre-processing optical imagery to generate surface reflectance and topographically correct imagery, enhancing replicability and ensuring output uniformity (Bunting, 2017). Therefore, this study employed ARCSI software to generate ARD data from the Landsat 8 imagery for this national forest study (Figure 4.3), including an implementation of the cloud masking algorithm FMASK (Zhu et al., 2015; Zhu and Woodcock, 2012).

PlanetScope images were acquired in the standard Analytic Product (Radiance) and processed to top-of-atmosphere reflectance and then atmospherically corrected to bottom-of-atmosphere reflectance. This ensures consistency across localized atmospheric conditions, minimizing uncertainty in spectral response over space and time (Tu et al., 2022).

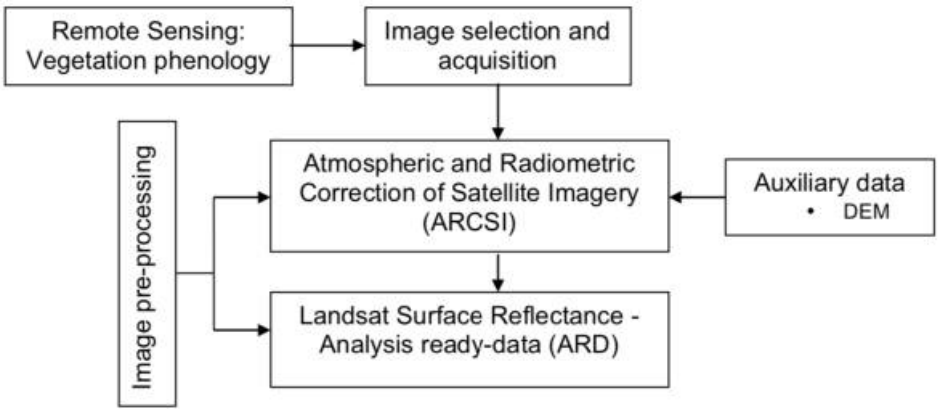

Figure 4.3: Image acquisition and pre-processing workflow

4.5.11 Earth Observation Data Downloader (EODataDown)

Acquisition of EO data at a national level for a country such as Tanzania requires automation of the data download and analysis. This is particularly important when considering the creation of a forest monitoring system where data will need downloading on a regular basis. For this study, the EODataDown[12] open-source tool was used. EODataDown can automatically download and process EO data to an analysis-ready data product (Bunting, 2018). It can be applied for batch downloading Landsat 8 for forest mapping and monitoring in Tanzania. One of the key advantages of this tool is that it allows user-defined plugins to be constructed for data analysis (e.g., change detection), allowing a full workflow to be automated. The software is written as a Python module and is built on top of a PostgreSQL database with dependencies on RSGISLib and ARCSI.

The PostgreSQL database keeps track of the images acquired for the study and their processing stage, i.e., processed to ARD and application of plugins for the change analysis. ARSCI provides the processing chain for the optical ARD generation where outputs include: FMask cloud masks, valid masks, topographic shadow, footprint vector, view angle, and finally standardised surface reflectance, which corrects for solar and local geometry (i.e., Bidirectional Reflection Distribution Function (BRDF) and topographic correction).

[12] https://eodatadown.remotesensing.info/

4.5.12 High-Performance Computing (HPC)

Establishing a National Forest Monitoring System (NFMS) requires a large volume of EO data to be processed and, therefore, a large amount of computational power and storage that exceed conventional processing from desktop computers (Kalluri et al., 2000). Therefore, HPC has emerged as a promising solution to process efficiently large datasets and generate ARD for forest classification and change analysis for scientific understanding over a large geographical area (e.g., Bunting et al., 2018, 2022).

This study implemented the acquisition and analysis of remotely sensed (Landsat 8) data for Tanzania through Super Computing Wales (SCW)[13], with high-speed memory and storage. Hence, this was achieved by utilising the RSGISLib remote sensing data processing algorithm (Bunting et al., 2014) through a massively parallel multi-processor from the SCW platform to expedite generating of forest information for Tanzania. The SCW environment's utilisation focused on improving the processing time and computational load. Typically, around 100 cores were used at each processing stage.

Therefore, the forest baseline for forest/non-forest, forest types classification, and forest change analysis for Tanzania was developed using multispectral data from the Landsat 8 Operational Land Imager (OLI) images (2013 to 2018) for May to November with cloud cover threshold of $> 80\%$. A total of 3200 Landsat 8 OLI images were downloaded using the Google Cloud API and deployed on the SuperComputing Wales (SCW) high-performance computing (HPC) infrastructure.

[13] https://www.supercomputing.wales/

Chapter 5

Preliminary Study and Methodology Piloting

5.1 Introduction

This study aims to provide a national-level forest monitoring system for Tanzania (approximately 945,100 km^2). However, this chapter focuses on developing and experimenting with methods for a smaller spatial area, the Rufiji basin. This allowed for an understanding of data volume and constraints associated with storage and processing time. Similarly, data acquisition limitations could be understood, such as cloud cover, and limited data availability. Therefore, this chapter aims to generate forest extent and forest type maps for 2017, using Landsat 8 for the Rufiji basin in Tanzania. Specifically, this chapter:

i. Examines seasonality separability between different vegetation types based on vegetation indices (VI)

ii. Explore algorithms for clouds and shadow detection on optical data

iii. Generate image composites based on maximum NDVI

iv. Use the resulting imagery composites (iii) for Forest and Non-forest classification. The classification of forest/non-forest and further into forest types; is based on the existing forest definition, with an area larger than 0.5 ha and forest cover over 10%. The classification of forest/non-forest and further into forest types; is based on the existing forest definition, with an area larger than 0.5 ha and forest cover over 10%. Landsat 8 data for 2017 was used together within a machine learning (Extremely Randomised Tree classifier (ERT). The classification accuracy was checked using NFI data.

v. Use the image composites and the forest map to create a forest types classification

Therefore, the findings will provide a roadmap for expanding to the country level.

5.2 Study site: Rufiji Basin

The Rufiji River Basin is the largest in East Africa, located between Longitudes 33^0 55' E and 39^0 25' E and between Latitudes 5^0 35' S and 10^0 45' S (Figure 5.1). The elevation rises from 0 meters in the Indian Ocean to nearly 3000 meters in the Mbeya region. It covers about 183,791 km^2 representing approximately 20% of the Tanzania land surface (Olson et al., 2015). The Rufiji River Basin varies greatly in climate from tropical humid in the east to temperate in the Southern Highlands and hydrological conditions, with a humid temperature of about 23^0C and a hot

climate of about 39^0C at the coast. The basin is divided into four sub-basins which are Great Ruaha (46.5%), Kilombero (21.9%), Luwegu (13.8%), and Lower Rufiji (17.7%).

The Rufiji basin's climate varies with a hot and dry climate in the north-western part. The mountainous regions experience a humid and cold climate, except for the lower parts, which experience two rainy seasons, the most significant portion of the basin characterised by unimodal rainfall. Rainfall is high along the mountain chain in the western Kilombero valley. The annual rainfall in Kilombero ranges from 1,000 mm to 1,800 mm, with a yearly average of about 1,400 mm. Rain decreases towards the middle of the Great Ruaha sub-basin, where annual rainfall ranges from 400 mm to 1,200 mm with an average of about 800 mm. High rainfall is also experienced around the Mahenge Hills in Morogoro region. The rain in the Luwegu sub-basin is estimated to range between 800 mm and 1,400 mm annually, with an average of 1,100 mm. Rainfall is also temporally uneven, with the majority falling from November to May and the remainder of the year receiving very little rain.

The variation in climatic conditions has characterised different forest types, with woodlands covering about 22,900 km^2 of the total area, and almost 4,480km^2 consisting of 92 protected forest reserves. Mangroves at the Rufiji river delta, which is the largest in the country, make a unique type of vegetation in the basin to protect the coastline and support various organisms. Different types of forests and a high level of the human population of more than 16% of the Tanzania population with diverse activities (agriculture, fisheries, tourism, mineral exploration, hydropower generation over 60%) cause high demand for land resources within the basin (Mwalyosi, 1990).

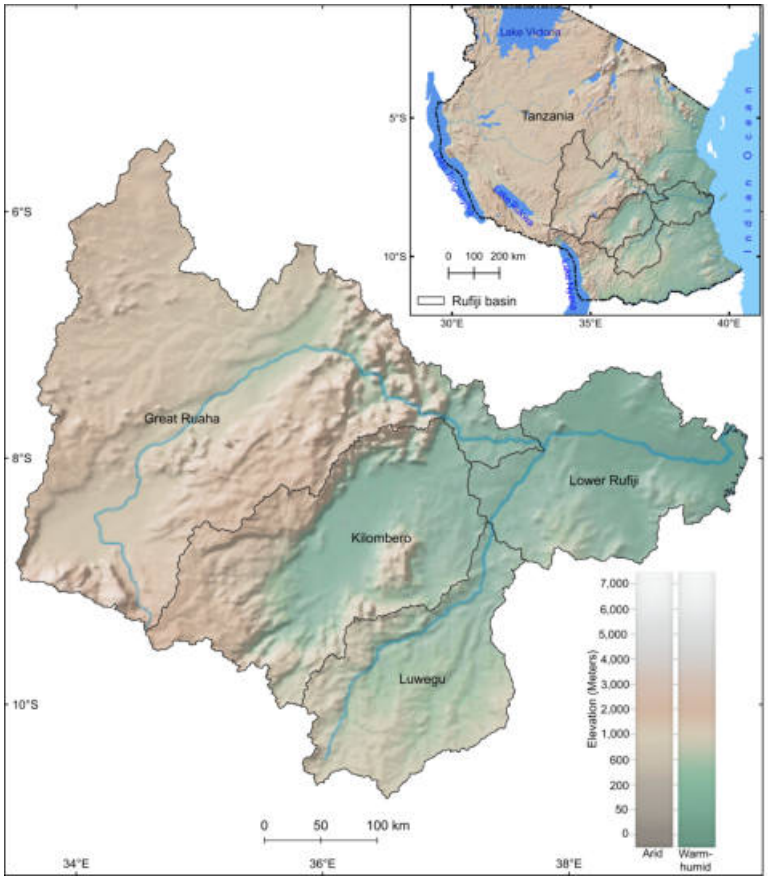

Figure 5.1: Rufiji Basin - preliminary study area. Created with Natural Earth data

5.2.1 Why Rufiji Basin?

The Rufiji Basin represents most of the climatic zones within Tanzania, including the hot-humid coastal plain, the semi-arid zone of the central plateau, and the temperate highland areas that support various vegetation types. The vegetation's seasonal behavior is strongly reflected in the phenological changes necessary for investigating the separation of forests from shrubs using remote sensing data. Similarly, the different climatic conditions support habitats for a wide range of

both plants and animals. It includes most of the ecosystems and land cover found across Tanzania, such as forests, woodlands, pastures, and agricultural and urban. Therefore, the basin preserves its unique natural heritage, which supports various development projects and human activities. Despite its national and international significance, the Rufiji Basin has received few scientific investigations on the states and dynamics of forests and their provision of resources.

The forests, woodlands, and wetlands in the Rufiji Basin have come under increasing pressure with numerous unsustainable off-take exploitation rates. These include the conversion of forests and woodland for dryland agriculture and cash crops, even the destruction of mangrove forests for agriculture, and over-harvesting of its woody biomass for other purposes (e.g., firewood) (Ochieng, 2002).

Therefore, as the population continues to increase in the Rufiji Basin, forest lands are anticipated to be involved in the conversion to other land uses. The conversion of land will likely include forested areas. Given this context, forest cover maps are required to assess the available forest resources and support national policies' formation and policing (Olson et al., 2015).

5.3 Methods

5.3.1 Image Acquisition and Pre-processing

A collection of multispectral Landsat 8 Operational Land Imager (OLI) images were downloaded from the T1 archives through the Google cloud[1] using an automated downloading process in the ARCSI command line. The downloaded USGS

[1] https://cloud.google.com/storage/docs/public-datasets/landsat

Collection 1 images are orthorectified, map-projected (UTM WGS84) images containing radiometrically calibrated data. The images were acquired in the year 2017±1 with a cloud cover threshold of $< 70\%$.

5.3.2 Image Pre-processing

The application of optical imagery requires appropriate pre-processing to derive surface reflectance (pSUR). Pre-processing to surface reflectance was undertaken using the ARCSI software, which uses a dark object subtraction in the visible bands to retrieve Aerosol Option Depth (AOD) (Bunting, 2017) from the image and then parameterises the 6S radiative transfer model (Vermote et al., 1997) and applies the resulting correction to the image data (Bunting et al., 2018). Both a bi-directionally corrected surface reflectance and horizontal surface for the observed top of atmosphere radiance were estimated using the 6S model (Flood et al., 2013). The Function of Mask (FMask) algorithm, available in the ARCSI software was applied for clouds and cloud shadows detection in the Landsat imagery (Zhu et al., 2015; Zhu and Woodcock, 2012) (Figure 5.2). Therefore, for each image valid area, cloud and shadow masks are produced alongside the standardised surface reflectance, which includes the topographic term into the bidirectional reflection distribution function (BRDF) correction as outlined by Shepherd and Dymond (2003).

Topographic correction is important, particularly for the mountainous areas, such as the Eastern Arc Mountains, Mbeya, and Poroto Mountains due to variations in sun and sensor view angles. Despite the fact that Landsat can point its sensors off-nadir at $\pm 7.5^0$ viewing angle, the correction improves the elimination of the effect

of shadows and relief, especially in steep slope areas (Li et al., 2014). Without topographic correction, it could influence the forest classification results as the surface reflectance is different with varying solar elevation and azimuth, slope, and aspect with respect to the location of individual trees and tree clusters (Huang et al., 2008).

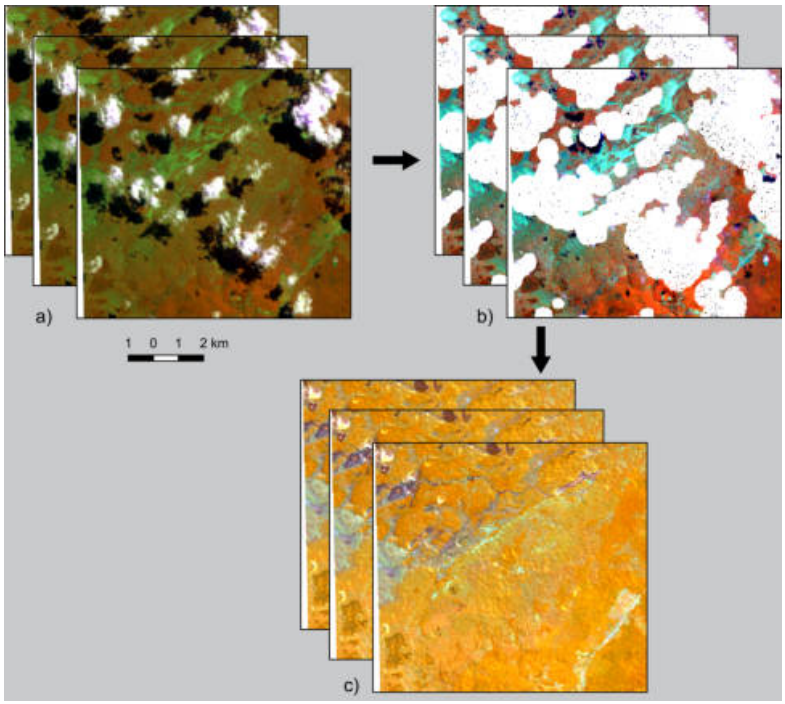

Figure 5.2: Image preprocessing. A Subset of Landsat 8 image p166r66 acquired on 13/08/2017 (dry season) (a) original image with clouds and shadows (b) showing clouds and shadows detected using the Fmask algorithm in the ARCSI software (c) final composite image

5.3.3 Forest Baseline Classification

The classification was achieved using the hierarchical approach, first delineating the forest/non-forest extent and then classifying it into forest types. The forest type definitions were based on the existing forest definition in Tanzania. The

non-forest class includes all classes related to bushland, grassland, cultivated land, settlement, bare land, rock outcrops, barren coastal lands, and ice cap/snow. The classification process followed the methodology of Clewley et al. (2014) and included: image segmentation, populating the raster attribute table (RAT) with reflectance values, populating the RAT with training, running a machine learning-based classification, and finally, accuracy and post-classification assessment (Figure 5.3).

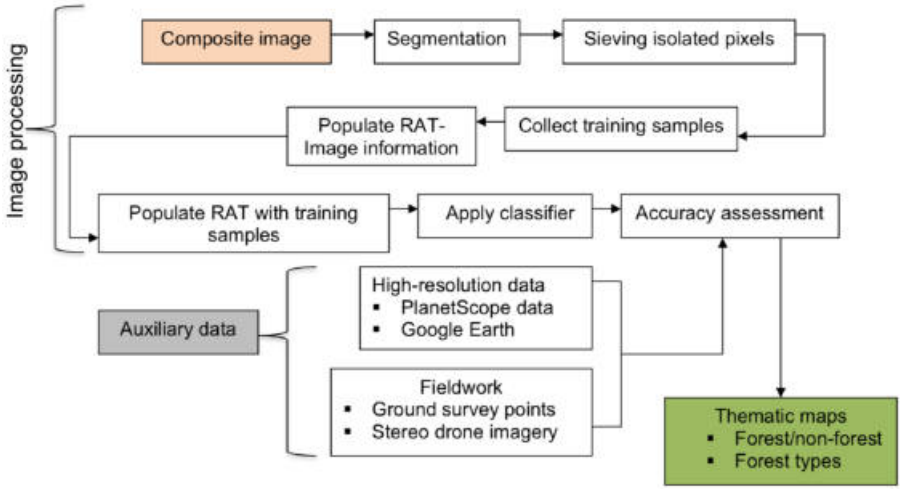

Figure 5.3: Composite image classification and accuracy assessment workflow

5.3.4 Image Segmentation

The segmentation process (Figure 5.4) assigns the image into discrete clumps of pixels and is implemented within RSGISLib software (Shepherd et al., 2019). The separation was based on spectral similarities in colour (Clewley et al., 2014). A K-means clustering was then used to initialise the segmentation creating groups of similar pixels (Witten et al., 2016). An advantage of K-means is that it reduces computation time as the image is classified block-by-block (mini-batches) and re-

duces memory error, especially when working with a large raster (Sculley, 2010). Similarly, it allows the use of a small amount of training data for each iteration, which significantly reduces training time (Mai and Park, 2016). Therefore, the pixels of the segments were predicted to carry the same information class.

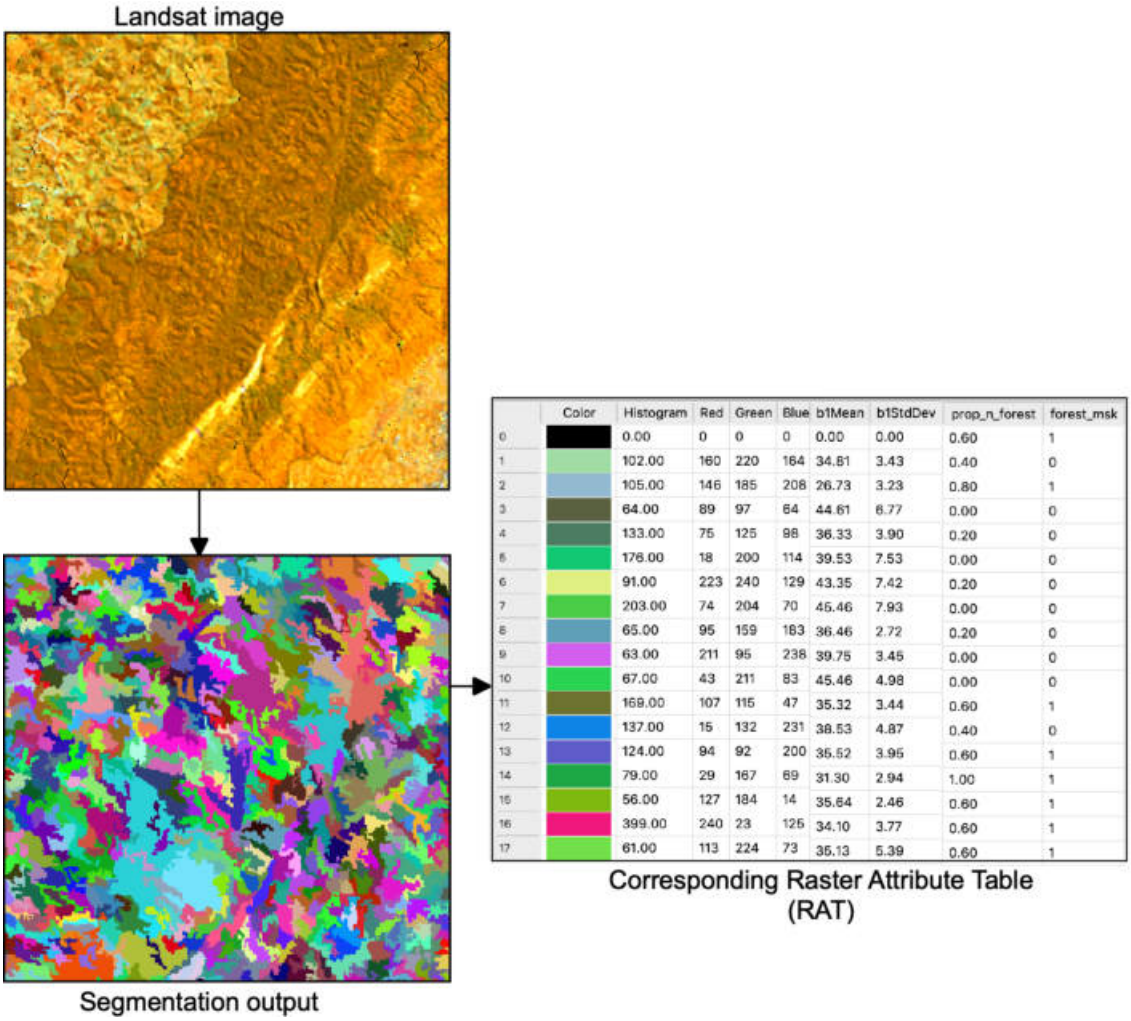

	Color	Histogram	Red	Green	Blue	b1Mean	b1StdDev	prop_n_forest	forest_msk
0		0.00	0	0	0	0.00	0.00	0.60	1
1		102.00	160	220	164	34.81	3.43	0.40	0
2		105.00	146	185	208	26.73	3.23	0.80	1
3		64.00	89	97	64	44.61	6.77	0.00	0
4		133.00	75	125	88	36.33	3.90	0.20	0
5		176.00	18	200	114	39.53	7.53	0.00	0
6		91.00	223	240	129	43.35	7.42	0.20	0
7		203.00	74	204	70	45.46	7.93	0.00	0
8		65.00	95	159	183	36.46	2.72	0.20	0
9		63.00	211	95	238	39.75	3.45	0.00	0
10		67.00	43	211	83	45.46	4.98	0.00	0
11		169.00	107	115	47	35.32	3.44	0.60	1
12		137.00	15	132	231	38.53	4.87	0.40	0
13		124.00	94	92	200	35.52	3.95	0.60	1
14		79.00	29	167	69	31.30	2.94	1.00	1
15		56.00	127	184	14	35.64	2.46	0.60	1
16		399.00	240	23	125	34.10	3.77	0.60	1
17		61.00	113	224	73	35.13	5.39	0.60	1

Figure 5.4: An example of the image segmentation process. The image is part of the Kilombero and Udzungwa mountain

The resulting output from the K-Means step was then iteratively eliminated, first removing isolated pixels and then segments of 2 pixels and so on in one-pixel in-

crements until the user-defined minimum segment size was met (6 pixels). For this study, the minimum mapping unit (MMU) was 0.5 ha (approx. six pixels) as per forest definition in Tanzania. The eliminated segments are merged based on their colour (closest in Euclidean distance) to their neighboring larger segments.

5.3.5 Populate Raster Attribute Table (RAT)

The Raster Attribute Table (RAT) can be populated with statistics such as the minimum, maximum, mean, and standard deviation (Figure 5.4) of each band's reflectance for each segment. These features are then used to classify each segment. The use of a RAT requires the use of the KEA file format (Bunting and Gillingham, 2013; Clewley et al., 2014). This analysis was performed using RSGISLib (Bunting et al., 2014). For this study, just the mean reflectance for each band was populated.

5.3.6 Create Training Samples

An adequate number of representative training samples are a prerequisite for successful classification (Lu and Weng, 2007). For this study, the training samples were generated by interpreting the Landsat 8 image composite and local expert knowledge. Polygons were drawn using QGIS to define the training samples for each forest and non-forest type. Expert knowledge of existing vegetation types in Tanzania was the key to generating the training samples, which were informed by field knowledge and reference to higher spatial resolution imagery (e.g., Google Earth) due to the complexity and heterogeneity of the study area landscape. Higher-resolution Google Earth imagery was particularly useful to identify where

mixed pixels occurred.

5.3.7 Populate the RAT with Training

RSGISLib provides functions to assign training data, in the form of vector files (e.g., shapefiles), to the RAT. It rasterises the training data and populates the segments with the mode of the rasterised training polygons. It updates the table with information about the classes based on the training dataset.

5.3.8 Apply a Classifier

The choice of a classifier for image classification depends on accuracy, reproducibility, robustness, ability to utilise data information, uniform applicability, and objectiveness (Cihlar et al., 1998). Due to different environmental conditions and datasets used, no one classifier can satisfy all these requirements across all datasets (Lu and Weng, 2007). The classification process was implemented using machine learning classifiers which form more advanced statistically supervised classifiers. Ensemble classifiers have gained more considerable application in pattern recognition and machine learning because of their superiority to single classifiers in terms of classification performance. Therefore, an Extremely Randomised Tree classifier (ERT) from the scikit-learn library was applied for this study.

ERT was selected for this study because it reduces bias in terms of sampling from the entire dataset during the construction of the trees. Different subsets of the data may introduce different biases in the results obtained and it prevents this by sampling the entire dataset (Marée et al., 2013). ERT reduces variance due to the

randomized splitting of nodes within the decision trees. Hence, the algorithm is not heavily influenced by certain features or patterns in the dataset. This makes ERT faster during classification since node splits are random and independent from the output values of the learning sample (Geurts et al., 2006).

5.3.8.1 Extremely Randomized Tree Classifier (ERT)

Since the ERT is an ensemble technique implemented for both supervised classification and regression where the randomisation process is robust as the choice of attributes and cut-points are responsible for a large proportion of variance while splitting a tree node (Geurts et al., 2006). The selection of this classifier is based on building randomised trees whose structures are independent of the outputs from the training samples. It enhanced computational efficiency and provide variance analysis in terms of geometric and kernel characterisation of the model. Therefore, the predictive accuracy and control of over-fitting are improved (Manaf et al., 2018).

During training, the ERT will construct trees over every observation in the dataset but with different subsets of features (i.e., it does not resample observations when building a tree). It essentially consists of randomizing strongly both attribute and cut-point choice while splitting a tree node. In the extreme case, it builds randomized trees whose structures are independent of the output values of the learning sample. The strength of the randomization can be tuned to the problem by the appropriate choice of a parameter (Marée et al., 2013).

ERT has been applied in different fields and found to be effective in high-dimensional classification problems such as biomedical imaging (Marée et al., 2007), forest cover

assessment and estimation (Devaney et al., 2015) and stream waters classification (Hannan and Anmala, 2021). Therefore, the ERT algorithm provides an effective, efficient, and free approach for information extraction on forest extent and mapping at the Rufiji delta.

5.3.9 Post-Classification

The post-classification correction was done as a quality check for the initial classification result by visual comparison with the raw images and high resolution from Google Earth to ensure a reliable forest map. In inadequately classified areas, additional training samples were collected and the classification was re-run until the classification was considered of sufficient quality to move ahead.

5.3.10 Forest Type Classification

Precise forest-type mapping is essential when evaluating forest ecological systems for environmental management practices. The process focused on classifying forested areas into more detailed forest types, consisting of seven dominant forest types according to the actual distribution in the study area. These included montane, lowland, mangrove, plantation forest, closed woodland, open woodland, and thicket. Therefore, using the same methodology as the forest / non-forest classification (Figure 5.3) and within the forest classification, a forest-type classification was undertaken for the Rufiji basin.

5.3.11 Accuracy Assessment

The reference data for forest types were obtained from the NFI collected between 2014 - 2018 (Figure 5.5). Since the field points have different timing except for 2018, with the baseline opted for the year 2017, it was necessary to check against high-resolution images (3 m) from PlanetLabs data (Planet Team, 2017), Google Earth, and a sample field survey for 2018 - 2019 using drone capture. The points found not to represent the current status were eliminated from the assessment. According to Congalton (1991), factors to consider during the accuracy assessment process include error sources, sampling design, such as sample scheme, the number of samples, and sample unit (ground data collection and sample size).

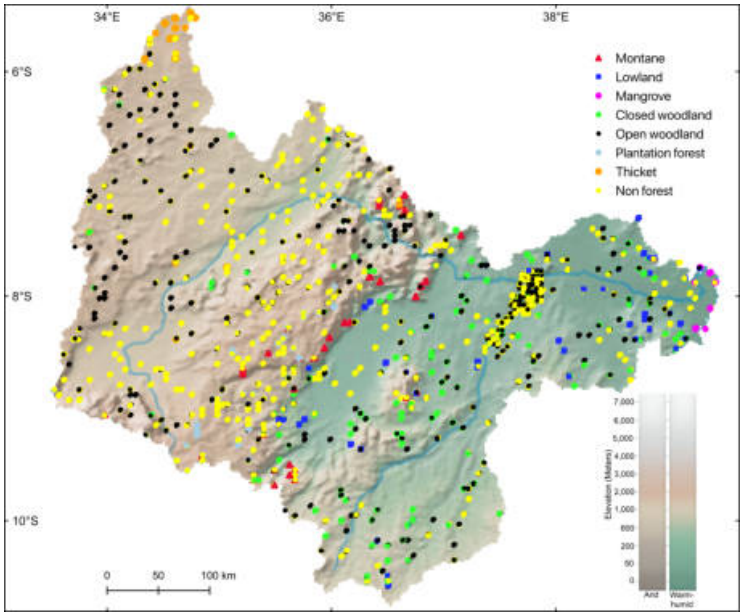

Figure 5.5: Reference data for the forest types distribution from the NFI at the Rufiji Basin.

5.3.11.1 Accuracy Assessment Sampling Unit

The sampling unit predicts the spatial location on the classified map and spatial location on the ground and forms the fundamental unit for the accuracy assessment process. Areal (such as pixels, polygon, or fixed-area plots) and point sampling units are applied in the accuracy assessment (Stehman and Czaplewski, 1998). The accuracy assessment was done using a point sampling unit used from the NFI in Tanzania (National Forest Resources Monitoring and Assessment (NAFORMA) (MNRT, 2015).

5.3.11.2 Map Accuracy Estimates

Forest/non-forest accuracy metrics: The accuracy assessment for the forest/non-forest binary classification was presented using five accuracy metrics: overall accuracy, producer accuracy, user accuracy, F1-score, and Matthews Correlation Coefficient (MCC). The overall classification accuracy represents the percentage of pixels classified correctly in the validation dataset (Congalton and Green, 2019). Producers' accuracy estimates the omission error for a particular class and presents the probability that a reference site has been correctly classified. Users' accuracy is used to determine the commission error and shows the probability that a pixel classified on the image means the same class on the ground. F1-score allows a better evaluation of the forest cover class-wise correctness and merges producer's and user's accuracy into a combined measure (Deus, 2018).

According to Schuster et al. (2012), the F1-score index depicts the harmonic mean among precision (p) and recall (r) for each class i equation (5.1). The score ranges between 0 and 1, whereby 0 means the worst results, and 1 is the most reliable.

Though F1-score is well known chosen accuracy metric in binary classification, it can severely exaggerate and inflate results, particularly on asymmetrical datasets (Chicco and Jurman, 2020). Therefore, further accuracy measure was done by using the MCC, which overcome the class imbalance issue. It ranges between -1 and $+1$, with extreme values -1 and $+1$ obtained when perfect misclassification and perfect classification, respectively, and 0 indicates the classification result was uncorrelated with the ground truth data (Boughorbel et al., 2017). MCC is explained in terms of True Positive (TP), True Negative (TN), False Positive (FP), and False Negative (FN) equation (5.2).

$$(F_1)_i = \frac{2p_i r_i}{(p_i + r_i)'} = 2 \times \frac{users \quad accuracy \times producers \quad accuracy}{users \quad accuracy + producers \quad accuracy} \tag{5.1}$$

$$MCC = \frac{(TP \times TN) - (FP \times FN)}{\sqrt{(TP + FP) \times (TP + FN) \times (TN + FP) \times (TN + FN)}} \tag{5.2}$$

Forest types accuracy metrics: The accuracy assessment was conducted based on (Olofsson et al., 2014, 2013). This approach was found useful for reducing the uncertainty of the classification results. Three stages were implemented during the accuracy assessment process. (i) estimate map accuracy based on the ground reference points, (ii) estimate area proportions adjusted for the map bias based on (i) above, and (iii) estimate standard errors for the confidence interval for the error-adjusted estimates from (ii). The map accuracy was presented in the form of an error matrix, and the accuracy measures derived were users, producers, overall accuracy equations (5.3)–(5.5), allocation disagreement, and quantity disagreement

(Pontius Jr and Millones, 2011).

$$U_i = \frac{p_{ii}}{p_i} \tag{5.3}$$

$$P_j = \frac{p_{jj}}{p_j} \tag{5.4}$$

$$O = \sum_{j=1}^{q} p_{jj} \tag{5.5}$$

Where U_i represents users accuracy, P_i denotes producer accuracy, and O denotes overall accuracy, subscript i represents the map class (rows), and the subscript represents the reference class (columns) in the error matrix table.

Since the accuracy measurements are based on sample estimates and hence subject to uncertainty (Olofsson et al., 2013), it is necessary to derive the confidence intervals (range of values) for all three accuracy measures. According to Olofsson et al. (2014), the variance estimators for each accuracy measure were obtained using the equations (5.6)–(5.8). The overall accuracy was evaluated based on the point counts while also weighted by each class area. It was useful for assessing the contribution of each class to the overall accuracy assessment.

(i) Overall accuracy

$$\hat{V}(\hat{O}) = \sum_{i=1}^{q} W_i^2 \hat{U}_i (1 - \hat{U}_i) | n_i - 1) \tag{5.6}$$

(ii) User's accuracy of map class i

$$\hat{V}(\hat{U}_i) = \frac{\hat{U}_i (1 - \hat{U}_i)}{n_i - 1} \tag{5.7}$$

(iii) Producer's accuracy of reference class j=k

$$\hat{V}(\hat{P}_j) = \frac{1}{\hat{N}_{.j}^2}\left[\hat{N}_{j.}^2(1-\hat{P}_j)^2\hat{U}_j(1-\hat{U}_j)|n_j - 1 + \hat{P}_j^2\sum_{i\neq j}^{q}\hat{N}_{ij}^2 n_{ij}|n_i.(1-n_i j|n_i.|n_i. - 1)\right] \tag{5.8}$$

Where $\hat{N}_{.j} = \sum_{i=1}^{q}\frac{N_{i.}}{n_{i.}}n_{ij}$ represents the measured marginal total number of pixels of reference class j, $N_j.$ is the marginal total of map class j, and n_j is the total number of sample units in map class j.

5.4 Results

5.4.1 Vegetation Phenological Separability

Seasonality has the most significant impact on the quality of the classification results as the phenological state, which defines the separation of different vegetation types, for example, deciduous trees from evergreen trees or shrubs and grasses. Selecting pixels with the highest NDVI values from the dry season (June to November) enabled the separation of the forest classes from the non-forest land covers. The NDVI values were extracted from the images (June to November) and used to identify the optimal time of the year (August to October) for separating grasses, bushes, and other non-vegetation from the main forest classes (Figure 5.6).

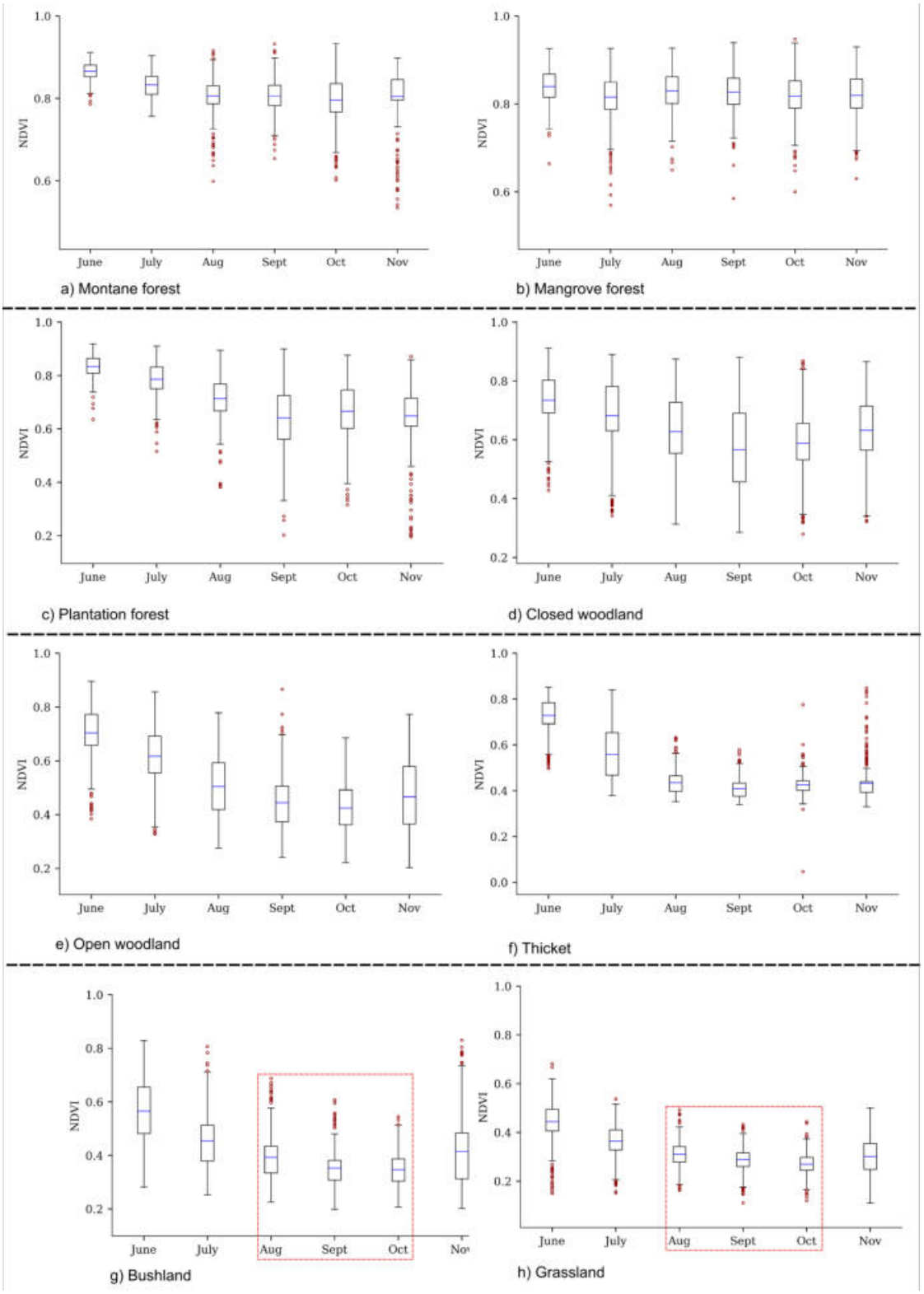

Figure 5.6: A seasonal pattern vegetation separability based on the NDVI. A red box for g and h indicates the lowest NDVI for bushland and grassland from August to October, which supports separation from the forests

5.4.2 Final Image Composite

The FMASK algorithm adequately detected clouds and their shadows (Figure 5.2) from Landsat 8 images to automatically generate a composite image for the Rufiji Basin. The final output images were generated as standardised reflectance and expressed as a standard set of azimuth and zenith angles for the sun and satellite. It hence eliminates the further disparity between illumination and viewing geometry between acquisitions of the image. Only pixels with maximum NDVI values for different vegetation covers were used to produce the composite output image. A total of 72 Landsat 8 images were used to generate the final composite for the Rufiji Basin (Figure 5.7).

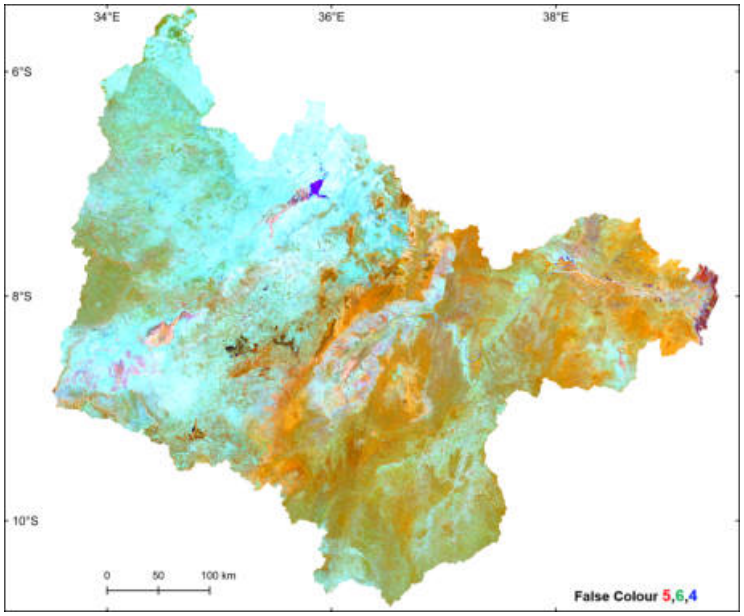

Figure 5.7: Final mosaic composite of Landsat 8 image over the Rufiji Basin

5.4.3 Forest/Non-forest Classification

The forest/non-forest binary classification (Figure 5.8) was evaluated using 6,684 sample points, including 3,706 forest sample points and 2,978 non-forest sample points. Classification accuracy measures for forest-based on sample units had high certainty with the producer's accuracy (PA), and user's accuracy (UA) of 92.47% and 96.50%, respectively. The accuracy metrics show an overall accuracy of 93% $\pm$ 0.02, F1-score of 0.94, and MCC of 0.87 (Table 5.1).

Table 5.1: Classification accuracy measures for the baseline

Cover type	**UA (%)**	**PA (%)**
Forest	96.50 ± 0.00	92.47 ± 0.00
Non - forest	90.82 ± 0.01	95.69 ± 0.00
Overall accuracy	$\mathbf{93.00 \pm 0.02}$	
F1-score	**0.94**	
MCC	**0.87**	

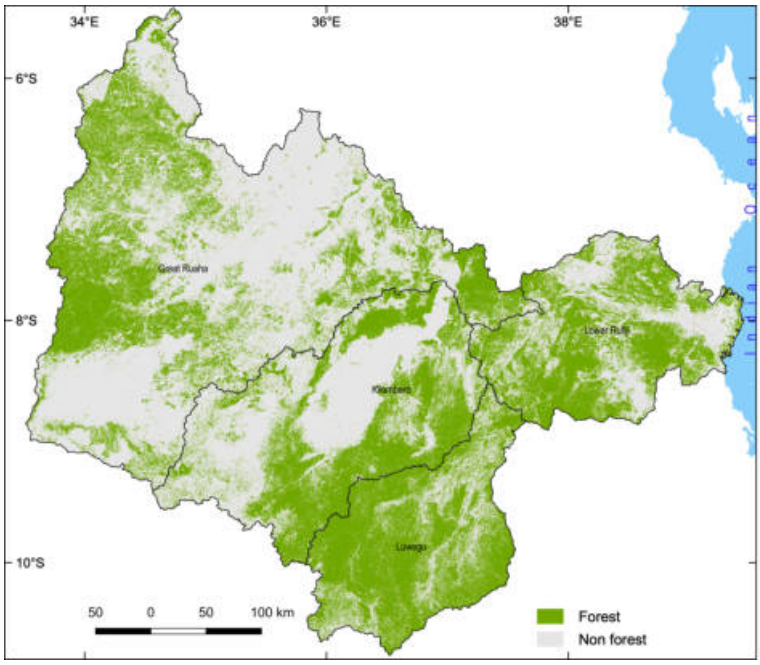

Figure 5.8: Forest/non-forest map of Rufiji Basin

5.4.4 Forest Types Classification

From the forest extent in the basin, the forested area was classified into seven types (Figure 5.9) and the mapped area (Table 5.3). Table 7.7 summarised the accuracy metrics with an overall accuracy of 91%, with a low quantity disagreement of 0.019 and an allocation disagreement of 0.062 between classification and actual ground points. It indicates a rational level of agreement with the reference field data (Figure 5.10 and Figure 5.11).

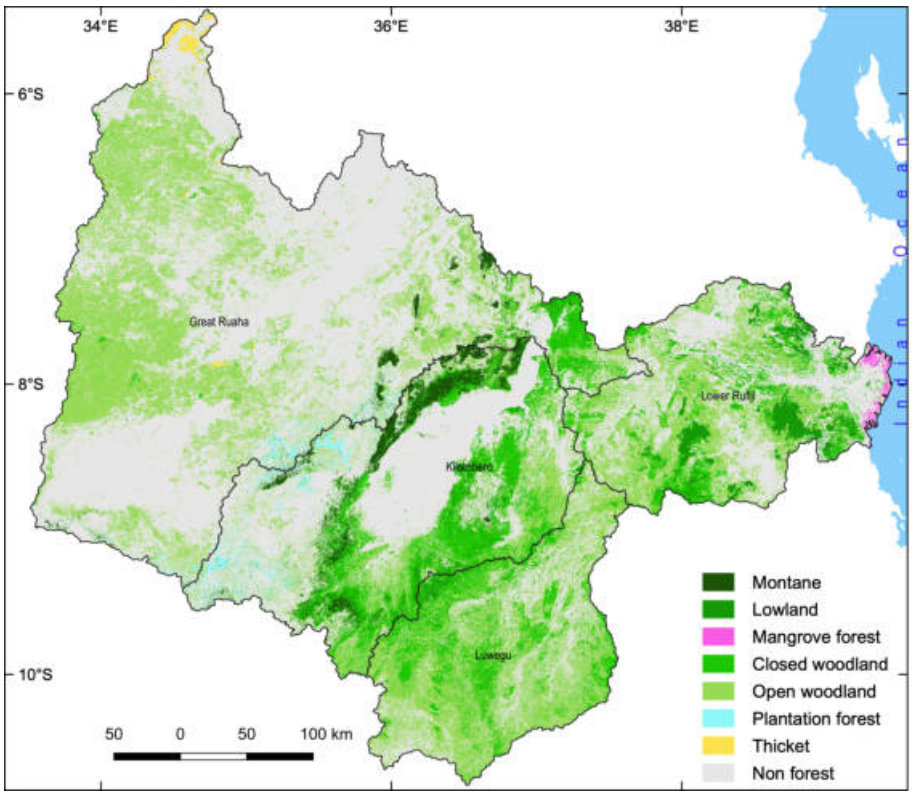

Figure 5.9: Map showing areal proportional of forest types at Rufiji Basin

Table 5.2: Classification accuracy measures

Forest type	**UA(%)**	**PA(%)**
Montane forest	89 ± 0.04	87 ± 0.04
Lowland forest	91 ± 0.03	75 ± 0.04
Mangrove forest	83 ± 0.12	91 ± 0.09
Closed woodland	73 ± 0.03	81 ± 0.02
Open woodland	92 ± 0.01	90 ± 0.01
Plantation forest	87 ± 0.05	78 ± 0.05
Thicket	72 ± 0.24	65 ± 0.08
Non - forest	97 ± 0.00	98 ± 0.00
Overall accuracy	91 ± 0.00	
Allocation disagreement	**0.062**	
Quantity disagreement	**0.019**	

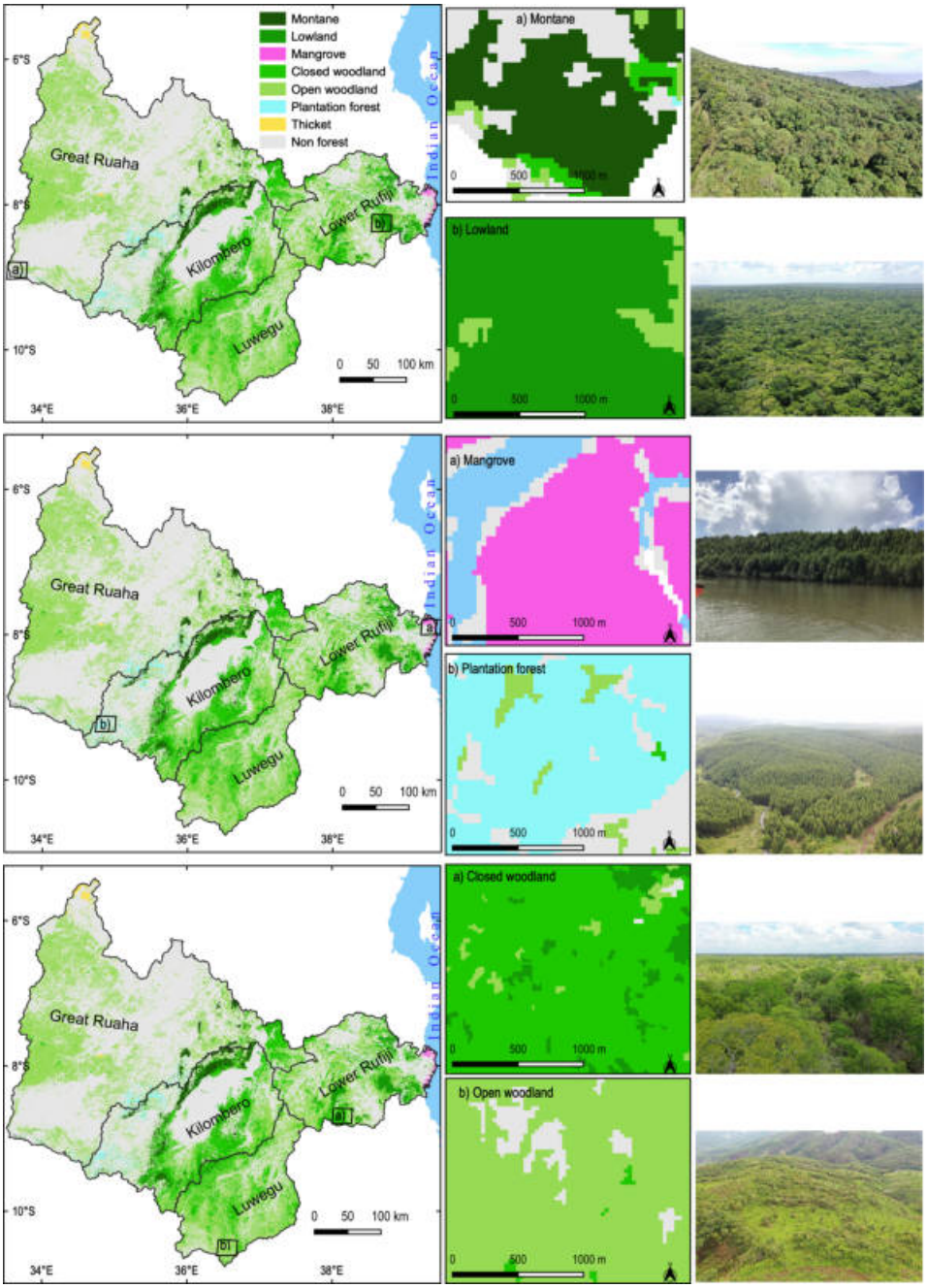

Figure 5.10: An illustration of the detailed samples of classification result for the forest types with a location of ground field photo at Rufiji Basin

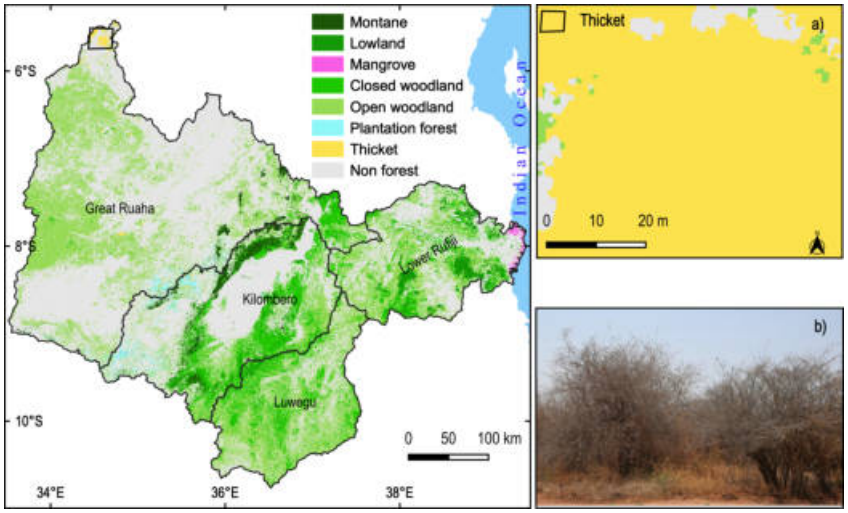

Figure 5.11: An illustration of the detailed sample of classification result for thicket woodland at Rufiji Basin

Table 5.3: Map area for each forest class based on the classification result

Forest type	**Field point**	**Map area (ha)**	**Weight (%)**
Montane forest	182	359,383.32	2.00
Lowland forest	206	484,058.88	2.70
Mangrove forest	37	35,678.34	0.20
Closed woodland	785	1904578.02	10.62
Open woodland	2,270	5,633,552.25	31.42
Plantation forest	149	173,927.34	0.97
Thicket	77	52,179	0.29
Non - forest	2978	9,288,447.12	51.80
Total	6,684	17,931,805.02	100.00

5.4.5 Main Causes of the Classification Errors

During the dry months of September to October, leafless deciduous vegetation in the country's arid areas was misclassified as bright or dark soil (non-forest) (Figure 5.12). It was caused by the low near-infrared response and higher visible reflectance bands compared to the evergreen vegetation and may reduce the forest area. A visual examination of the sample points occurring on the edge of different

forest types caused the omission error from one class or commission error.

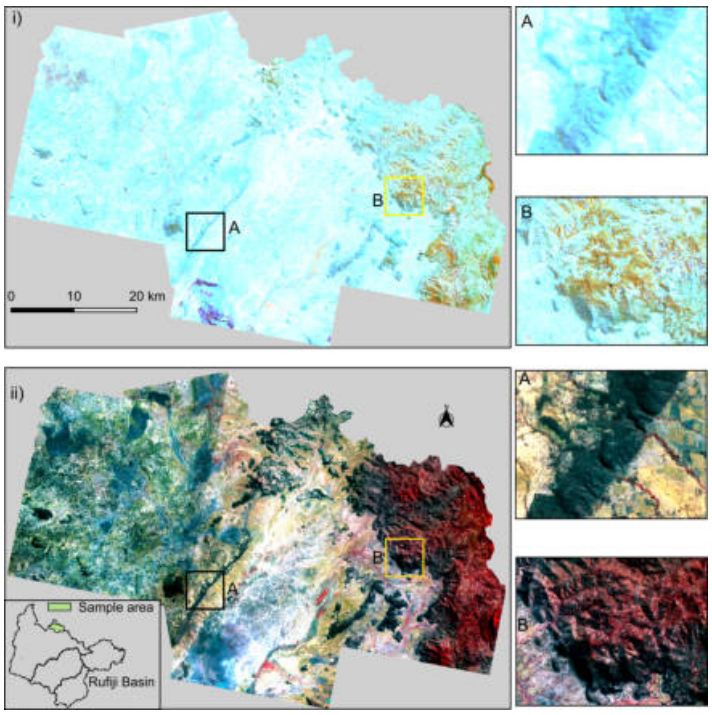

Figure 5.12: Dry season images comparison. Illustrations of (i) Landsat 8 image from a semi-arid area captured during the dry season of the year (August - October) with high soil reflectance depict less forest compared with high-resolution (ii) PlanetScope scene (3 m spatial resolution) captured on 24/06/2019.

5.5 Discussion

5.5.1 Classification Performance

Persistent cloud cover often hinders tropical forest mapping and monitoring with optical data. The proposed automated cloud and shadow detection using the FMASK algorithm and $NDVI_{max}$ image composites have successfully allowed the mapping of the forests within the Rufiji Basin. The overall accuracy for the

forest/non-forest cover was 93%, with a F_1 score of 0.94 and MCC of 0.87 (Table 5.1) with a similar overall accuracy of 91% for the classification of forest types with a low quantity disagreement of 0.019 (Table 7.7). It indicates a rational level of agreement with the reference data.

However, in comparing the MCC and F1-score in evaluating binary classification, MCC reduced the accuracy by 7% compared to F1-score. Yet, MCC could be a reliable measure of certainty for forest binary classification because its accounts for the comparative of both positive components and the negative elements in the dataset (true positives, false negatives, true negatives, and false positives) (Chicco and Jurman, 2020).

5.5.2 Potential Forest Areas in the Basin

The maps shown in Figures 5.8 and 5.10, present the forested area in Rufiji Basin, which was mapped as 8,643,358 ha for 2017. The major forested area found in the eastern part of the basin comprises of the sub-basins of Kilombero, Luwengu, and lower Rufiji (Figure 5.8). The classification results indicate that the woodland class (open and closed woodland) constitutes 42.04% of the study area (Table 5.3). It is associated with an ecological niche, primarily associated with climate and a diverse set of environmental conditions which may occur in a mosaic with other forest types (Abdallah and Monela, 2007). As such, the availability of the protected areas network in the basin enhances forest cover and could be important in protecting the country's remaining forests (Riggio et al., 2019; Pfeifer et al., 2012; Brockington, 2007).

5.5.3 Implications for Informing Conservation Planning

Rufiji Basin harbours the world-famous tropical montane rivers, descending from the montane forests, including the Eastern Arc Mountains feeding major rivers, floodplains, and ocean (Encalada et al., 2019). From the classification maps, the extent of the forest in the Rufiji Basin is about 48.20% of the total area, and montane forests occupy 2%, providing vital ecosystem services to the livelihood of the area's inhabitants.

Similarly, the construction of immense hydropower at Stiegler's Gorge in the Rufiji Basin (Duvail et al., 2014) will depend on forest conservation in the catchment, especially upland forests, to reduce siltation. However, also to the Selous Game Reserve, is home to a wealth of flora and fauna for the long-term resource sustainability base for the nation at large. Consequently, these forests' management demands that management decisions are based on the most reliable scientific information possible. Therefore, it is proposed that similar information to that derived here for the Rufiji Basin should be derived for the whole country of Tanzania as an operational tool for monitoring forest mapping at wall-to-wall coverage.

Establishing a forest baseline extent provides a road map for the assessment of forest cover change to be covered in the subsequent chapters. The output maps developed can be applied to assessing the deforestation in the country and predicting the location and future deforestation rates. It will inform the design of government policy and provide a baseline for examining forest conservation programmes such as REDD+. Similarly, it can also be used to analyse protected area management effectiveness.

5.5.4 Limitations

Although a high level of accuracy was attained for both binary forest/non-forest and forest type classification, there were errors in the classification results due to season variability (Figure 5.12). For example, this study's images were sourced from the dry period, and Rufiji Basin consists of different climatic zones influencing both forests and woodlands. Therefore, the selection of images should be considered differently among climatic zones. For instance, images from semi-arid areas (Figure 5.12) should be selected around June - July (Table 4.1) before the complete shedding of leaves to reduce high soil reflectance and minimise forest areas' underestimation.

5.5.5 Direction for National Forest Mapping and Monitoring

5.5.5.1 Image Composite and Individual Scene Classification

The image mosaic composite has the advantage of reducing data volume and therefore processing time for the classification process with small area coverage. However, in some cases, this also reduces the variability between the classes which are present within individual scenes. Moreover, creating just a single output image means that any errors within that composite (e.g., missed clouds or cloud shadows) directly result in errors in the final classification. Therefore, it is proposed that an individual scene-based approach is considered where the scenes are classified independently, and the resulting classification is merged or composited rather than compositing the reflectance data.

5.5.5.2 Image Segmentation versus Pixel-Based Classification

Within the literature, the number of studies making use of segmentation-based approaches versus pixel-based approaches is mixed with no clear consensus as to the optimal solution. Segmentation-based approaches in effect compress the image data, therefore, resulting in fewer classification decisions. However, the segmentation has also predefined the class boundaries between classes, and without clearly defined and spectrally distinct boundaries can result in classification error. For example, the boundary definition between open and closed woodlands was poorly defined by the segmentation. Additionally, classes with a small geographic extent (e.g., mangroves or montane forests) within the area to be classified might only result in a small number of segments available to train a classifier and due to the need to balance the number of training samples between the classes provided to the classifier can result in an overall reduction in the classifier performance. Therefore, a pixel-based approach rather than a segmentation-based approach might also be considered when producing the national map.

5.5.5.3 Choice of Classifier

The Extremely Randomized Tree Classifier was used, and it achieved high-quality results across the basin for both the forest/non-forest and forest-type classifications. However, the classifier is limited in the amount and variability of the training data which can be provided and used by the classifier. Alternative approaches, such as the XGBoost classifier, can use much larger training datasets. Larger training datasets could easily be generated if the analysis was performed on an individual scene basis using a per-pixel-based approach.

5.5.5.4 Forest Habitat Suitability Analysis

For the forest type classification, reducing the number of classes the classifier is comparing to make a decision will result in an increase in classification accuracy and avoid extreme errors such as mangroves being classified on top of a mountain, for example. The forest types in Tanzania have defined ecological niches. Identifying and mapping those niches could significantly improve the resulting forest types classification when scaled nationally.

Establishing the areas which are potentially suitable habitats for the different forest types is also useful for biodiversity conservation, policy-making, and climate change mitigation (Bonan, 2008; Gibbs et al., 2010). Forest habitat suitability models are increasingly used as planning tools for highlighting potential forest conservation areas. It is, therefore, useful to complement remote sensing data on forest mapping and monitoring with information about suitable forest habitats. For example, forest restoration efforts (Seidl et al., 2017; Tobón et al., 2017) will require habitat suitability models considering the requirement of forest species across the landscape in the context of current and future climates.

5.6 Conclusions

The method described in this study presents an initial technique for generating forest / non-forest and forest types mapping in a robust manner using data and software which is affordable and scaleable across the Rufiji Basin. The progress of remote sensing technologies can provide periodic observations for inconsistent forest statistics, fill critical data gaps, and ensure data availability. Utilising the

open-source approach for processing and analysis will enable users, such as land management agencies in forestry, to benefit from freely available software products and access to source code as new algorithms can be integrated and managed.

The method has been implemented on Landsat 8 data but is entirely compatible with different Landsat TM and ETM+ and Sentinel-2 images. The high accuracy achieved (91 - 93%) demonstrates the potentiality of the proposed method in distinguishing between the dominant forest cover types in areas with limited Earth Observation data due to frequent cloud cover. However, areas for improvement include testing other machine learning classifiers such as extreme gradient boosting (XGBoost) and Light Gradient Boosting Machine (LightGBM) (Chen and Guestrin, 2016; Ke et al., 2017) since a limited number of studies have used these classifiers in tropical forest mapping with few focused on crops mapping (Ustuner and Balik Sanli, 2019). Additionally, moving away from image composites might also provide an advantage, where errors in the cloud and cloud shadow masking result in areas of composites having poor image quality. While processing individual scenes might provide an option for avoiding the generation of image composites, it will require significantly more data processing. Finally, while a segmentation-based approach was used for this study, some of the open forest boundaries were relatively poorly defined by the segmentation. Therefore pixel-based approaches might be considered.

Chapter 6

Climate Change and Tanzanian Forests

This chapter is based on:

John, E., Bunting, P., Hardy, A., Roberts, O., Giliba, R., Silayo, D. S., 2020. Modelling the impact of climate change on Tanzanian forests. *Diversity and Distributions* 26:1663-1686, https://doi.org/10.1111/ddi.13152.

6.1 Introduction

Tropical forests form the most abundant terrestrial reservoir of carbon storage and biodiversity (Newmark, 2006), but have experienced climate change impact, deforestation, and habitat fragmentation (Bonan, 2008; Gibbs et al., 2010). The projected increase in global mean temperature of $4.3 \pm 0.7\ ^0$C by 2100 for RCP8.5 is likely to further affect the geographic distribution, composition, and productivity of tropical forest ecosystems (IPCC, 2014) adversely affecting vital ecosystem services. Sub-Saharan Africa has been identified as one of the most vulnerable parts of the world to the effects of climate change (Serdeczny et al., 2017; Chidumayo et al., 2011). Climate change is predicted to increase hazards such as flood and fire hazards, disease, food insecurity, and habitat degradation (Serdeczny et al., 2017).

The effects of climate change on African tropical forest habitats mostly result from changes in precipitation patterns (particularly the influence of the El Niño-Southern Oscillation (ENSO)) (Butt et al., 2015) and the Subtropical Indian Ocean Dipole (SIOD) and subsequent effects on soils and groundwater availability (Müller et al., 2014), alongside increases in atmospheric availability of CO_2 concentration and nitrogen deposition (Serdeczny et al., 2017). Even though the effect of climate change has already been felt, its impact on the tropical forests remains relatively understudied (Pacifici et al., 2015; Delire et al., 2008; Markham, 1998), especially in resource-poor sub-Saharan Africa where data is scarcely creating a barrier to incorporating climate change scenarios into land management and conservation planning (Lee and Jetz, 2008).

Increasingly, global initiatives and commitments are considering African tropical forests as critical components of climate change mitigation strategies such as the Bonn Challenge on Forest Landscape Restoration (FLR) (Seidl et al., 2017), the UNFCCC on REDD+(Romijn et al., 2012), the Rio+20 land degradation neutrality (Grainger, 2015), Aichi Target 15 on the restoration of degraded ecosystems (Tobón et al., 2017), and the 2030 agenda of the United Nations for Sustainable development goals (SDGs) 13 and 15 (Swamy et al., 2017). To ensure that these strategies are successful and enable effective conservation it is essential to establish a baseline in terms of forest habitat extent and resilience to climate change pressures (Verdone and Seidl, 2017; Clark et al., 2014). This should be determined in a scalable and tractable manner, including modelling projections of future distributions to bridge the gap of data deficiency regarding Sub-Saharan forests (Montagnini et al., 2005).

Habitat Suitability Modelling (hereafter referred to as HSM) or Species Distribution Modelling is widely applied in estimating changes in habitat suitability and counteracting negative impacts of climate change (Lim et al., 2018; Title and Bemmels, 2017; Edenius and Mikusiński, 2006). It represents a valuable tool for informing policy-makers about the effects of climate change on the forest community (Seidl et al., 2017). HSM focuses on identifying both the most influential environmental and climatic variables describing the presence/absence, abundances, or even growing conditions of forest species and the optimal relationships between their distributions and these explanatory variables (Jiménez-Alfaro et al., 2018). The provision of environmental and climatic variables from globally, often freely, available Earth Observation (EO) datasets, enables simulations and subsequent information to be determined over scales that are suitable for national, regional,

and even global decision-making (Edenius and Mikusiński, 2006).

Maximum Entropy (MaxEnt) modelling (Phillips et al., 2006; Renner and Warton, 2013) has been used to successfully predict forest species habitat suitability under current and future climate scenarios for a range of sites across the world. For example, climate change impacts on forest habitat suitability and diversity in the Korean Peninsula (Lim et al., 2018); how much does climate change threaten European forest tree species distributions (Dyderski et al., 2018); climate change impact on the distribution of Dipterocarp trees in Asia (Deb et al., 2017); induced range shift in miombo woodland due to climate change in Southern Africa (Pienaar et al., 2015). However, most of these studies are limited to a single-tree species, lacking multiple tree species (such as Jiménez-Alfaro et al., 2018; Edenius and Mikusiński, 2006; Rondinini et al., 2005). In contrast, modelling multiple-tree species tend to yield better results (Edenius and Mikusiński, 2006) as this approach relies on detecting the shared pattern of the environment response for sparsely recorded species, thereby simplifying intricate species-specific patterns. It also enables direct interpretation by decision-makers (Ferrier and Guisan, 2006) that would typically be at the community level, except for studies into particular threatened species (Brummitt et al., 2015).

Approaches like MaxEnt rely on the availability of species or habitat presence data, typically based on field observations of a particular species or habitat. In the United Republic of Tanzania, the National Forest Inventory (NFI) provides a comprehensive dataset that includes over 19 thousand observations of forest types with over 50 thousand points for dominant forest types in overall ecological zones across the country (Tomppo et al., 2014; Minunno et al., 2019; Storch et al., 2018) providing an exciting opportunity to provide baseline maps of forests and

woodlands extent and the subsequent influence of climate change (Lim et al., 2018).

This study uses MaxEnt to map the distribution of forest types in Tanzania centered on two climate Representative Concentration Pathways (RCPs) scenarios (RCP4.5 and RCP8.5) and the future period of 2055 and 2085. Specifically, this chapter addresses the following research questions:

1. What are the vital climatic factors that affect the distribution of forest types based on dominant tree species in Tanzania?
2. What are the impacts of climate change on the distribution of the prevalent tree species habitats?
3. What are the implications for changes in the distribution of forest habitats on the conservation of globally significant indigenous flora and fauna?

6.2 Methods

A piece of detailed information on the study area is discussed in Chapter 3 and Figure 6.1 for the distribution of the presence points for dominant tree species from natural forest types in Tanzania (Figure 6.2).

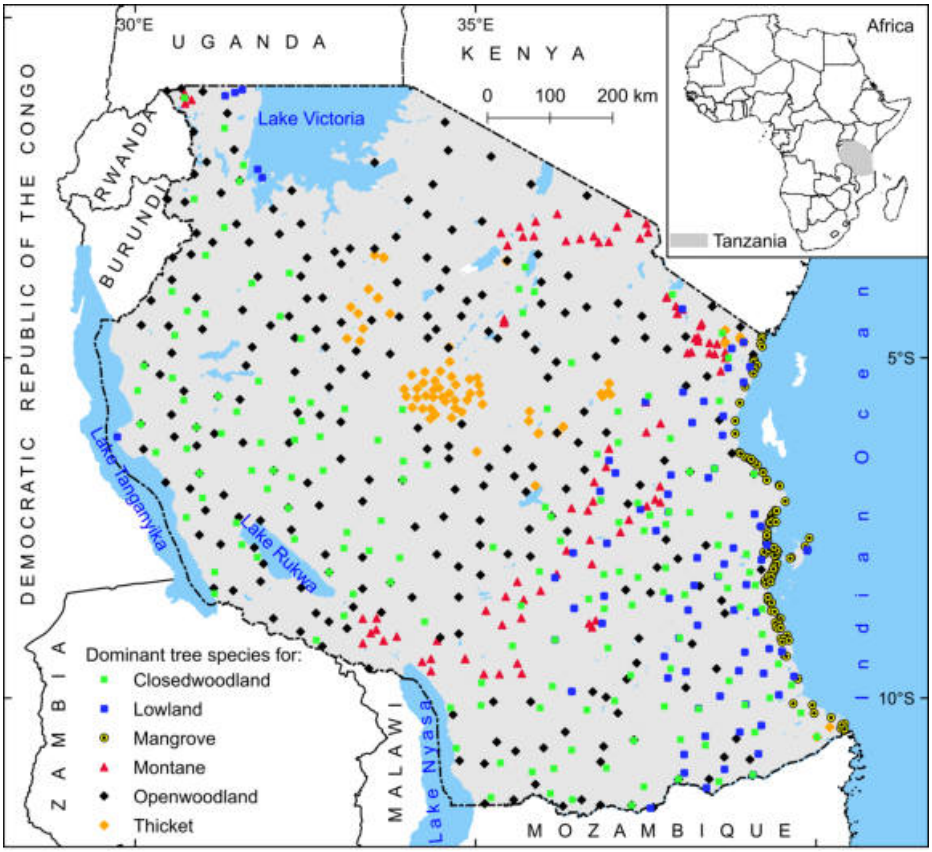

Figure 6.1: Distribution of the presence points for dominant forest types in Tanzania. EPSG: 4326, WGS84 projection

.

Table 6.1: Descriptions and main characteristics of the natural forest types in Tanzania

Level 1	**Level 2**	**Description**	**Altitude(m)**	**Crown cover(%)**	**Height (m)**
Forest	Montane	Catchment forests found in mountainous areas and changes with elevation	1400 – 1850	≥ 40	> 5
	Lowland	Include groundwater forest and mainly located near the coast of the Indian ocean and in small portion of the mixture with woodlands and montane forest	540 – 810	> 40	> 5
	Mangrove	Grow on the upper part of the inter-tidal zone of the sheltered shores of the delta, alongside the river estuaries and the creeks, mainly along the Indian Ocean. May occur with other wooded land vegetation	≤ 25	> 40	≥ 5
Woodland	Closed	Dominated with perennial C4-grasses which induce regular fire occurrences in the month of May to November before rain season	100 – 1400	> 40	> 5
	Open	The same description as closed woodland with the difference in canopy cover	100 – 1400	10 – 40	≥ 5
Thicket	Thicket	Dense evergreen or deciduous thorn woodland. Grow interlocked and make impassable community	1244 – 1300	5 – 10	< 5

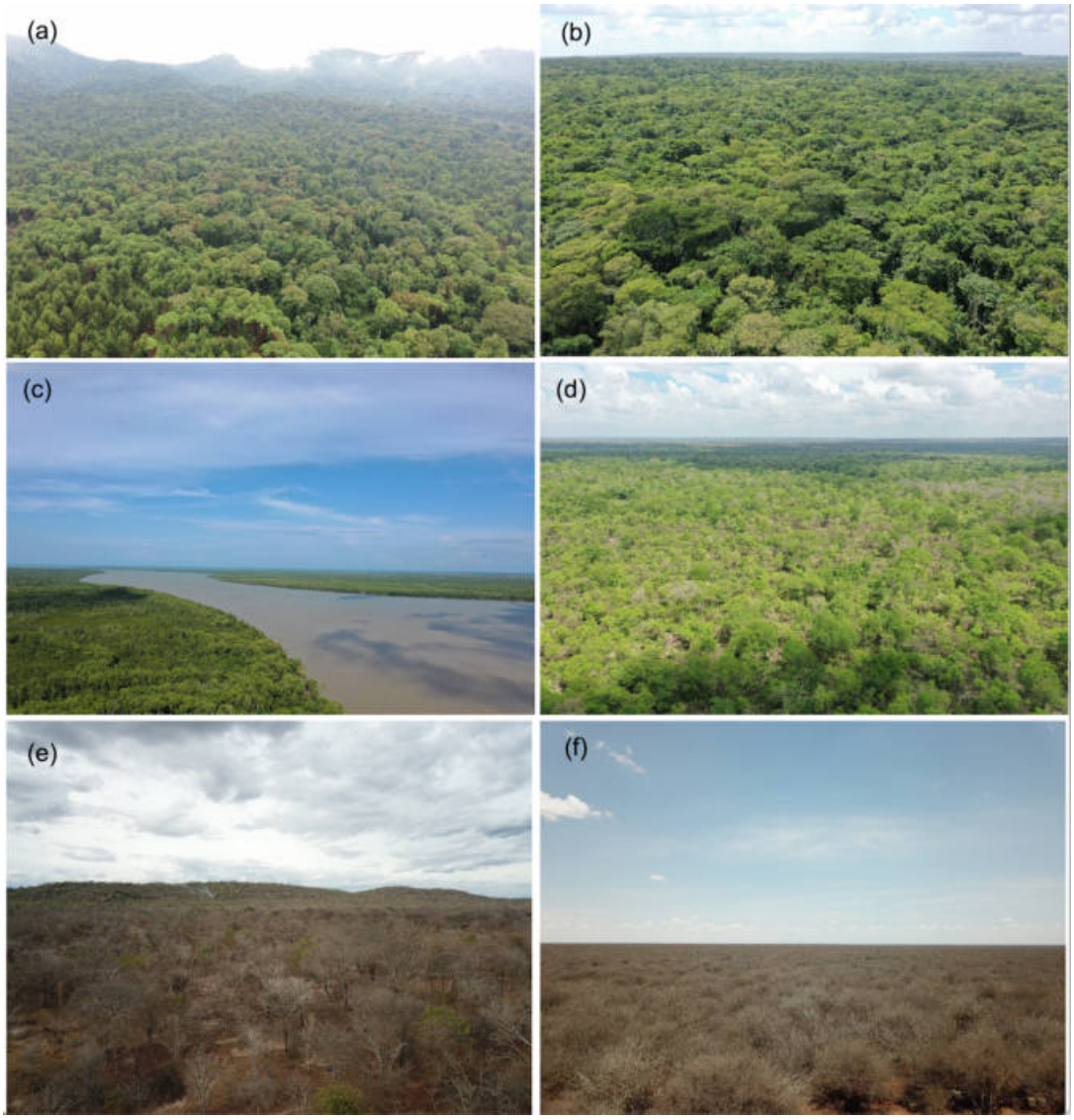

Figure 6.2: Aerial photographs for the natural forest types in Tanzania based on drone capture (height $\approx$ 60 m), October 2019: (a) montane forest, (b) lowland forest (c) mangrove forest, (d) closed woodland, (e) open woodland and (f) thicket

6.2.1 Datasets

6.2.1.1 Forest occurrence data

A piece of detailed information on forest occurrence records is discussed in Chapter 4. The dominant forest types (59,208 points) were selected as proxy indicators of habitat types for different existing forest types and dependent species (e.g., epiphytes of montane forests). Therefore, when dominant species change, this may impact connected species in the ecosystem. Hence, they provide long-term forest monitoring of habitat in response to climate change (Dyderski et al., 2018). The presence-only records were chosen based on abundance from the plot measurements for each forest type (Figure 6.2 and Table 6.1). The selection included both percentage frequency (occurrence) and abundance (proportional of individuals). This implies that only the most frequent and abundant species from each forest type were selected. The Plantation forest was excluded from the analysis as their habitat changes are mainly the result of different non-climatic anthropogenic drivers such as land management decisions (e.g., Bodin et al., 2013).

6.2.1.2 Spatial rarefaction

Geographical bias in the habitat or species occurrence data is likely to result in model overfitting and artificial inflation of model performance (Boria et al., 2014; Veloz, 2009). Therefore, the original 59,208 dominant forest-type points underwent a step-wise spatial rarefaction process, based on the random selection of a single location within grids of increasing size (Brown et al., 2014). Specifically, a 5 x 5 km fishnet grid was created over the entire extent, to produce a single

distribution point selected in each grid, with at least the distribution points be at 5 km apart. It was performed for each forest category separately to avoid eliminating too many observations from less extensive forest types, such as mangrove and montane. This procedure resulted in the selection of 1,307 occurrence points (n = 103 montane, n = 276 lowland, n = 168 mangrove, n = 378 closed woodland, n = 301 open woodland, and n = 81 thicket) that were considered to be spatially independent.

6.2.1.3 Environmental variables

The selection of environmental variables was based on a conceptual model that encompasses factors deemed to control the presence, or in some cases, absence, of a particular species (Jiménez-Alfaro et al., 2018). In this instance, the variable selection was based on the parameters that control the physically-based forest growth model 3-PG (Physiological Principle in Predicting Growth) (Landsberg and Waring, 1997; White et al., 2006). The use of the 3-PG model provides a robust approach to understanding the growth dynamics of forests based on an ecosystem's physiological processes (White et al., 2006). It incorporates the dimension of climatic changes in the growth and productivity prediction to understand the impact of climatic variations on the forest's ecosystem (Franklin et al., 2016). This can be used to evaluate site potential and analyze the probable effects of varying growing distribution under changing climatic conditions. The 3-PG model performs well for a diverse range of conditions for many forest types and species and can be integrated with other models and approaches in order to widen its functions and applications (Gupta and Sharma, 2019). The model includes a large number of parameters, but the selection was limited to those parameters listed in

Table 6.2.

Table 6.2: Environmental variables are based on the 3-PG model and bold abbreviated variables are used in the final model after testing for collinearity using a pairwise Pearson correlation.

Variable name	Explanation	Unit
PET seasonality **(PETseason)**	Monthly variability in potential evapotranspiration	mm/month
PET Warmest Quarter **(PETWarmQ)**	Mean monthly PET of warmest quarter	mm/month
PET wettest quarter **(PETWetQ)**	Mean monthly PET of wettest quarter	mm/month
Thermicity index **(ThermicitI)**	Sum of mean annual temp., min. temp. of the coldest month, max. temp. of the coldest month, x 10, with compensations for better comparability across the globe	^{0}C
Elevation **(Elv)**	Height above or below sea level	m
Terrain ruggedness index **(Tri)**	Calculates the difference in elevation values from a center cell and the eight cells immediately surrounding it	m
Topographic wetness index **(TopoWet)**	This quantifies topographic control on the hydrological process	-
Soil water availability capacity **(SoilwaterA)**	Plant available water holding capacity (v%) of the soil	mm
Soil types **(ST)**	Characterised by a variety of textures and nutrients	-
Potential evapotranspiration **(PET)**	Amount of evaporation taking place when sufficient water is available	mm
Mean annual temperature **(Bio1)**	The average temperature for each month	^{0}C
Mean annual rainfall **(Bio12)**	This is the sum of all total monthly precipitation values	mm
Rainfall wettest month **(Bio13)**	This index identifies the total rainfall that prevails during the wettest month	mm
Rainfall driest month **(Bio14)**	This index determines the total precipitation that prevails during the driest month	mm
Annual moisture index **(Mi)**	Mean annual rainfall/Potential evapotranspiration	-

Current and future bioclimatic variables were obtained from the KITE dataset (AFRICLIM)[1] (Platts et al., 2015). Future climate data were ensemble mean downscaled to the resolutions ($\approx$ 1 km) using 18 pairwise combinations of five regional climate models (RCMs) driven by 10 general circulation models (GCMs). A detailed explanation of data downscaling is found in Platts et al. (2015). The

[1] https://webfiles.york.ac.uk/KITE/AfriClim/ByCountry/Tanzania/

ensembles were projected under two RCPs (RCP4.5 and RCP8.5) based on the Fifth Assessment Report (AR5) of the United Nations Intergovernmental Panel on Climate Change (IPCC). It represents independent trajectories on emissions, socioeconomic, and policy (Moss et al., 2010). RCP4.5 is an intermediate stabilizing pathway of the average 2041–2070 referred to as RCP4.5–2055, and it is the optimistic pathway without an overshoot scenario at 4.5W/m^2 ($\approx$ 650 ppm CO_2 eq.) by 2100 (Wise et al., 2009). It supports climate policies on reducing emissions, with moderate population and economic growth with reforestation programmes, and increases areas of natural vegetation (Van Vuuren et al., 2011b). RCP8.5 as a long term was the average of 2071–2100 referred to as RCP8.5–2085, and it is a pessimistic pathway with rising radiative forcing pathway leading to 8.5W/m^2 ($\approx$ 1370 ppm CO_2 eq.) by 2100 (Moss et al., 2010). This scenario assumes no policy change to reduce emissions, with high population growth, low income, increased energy demand, and deforestation, especially in the least developed countries (Riahi et al., 2011; Hurtt et al., 2011).

Other variables selected included those related to terrain and soil characteristics. The Shuttle Radar Topography Mission (SRTM) 1-arc second elevation data were obtained from the USGS Earth Explorer to generate a terrain ruggedness index, a proxy measure of topographic heterogeneity (Riley et al., 1999). Soil characteristic variables were obtained from the World Soil Information (ISRIC)[2] included soil type (see Appendix 1 as Table A.1) (Hengl et al., 2015). Pairwise Pearson correlation (r) was used to test for collinearity between predicting variables, taking a relationship r $>$ 0.7 or $<$ -0.7 as highly correlated (Dormann et al., 2012; Braunisch et al., 2013) (see Appendix 1 as Table A.2). Table 6.3 summarizes the

[2] https://www.isric.org

general statistics of the selected bioclimatic and topographic profiles of dominant forest types under current conditions based on the occurrence data used in this study.

Table 6.3: Summary statistical information for major bioclimatic profiles of dominant forest types based on the occurrence data used in this study. Bio1: Mean annual temperature; Bio12: Mean annual rainfall; Bio14: Rainfall driest month; Elv: Elevation; Tri: Terrain ruggedness index

Forest type	Dominant tree	Code	Unit	Mean	SD	Min.	Max.
Montane	*Ekerbergis capensis*,	Bio1	^{0}C	17.01	0.10	10.40	26.10
	Olea capensis, *Albizia*	Bio12	mm	1247.61	10.72	850.00	2686.00
	gummifera, *Ocotea*	Bio14	mm	14.80	0.64	0.00	66.00
	usambaraensis,	Elv	m	1760	19	235	3039
	Newtonia buchananni	Tri	m	92.11	1.94	8.38	229.88
Lowland	*Antiaris toxicaria*,	Bio1	^{0}C	24.72	0.04	15.00	27.30
	Scorodophloeus	Bio12	mm	1219.44	6.47	610.00	2735.00
	fischeri, *Soriendea*	Bio14	mm	11.20	0.33	0.00	56.00
	madagascariensis,	Elv	m	363.32	7.34	9.00	2377.00
	Milletia stuhlmannii,	Tri	m	36.40	1.20	1.12	279.25
Mangrove	*Milicia excelsa*	Bio1	^{0}C	26.69	0.04	25.90	27.50
	Avicennia marina, ,	Bio12	mm	1342.84	4.46	992.00	1869.00
	Sonneratia alba,	Bio14	mm	17.00	0.15	7.00	49.00
	Rhizophora mucronata	Elv	m	8.82	0.08	1.00	22.00
		Tri	m	2.60	0.06	0.12	2479.80
Closed woodland	*Brachystegia speciformis*,	Bio1	^{0}C	22.56	0.01	13.7	27.20
	Julbernardia globiflora,	Bio12	mm	1139.84	1.16	556.00	2377.00
	Brachystegia microphylla,	Bio14	mm	1.64	0.01	0.00	35.00
	Erythrophleum africanum,	Elv	m	1040.06	2.00	14.00	2039.00
	Burkea africana	Tri	m	29.96	0.16	0.38	248.12
Open woodland	*Combretum spp*,	Bio1	^{0}C	22.97	0.01	13.90	27.30
	Acacia spp,	Bio12	mm	1021.89	1.86	519.00	2715.00
	Commiphora spp,	Bio14	mm	3.59	0.04	0.00	48.00
	Lonchocarpus sp,	Elv	m	942.05	3.54	10.00	2276.00
	Lannea spp,	Tri	m	22.88	0.21	0.25	231.12
Thicket	*Terminalia spp*	Bio1	^{0}C	22.19	0.10	20.10	25.60
	Pseudoprosopis fischeri,	Bio12	mm	766.08	11.45	566.00	1243.00
	Combretum celastroids,	Bio14	mm	3.27	0.80	0.00	38.00
	Dicrostachys cinerea	Elv	m	1160.47	28.57	106.00	1516.00
		Tri	m	8.78	0.67	2.38	45.38

6.2.2 Forest modelling

The modelling process focused on forest types (Table 6.1, Figure 6.2) based only on dominant tree species (Table 6.3). The inventory data adequately presented the distribution of forest types at different compositional gradients to predict suitable

habitats for both current and future climates. The approach involves modelling forest types independently and then ensemble the results (Ferrier and Guisan, 2006). In this manner, the distribution of forest types can be predicted in a grouped way based on the trait characters (D'Amen et al., 2017). The method follows the assumption that similar populations group have the same response to the environmental gradients based on the relative importance of environmental-predictors (Rose et al., 2016).

6.2.2.1 MaxEnt modelling and calibration

MaxEnt software version 3.4.1 (Phillips et al., 2017) was used to model forest and woodland types at the national scale. The data (occurrence and environmental data) were prepared using QGIS 3.6 version[3] and the Remote Sensing and GIS software library (RSGISLib; (Bunting et al., 2014)[4].

MaxEnt simulations were performed for each forest type using 50 replicates with 10,000 randomly sampled pseudo-absence points. The maximum number of iterations was set to 1000, while the convergence threshold was defined at 0.001, to enable each replicate to converge within an acceptable time frame. Cross-validation was used to partition the 1,307 occurrence records for model calibration and evaluation purposes, whereby 75% of the occurrence records were used for model calibration while the remaining 25% were retained for model validation.

A regularisation multiplier of one was used to limit model overfitting and enable the formulation of smooth response curves (Merow et al., 2013). The log-log (clog log) output format was selected based on a sampling design that typically reflects

[3] https://www.qgis.org
[4] https://www.rsgislib.org/

the presence of localities and abundance of each dominant tree specie (each forest type) per quadrant at the presence probability of 0.63 (Phillips et al., 2005) and the location of occurrence is well estimated (Phillips et al., 2017). A jackknife approach was used to examine the importance of each variable contribution to the potential distribution of vegetation types (Olivier et al., 2013).

6.2.3 Construction of baseline and change maps

The final habitat suitability maps were generated by transforming the continuous probability values, ranging from 0 to 1 representing low and high probability, respectively, to discrete values of being either suitable or not suitable for the baseline. Following Spiers et al. (2018), the 10^{th}-percentile training presence threshold was used to define suitable and unsuitable habitats for current and future projections. The future predicted habitat is calculated, for each forest type and taken as the difference between the baseline model and the future models to generate change maps (Maharaj and New, 2013) at RCP4.5 and RCP8.5, respectively, and presented with four predicted habitats of unsuitable, suitable, expansion and contraction (Table 6.4).

Table 6.4: Summary of predicted habitat suitability changes for the forest types

Pixel value			
Baseline	**Future**	**Predicted habitat suitability change**	**Description**
0	0	Unsuitable (no change)	Not suitable habitat at the current and future climate
0	1	Expansion (gain)	Not suitable habitat at the current climate but may be suitable in the future climate
1	0	Contraction (loss)	Suitable habitat at present but not in the future climate
1	1	Suitable (stable, no change)	Suitable habitat at both, current and future climate

6.2.4 Model performance evaluation

The models were evaluated using the qualitative statistic for the Area Under the Curve (AUC) of the Receiver Operating Characteristic (ROC) curves of the test data for the predicted mean accuracy model output for each forest type (Merow et al., 2013; Fielding and Bell, 1997). Model over-fitting was quantified using $AUC_{DIFF} = AUC_{training} - AUC_{testing}$ (Warren and Seifert, 2011) with excellent model performance when AUC_{DIFF} is close to 0 (Bosso et al., 2016).

6.2.4.1 Baseline model accuracy assessment

AUC values have received criticism as they are vulnerable to overinflation of model performance where spatial autocorrelation exists within the model variables and where a modelled habitat niche is small relative to the extent of the modelled area (Williams et al., 2015). To alleviate these issues, an independent measure of model

accuracy using the forest tree species data was conducted, removed during the spatial rarefication process, including a total of 57,901 points. The agreement was quantified using three metrics: 1) Overall % accuracy and associated confidence interval (CI) (Olofsson et al., 2014; Pontius Jr and Millones, 2011), 2) F1 score index which depicts the harmonic mean among precision (p) and recall (r) for each class (Sofaer et al., 2019) and 3) Matthews Correlation Coefficient (MCC), which is explained in terms of True Positive (TP), True Negative (TN), False Positive (FP) and False Negative (FN) (Boughorbel et al., 2017).

6.3 Results

6.3.1 Model performance and habitat suitability estimation

Mean test AUC score demonstrated a high degree of accuracy (AUC $>$ 0.9) for modelling the suitability of montane, lowland, mangrove forests and thicket (Table 6.5, Figure 6.3a-c, Figure 6.5). Closed woodland also showed a good level of accuracy (AUC = 0.72) (Table 6.5, Figure 6.4a). The relatively low standard deviation in AUC (ranging from 0.005 to 0.082) demonstrated a degree of model stability (Table 6.5). The models for open woodland calibrated inadequately (AUC = 0.6) (Table 6.5, Figure 6.4b). This result was expected since open woodlands are dynamic with an unconstrained habitat niche, leading to a great deal of overlap with other forest communities, especially closed woodland, lowland, and thicket. The results of the accuracy assessment using an independent dataset also indicated a good level of agreement. A mean overall accuracy of 90% ranging from 85% to

97%, F1 score of 0.9 (range of 0.84 to 0.98) and an MCC mean value of 0.83 ranging from 0.75 to 0.95 (Table 6.6) were attained. Therefore, the accuracy metrics indicated that the models are reliable to explain the potential habitats of the dominant tree species and can effectively reflect the distribution of the forest types in Tanzania in the present and future time. The main source of confusion occurred along the boundaries between forest types. These transitional zones rarely occur as sharp boundaries and are therefore likely to include a mix of forest types.

Table 6.5: Model performance evaluation under AUC for the potential distribution of forests and woodlands

Forest type	AUC_{test}	AUC_{DIFF}	AUC_{SD}	Cloglog threshold
Closed woodland	0.72	0.056	0.082	0.425
Open woodland	0.60	0.068	0.079	0.479
Montane	0.96	0.003	0.014	0.245
Lowland	0.93	0.007	0.021	0.325
Mangrove	0.97	0.000	0.005	0.521
Thicket	0.92	0.012	0.039	0.183

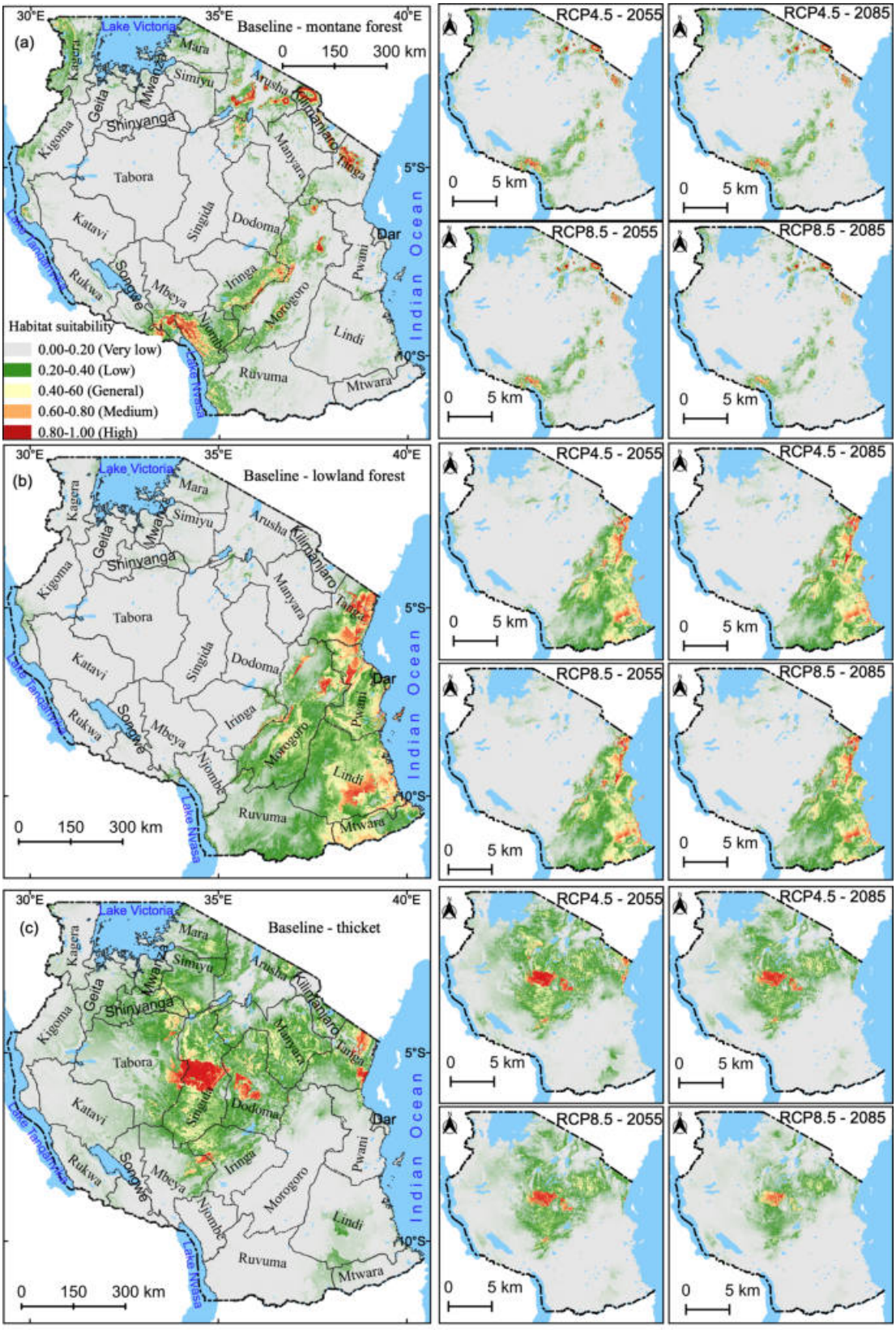

Figure 6.3: Predicted potential suitable habitat distribution area for (a) montane, (b) lowland forest and (c) thicket under current and future climate scenarios in Tanzania. EPSG: 4326, WGS84 projection

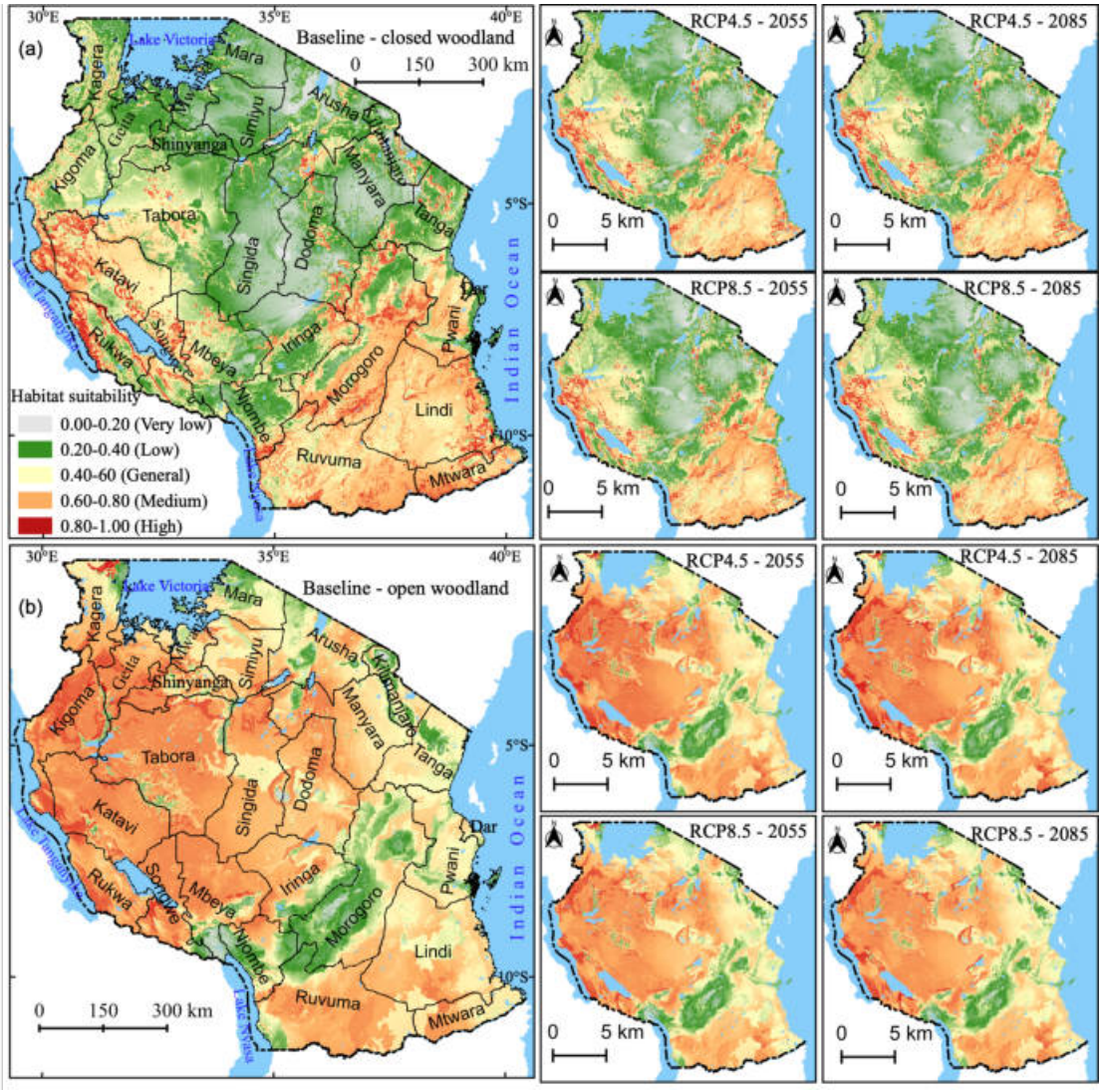

Figure 6.4: Predicted potential suitable habitat distribution area for (a) Closed woodland, (b) Open woodland and under current and future climate scenarios in Tanzania. EPSG: 4326, WGS84 projection

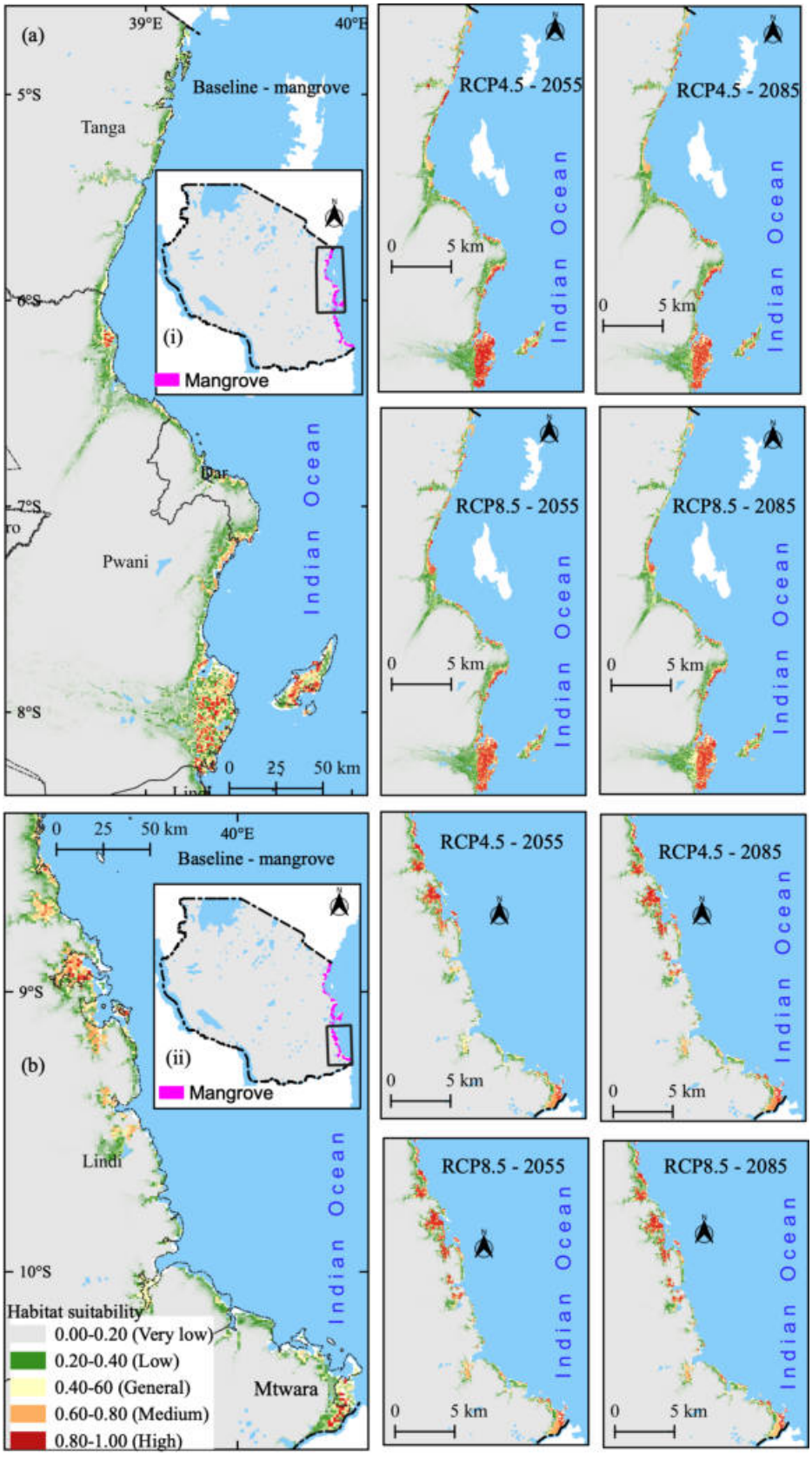

Figure 6.5: Predicted potential suitable habitat distribution area for mangrove forest under current and future climate scenarios in Tanzania (a) northern coastline of Tanzania (b) southern coastline of Tanzania. EPSG: 4326, WGS84 projection

Table 6.6: Summary of the accuracy metrics: overall accuracy, F1 score, and MCC

Forest type	Overall Accuracy	F1 score	MCC
Montane	0.943±0.014	0.93	0.88
Lowland	0.925±0.010	0.92	0.85
Mangrove	0.976±0.006	0.98	0.95
Closed woodland	0.879±0.002	0.88	0.75
Open woodland	0.852±0.003	0.84	0.77
Thicket	0.894±0.039	0.89	0.78

6.3.2 Variables importance to each model

Precipitation and temperature (Mean annual precipitation, rainfall driest month and mean annual temperature) (Table 6.7) were the main determinants for explaining the current and future distribution of the six forest types based on the candidate tree species in Tanzania. However, non-climatic variables, reflecting the topographic (elevation and terrain ruggedness) and soil constrain the distribution of these forest types, especially mangrove forests on the flat coastal plains. For example, removing elevation from the mangrove model resulted in a shift from the known areas of mangrove occurrences to inland lakes and rivers.

6.3.3 Predicted Forest Habitat Distribution

The climate change scenarios indicate a projected change of suitable habitat for most forest communities (Table 6.8 and Table 6.9). Montane forests, located at moderate to high altitudes, are predicted to suffer a loss of more than 47% in suitable habitat extent by 2085 under even the most optimistic emission scenario (RCP4.5), and losses of 64% under a high emission scenario (RCP8.5). Thicket forests are predicted to lose more than 70% of their habitat under the high emission

Table 6.7: Independent variables and their explanatory contributions to the distribution of the six forest types. It indicates habitat suitability changes within the range of the predictor variables. See Appendix 1 as Table 1 for a definition of the soil types.

Forest type	Variable name	Unit	%	Mean	SD	Min.	Max.
Montane	Rainfall driest month	mm	59.8	14.80	0.64	0.00	66.00
	Terrain ruggedness	m	14.1	92.11	1.94	8.38	229.88
	Soil type (Nitisols, Histosols)	-	8.6	-	-	-	-
	Potential evapotranspiration	mm	8.1	1387.70	127.69	1051.00	1791.00
	Mean annual temperature	^{0}C	6.2	17.01	0.10	10.40	26.10
	Annual moisture index	-	1.2	90.74	22.51	47.00	209.00
	Mean annual rainfall	mm	1.0	1247.61	10.72	850.00	2686.00
	Elevation	m	0.5	1760	19	235	3039
	Rainfall wettest month	mm	0.4	232.18	65.15	143	514.00
Lowland	Rainfall driest month	mm	49.8	11.20	0.33	0.00	56.00
	Elevation	m	21.7	363.32	7.34	9.00	2377.00
	Terrain ruggedness	m	12.5	36.40	1.20	1.12	279.25
	Soil type (Arenosols, Fluvisols)	-	4.6	-	-	-	-
	Mean annual rainfall	mm	4.3	1219.44	6.47	610.00	2735.00
	Potential evapotranspiration	mm	3.3	1606.03	111.83	1385	1787
	Annual moisture index	-	1.5	76.46	19.83	48.00	130.00
	Mean annual temperature	^{0}C	1.2	24.72	0.04	15.00	27.30
	Rainfall wettest month	mm	1.1	223.05	58.65	150.00	405
Mangrove	Mean annual temperature	^{0}C	21.0	26.69	0.04	25.90	27.50
	Elevation	m	72.0	8.82	0.08	1.00	22.00
	Soil type (Solonchanks, Arenosols)	-	2.8	-	-	-	-
	Terrain ruggedness	m	2.5	2.60	0.06	0.12	2479.80
	Potential evapotranspiration	mm	1.3	1502.64	67.23	1388.00	1791.00
	Rainfall wettest month	mm	0.3	297.59	66.62	154.00	467.00
	Mean annual precipitation	mm	0.1	1342.84	4.46	992.00	1869.00
	Annual moisture index	-	0.0	89.93	13.77	56.00	135.00
	Rainfall driest month	mm	0.0	17.00	0.15	7.00	49.00
Closed woodland	Mean annual precipitation	mm	40.0	1139.84	1.16	556.00	2377.00
	Terrain ruggedness	m	14.2	29.96	1.16	0.38	248.12
	Rainfall wettest month	mm	11.7	215.98	48.38	111.00	359.00
	Mean annual temperature	^{0}C	9.0	22.56	0.01	13.7	27.20
	Elevation	m	7.1	1040.06	2.00	14.00	2039.00
	Soil type (Acrisols, Ferralsols)	-	7.1	-	-	-	-
	Rainfall driest month	mm	6.8	1.64	0.01	0.00	35.00
	Potential evapotranspiration	mm	2.5	1626.70	14.65	1365	1869
	Annual moisture index	-	1.6	71.87	17.65	40	126
Open woodland	Rainfall driest month	mm	41.7	3.59	0.04	0.00	48.00
	Terrain ruggedness	m	27.0	22.88	0.21	0.25	231.12
	Soil type (Ferralsols, Gleysols)	-	18.2	-	-	-	-
	Mean annual precipitation	mm	8.3	766.08	11.45	566.00	1243.00
	Annual moisture index	-	1.7	62.44	15.87	24.00	114.00
	Elevation	m	1.3	942.05	3.54	10.00	2276.00
	Rainfall wettest month	mm	0.9	187.25	44.80	66.00	308.00
	Potential evapotranspiration	mm	0.5	1657.27	101.82	1409.00	1890.00
	Mean annual temperature	^{0}C	0.3	22.97	0.01	13.90	27.30
Thicket	Mean annual precipitation	mm	32.5	766.08	11.45	566.00	1243.00
	Soil type (Acrisols and Arenosols)	-	27.3	-	-	-	-
	Terrain ruggedness	m	13.1	8.78	0.67	2.38	45.38
	Rainfall driest month	mm	12.3	3.27	0.80	0.00	38.00
	Rainfall wettest month	mm	7.4	144.09	17.03	114.00	219.00
	Annual moisture index	-	6.2	44.93	7.91	32.00	75.00
	Potential evapotranspiration	mm	0.9	1707.40	55.27	1580.00	1891.00
	Elevation	m	0.1	1160.47	28.57	106.00	1516.00
	Mean annual temperature	^{0}C	0.1	22.19	0.10	20.10	25.60

scenario (RCP8.5) by 2085. Mangrove forests are predicted to increase by 40% in both emission scenarios (RCP4.5 and RCP8.5). Lowland forest habitat, occurring in a mosaic of montane and woodland is predicted to have lost a suitable habitat of more than 10% by 2085 (RCP8.5). Woodland vegetation, the most geographically extensive forest type in Tanzania, is predicted to lose approximately 5% of its suitable habitat by 2085. Projected change maps (Figure 6.6, Figure 6.7 and Figure 6.8) present the anticipated changes in the forest suitable habitats from the projected baseline to the future climate in Tanzania.

Table 6.8: Predicted changes in forests habitat in km^2 and percentage (%) from the baseline for RCP4.5 (2055) and RCP4.5 (2085)

	Baseline		RCP4.5 - 2055				RCP4.5 - 2085			
Forest type	**Suitable**	**Not suitable**	**Loss** (%)	**Gain**	**Suitable**	**Not suitable**	**Loss** (%)	**Gain**	**Suitable**	**Not suitable**
Closed woodland	450,151	484,756	14,319(3.18)	15,026 (3.34)	435,832	469,730	22,061 (5.00)	11,608 (2.58)	428,090	473,148
Open woodland	662,595	272,312	16,676 (2.52)	13,145 (2.00)	645,919	259,167	24,088 (3.64)	116,989 (2.56)	638,507	255,323
Montane forest	58,019	876,888	23,619 (40.70)	133 (0.24)	34,400	876,755	27,400 (47.22)	119 (0.20)	30,619	876,769
Mangrove forest	1,467	933,442	319 (21.75)	652 (44.44)	1,148	932,790	222 (15.13)	681 (46.42)	1,245	932,761
Lowland forest	117,178	817,731	3,872 (3.30)	9,849 (8.40)	113,306	807,882	4,810 (4.10)	10,198 (8.70)	112,368	807,533
Thicket	172,662	762,245	0(0)	0(0)	177,881	757,026	65,061 (37.68)	3,729 (2.15)	107,601	758,516

Table 6.9: Predicted changes in forests habitat in km^2 and percentage (%) from the baseline for RCP8.5 (2055) and RCP8.5 (2085)

	Baseline		RCP4.5 - 2055				RCP4.5 - 2085			
Forest type	**Suitable**	**Not suitable**	**Loss** (%)	**Gain**	**Suitable**	**Not suitable**	**Loss** (%)	**Gain**	**Suitable**	**Not suitable**
Closed woodland	45,0151	484,756	17,951 (4.00)	9,625 (2.14)	432,200	475,131	15,066 (3.35)	16,681 (3.71)	435,085	468,075
Open woodland	662,595	272,312	26,710 (4.03)	9,039 (1.36)	635,885	263,273	20,420 (3.08)	18,145 (2.74)	518,376	254,167
Montane forest	58,019	876,888	28,827 (49.68)	114 (0.19)	29,191	876,774	37,343 (64.36)	128 (0.22)	20,676	876,760
Mangrove forest	1,467	933,442	199 (13.56)	714 (48.67)	1,268	932,728	257 (17.51)	626 (42.67)	1,210	932,816
Lowland forest	117,178	817,731	7,746 (6.61)	8,011 (6.84)	109,432	809,720	11,891 (10.15)	7,377 (6.30)	105,287	810,354
Thicket	172,662	762,245	70,589 (40.88)	3,256 (1.88)	102,073	758,989	127,588 (73.89)	1,267 (0.73)	45,074	760,978

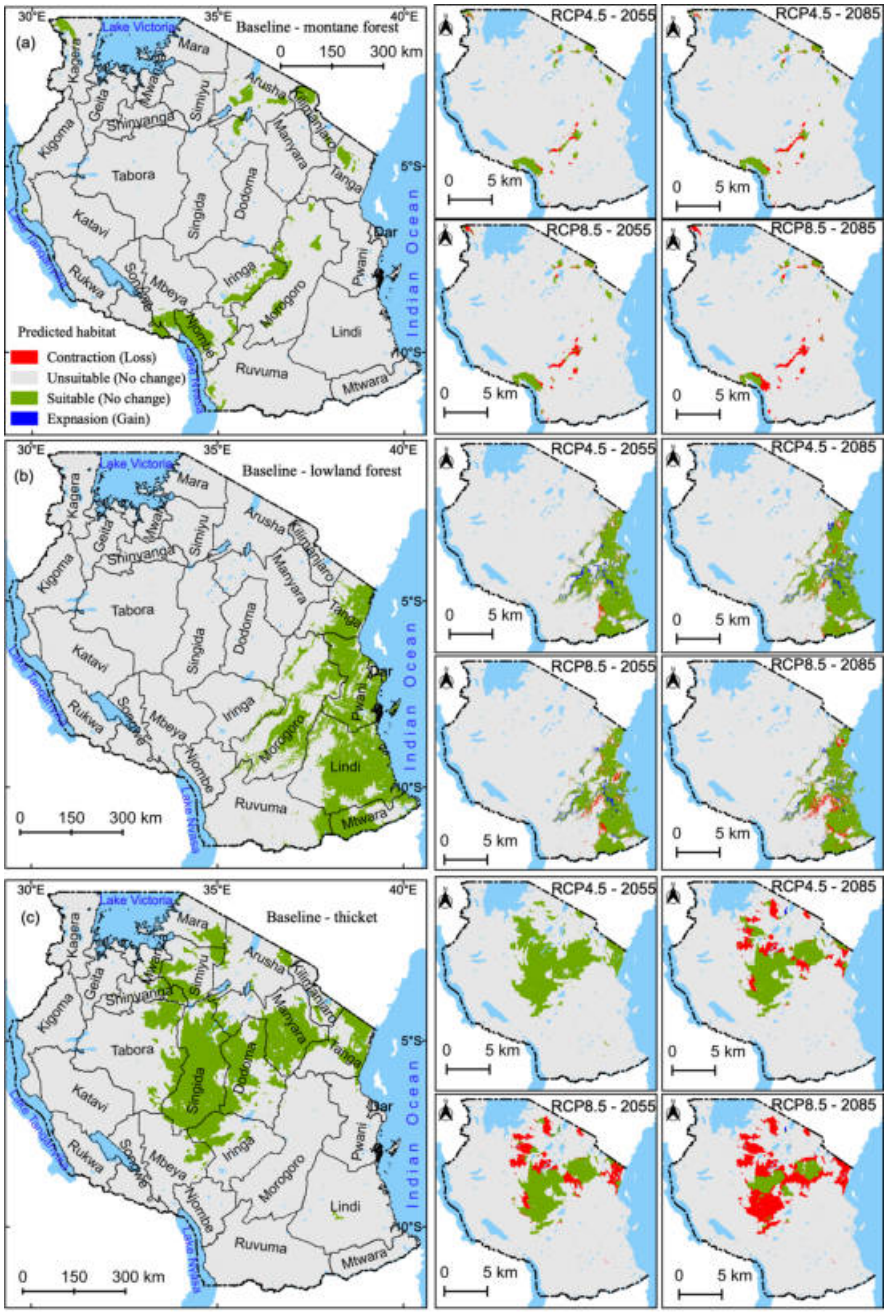

Figure 6.6: Predicted spatial changes in the potential habitat distribution area based on the thresholds provided in Table 4 for (a) montane (b) lowland forest (c) thicket under current and future climate scenarios. EPSG: 4326, WGS84 projection

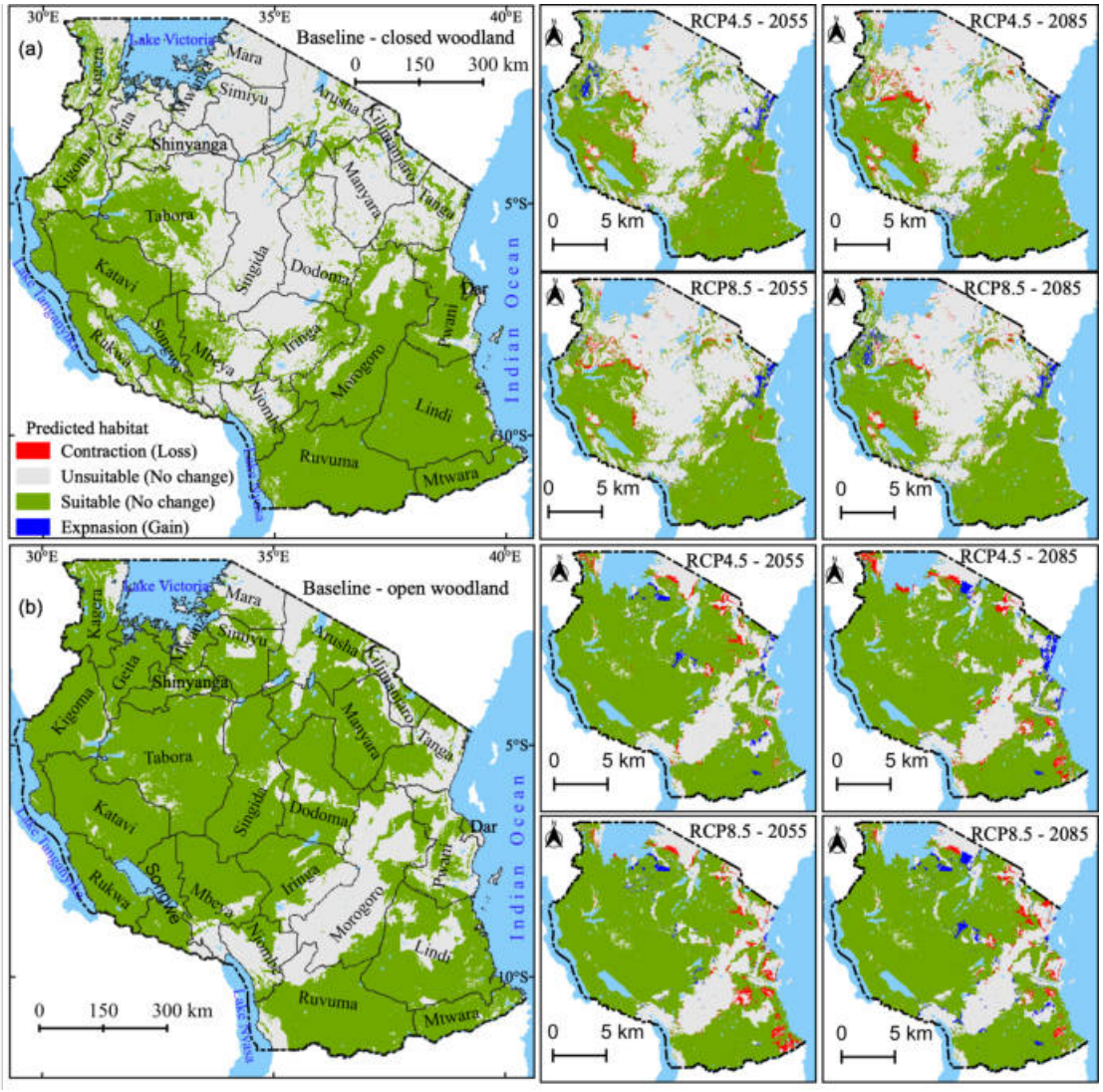

Figure 6.7: Predicted spatial changes in the potential habitat distribution area based on the thresholds provided in Table 4 for (a) closed woodland (b) open woodland under current and future climate scenarios. EPSG: 4326, WGS84 projection

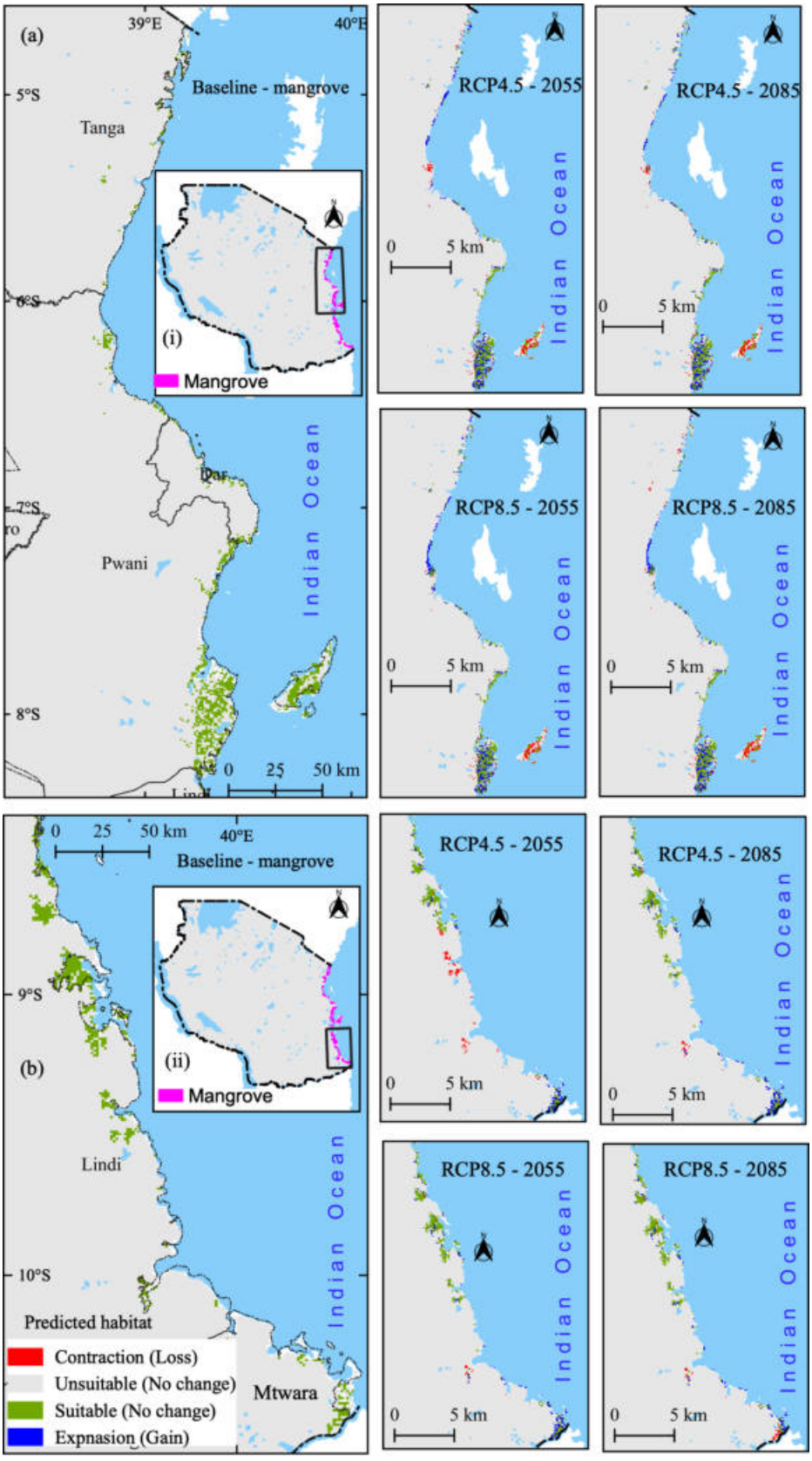

Figure 6.8: Predicted spatial changes in the potential habitat distribution area of mangrove under current and future climate scenarios based on the thresholds provided in Table 4: (a) northern coastline of Tanzania (b) southern coastline of Tanzania. EPSG: 4326, WGS84 projection

6.4 Discussion

6.4.1 Predicted Forests Habitat Change

The impact of climate change on forest extent in Tanzania was assessed using the national forest inventory data (Tomppo et al., 2014). The results indicate that climate changes will affect all forest habitats' suitability across Tanzania. Similarly, the results reveal that climate change will threaten forests at various scales: forests with a narrow geographical range occurring at high altitudes (i.e., montane forests) will experience more loss of their current habitat in the future. This may be associated with fragmented strips of montane forests, and particularly high endemism has increased a great sensitivity to climate change (Foster, 2001). Moreover, future climate change will extensively threaten microhabitat forests (i.e., thickets) occurring in a semi-arid climate (Moncrieff et al., 2015). These projections indicate that climate change, especially temperature rise, will accelerate habitat loss of already vulnerable forests such as thickets (Chidumayo et al., 2011). Mangrove forests are predicted to expand their current range as a response to climate change (Godoy and Lacerda, 2015), although the future extent shift is more likely to be driven by sea-level rise, which was not factored, into the present study (Alongi, 2008). Similarly, climate extremes such as drought, storms, cyclones, and wildfires (Deb et al., 2017) are expected to alter the forest types' distribution, composition, phenology, and structure (e.g., through increased tree mortality).

6.4.2 Potential Suitable Habitat Impacted

The loss of suitable habitat for the montane forest is projected to be extensive, with losses exceeding 40% even under the optimistic RCP4.5 scenario by 2055 (Table 6.8 and Table 6.9). This predicted loss is particularly pronounced in the high biodiversity areas of the Eastern Arc Mountains, a foothill of Rungwe and Livingstone mountain range along Lake Nyasa (Figure 6.6a). A projected reduction in rainfall results in a contraction of montane forests to higher elevations, illustrated by the projected loss of montane forest communities at lower elevations around Mount Kilimanjaro. The isolated nature of these montane habitats sometimes termed "forest islands" (Fjeldså, 1999), form essential refugia for several species including 15 mammal species identified as vulnerable or high-risk status within the Udzungwa Mountains (Rovero et al., 2006). Forest loss in montane regions has severe implications for wildlife migration as these forests provide vital corridors linking reserves in Ruaha to the Selous Game Reserve via the montane forests of the Udzungwa Mountains (Jones et al., 2012). Additionally, the loss of suitable habitat for forests in these regions is likely to increase sediment supply within the Rufiji basin, affecting downstream wetlands dynamics and water resources (Ochieng, 2002).

Rising temperatures and reduced rainfall during the dry season are projected to result in the loss of suitable lowland forest habitats above 10% by 2085 (Table 6.9). Given the extent of lowland forest in Tanzania, the effects of this loss have broad-reaching implications, including reduced landscape connectivity impacting wildlife migrations (Ntongani et al., 2010). Projected losses are particularly pronounced in the southeast of the country in the regions of Ruvuma, Mtwara, and

Lindi (Figure 6.6b), which provides an extensive transboundary wildlife corridor between the Selous and Niassa (Mozambique) game reserves. Lowland forest communities in this area mosaic with one of the World's largest miombo woodland ecosystems with a projected decline of above 4% (Table 6.8 and Table 6.9) providing migratory routes for a number of species including the largest populations of elephants, as well as globally significant populations of Roosevelt's sable antelope, Liechtenstein's hartebeest, Nyasa wildebeest, eland, greater kudu and carnivores including African wild dog, lion, and leopard (Hofer et al., 2004). Conversely, a small degree of expansion of woodlands (closed and open) is projected into wetter areas, for instance, into the Lake Tanganyika, Victoria, and Pangani basin (Figure 6.7). However, there are predicted severe losses (over 40% by 2085 even under optimistic conditions) (Table 6.9) in suitable habitats for thickets in central and north-eastern Tanzania in the regions around Singida, Dodoma, and Manyara (Figure 6.6c). Habitat fragmentation and reduced ecological resilience are anticipated, impacting the vital ecosystem for several game reserves and national parks with regionals and even global significance, including Mkungunero, Swagaswaga, Muhezi, Rungwa, Maswa, Mkomazi, Saadani, the Serengeti national park ecosystem and bee reserves in Manyoni district. These forest communities represent vital habitats for fauna such as birds, small browsers, and larger animals such as rhinoceros, particularly in dry regions where thickets represent the only closed-canopy habitat (Medley, 1996; Sharam et al., 2006).

Mangrove forests represent a valuable economic resource for local communities as well as maintaining the seascape. Importantly, mangrove forests play an essential role in carbon storage (natural carbon sinks), capturing CO_2 from the atmosphere and storing it in their biomass than terrestrial trees (Ray and Jana, 2017; Alongi,

2012). Under projected climate change scenarios, habitats suitable for mangrove forests are predicted to expand their range by 40% (Table 6.8 and Table 6.9) at both low and high emissions (Figure 6.8). It is chiefly due to rising temperatures and subsequent evaporation, coupled with reduced annual rainfall totals leading to increased salinity, a favorable condition for the mangrove ecosystem (Alongi, 2015). Therefore, an increase in temperature would be positive for the mangrove ecosystem as more accelerated growth, changes in community composition, diversity, and latitudinal expansion (Hanebuth et al., 2013; Alongi, 2015). Similarly, a rise in sea level influenced by future climate change is expected to alter mangrove forests significantly as they are susceptible to any shift in sea level (Crase et al., 2015; Alongi, 2008). The relative sea-level rise may cause landward retreat in mangrove forests supported by sediment composition on the upland habitat (Godoy and Lacerda, 2015). However, the ability of mangroves to migrate inland may be constrained by local conditions, such as infrastructure (e.g., roads, agricultural fields, dikes, urbanization, seawalls, and shipping channels) and topography (e.g., steep slopes) (McLeod et al., 2006). For example, the construction of coastal engineering structures along the coast of Tanzania obstructs the natural inland migration of mangroves even when the sea level rises.

6.4.3 Implications for Forests Conservation Planning

A dramatic decline in the projected extent of Tanzanian forests over the next 50 years is expected to be driven by regional and national climatic factors. The study, therefore, identifies a tractable method of using existing forest inventory data to predict the distribution of future habitats capable of sustaining forest ecosystems in spite of the challenges posed by future climate change. Information

on forest extent and change of this nature can directly inform schemes such as the Clean Development Mechanism (CDM) and REDD+ (Pelletier and Goetz, 2015) as an incentive and alternative plans to reduce pressure on the remaining suitable forest habitats and enhance forest conservation, sustainable forest management and enhanced of forest carbon stocks and payment of ecosystem services (Romijn et al., 2012).

The habitat modelling procedure demonstrated that climate has a substantial control on the distribution of Tanzanian forest communities. As a result, even under an optimistic climate change scenario (RCP4.5), forest communities in Tanzania are projected to decrease in an immense range. Notably, the montane forests of Tanzania are globally significant in terms of biodiversity (Fjeldså, 1999; Rovero et al., 2006; Jones et al., 2012), yet they are projected to halve in extent by 2085. Whereas forest communities like closed, open woodland and mangrove forests may expand into other regions in response to climate change, montane forests are constrained by elevation and therefore show particular vulnerability to changes in temperature. As such, montane species may well act as a barometer for regional climate change (e.g., Kimball et al., 2000). Focusing on monitoring efforts in these regions may be vital in identifying changes in forest composition and biodiversity in response to climate change, in the hope that this can steer policy before a crucial tipping point is reached. For instance, through efforts like the African Forest Landscape Restoration initiatives (FLR) with a target of restoring 100 million hectares of deforested and degraded landscape across Africa by 2030 (Mills et al., 2015).

Other more direct anthropogenic factors compound the threat from climate change as these forest communities undergo extensive felling for building material and

charcoal production, as well as increasing frequency of forest fires (Sharam et al., 2006). These forest habitats extend across approximately half of Tanzania, and habitat degradation or loss of this magnitude can have serious implications, particularly in terms of loss of carbon sink (Makundi and Okiting'ati, 1995) and their role in wildlife migratory patterns: projected losses coincide with wildlife corridors with regional significance such as the Selous-Niassa, Udzungwa-Ruaha and Muhezi-Swagaswaga migratory routes (Hofer et al., 2004; Medley, 1996; Sharam et al., 2006).

6.4.4 Relevance of Habitat Suitability Models for Image Classification

The baseline habitat suitability maps (Figure 6.6, Figure 6.7 and Figure 6.8) provided the basis for the forest types' identified habitat preferences in Tanzania. They can be an essential model for training data selection in future image classification for the forest types. Collecting adequate and representative training samples at a country level may be challenging, impacting classification results. Therefore, to improve the classification result at a country scale, it is proposed to include habitat suitability models for the forest types as suitable habitats, and identify forest types with higher location specialisation that suitably characterise the class being mapped (Foody and Mathur, 2004).

6.4.5 Limitations of the study

This study adopted a widely accepted methodology (e.g., Merow et al., 2013; Elith et al., 2006; Lim et al., 2018) that facilitates the mapping of forests' habitat suitability and their alteration due to climate change; however, it suffers from the same limitations associated with known uncertainties of the data and climate models (e.g., Watling et al., 2013). Similarly, the forest habitats prediction focused at a county level, and therefore, the results should be interpreted at the national scale rather than a regional or small local scale.

6.4.6 Future research perspectives

Future simulations should consider using the information on the spatial pattern of change, such as proximity (distance rasters) to urban centers and road networks, and density rasters of projected population growth (population data surface). Construction of road networks across forests is likely to trigger increased forest degradation and fire incidences that in turn are expected to alter regional climate (Nepstad et al., 2001; Fonseca et al., 2019). Future work also should explicitly consider the impact of sea-level rise and geomorphology on Tanzanian mangroves to fully understand how these essential habitats might change as a result of climate change.

6.5 Conclusions

Climate change will alter Tanzanian forests by accelerating habitat loss, and fragmentation and hence reducing ecological connectivity. The effect of forest fragmentation will compromise the potential plant pollinators' movement and seed dispersal. The induced fragmentation is especially severe when essential wildlife corridors, such as riparian zones that connect different areas of the landscape, are impacted. The optimal management solution in this regard is to increase ecological connectivity in current forest planning and management. Ecological connectivity should be maintained in habitats that are predicted not to change and expand under future climate change by preserving native forests and, where possible, protecting the remaining forest areas from other anthropogenic disturbances. Improving ecological connectivity would significantly enhance not only sustainable forest management but also improve the design and implementation of forest projects and programmes. For example, ecological connectivity in forests will improve wildlife movement. This is more prominent for the dispersed population of large mammals (e.g., elephants) (Ntongani et al., 2010), when enclosed, increases the destructions of the highly diverse forest habitats (Ripple et al., 2015). Therefore, increasing forest connectivity will enhance the natural resilience of the remaining forests to the predicted effects of climate change. Consequently, the findings call for conservation planning in different dimensions: improving the management of the existing protected areas which can absorb the impact of climate change, but also expanding to newly suitable areas with effective land-use planning, conservation, and land reclamation.

Chapter 7

Forest Baseline Classifications of Tanzania

This chapter is based on:

John, E., Bunting, P., Hardy, A.; Silayo, D.S., Masunga, E., 2021. A Forest Monitoring System for Tanzania. *Remote Sensing* 13, 3081. https://doi.org/10.3390/rs13163081

7.1 Introduction

Reliable and current information on the status (extent, location, and type) of forest resources can promote effective conservation for sustainable forest management in Tanzania, supporting transparent National Forest Monitoring Systems (NFMS), REDD+ payments, more efficient allocation of scarce conservation resources, and an improved understanding of the significance of forest conservation investments. The establishment of a reliable forest baseline considering trees in forests (TIFs) and trees outside forests (TOFs), such as those located on farmland and in built-up areas (rural and urban) (Chakravarty et al., 2019) is a key first step. Including TOFs in forests, monitoring is essential due to their economic, ecological, and climatic role and contributes substantially to national biomass and carbon stocks and to the livelihood of people (Jain et al., 2020). Therefore, this chapter explores a novel method for generating wall-to-wall forest mapping across Tanzania with the application of a machine-learning classifier using Landsat 8 OLI images. The methodology builds on the lessons learned from Chapter 5.

7.2 Methods

7.2.1 Image Acquisition and Pre-processing

As outlined in Chapter 5, issues due to clouds and cloud shadows, particularly in the eastern coastal areas, provide a challenge when using optical imagery. Therefore, at a national scale, Landsat 8 OLI-TIRS data from collection 1 archive from 2013 to 2018 for the months of May to November with a cloud cover threshold of

$>$ 80% were downloaded for analysis. The pre-processing was undertaken using the ARCSI software as described in Chapters 4 and 5 (Figure 4.3).

The whole process was implemented on the SuperComputing Wales (SCW[1]) platform, as discussed in Chapter 4. This was important for handling the large data volume, amounting to 3,200 Landsat 8 OLI images, by reducing the computational processing time, as up to 100 cores were simultaneously used for the analysis. Following the steps outlined in Chapter 5, an image composite was also created to visualise and compare the classified products but was not used for the classification.

7.2.2 Overview of Classification Methodology

The classification followed a hierarchical approach, first delineating the forest as one class (level 1) and then classifying the forest pixels into forest types (level 2) (Figure 7.1), generating the forest baseline for Tanzania. Level 1 focused on producing general forest extent information, whilst level 2 classified forested areas (level 1) into more detailed forest types distribution, effectively supporting monitoring and management. The XGBoost classifier (Section 4.5.5) was used for the analysis where the training data were split into 100 sets creating 100 training classifiers. The 100 trained XGBoost classifiers were applied to each of the 3,200 scenes, resulting in 320,000 individual classifications. The analysis was carried out on a per-pixel and individual-scene basis. The 100 classifications for the scene were first merged by thresholding the number of times a pixel had been classified to an individual class, resulting in 3,200 hard classifications. The resulting 3,200

[1] https://portal.supercomputing.wales/

scene-by-scene classifications were then merged using the same process, creating the final national map.

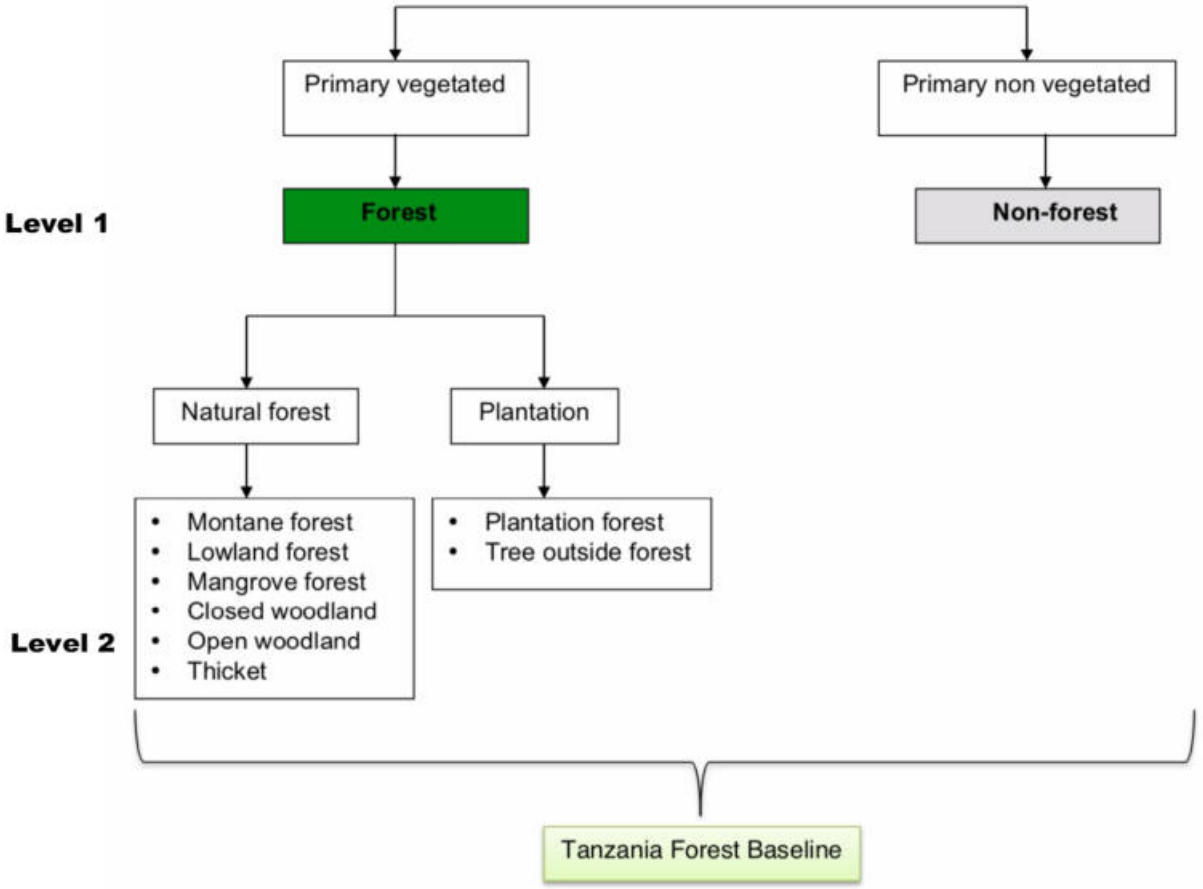

Figure 7.1: Classification hierarchical scheme

7.2.3 Forest/Non-forest Classification

7.2.3.1 Defining Training Data

The training polygon regions of interest (ROIs) for the forest/non-forest classification were generated with reference to the composite image and higher resolution Google Earth imagery by identifying pure forest and non-forest areas. Due to the

higher spatial resolution of Google Earth aerial imagery (Connette et al., 2016), it is much easier to distinguish forests and forest types from other vegetation classes (i.e., bushes, grasses, and crops) and hence improve classification results. This minimised the potential of misclassification influenced by other land covers. A total of 46,176 training polygons were collected (forest, n = 22,440 and non-forest, n = 23,736). These samples were then rasterised onto each of the 3,200 images and the associated image pixels were extracted, creating 435,808,135 forest samples and 1,423,875,598 non-forest samples.

Training with this number of samples would create an XGBoost classifier with many levels and large trees, which might be very slow to apply. To use this large training dataset, the data were split into 100 sets by randomly selecting 500 scenes (of the 3,200), merging the associated training samples, and then balancing the number of non-forest samples by randomly selecting a subset of non-forest samples to match the number of forest samples. The number of samples for each class used for each of the 100 classifiers varied, but the minimum was 60,874,216, the maximum was 78,833,485, the mean was 68,118,012, and the standard deviation was 35,37,652. The resulting data was split by taking random non-overlapping samples to create training (50%), validation (25%), and testing (25%) datasets.

7.2.3.2 Optimising the XGBoost Parameters

The XGBoost algorithm (Section 4.5.5) has a large number of hyperparameters to optimise. For this study, a Bayesian optimisation was used, as implemented within the RSGISLib software. The full training and validation datasets could not be used for the parameter optimisation as it would have taken a very long time (many months) to perform the optimisation. Therefore, subsets of the training

and validation data were randomly extracted for each of the 100 sample sets. For the optimisation, 60,000 training samples of forest and non-forest were used (i.e., 120,000 in total) and 20,000 for the validation dataset.

7.2.3.3 Training the XGBoost Classifiers

Once the parameters had been optimised, the 100 classifiers could be trained using the full training dataset. Therefore, generating 100 classifiers trained with different datasets and hyperparameters. Given the large number of training samples used to train these classifiers, training was conducted using multiple cores with 40 cores used to train each model. The training was therefore conducted consecutively, with each classifier trained in turn. It took 35 days for all 100 models to be trained. Using the testing datasets, the average accuracy of the classifiers was 99%.

7.2.3.4 Creating the Final Forest Extent Map

As described in Section 7.2.2, the 100 classifiers were applied to each of the 3200 scenes. The 100 classifications were summarised on a per-pixel basis providing a percentage for the number of times a pixel was classified as forest. The scene was then thresholded using at 30%, 50%, and 80%. The thresholds were selected based on a visual inspection of the subsample of scenes and chosen to capture the probability of pixels classified as a forest at the three different levels. For example, if a threshold is $> 80\%$ of pixels (on a per-scene basis) classified as forest, then the pixel will be assigned as forest.

To merge the scene-based classifications, and to create a national forest mask, 100 km tiling was used with this allowing parallel processing. The percentage of times

a pixel was classified as the forest was calculated for each pixel, resulting in three output images for each scene-based threshold (i.e., 30%, 50%, and 80%). Those outputs were subsequently thresholded using the same 30%, 50%, and 80% levels, creating 9 forest extent maps for Tanzania (e.g., scene threshold of 50% and national threshold of 80%). However, a further refinement of the threshold selection can be made in future studies. Finally, an independent accuracy assessment was undertaken to identify the optimal forest extent map.

7.2.4 Forest Types Classification

The second step in the hierarchy (Level 2) (Figure 7.1) of forest classification was to classify the forested pixels into forest types (montane, lowland, mangrove, plantation forest, closed woodland, open woodland, and thicket). Forest types classification is necessary for generating detailed forest distribution for evaluating forest ecological systems and supporting monitoring and management practices. To constrain this analysis, each forest type's habitat suitability from Chapter 6 was used in Figures 6.3, 6.5 and 6.4. This novel approach was selected to minimise the classification error such that a pixel was only considered for the forest types that the habitat suitability analysis had identified. Therefore, it constrained the classification of forest types based on their adaptation and corresponding bioclimatic patterns, minimising misclassification and reducing the time for the classifier for searching similar pixels outside the suitable habitat of the given forest type. For example, mangroves would not be classified around freshwater lakes and at altitudes above high tide levels.

7.2.4.1 Forest Types Mask

The habitat suitability extent maps were intersected to merge the individual forest type suitability maps, identifying 34 combinations (Figure 7.2b). For a small number of areas, the habitat suitability result provided suitability for only a single class (e.g., open woodland) (Table 7.1). However, this would not allow the classifier to perform classification, so a second class was added in these cases. For example, for the areas which only had suitability for open woodland, then closed woodland was added (Table 7.1). Therefore, for the first time, the study proposes a novel technique, exemplified by the case of combining forest habitat suitability models as input data to constrain the classification of forest types based on their adaptation and corresponding bioclimatic patterns, minimising misclassification. It aimed at improving the overall forest classification over a large area and a complex forest landscape.

Table 7.1: A sample of predicted combined forest types suitability depicting single class occurrences. Therefore, a second class was added in these situations to enable the classifier to perform classification.

	Predicted combination		
Value	**Habitat type predicted**	**Yes = 1/ No = 0**	**Added class**
2	Montane forest	1	Lowland forest, plantation forest
	Lowland forest	0	
	Mangrove forest	0	
	Plantation forest	0	
	Closed woodland	0	
	Open woodland	0	
	Thicket	0	
4	Montane forest	0	
	Lowland forest	0	
	Mangrove forest	0	
	Plantation forest	0	
	Closed woodland	0	
	Open woodland	0	
	Thicket	1	Open woodland, closed woodland
8	Montane forest	0	
	Lowland forest	0	
	Mangrove forest	0	
	Plantation forest	1	Montane, lowland forest
	Closed woodland	0	
	Open woodland	0	
	Thicket	0	
16	Montane forest	0	
	Lowland forest	0	
	Mangrove forest	0	
	Plantation forest	0	
	Closed woodland	0	
	Open woodland	1	Closed woodland, lowland forest
	Thicket	0	
32	Montane forest	0	
	Lowland forest	0	
	Mangrove forest	0	
	Plantation forest	0	
	Closed woodland	1	Open woodland, lowland forest
	Open woodland	0	
	Thicket	0	
64	Montane forest	0	
	Lowland forest	1	Montane forest, closed woodland
	Mangrove forest	0	
	Plantation forest	0	
	Closed woodland	0	
	Open woodland	0	
	Thicket	0	
128	Montane forest	0	
	Lowland forest	0	
	Mangrove forest	1	Lowland forest, closed woodland
	Plantation forest	0	
	Closed woodland	0	
	Open woodland	0	
	Thicket	0	

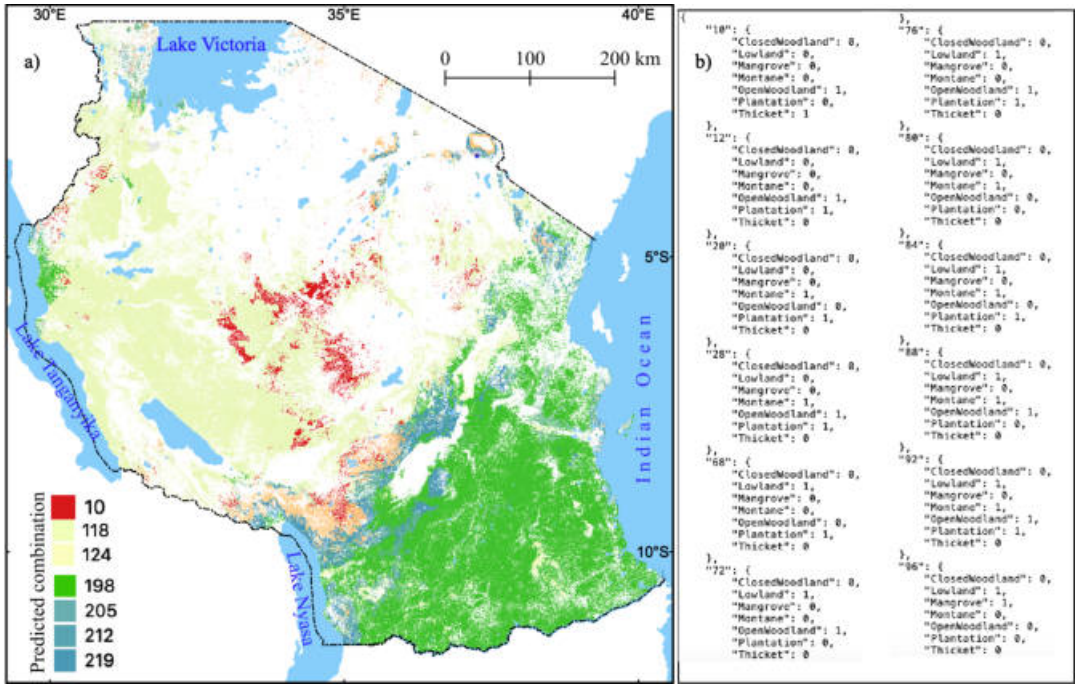

Figure 7.2: A sample of forest habitat formation combination: a) Combined habitat map b) JavaScript Object Notation (JSON) file indicating possible forest types combination

The habitat suitability analysis was undertaken at a pixel resolution of 1 km to capture local environmental variability (Hijmans et al., 2005; Fick and Hijmans, 2017) at a country scale, and corresponding bioclimatic patterns enable inferring of relationships between different forest types' habitats. Therefore, the nearest neighbour resampling was used to create a 30 m resolution product required for the Landsat classification. However, due to this resolution change, there were 30 m pixels that were within the forest mask but did not have habitat suitability. For example, along the coast and other forests/non-forest boundaries present at 1 km (e.g., wetlands and lakes). The k-NN is a non-parametric model which does not require a normal distribution and homoscedasticity of data and was used to fill these pixels where an unknown pixel was filled with the mode of the k spatially

nearest pixels. Therefore, the model is effective as it searches for the k nearest pixels based on the greatest similarities of each un-observed location to all sample pixels in a feature space consisting of predictors and then generates an estimate of the location by weighting the observations from k nearest pixels (Jiang et al., 2020). For this analysis $k = 5$. The algorithm was found to be efficient and is suited for the samples across multiple classes (Cortijo and De La Blanca, 1997). Therefore, the resulting map (Figure 7.2a) was used to define the classes considered for each pixel during the classification.

7.2.4.2 Defining the Training Dataset

Similar to the forest/non-forest classification, the training polygons were defined for each forest type and extracted from all the Landsat scenes. A total of 20,370 sample polygons were defined for the forest types (montane, $n = 1,272$, lowland, $n = 2,053$, mangrove, $n = 1,407$, plantation forest, $n = 794$, closed woodland, $n = 3,264$, open woodland, $n = 11,070$ and thicket, $n = 510$). This resulted in the following number of pixel samples:

Montane Forest $n = 7,638,017$

Lowland Forest $n = 19,192,926$

Mangroves $n = 2,225,183$

Plantation Forest $n = 2,118,903$

Closed Woodland $n = 34,636,347$

Open Woodland $n = 165,439,923$

Thicket $n = 18,051,337$

To define the number of samples for each of the 34 class combinations, the data were combined, and if one class had more samples than the others in the combination, then a random subsample was generated. However, if the minimum number of samples was over 10,000,000, then all classes were limited to 10,000,000 samples to balance the training samples across a landscape and ensure that they are representative of each forest class proportions. It aimed at maximising the accuracy of all forest types and avoiding bias towards the majority class, compared to forest types with small geographical area coverage. For example, for a combination of Mangroves, Lowland Forest, and Closed Woodland, then the Lowland Forest and Closed Woodland samples were subset to 2,225,183 (i.e., the number of samples of mangroves as this was the smallest of the three classes). However, if the combination were Closed Woodland and Open Woodland, then the number of samples would have been limited to 10,000,000.

7.2.4.3 Training the Classifiers

For this analysis, just a single classifier was trained for each combination where the samples were split into training (50%), validation (25%), and testing (25%) sets (Figure 7.3). A 10% sample of the training and validation datasets was randomly extracted to optimise the XGBoost hyperparameters using Bayesian optimisation.

Bayesian optimization trains a machine-learning model to predict the best hyperparameters. For each set of hyperparameters, a different model performance is produced and thus a different result under the performance metric. Grid search was used in searching the whole parameters space. But for models with a large parameter space, such as XGBoost, are slow and inefficient. Thus, an iterative pro-

cess was undertaken to train the model within this resulting in a more accurate estimation. The XGBoost model had the following hyperparameters, eta, gamma, max_depth, min_child_weight, max_delta_step, subsample, nthread, eval_metric, objective, and num_class. A dictionary of class information, such as ClassInfoObj objects, is defined with the training and validation data. The training data inputted into this function might well be a smaller subset of the whole training dataset to speed up processing. Therefore, Bayesian optimisation builds a model for the optimization function and explores the parameter space systematically, which improves the classification results.

The XGBoost classifiers were trained using the optimised hyperparameters and full training and validation datasets. Using the independent testing dataset, the average classifier accuracy was 99%.

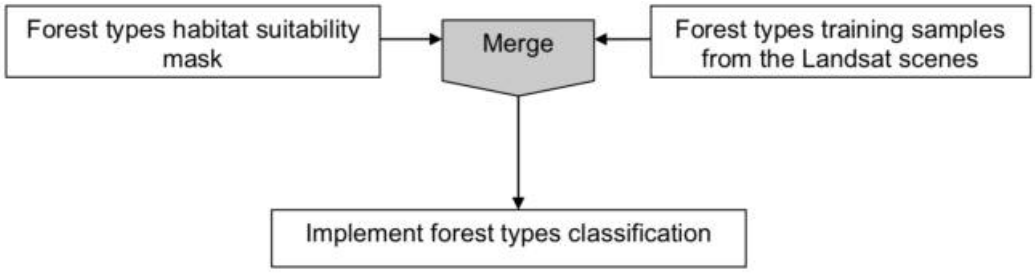

Figure 7.3: Workflow of collecting training dataset

7.2.4.4 Final Forest Types Map

As with the forest/non-forest classification, the classification was applied on an individual scene basis. The habitat suitability-derived mask was used to define the pixel combination and the associated classifier was applied. Therefore, each pixel was only considered for the classes defined by the habitat suitability analysis.

To summarise the scene-based forest type classifications, creating a national map, the mode of each pixel was taken, with the analysis undertaken using 100 km tiles.

7.2.5 Accuracy Assessment

7.2.5.1 Forest/Non-forest

The National Forest Inventory (NFI; NAFORMA) collected by Tanzania Forest Services from 2011 – 2014 (MNRT, 2015) and other local forest inventories for 2016 – 2018 were considered for this assessment of accuracy, but the temporal and spatial scale differences in defining the forest extent from these data were found to be difficult. Therefore, the NFI data was not considered as reliable reference data to assess the forest extent map against.

Therefore, accuracy assessment was conducted using a point-based sampling with reference to freely available virtual globe web-based maps (ESRI Satellite, Bing Satellite, and Google Satellite) available on QuickMapServices in QGIS 3.10. The satellite imagery accessible within these references originates from different data providers and is usually 65 cm resolution with a span range of dates for image acquisition (Connette et al., 2016). The three base-map layers (Figure 7.4) were used to check the sample points for positional accuracy, inconsistent quality of images, image acquisition date, and different temporal frequencies (Yu and Gong, 2012). Therefore, the high-resolution images in base-map layers were found to be adequate for validation (Yu and Gong, 2012), which is challenging to acquire and accomplish the requirement of ground truth points on a country-level mapping.

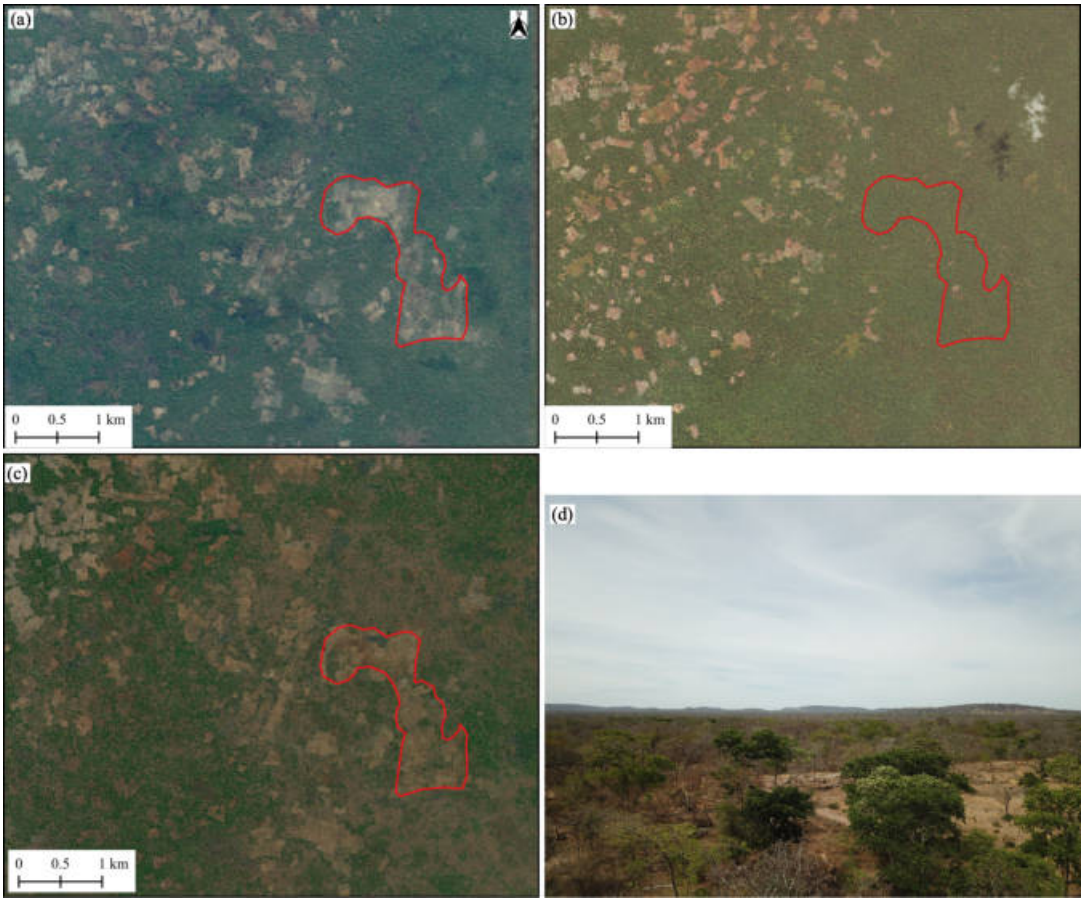

Figure 7.4: Sample virtual globes web-based map comparison: (a) Google Satellite (b) Bing Satellite (c) ESRI Satellite (d) ground field photo; red polygon indicating timing variation on image updates, especially for Bing Satellite.

The accuracy assessment points were generated using a stratified random sampling approach (Olofsson et al., 2013, 2014) from the classified images and visually interpreted using the virtual globes web-based maps (Figure 7.4). A proportional-to-class allocation was used to minimise standard errors in accuracy estimation (Myroniuk et al., 2020). Therefore, at least 1,000 sample points would fall into each class (forest/non-forest), and a total of 2,000 points were used for each sample area (185 km by 180 km) within nine sampled sites over the country (Figure 7.5).

Hence, a total of 18,000 sample points were used for accuracy assessment using the classification accuracy QGIS plugin[2] (Bunting et al., 2018) with a buffer of 45 m around each sample-point on the base-map layer (about 3 pixels on Landsat image) (Figure 7.6). This followed the characterisation method, whereby if half of the buffer area has reached the absolute majority of the cover inside the sample unit, then assigned to the majority class. The tool extends the possibility of panning all samples, specifying cover class using a drop-down menu with an overlay on virtual globes web-based maps (Figure 7.4) to understand each cover class better.

[2] https://www.remotesensing.info/tag/accuracy-assessment.html

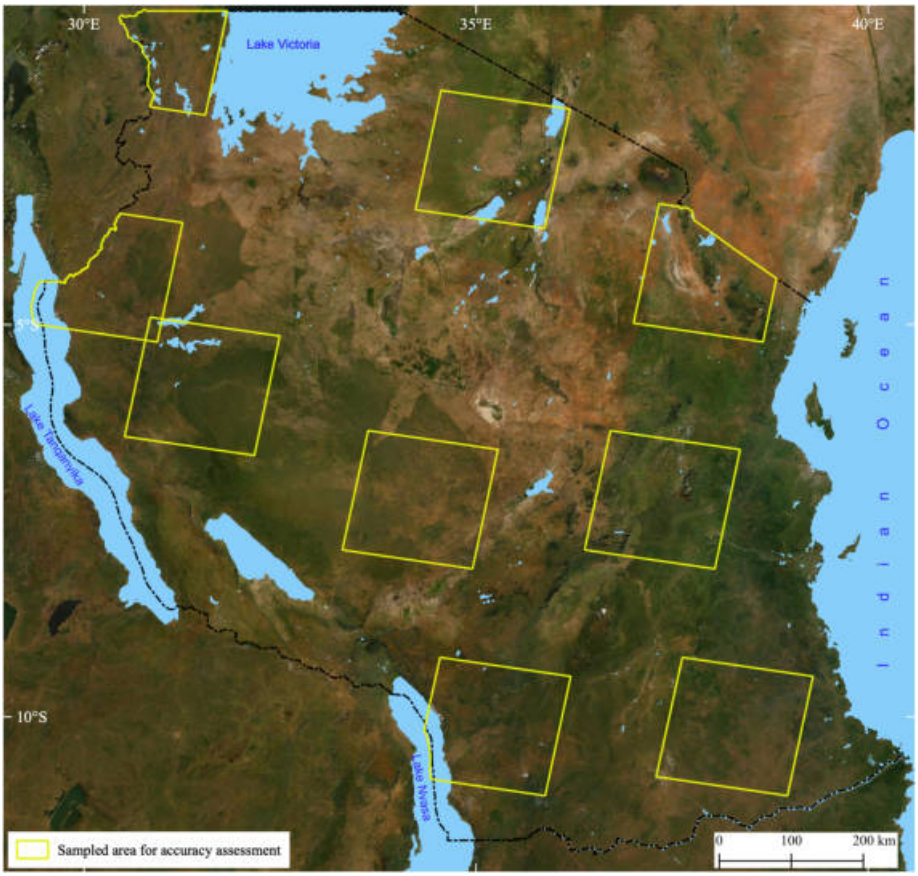

Figure 7.5: Accuracy assessment sample areas for binary forest/non-forest classification on Google satellite base-map

Further sample validation was done using high-resolution images from PlanetScope (3 m) and drone images across the classified forest and non-forest boundaries. The product accuracy metrics are summarised with an overall accuracy (OA), user and producer accuracy (UA and PA), allocation disagreement (AD), quantity disagreement (QD), proportional correct, total disagreement (Olofsson et al., 2014; Pontius Jr and Millones, 2011), F1-score, precision, recall, omission, commission error, and Matthews Correlation Coefficient (MCC) allowing the users to understand the distribution of error in the products (Boughorbel et al., 2017). The error distribu-

tion will not be equal throughout the classification as more uncertainty is found on the class boundaries (Foody, 2002). Explicitly considering these ensures a robust approach is followed reliably informing the community of the map quality.

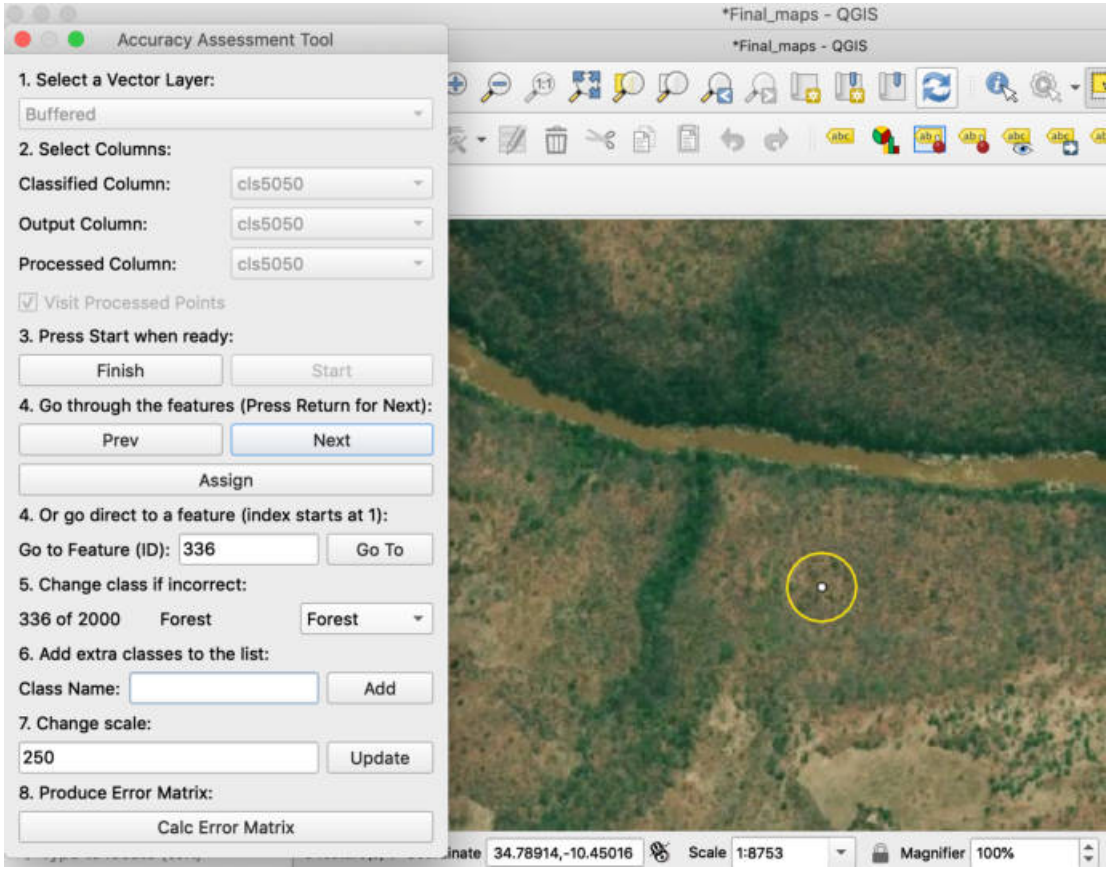

Figure 7.6: Illustrates the application of accuracy assessment tool used in verification of validation points for ground truth purposes on Google satellite base-map. Sample point buffered with 45 m (yellow circle).

7.2.5.2 Forest Types

To assess the forest type map, the National Forest Inventory (NFI; NAFORMA; (MNRT, 2015)) (Figure 7.7) was used where it was masked using the forest mask from forest/non-forest. Any remaining points within the NFI defined as being

outside of a forested area were then removed and the points for 2011 – 2014 were checked for validity using virtual globe web-based maps in QGIS (e.g., Google Earth data). While the temporal differences prevented the use of this data for assessing the forest extent map for the forest types masking to the forested extent defined in this analysis removing the majority of the temporal change from the dataset. If a pixel was defined as a forest in the 2013 – 2018 baseline mapping and with the NFI data (2011 – 2014), then it was very unlikely that the forest type could have changed. Forest types are also more difficult to assess through the analysis of high spatial resolution remotely sensed data, particularly the differences between classes such as open and closed woodlands, and therefore access to a field-derived dataset is strongly preferred. For further information and the field collection process of NAFORMA data, see Chapters 4, 5, and 6.

Therefore, a final total of 13,200 field points for the forest types were used for the accuracy assessment (n = 3,895 closed woodland, n = 1,708 lowland forest, n= 57 mangrove forest, n= 401 montane forest, n= 6,721 open woodland, n= 216 plantation forest and n= 202 thicket). Thematic accuracy measures of the forest types classification were summarised as overall accuracy, user and producer accuracy, F1-score, quantity disagreement, allocation disagreement, total disagreement, proportion correct, precision, recall, commission, and omissions error (Pontius Jr and Millones, 2011).

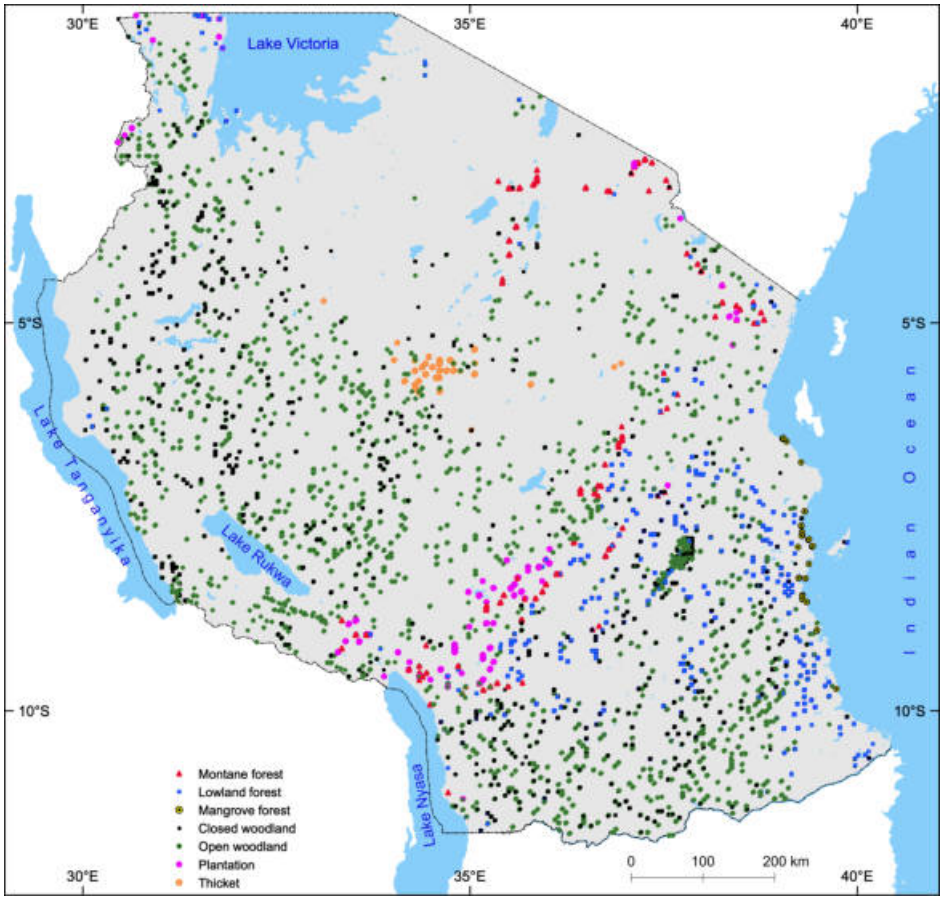

Figure 7.7: NFI accuracy assessment points distribution for the seven forest types

7.3 Results

7.3.1 Summary of results

The individual scene classification with the XGBoost algorithm had the advantage of reducing seasonality's effects on images captured at different times of the year, but it had the disadvantage of being time-consuming to execute. However, it could use the large training datasets available by following the individual scene

approach. Since the final outputs were free from seasonality disparity, the method was suitable for Tanzania's forest baseline classification.

7.3.2 Forest/Non-forest Classification

The binary forest/non-forest analysis produced 9 forest/non-forest maps of Tanzania (Table 7.2). The accuracy assessment was used to identify the map to take forward for further analysis.

7.3.2.1 Accuracy Assessment and Model Selection

The accuracy reported with this method for the nine models exhibited a satisfactory level of overall accuracy ranging from 68.46 ± 0.50% to 89.66 ± 0.40% (Table 7.2). The best three models were further evaluated to select the final model. Therefore, the final chosen model (Figure 7.10) with a single-scene threshold of 80% and multi-scene threshold of 50% when combining the results from the different scenes which depicted an overall accuracy of 89.66 ± 0.40%, F1-score of 0.87 and MCC value of 0.78 (Table 7.3), sufficiently separated primary forests from non-forest classes (Figure 7.8 and Figure 7.9).

Table 7.2: Evaluating classification models performance using accuracy assessment metrics for binary classification (forest/non-forest). The highlighted (coloured) indicates the three classification models with high accuracy. OA: Overall Accuracy; AD: allocation disagreement; QD: Quantity Disagreement; PC: Proportional Correct; TD: Total Disagreement; MCC: Matthews Correlation Coefficient

Classification model							
Single-scene (%)	**Multi-scene (%)**	**OA %**	**AD**	**QD**	**PC**	**TD**	**MCC**
30	30	68.46 ± 0.50	0.009	0.202	0.787	0.212	0.50
30	50	81.77 ± 0.50	0.029	0.123	0.847	0.152	0.67
30	80	88.17 ± 0.40	0.065	0.047	0.887	0.112	0.75
50	30	73.16 ± 0.50	0.016	0.181	0.802	0.197	0.56
50	50	88.11 ± 0.40	0.049	0.061	0.889	0.110	0.77
50	80	85.93 ± 0.40	0.039	0.080	0.879	0.120	0.72
80	30	80.84 ± 0.50	0.034	0.127	0.838	0.161	0.66
80	50	89.66 ± 0.40	0.100	0.003	0.896	0.103	0.78
80	80	81.24 ± 0.40	0.014	0.111	0.873	0.126	0.64

Table 7.3: A detailed accuracy metrics for the three classification models with high accuracy highlighted on Table 7.2: UA: User Accuracy; PA: Producer Accuracy

Classification model								
Single-scene (%)	**Multi-scene (%)**	**Cover type**	**UA %**	**PA %**	**F1**	**Precission**	**Recall**	**Commission**	**Ommision**
80	50	Forest	87.69 ± 0.70	87.86 ± 0.60	0.87	0.87	0.87	0.053	0.050
		Non-forest	91.11 ± 0.50	90.98 ± 0.40	0.91	0.90	0.91	0.050	0.051
30	80	Forest	79.35 ± 0.90	91.59 ± 0.60	0.85	0.91	0.79	0.080	0.032
		Non-forest	94.65 ± 0.40	86.20 ± 0.50	0.90	0.86	0.94	0.032	0.080
50	50	Forest	95.02 ± 0.40	80.43 ± 0.60	0.87	0.80	0.95	0.024	0.085
		Non-forest	83.04 ± 0.70	95.79 ± 0.40	0.88	0.95	0.83	0.085	0.024

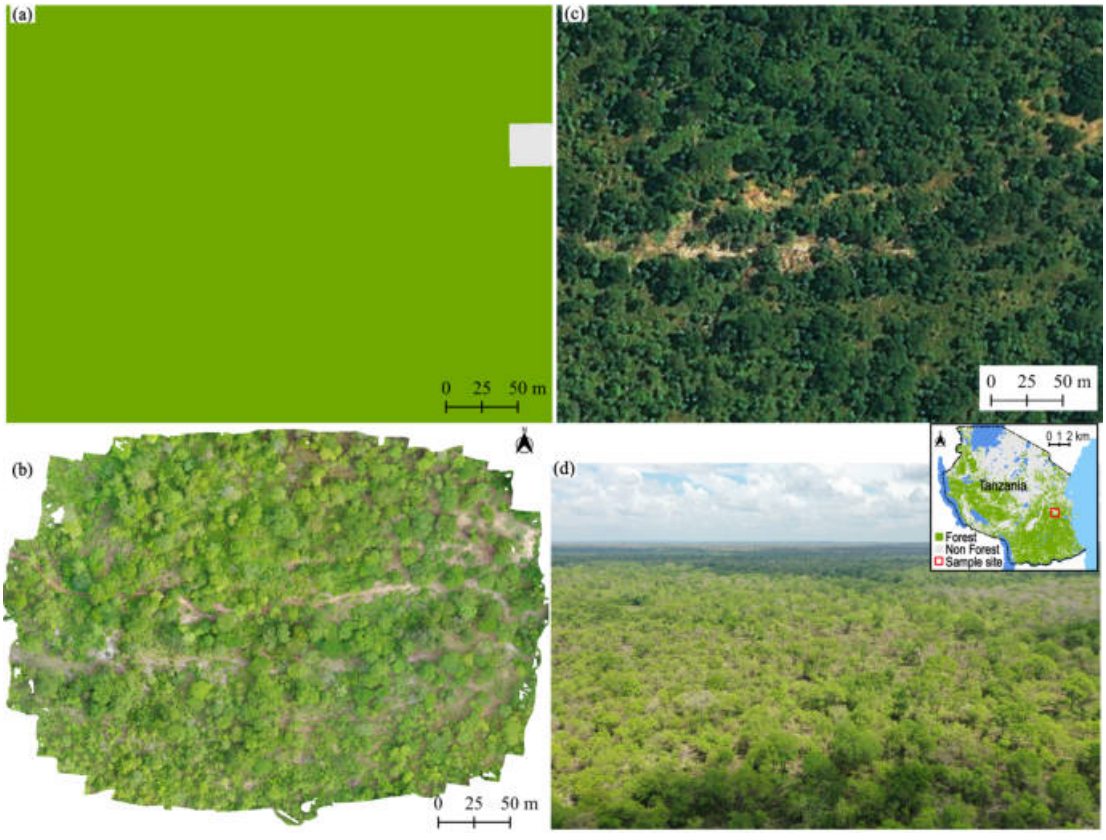

Figure 7.8: A detailed sample visual comparison of classification result at Ngulakula forest reserve-Rufiji based on field survey, November 2018: (a) Classification output (b) Drone orthomosaic (c) Bing Satellite (d) Field photo. Photo acquired by the author

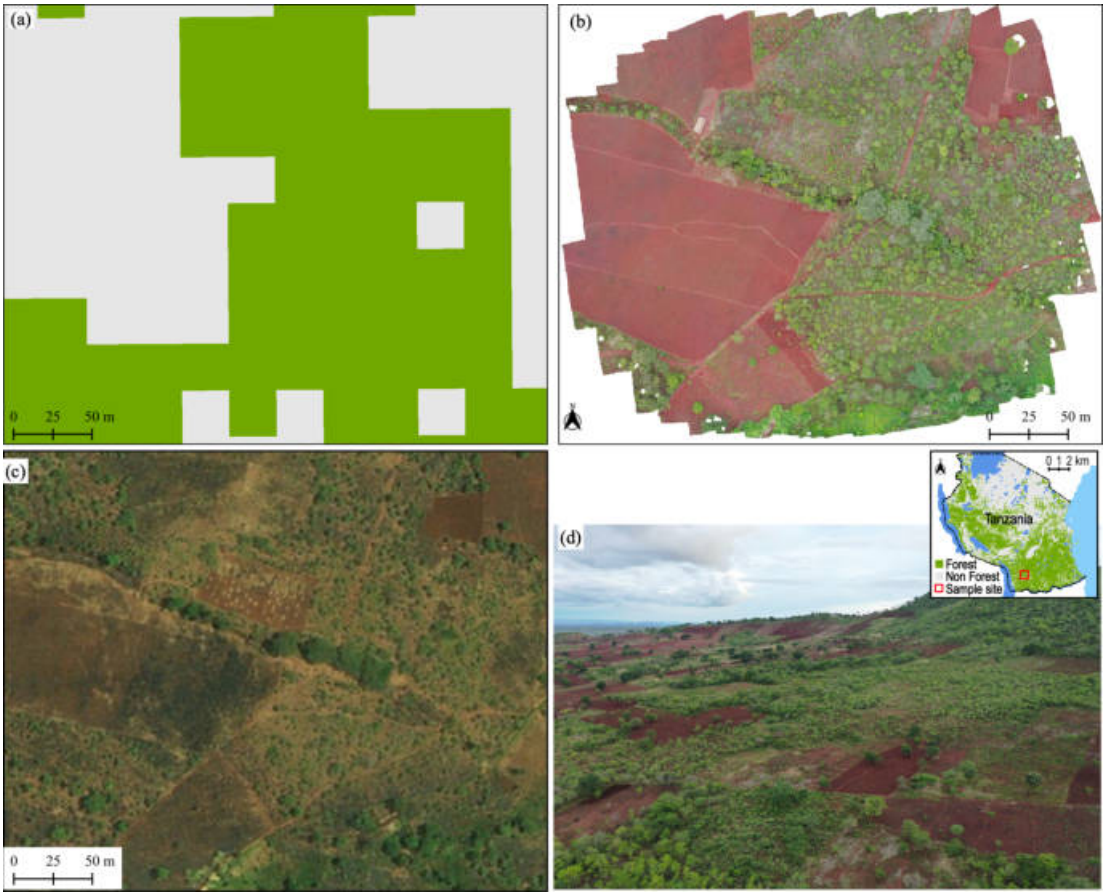

Figure 7.9: A detailed sample visual comparison of classification result on forest area cleared for farming at Lihanje forest reserve-Songea based on field survey, November 2018: (a) Classification output (b) Drone orthomosaic (c) Bing Satellite (d) Ground field photo. Photo acquired by the author

Figure 7.10: Map showing areal proportional of forest/non-forest cover from classification result in Tanzania

7.3.2.2 Source of Classification Error

The classification result was generated by isolating the generic forest class, and other vegetation types such as grassland and bushland, and this resulted in a high overall accuracy of 89.66 ± 0.40%. However, this still resulted in 10% error in the classification. From a visual assessment of the map, the likely sources of error were ascertained to be forest intermixed with edaphic areas and disturbances often by frequent fire, especially in woodland areas. Similarly, wetland areas (Figure 7.11) (yellow circle) and forest-grassland mosaic (Figure 7.12) remain evergreen

throughout the year.

The wetland classification is often challenging due to the seasonal vegetation dynamics and hydrological change following vegetation phenological differences in its growth period. Also, the complexity of the mountain terrain, such as those found at Mt. Kilimanjaro, Meru, and the Eastern Arc Mountains due to differences in the surface illumination between shaded and illuminated areas, impacts the classification accuracy results.

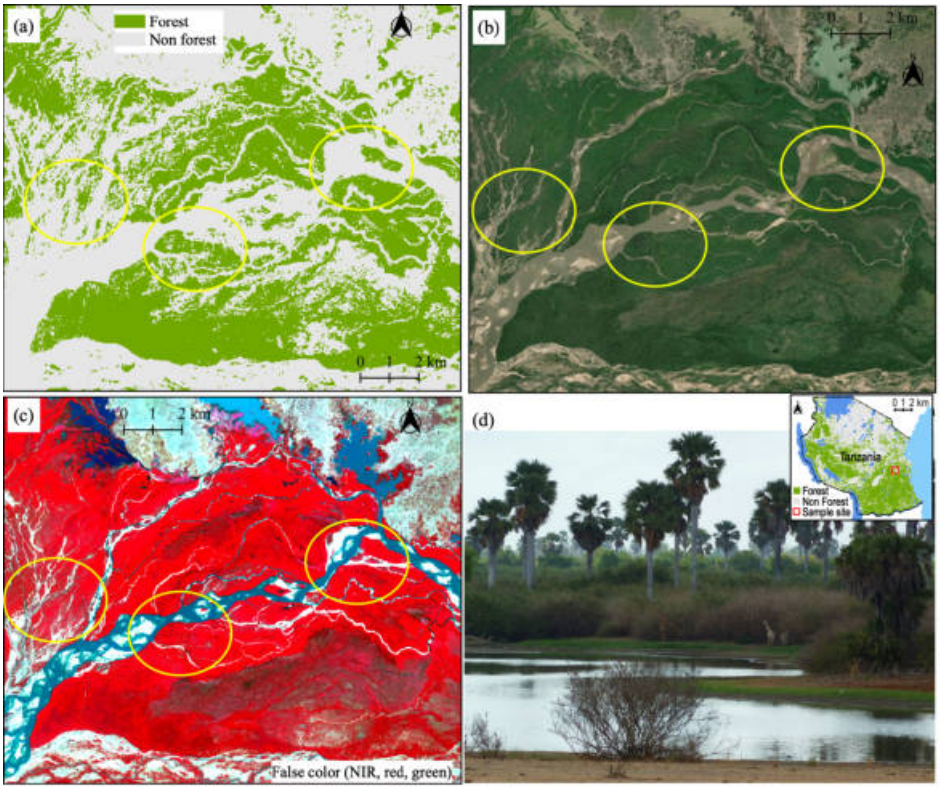

Figure 7.11: A detailed sample of classification error (yellow circle) on wetland area at Rufiji river- Selous Game Reserve: (a) Classification output (b) ESRI Satellite (c) PlanetScope image (pixel size = 3 m) (d) Ground field photo. Photo acquired by the author

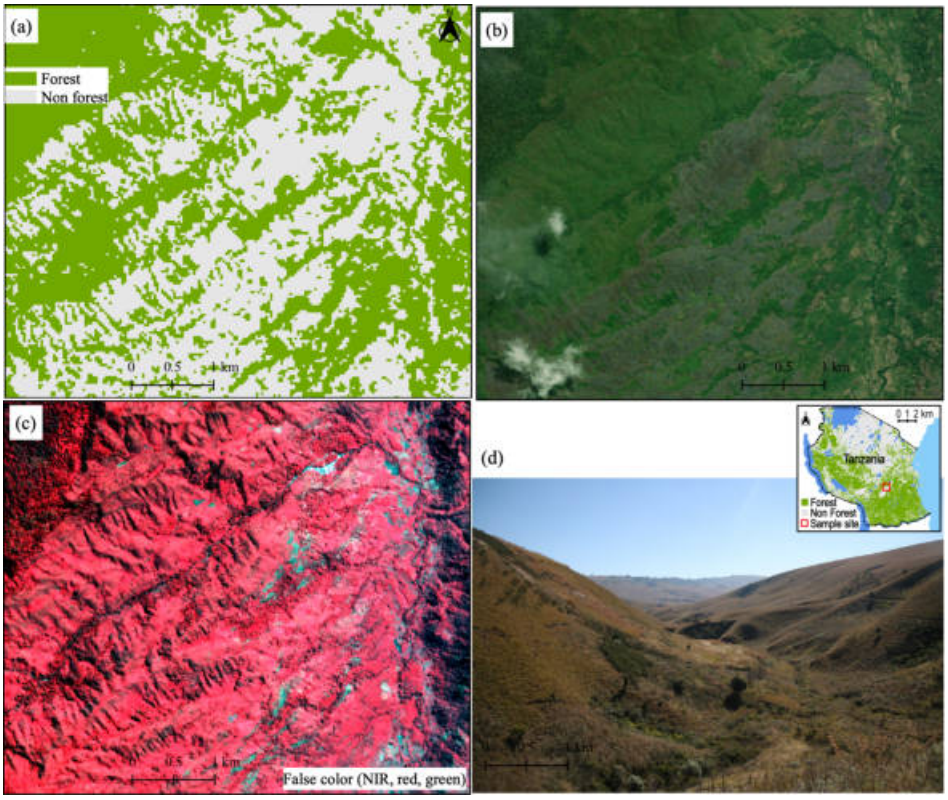

Figure 7.12: A detailed sample of classification error on mountain area with dense grassland, part of Uzungwa Scarp Nature Forest Reserve: (a) Classification output (b) ESRI Satellite (c) PlanetScope image (pixel size = 3 m) (d) Ground field photo. Photo acquired by the author

7.3.2.3 Forest Area Estimates

Table 7.4 presents the forest cover extent for Tanzania, as generated from the nine classification models. The results were compared with the previous national field inventory (NAFORMA) on a national scale. As shown in Table 7.4, the classification identified as being the best resulted in forest area estimates close to the NFI. Table 7.4 also demonstrates a relationship between the forest area mapped and the single-scene and multi-scene thresholds. As seen, the steps in the area mapped between the thresholds are also quite large. This might imply

that an improvement in the classification accuracy might be possible with further refinement of the threshold selection and is an area for further study.

Table 7.4: Estimated forest area from the classification results for the nine models compared with national forest inventory (NFI) - NAFORMA, with a relative sampling error of 8.89% on forests and woodlands, estimated at a total land area of 883,000 km^2 (MNRT, 2015). The highlighted (coloured) indicates the three classification models with high accuracy from Table 7.2.

Classification model						
Single-scene (%)	**Multi-scenes (%)**	**Cover type**	**Estimated area (km^2)**	**Area (%)**	**NFI area (km^2)**	**Area (%)**
30	30	Forest	756,686	84.87		
		Non-forest	134,913	15.13		
30	50	Forest	612,041	68.65		
		Non-forest	279,558	31.35		
30	80	Forest	321,124	36.02		
		Non-forest	570,476	63.98		
50	30	Forest	708,875	79.51		
		Non-forest	182,725	20.49		
50	50	Forest	521,238	58.46		
		Non-forest	370,361	41.54		
50	80	Forest	249,171	27.95		
		Non-forest	642,428	72.05		
80	30	Forest	614,830	68.96		
		Non-forest	276,770	31.04		
80	50	Forest	407,976	45.76	481,000	54.4
		Non-forest	483,624	54.24	402,000	45.6
80	80	Forest	156,134	17.51		
		Non-forest	735,466	82.49		

7.3.2.4 Forest Area Estimates Ranked by Region

Country-level forest statistics provide information on forest resource status and trends for policy formulation and progress in complying with regional and international commitments. However, it is also necessary to report forest extent (Figure 7.10) based on the regional administrative areas and streamline forest-related reporting to increase its usefulness and relevance at the local level. Table 7.5 summarises forest extent by region in Tanzania.

Table 7.5: Forest extent summarised using a map ranked by regions

Rank	Region	Area (ha)	Percentage (%)
1	Lindi	5,526,955	13.55
2	Ruvuma	5,059,867	12.40
3	Morogoro	4,295,711	10.53
4	Katavi	3,478,155	8.53
5	Tabora	3,054,801	7.49
6	Mbeya	2,163,746	5.30
7	Kigoma	1,988,670	4.87
8	Iringa	1,803,936	4.42
9	Pwani	1,739,369	4.26
10	Singida	1,689,458	4.14
11	Njombe	1,427,548	3.50
12	Songwe	1,220,258	2.99
13	Mtwara	1,203,790	2.95
14	Kagera	1,105,736	2.71
15	Tanga	951,165	2.33
16	Manyara	861,542	2.11
17	Rukwa	768,848	1.88
18	Geita	736,440	1.81
19	Dodoma	644,469	1.58
20	Kilimanjaro	377,028	0.92
21	Arusha	265,288	0.65
22	Shinyanga	177,709	0.44
23	Mara	92,345	0.23
24	Mwanza	89,022	0.22
25	Dar Es Salaam	43,970	0.11
26	Simiyu	31, 773	0.08

7.3.2.5 Forests in Protected Areas

The forest cover of *in-situ* conservation strategies such as protected areas is necessary for biodiversity and ecosystem protection in Tanzania. Therefore, this study also provides systematic information on how different protected areas (forest re-

serves and wildlife-managed areas) support critical forest cover extent as an ecological parameter required to produce desired conservation outcomes. Table 7.6 provides the forest extent in forest reserves and wildlife management areas in Tanzania. See Appendix 4 (Tables A.3, A.5, and A.6) for detailed forest extent in the individual protected area category.

Table 7.6: A summary of forest extent (ha) in protected areas

	Protected area category			
Cover	Forest reserve	Percentage (%)	Wildlife area	Percentage (%)
Forest	6,911,300	17	11,339,583	28

7.3.2.6 Trees Outside the Forest in Urban and Agroforestry Systems

Figure 7.13 shows a detailed sample result for the TOFs in an urban area (Dar Es Salaam). Similarly, Figure 7.14 displays an example area of the agroforestry system, which has vast potential in affording multiple advantages to individual farmers and communities. The performance of the classification algorithm proved to be suitable for mapping TOFs. However, not every single tree can be depicted, considering the spatial resolution of 30 m, and liable to exclude young trees due to their small and scattered canopies and moderate height.

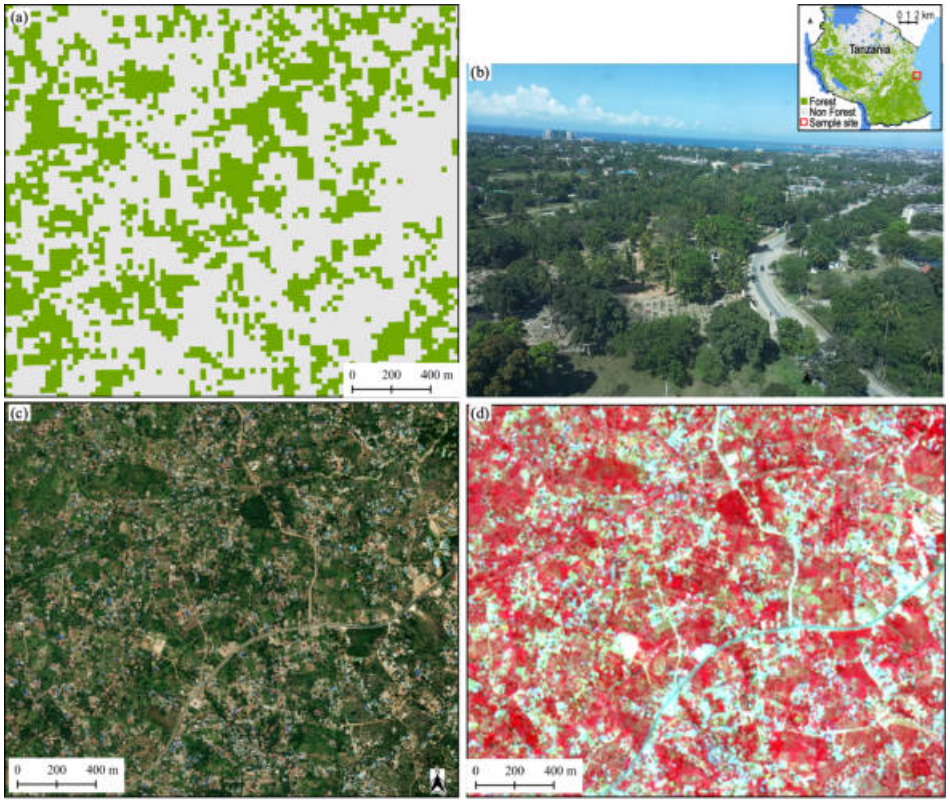

Figure 7.13: A detailed sample of classification result for the TOF (Dar es Salaam city). The spatial distribution and extent of TOF were not well understood earlier due to the complexity involved in accurately mapping in mixed tree/crop/ human settlements. This mapping includes all lands predominantly under urban use with trees and/or shrubs whatever their spatial pattern (in lines or strips, in discrete stands or scattered): (a) Classification output (b) Ground field photo (c) ESRI Satellite (d) PlanetScope image (pixel size = 3 m). Photo acquired by the author

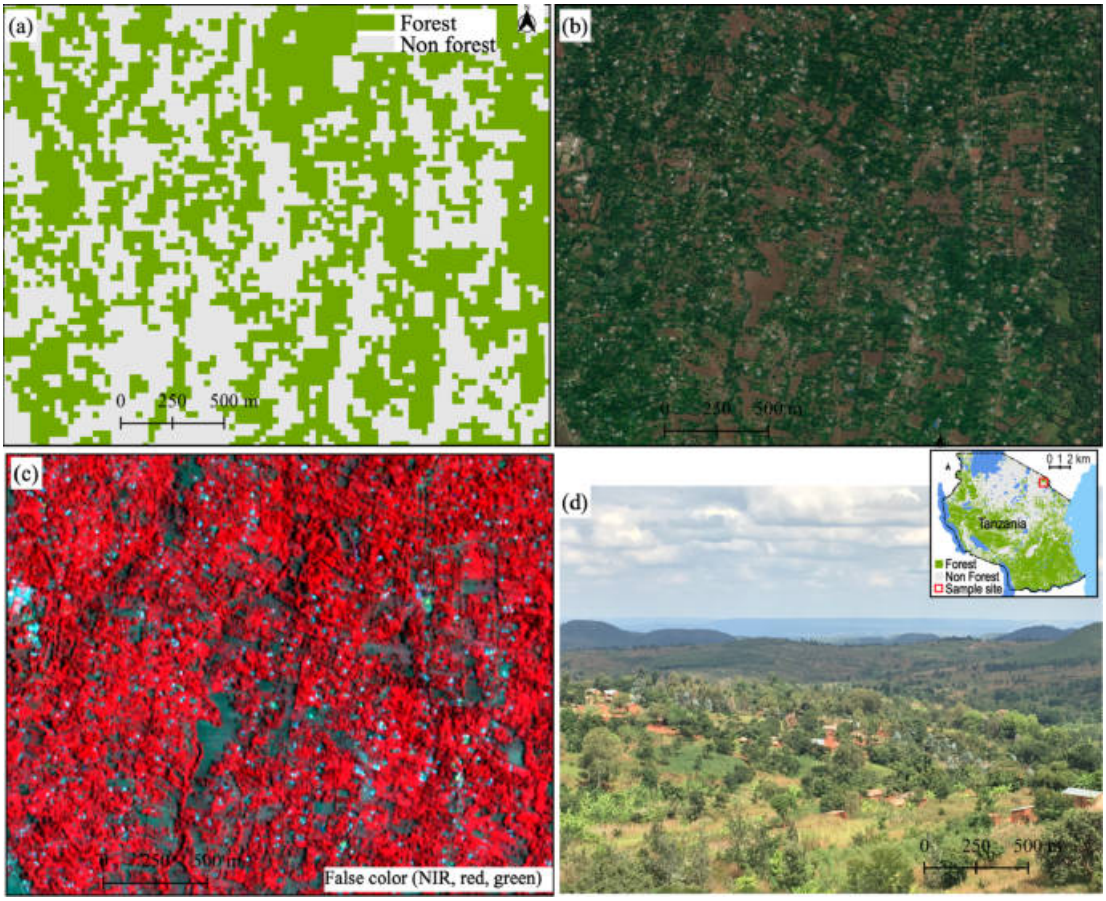

Figure 7.14: A detailed sample of classification result for agroforestry system: (a) Classification output (b) ESRI Satellite (c) PlanetScope image (pixel size = 3 m) (d) Ground field photo. Photo acquired by the author

7.3.2.7 Post Disturbance Forest Regeneration

The classification result also identified areas recovering from anthropogenic disturbance as a noticeable measure of forest ecosystem resilience. However, there is a limited forest recovery in unmanaged compared to managed forests derived from the Landsat. Long-term post-disturbance recovery on unmanaged forests is limited to the short fallow period due to human-induced perturbations and dependency that hampers forest recovery capacity. Therefore, capturing forest regeneration

in unmanaged forests remains a challenge as it rarely occurs. Hence monitoring forest recovery in managed forests is necessary for enhancing the management of the remaining forests. Figure 7.15 presents a sample area at Mohoro forest reserve in the Rufiji district that was highly deforested. Accordingly, the result provides quantitative evidence for using a Landsat sensor to monitor forest recovery from anthropogenic and natural disturbance events.

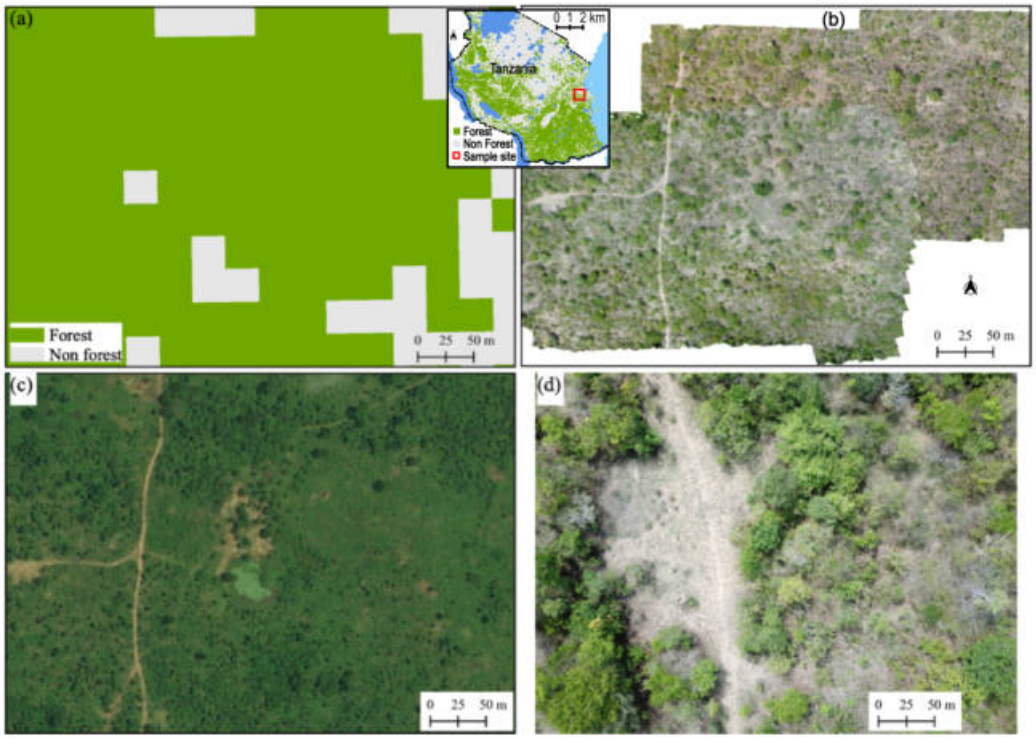

Figure 7.15: A detailed sample of classification results for forest recovering from human disturbances at Mohoro forest reserve. The classification result demonstrated that remote sensing can i) provide spatially meaningful recovery baselines on the nature of disturbance-recovery dynamics in forested ecosystems in Tanzania and ii) retrospectively quantify and characterise historic forest recovery trends that have implications for forest management, climate change mitigation, and restoration initiatives in the near term: (a) Classification output (b) Drone orthomosaic of October 2019 (c) Bing Satellite (d) Ground field photo. Photo acquired by the author

7.3.3 Forest Type Classification

The application of forest habitat suitability for constraining the forest types classification at a national scale was the challenge of differentiating the forest types by their spectral differences into distinct forest types, such as open and closed savanna woodlands that occur due to seasonal abscission (leaf-on/leaf-off) cycles of the year. Therefore, the approach adequately separated a range of distinct forest types and contributed important information on the current status of unique forest ecosystems and patterns in Tanzania (Figure 7.16).

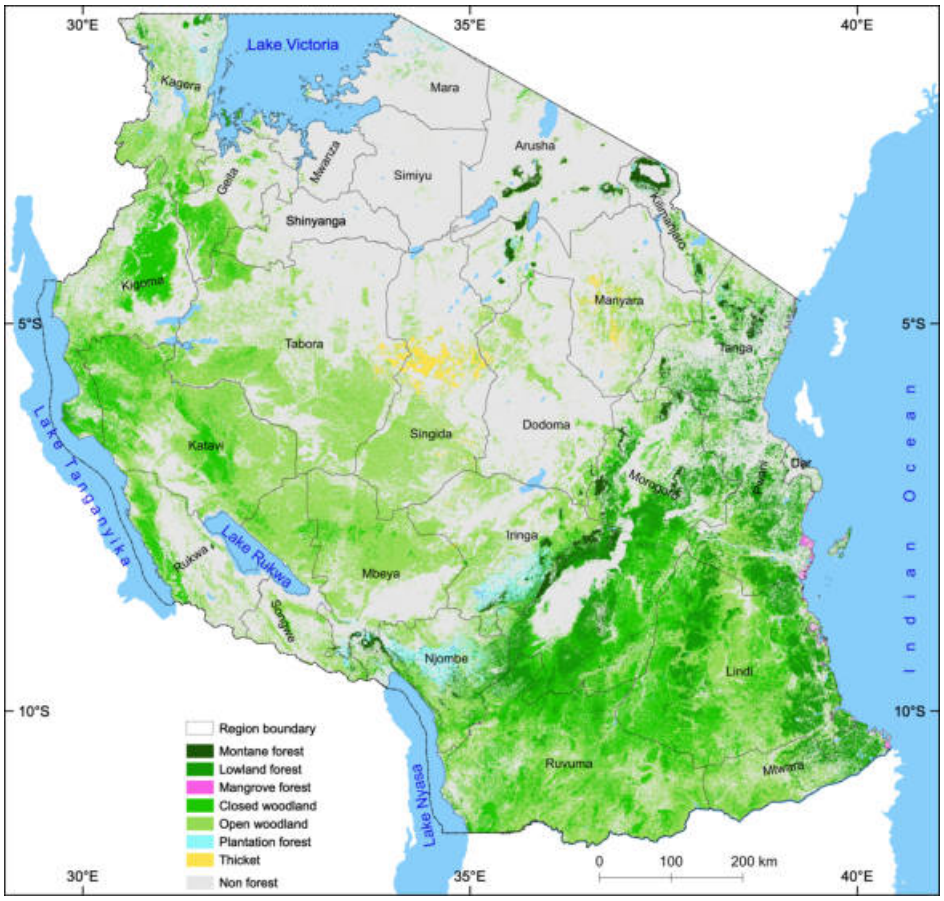

Figure 7.16: Map showing areal proportional of forest types in Tanzania

7.3.3.1 Accuracy Assessment

The forest types classification map's overall accuracy was 85%, with F1 scores ranging from 0.77 to 0.99. The areas distinguished as the different forest types can also be considered accurate due to the low quantity disagreement of 0.02 (Table 7.7). Therefore, the proposed method has produced a desirable classification result in a complex forest landscape with varying climatic conditions, from dry savanna to moist montane forest (Figure 7.18 and Figure 7.17). It showed an adequate level of agreement with the forest status on the ground.

Table 7.7: Thematic accuracy measures of the forest types classification: UA = User accuracy, PA= Producer accuracy

Forest type	**UA(%)**	**PA(%)**	**F1 score**	**Precision**	**Recall**	**Commission**	**Ommision**
Montane forest	88.53 ± 3.10	89.65 ± 2.80	0.89	0.89	0.88	0.002	0.003
Lowland forest	96.02 ± 0.90	88.55± 1.30	0.92	0.88	0.96	0.005	0.015
Mangrove forest	98.24 ± 0.34	100 ± 0.00	0.99	1	0.98	0.000	0.000
Closed woodland	72.35 ± 1.40	82.76 ± 1.10	0.77	0.83	0.72	0.067	0.049
Open woodland	89.73 ± 0.70	85.23 ± 0.60	0.87	0.85	0.89	0.057	0.068
Plantation forest	77.78 ± 5.5	90.32 ± 4.00	0.84	0.90	0.77	0.004	0.001
Thicket	89.60 ± 4.20	79.04 ± 4.00	0.84	0.79	0.89	0.001	0.003
Overall accuracy (OA)	**85.22 ± 0.50**						
Allocation disagreement (AD)	**0.11**						
Quantity disagreement (QD)	**0.02**						
Proportion Correct (PC)	**0.86**						
Total Disagreement (TD)	**0.13**						

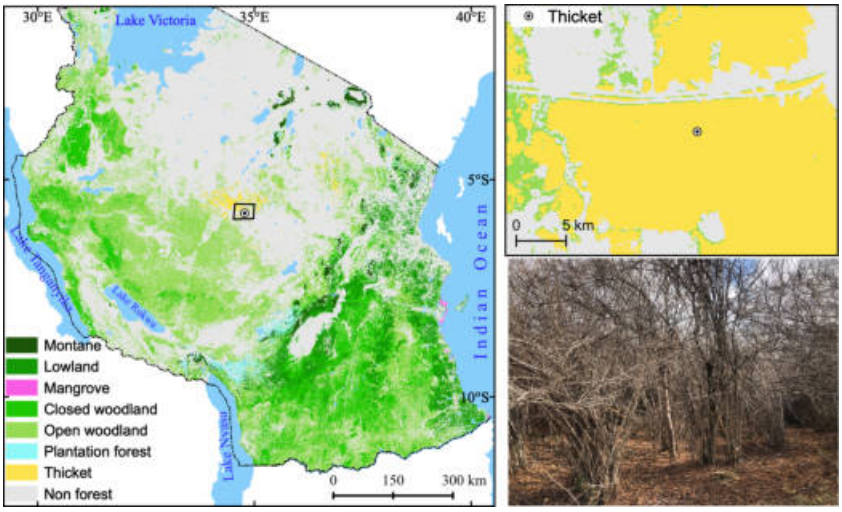

Figure 7.17: An illustration of a detailed sample of classification result of thicket woodland with a location of ground field photo. Photo acquired by the author

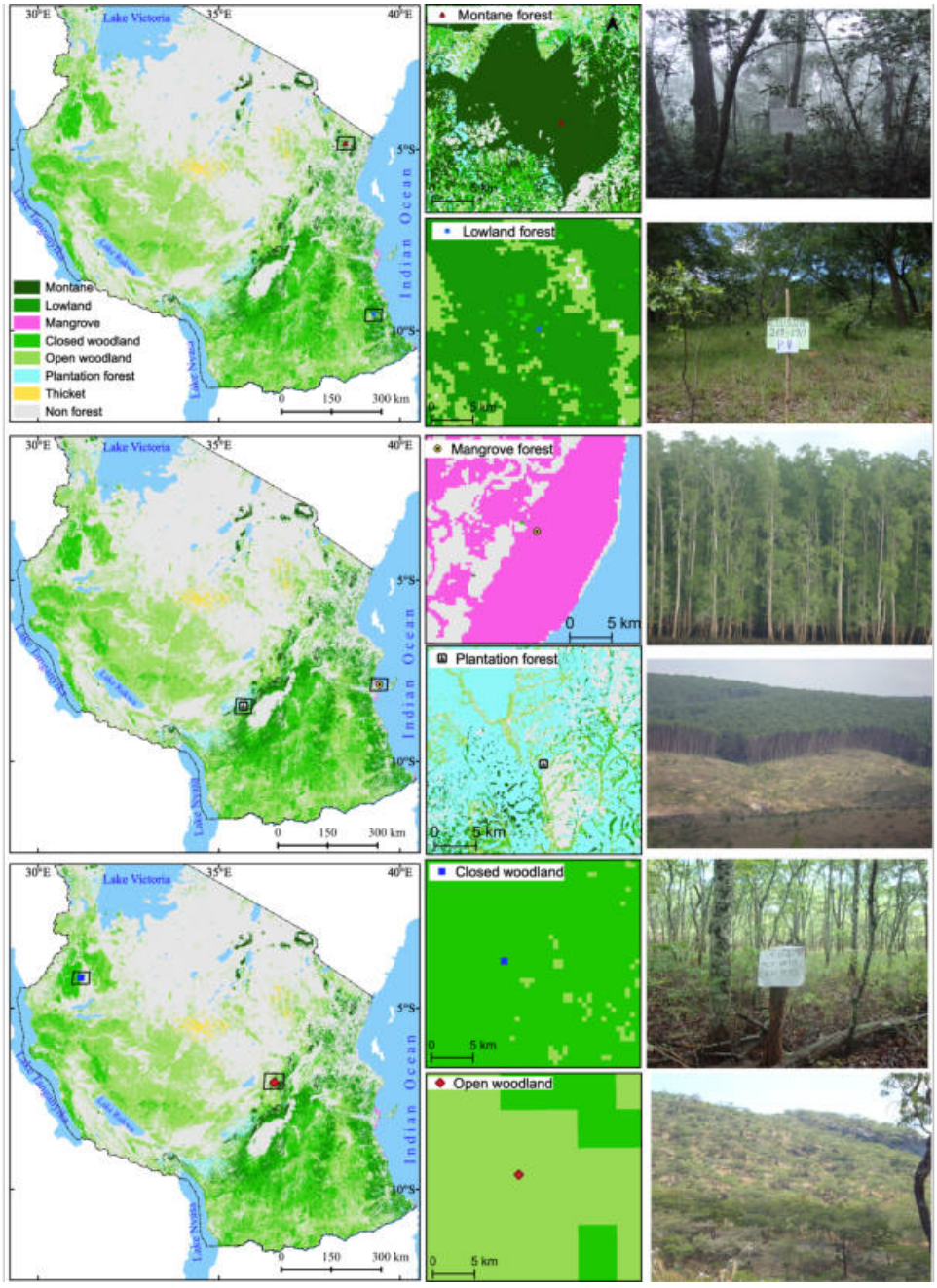

Figure 7.18: An illustration of a detailed sample of classification result for the forest types with a location of ground field photo. Photo acquired by the author

7.3.3.2 Sources of Classification Error

The main confusion within the error matrix lies among the deciduous forest types (closed and open woodland) (Table 7.8) as about 25% of closed woodland points were classified as open woodland, and 8% of open woodland points were classified as closed woodland. It remains a challenge to obtain a definite boundary between the two classes (Figure 7.19) as the difference is related to tree cover rather than species composition. Therefore, the spectral difference is associated with the percentage of background soil and/or grassland reflectance versus canopy leaf reflectance. This is associated with a broad overlap between an open and closed woodland and other forest communities (Figure 7.21). For example, the possibility of habitat overlap between closed and open woodland is estimated at 80%, and closed woodland and lowland is about 40% (Figure 7.21) and often results in misclassification.

Likewise, in the country's arid regions (Dodoma, Singida, Shinyanga, Simiyu, and parts of the Manyara region) (Figure 7.16), forests are primarily limited by the lack of water. They typically have low vegetation cover (Figure 7.20), which has led to significant hurdles to accurate retrieval of forest cover in these areas using remote sensing compared to humid regions. It remained with a sparse covering of vegetation (leafless drought-deciduous plants), with increased soil brightness. However, it is feasible to retrieve quantitative information about forest types in a heterogeneous landscape across a national level, necessary for forest monitoring despite these challenges.

Nevertheless, to minimize these classification errors, future studies could include mapping direct measures of canopy openness allowing the identification of spatial patterns of forest structure including discerning boundaries of forest structure

across gradients. Classifying the openness of the canopy of dry tropical forests remains a challenge when only using optical sensors and could benefit from a combination of other EO data such as from Sentinel-1 (S1) SAR or higher resolution Sentinel-2 (S2) optical sensors to capture and measure canopy openness (Verheghen et al., 2022).

Similarly, canopy height is a fundamental parameter for determining forest ecosystem functions such as biodiversity and above-ground biomass in Tanzania. The availability of Global Ecosystem Dynamic Investigation (GEDI), has provided sampled observations of the forest vertical structure at a near-global scale allowing for examining the vertical structure of vegetation spatially and temporally (Adrah et al., 2022). Using these data would help better comprehend the variation in canopy height in tropical forests, thereby supporting forest management practices, and monitoring forest response to climatic changes.

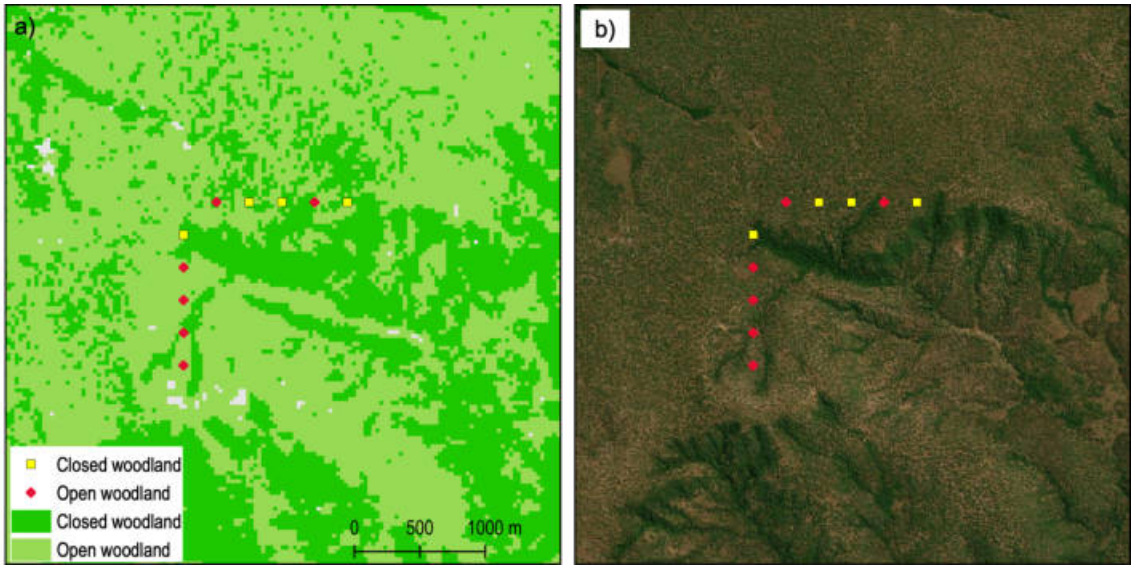

Figure 7.19: An illustration of a detailed sample of woodland landscape with a mosaic of closed and open woodland a) Classification result b) ESRI satellite image

Figure 7.20: Example of the sparse woodland area from the semi-arid region of the country. Semi-arid woodlands are eco-sensitive with minimal water resources and experience fluctuations in plant biomass. Soil brightness can interfere with signals for green vegetation classes due to both the comparatively low concentration of green vegetation in these areas and the physiological factors of the plants themselves leading to less pronounced spectral curves than related forests in wetter areas. Thus, given the sparseness and patchiness of vegetation in the landscape, the use of Landsat data at 30 m resolution may increase the possibility of excluding the spectral contribution of vegetation within individual pixels leading to classification error. High-resolution images such as Sentinel 2 imagery may provide a better solution for classifying these forest types in semi-arid areas. (Source: NAFORMA 2013)

Table 7.8: A contingency table for the forest types classification accuracy assessment. The highlighted points (red) for closed and open woodland indicated more mixing among the two classes. Cw=Closed woodland, Lo= Lowland, Ma= Mangrove, Mo= Montane, Ow= Open woodland, Pf= Plantation forest, Th= Thicket

		NFI field data						
		Cw	Lo	Ma	Mo	Ow	Pf	Th
Classification	CW	**2818**	67	0	5	987	0	18
	Lo	33	**1640**	0	17	18	0	0
	Ma	1	0	**56**	0	0	0	0
	Mo	1	35	0	**355**	4	6	0
	Ow	547	94	0	7	**6031**	12	30
	Pf	5	16	0	12	15	**168**	0
	Th	0	0	0	0	21	0	**181**

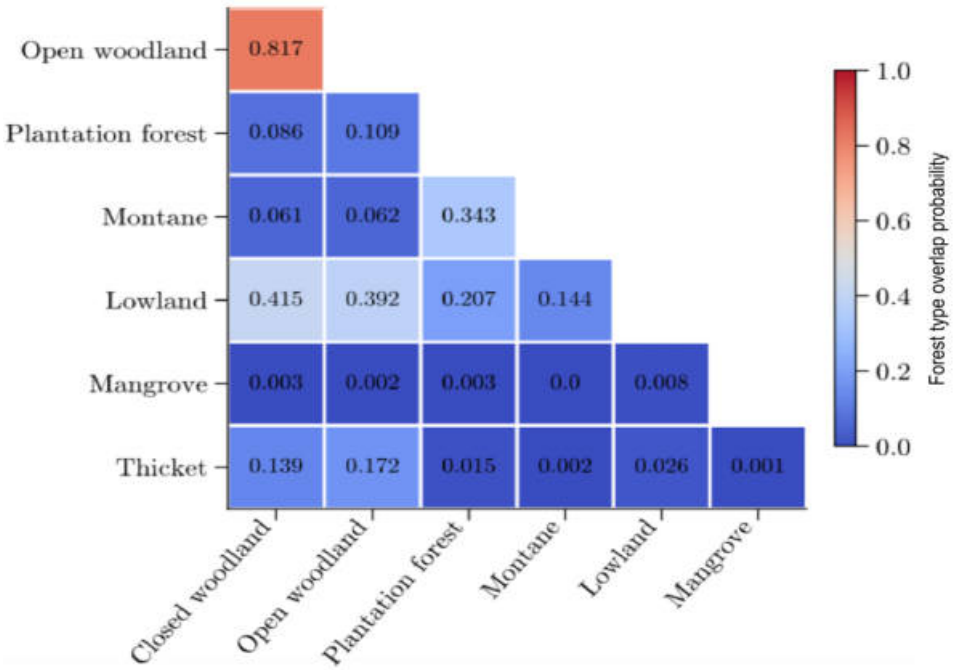

Figure 7.21: Estimated probability of forest types overlap (mosaic) in Tanzania based on national forest inventory measurements. The mosaic pattern tends to increase on the woodland landscape as compared to other forest types. This has a challenge on separability and hence accuracy assessment.

7.3.3.3 Forest Types Area Estimates

The forest type classification model produced compatible areal estimates compared with the national forest inventory (NAFORMA) with some minor differences among the forest types (Table 7.9), mostly open woodland with difficulty distinguishing from other related forest types such as closed woodland and lowland forest. The largest forest type by area is open woodland presenting 57%, followed by closed woodland with 22%. Therefore, woodlands occupy around 79% of the forest types, spreading from the central to the western part of the country and with a mosaic of lowland forest along the coast and southern Tanzania (Figure 7.16). The observed differences for the lowland forests are due to the challenges of differentiating lowland from the montane forest and open and closed woodland during inventory. The majority of the lowland forests were categorised as closed and open woodland.

Table 7.9: Estimated area for the forest types classification as compared with National Forest Inventory (NFI)-NAFORMA assessment

Forest types	**Map area (km^2)**	**Percentage (%)**	**NFI area (km^2)**	**Percentage (%)**
Montane forest	9,716	2.35	9,953	2.03
Lowland forest	60,670	14.65	16,565	3.38
Mangrove forest	767	0.19	1,581	0.32
Closed woodland	93,004	22.45	87,290	17.79
Open woodland	237,052	57.22	359,973	73.37
Plantation forest	6,695	1.62	5,545	1.13
Thicket	6,368	1.54	9,719	1.90

7.3.3.4 Forest Types Area Estimates Ranked by Region

The generated forest types (Figure 7.16) spatial distribution has also summarised by regions (Table 7.10) potentially important for production forestry, conservation

and planning.

Table 7.10: Forest types extent ranked by region

Rank	Region	Forest type (area (ha))						
		Montane	Lowland	Mangrove	Closed woodland	Open woodland	Plantation forest	Thicket
1	Lindi	-	1,377,894	7,691	2,057,557	2, 082,704	1,046	-
2	Ruvuma	12,125	332,343	-	2,009,182	2,699,130	7,088	-
3	Morogoro	186,449	1,561,300	-	1,606,680	926,625	14, 353	303
4	Katavi	-	3,101	-	1,022,021	2,452,964	-	-
5	Tabora	-	-	-	182,788	2,801,021	-	70,992
6	Mbeya	54,322	15,047	-	150, 698	1,903,027	38,881	-
7	Kigoma	771	36,955	-	1,023,376	920,846	6,722	-
8	Iringa	172,536	210,891	-	128,863	1072,248	210, 092	9,305
9	Pwani	276	971,532	36,433	342,745	387,265	1116	-
10	Singida	-	-	-	4,324	1,379,695	-	307,215
11	Njombe	76,484	204,612		178,271	652,490	315,705	-
12	Songwe	7,022	73,34	-	117,659	1,075,793	12,450	-
13	Mtwara	-	321,153	1,717	191,003	689,912	-	-
14	Kagera	1,522	65,396	-	191,273	841,122	6,422	-
15	Tanga	109,982	376,893	2,194	121,568	318,368	22,724	77
16	Manyara	41,316	6234	-	53,565	633,332	11,490	115,604
17	Rukwa	2,062	330	-	277,576	488,638	376	-
18	Geita	-	14,400	-	254,730	466,922	373	-
19	Dodoma	8,626	232	-	39,694	563,069	-	32,719
20	Kilimanjaro	137,233	13797	-	33,472	172,667	19,493	365
21	Arusha	121,967	4,346	-	16,547	116,442	5963	23
22	Shinyanga	-	-	-	25,980	151,725	-	-
23	Mara	-	7520	-	13,700	51,877	18,768	-
24	Mwanza		12,902	-	6,984	65,886	3248	-
25	Dar Es Salaam	-	8,909	584	4,929	29,451	97	-
26	Simiyu	-	-	-	465	31,272	-	-

7.3.3.5 Estimated Area of Forest Types in Protected Areas

The study also presented a forest baseline under different forest management regimes regarding the forest cover amount within each protection category based on the forest types (Table 7.11) as an essential component in enhancing the protection of distinct species assemblages. See Appendix 4 as Tables A.3, A.5 and A.6 for detailed forest types in the individual protected area category.

Table 7.11: Forest types in protected areas

	Forest type (area (ha))						
Protected area	Montane	Lowland	Mangrove	Closed woodland	Open woodland	Plantation forest	Thicket
Forest reserve	379,626	643,797	58,336	1,254,700	4,426,201	127,952	20,686
Wildlife area	268,842	1,171,620	-	3,551,964	6,201,071	-	146,087

7.4 Discussion

7.4.1 Classification Results

This study has demonstrated the application of a machine learning classifier (XGBoost) and EO data on forest and forest types classification for Tanzania. The evaluation of independent nine classification models for the forest/non-forest (Table 7.2) presented the model with a single-scene threshold of 80%, and a multi-scene threshold of 50% showed the highest overall accuracy of 89.22% with an F1-score of 0.87 sufficient for reporting of forest extent in Tanzania. However, future studies could try to optimise these thresholds further. The overall accuracy for forest types classification was slightly lower at 85%, with an F1-score ranging from 0.77 - 0.99. However, the unique introduction of habitat suitability modelling constrained the classification such that a forest type was only considered for classification in appropriate geographic regions (Figure 7.16). A particular challenge for the classification of forest types was differentiating closed and open woodland areas, as the boundary between these classes is based on the tree cover rather than the species composition of the woodlands. Future studies could also consider approaches that aim to retrieve associated biophysical parameters such as canopy cover. However, the result is considered the best mapping of Tanzania currently

available and could be applied to other neighbouring countries (e.g., Kenya and Mozambique) which have similar ecosystems.

The available training data played an important role in the classification and was a determining factor in terms of the accuracy of the thematic classifications. Three aspects were considered during training data collection: sample size, proportions of the training data to be representative of the actual class in the landscape, and minimal spatial autocorrelation. Therefore, the quality of the training data set was a determining factor for the accuracy of the classification thematic maps.

These maps will help to establish a structure and long-term forest monitoring system in Tanzania. Forest cover information is needed to support the national forest policy to manage sustainably, conserve, restore and utilise forests and associated resources for Tanzania's socio-economic growth and climate resilience. Importantly for addressing issues of REDD+ and GHG as international reporting commitments and the 2030 Agenda for SDGs over fighting deforestation (Anderson et al., 2017).

A further consideration is that the study used imagery over a 5-year period (2013 – 2018) to mitigate the issue of sufficient data availability given the high level of cloud cover, particularly in the coastal areas. However, change will have occurred in the forest extent during this period. Therefore the forest extent and type maps represent the forest cover for the majority of the scenes within the period. Within Chapter 8, the maps are updated to be up to date for the end of 2018.

7.4.2 Forest Area Estimates

Given the increasing trend in Tanzanian population growth (Figure 3.9) (World Bank, 2019), the need for food, water, and other products will increase pressure on the remaining forest resources. Therefore, it is timely to update forest cover mapping with the aim of enhancing forest cover and climate change mitigation and adaptation at a national level. The forest cover extent over the country was estimated with an area of 407,976 km^2, which accounts for 45.76% (Table 7.4) of the country landmass area.

From the forest types classification, the woodlands (closed, open woodland, and thickets) are the most prominent class and an important ecosystem of great significance to human economies (Mitchard and Flintrop, 2013; Campbell et al., 2007), estimated to cover about 336,405 km^2 which makeup 81.20% of the forested land in Tanzania and mainly covering the central and western part of the country. The montane forest as a biodiversity hotspot along a chain of isolated mountain ranges (Figure 7.16) supports a diversity of endemic species (Fjeldså, 1999) and was estimated at 9,717 km^2 representing 2.35% of the forest cover (Table 7.9). The lowland forest habitat overlapping with montane forest and woodlands with the most significant biological value and source of water supply for wildlife and people; was estimated to cover 60,718 km^2, presenting 14.16% of the forest cover, next to closed woodland (Table 7.9).

Compared to previous forest assessment results in Tanzania from the national forest inventory, this analysis's output is comparable with some differences, especially for the delineated woodlands (Table 7.8). The National Forest Inventory (NAFORMA) conducted from May 2011 to June 2014 estimated the total forested

land in Tanzania at 481,000 km^2 of land, equivalent to 54.4% of the total land area of 883,000 km^2, with a detailed of forest types extent summarised on Table 7.9.

The differences between forest inventory and this result can be explained as different timing between the two analyses. The field inventory data were collected at the sampling plot level and typically aggregated to the forest stand level at a country size (Hościło and Lewandowska, 2019). It is mainly associated with challenges of reaching some areas with traditional forest inventory and pushing in sampling intensity reduction and focused sampling effort with few samples/plots selected from these areas (Mitchell et al., 2017) particularly in the mountains. For example, from the national forest inventory (NAFORMA), the number of plots in a cluster varies from six to ten, depending on the determined challenge to reach the plots (Vesa et al., 2010) resulting in a relative sampling error of 6.87% for forests, 2.02% woodlands and 6.91% for thickets (bushlands) (MNRT, 2015).

7.4.3 Potential Forested Areas in Tanzania

Analysis of the distribution of forests in Tanzania indicates that the coastal, southern highlands and western parts of the country are mostly covered with forests (Figure 7.10 and Figure 7.16). These areas occupy a significant portion of the designated areas for forest reserves and wildlife-managed areas in Tanzania (see Appendix 3 and 4 as Figure A.1 and Tables A.3, A.5 and A.6). Management of protected areas highlights an efficient management approach for forest conservation efforts (Rosa et al., 2018). With the economy's progress, industrial forest plantations have grown enormously in Tanzania. The increase in plantation forests

from government, community, and individual farmers with most of the planted area situated in the southern highlands (Figure 7.16), supports this part of the country mapped with high forest extent (Kimambo and Naughton-Treves, 2019).

Future expansion of forest plantations in Tanzania will significantly improve landscape-scale restoration and can bring degraded land back into production, and improve the provision of ecosystem services in enhancing the ecological integrity and tackling climate and environmental challenges. If managed effectively, forest plantations provide the potential to sustainably supply a substantial proportion of the goods and services required by the communities, and therefore allow other forest areas to be managed for conservation and protection objectives in mitigating climate change impacts. Plantation forestry also is also likely to change from large-scale investments to those that are small or medium-scale in which local households and communities are owners or co-owners or be employed in forestry and wood processing. This is anticipated to new livelihood opportunities for Tanzanian communities.

7.4.4 Implications for Forest Management

Application of EO data will enhance timely sustainable forests and forest types management on the status, extent, and location, and forms an essential component of implementing the 2030 Agenda for achieving the Sustainable Development Goals (SDGs), particularly SDG15 (Sayer et al., 2019) in developing countries. Management of forests in Tanzania is mainly challenged by rapid population growth and ongoing climate change and hence remains a matter of debate. Consequently, the updated forest classification results will also promote the management of the

TOFs (Figure 7.13 and Figure 7.14) as an essential component, contributing to the scenic value of the landscape and carbon storage functions (Chakravarty et al., 2019). Therefore, information on TOFs is relevant as a basis for improving forest monitoring and land management decisions to help sustain tree cover and reduce pressure on TIFs in Tanzania.

Similarly, the classification method also captured the regenerating forests (Figure 7.15), which is essential for attaining the current and future forest management aimed at ensuring forest sustainability (Ligate et al., 2019). Monitoring forest recovery is a fundamental determinant in understanding forest status, extent, location, and dynamics, as functional conservation and forest management. The information from regenerating forests is crucial, especially for measuring conservation efforts necessary for environmental policy intervention and protection to mitigate biodiversity losses (Crouzeilles et al., 2017).

Therefore, the development of a baseline for forest recovery will subsequently provide trends and a framework to complement and integrate existing information on forest recovery from disturbance, including ground measurements. Such baseline information is essential for identifying spatial and temporal trends regarding forest disturbance and recovery that can be used to inform and bound questions related to forest management and climate change and support policy development. These are essential measures associated with the return of vegetation and trees to the land.

However, future analysis will require the use and application of airborne laser scanning (ALS) data that provide robust canopy height and cover measures to enable assessments that should provide insights into the return of forest structure (White et al., 2022).

This study's outcomes describe the ability to provide a reliable, comprehensive, and up-to-date forest map over a large area on a national scale. This information is essential to improve forest management, monitoring changes, habitat and biodiversity assessment, and forest carbon estimation. The spatial distribution and areas of forests in Tanzania gained immense attention to reduce the environmental and social impacts of forest exploitation. This information can help identify and plan for conservation efforts and opportunities to minimize the effects on biodiversity and livelihoods. Hence, the methodology developed is transparent, transferable, and presents a timely national forest and forest-type extent.

7.5 Conclusions

The establishment of a forest baseline is an important step towards creating a forest tract and related changes for future monitoring in support of decision-making. The changes in Tanzanian forest cover are still alarming; for example, according to the FAO report of 2020, Tanzania is placed among the countries with large forest area declines since the 1980s. The rate of changes based on the compound annual change rate indicates the increase in forest loss from 1990 - 2020 for about 0.88% representing 420,500 ha of forests deforested annually (FAO, 2020).

Therefore, advancements in remote and close-range sensing techniques are essential in attaining scientific output and improving forest monitoring in Tanzania for future development. This study's method produces the first consistent and robust estimates of forests and forest types covered in Tanzania using machine learning classification and EO data. These results reduce the uncertainty concerning forests and forest types extent as previous studies provided inadequate coverage.

This study has also contributed essential information for both science and forest management in Tanzania. However, clouds and shadows remain a critical challenge for the number of observations with free pixels, especially along the coast of Tanzania. To overcome this problem, the algorithms generated in this study could be implemented and further enhanced with the fusion of both optical and SAR imagery. Sentinel-2 images are ideal for large-scale analysis due to an extensive swath and dense series (Hościło and Lewandowska, 2019). The methods developed in this study could be directly transferred to these data, allowing up-to-date forest cover and forest-type maps with an increased spatial resolution of 10 m to be generated. SAR images from Sentinel-1 and PALSAR-2 could be used to offset the impacts of clouds, haze, and dust, which are freely accessible to map forest cover in Tanzania. Similarly, single-scene and multi-scene thresholds were arbitrarily selected to maintain computational viability, but future work can experiment with other thresholds to improve large-scale classification results and obtain an optimal value.

Chapter 8

Forest Change Extent and Monitoring of Tanzania

This chapter is based on:

John, E., Bunting, P., Hardy, A.; Silayo, D.S., Masunga, E., 2021. A Forest Monitoring System for Tanzania. *Remote Sensing* 13, 3081. https://doi.org/10.3390/rs13163081

8.1 Introduction

This chapter aims to create a forest change and monitoring framework for Tanzania centered on reporting change estimates derived from Earth Observation (EO) data. Consideration is needed for the availability of imagery, production of analysis-ready data products, the management of computational resources (compute and storage), and appropriate image processing and change detection approaches. The changes within forested regions result in two types of responses, abrupt changes (e.g., deforestation or fire) or gradual changes (e.g., disease, pests, or climatic). Natural changes within the system are often gradual or cyclic, such as fire burning, a key part of the savanna ecosystem. However, anthropogenic changes usually result in abrupt deforestation events that also result in long-term land use changes. Therefore, this monitoring system's primary focus is to identify abrupt changes, which are likely to result in long-term changes in land cover and use.

Therefore, the forest monitoring system should provide the capability for observing changes in forest resource extent, understanding the volume and frequency of unplanned deforestation, restoring degraded forest landscapes, and evaluating the vital function of carbon sequestration by forests and wooded lands. This provides the opportunity to develop a sound forest resource information system based on up-to-date and reliable information and to create national forest policies, planning, and sustainable development (Romijn et al., 2015).

Large-scale forest monitoring by remote sensing has been widely reported from global forest change datasets and gives reasonable initial forest loss estimates (Galiatsatos et al., 2020; Chen et al., 2020). The Hansen et al dataset[1] version 1.7 at

[1] http://earthenginepartners.appspot.com/science-2013-global-forest

the resolution of 30 m that provides a global forest loss estimate from 2001 - 2020 (Hansen et al., 2013). As a global and freely available dataset offers extensive forest change analysis, the accuracy of which should be assessed for Tanzania and a comparison made with the results of this study.

Therefore, this chapter provides a practical quantification of forest monitoring in Tanzania and uses long-term datasets to capture occurrences and trends linked to forest changes. The change analysis is based on the forest baseline developed in Chapter 7. It is focused on explaining the changes in forest extent and assessing the potential effectiveness of the system in forming the basis for and enhancing the national forest monitoring system in Tanzania. A further consideration is that the system should be as automated as possible, requiring little or no operator input while scalable to provide national coverage of Tanzania.

8.2 Method

8.2.1 Datasets

8.2.1.1 Benchmark Forest Mask

The forest/non-forest map from Chapter 7 (Figure 7.10) was utilised for forest change analysis at a country level (Figure 3.1), where only deforestation changes within the forest/non-forest mask were considered (Figure 8.1).

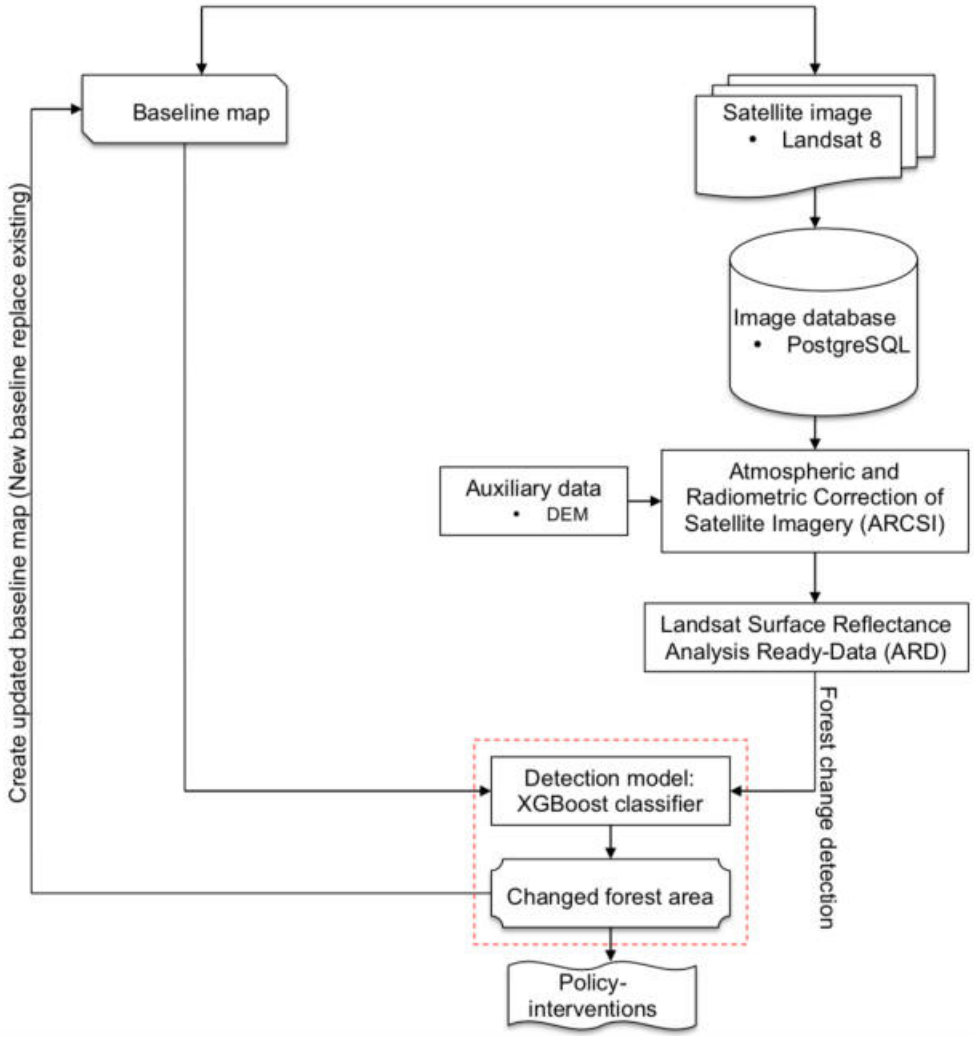

Figure 8.1: Forest monitoring system design for change detection in Tanzania

8.2.1.2 Satellite Images (Landsat 8)

The Landsat 8 (OLI-TIRS) images from the collection 1 archive were used for this analysis and processed to the same ARD produced as detailed in the earlier chapters (see Chapter 4 for details). Data were downloaded and processed for the period of May to October 2018, 2019, and 2020. The FMask detection algorithm

(Zhu et al., 2015; Foga et al., 2017) was used for cloud masking, but an addition 'clear-sky' produced was also derived through the RSGISLib software (Bunting et al., 2014).

Following clouds and cloud shadows masking, it is common to get many small areas of imagery between the clouds left over. In many cases, those small regions of imagery are either not useful for a given application and/or atmospheric correction of the regions is of poor quality due to adjacency effects from the clouds and atmosphere associated with a cloudy environment. The clouds and cloud shadows omissions are also commonly found in these regions around the identified clouds.

A solution to this problem is to select only the areas of the scene above a particular size threshold as being 'useful', discarding the rest. Within RSGISLib, this is referred to as a 'clear-sky' mask. The generation of the 'clear-sky' product is a two-step process. The first step is to buffer the identified cloud by 30 km. Those regions outside of the resulting mask were clumped, and only those with a size greater than 3,000 pixels were selected. They were grown, so they were not within 10 km (30 Landsat TM pixels) of an FMask cloud or cloud shadow object.

The application of the 'clear-sky' analysis results in a reduction in the available data, with useful data being lost. However, it also reduces errors in the following change analysis associated with omissions in the cloud masking.

8.2.2 Software System

At the core of the monitoring system is the EODataDown[2] software (Bunting, 2018). EODataDown can be configured to automatically download and process Landsat, Sentinel-2, and Sentinel-1 data to an analysis-ready data product. The analysis is executed in date order with the oldest image first. Following the generation of an analysis-ready data product, EODataDown can execute a set of user-defined plugins that perform a set of data analysis tasks. Each time the system is executed, the latest imagery is downloaded and analysed. However, by using a tool such as cron[3], the system can be automated to execute independently at a set time interval (e.g., daily or weekly) and therefore create a monitoring system.

For this study, EODataDown was configured to download, and process Landsat 8 imagery for Tanzania with a set of user-defined plugs implemented to create a monitoring system for forest change in Tanzania. The plugins implemented were:

1. Generate the clear-sky mask
2. Generate initial per-scene change masks
3. Apply XGBoost classifiers to generate the final change product for the scene

The advantage of the EODataDown system is that it allows the end-user to focus on their data analysis while the EODataDown architecture manages the system data storage and processing, creating a monitoring system.

[2] https://eodatadown.remotesensing.info/, https://github.com/remotesensinginfo/eodatadown
[3] https://en.wikipedia.org/wiki/Cron

8.2.3 Mapping Forest Change

8.2.3.1 Forest Change Definition

Changes in forest cover can start with modification or direct conversion. Forest modification results in changes in the structure, composition, and function of forests causing the reduction of many ecosystem benefits, including loss of connectivity. It is often also a precursor to outright deforestation (Grantham et al., 2020). However, the conversion of forests consists in clearing natural forests (deforestation) to use the land for other purposes, often agricultural (crops or creation of pastures for livestock), but also for mining, infrastructure, or urbanisation.

Therefore, forest change is described as the complete or partial removal of forest cover (Figure 8.2) that causes changes in forest structure (Reiche et al., 2021). In the context of remote sensing, this needs to consider the resolution of the imagery being used. For this study, it is considered that at least three pixels (30×30 m), an area of about 0.27 ha, were considered the minimum mapping unit. Defining the minimum mapping unit helps to minimise the number of false-positive changes due to the complex land surface conditions, especially in the savanna ecosystems, which are naturally more variable.

Forest change detection is designed to detect and track abrupt forest change events from anthropogenic and natural catastrophes (Coppin and Bauer, 1996). It augments the forest information as a novel source of forest change map products in Tanzania. As a result, changes in forest cover may be attributable to human activities, such as converting forests to other land uses, such as pastures, settlements, roads, and infrastructure construction. In addition, illegal and non-sustainable

logging, firewood extraction, and mining are altering forest cover. Natural phenomena include insect infestations and floods, droughts, desertification, fires, landslides, windthrow and tsunamis. A summary of the forest change detection process is presented in Figure 8.2.

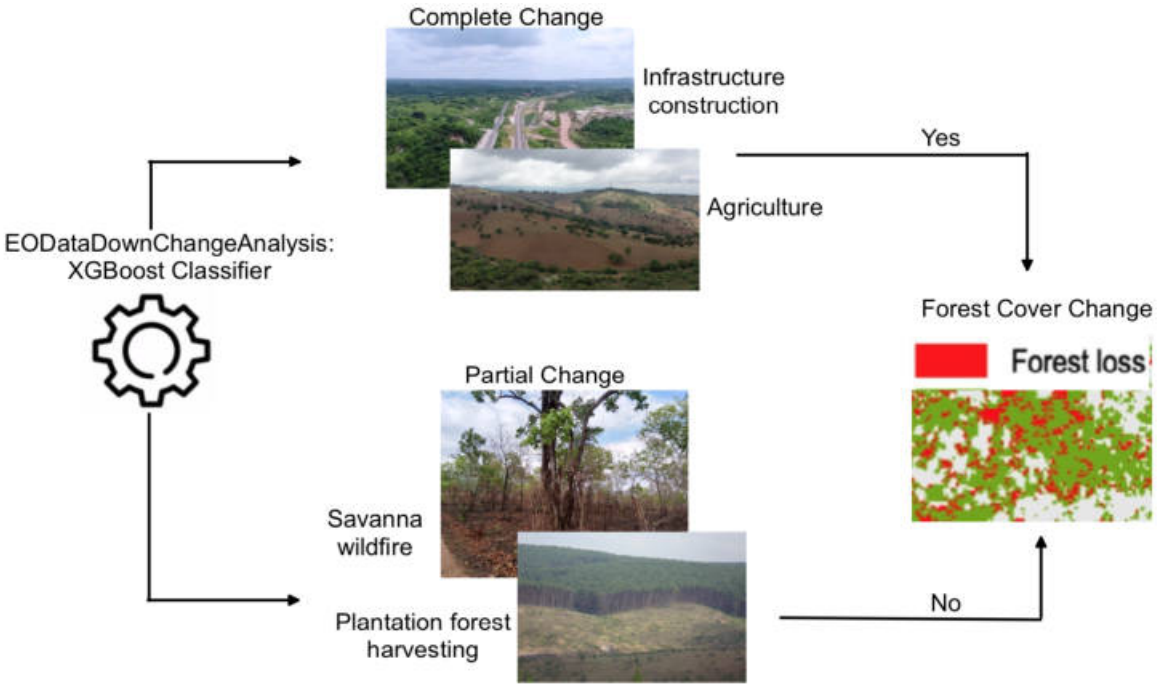

Figure 8.2: A flowchart of forest change detection analysis

8.2.3.2 Masking Burnt Areas

Fire is a vital ecological factor influencing tropical savannas' composition, structure, and distribution. Fire has become a part of tropical savannas throughout recorded history. These savannas burn more frequently and more extensively every year than any other biome. Therefore, fire occurrences create temporal changes to the Tanzanian woodlands and were not considered a permanent forest cover change. It is normal for these ecosystems to have a patchwork of burnt areas and

rarely produce long-term changes to the ecosystem (Figure 8.3). In the context of this study, these changes are not considered "real change". Human-made fires in Tanzania's forest areas remain more common than natural fires and occur more frequently in woodlands than in evergreen forests (Mugasha et al., 2004). Anthropogenic forest fires in Tanzania are often caused by traditional shifting cultivation or illegal logging. It occurs from May to November with a peak from August to October (Mugasha et al., 2004). The proper use of fire in woodland (savannas) is essential for maintaining these ecosystems as early burning is carried out to reduce more severe fire damage later in the fire season. Similarly, the recruitment of trees into larger-sized classes is heavily influenced by fire intensity due to the amount of fuel (grasses), the fuel's physical and chemical properties, climatic conditions, soil moisture, and topography (Govender et al., 2006).

Figure 8.3: A sample of a burnt area in the savanna and the quick recovery from field survey, October 2019. Therefore, this indicates a partial forest cover change. Photo acquired by the author

To separate fire from other changes within the analysis, the Normalised Burn Ratio (NBR) index equation (8.1) and Burn Area Index (BAI) equation (8.2) were used. The NBR index was used to identify burned areas that use the shortwave-infrared (SWIR) and near-infrared (NIR) portions of the electromagnetic spectrum (García and Caselles, 1991) and BAI highlights the burned area in the red to near-infrared (NIR) spectrum (Chuvieco et al., 2002). The thresholds of NBR > -0.02 and BAI < 100 were used to define the unburnt areas, and it was within these areas that the remaining change analysis was undertaken.

$$NBR = \frac{NIR - SWIR}{NIR + SWIR} \tag{8.1}$$

$$BAI = \frac{1}{(0.1 + R)^2 + (0.6 + NIR)^2} \tag{8.2}$$

Where for Landsat 8: R = band 4 and NIR = band 5 and SWIR = band 7

8.2.3.3 Plantation Forests

Plantations are heavily managed forests within the landscape and are not considered in terms of national forest change statistics as they are already considered 'changed' due to anthropogenic modification. Change regularly occurs with plantation forests with partial forest loss after harvesting, but replanting occurs shortly after, and therefore, while the land cover may have temporally changed, the land use has not. To mask the plantation forest areas, a mask was extracted from the forest type classification result (Figure 7.16) from Chapter 7.

8.2.3.4 Scene Based Change Detection

The change analysis was undertaken in two steps. The first identifies possible change pixels within the forest/non-forest mask, defined in Chapter 7, following masking for burnt areas and plantations, using an NDVI threshold of < 0.35. Additionally, a threshold ($< 30\%$) for the percentage of pixels identified as a potential change is applied, where if more than 30% of forested pixels have been identified as a possible change, then it is assumed that this is a seasonal change (i.e., loss of leaves due to phenology) and therefore should be ignored. At the scale of the Landsat scene, even with data removed due to cloud cover, the percentage of expected change is small. Finally, features of less than 3 pixels are removed from the layer to reduce noise.

Using the pixels identified in the first stage, the second identifies the change through a classification, using the same XGBoost classifiers (Section 4.5.5) trained in Chapter 7. The 100 classifiers are only applied to the pixels identified in the first stage, which significantly speeds up the application of the classifiers to the image as only a small percentage of the total number of pixels within the scene are being classified. The 100 classifications are merged, and a threshold of 50% was applied to identify forest and non-forest regions. The resulting non-forest regions are considered the final change features for the scene.

8.2.3.5 Summarising Forest Changes and Updating Baseline

To update the forest baseline (Figure 8.4) and confirm changes, the noise (i.e., false-positives) from the individuals' scenes needs to be taken into account, which can be considerable, particularly where the FMask cloud and cloud masking has performed poorly. Therefore, to confirm a change, it needs to have been identified several times. Through experimentation, a threshold of 5 was selected to confirm a change.

For this study, the changes were summarised to provide annual products, as required for national reporting, where the date of a change was associated with the date of the first observation of change. However, a scoring system could also be used within an additional EODataDown plugin to provide alerts of confirmed changes.

Change occurrence summaries were therefore generated for 2018, 2019, and 2020. The 2018 change layer included all the changes identified in the forest/non-forest extent for the 2013 to 2018 period and therefore updated the existing forest base-

line to the discrete date of January 1st, 2019. The change alerts for 2019 were identified and applied to generate a baseline for January 1st, 2020. Finally, while the Landsat imagery was processed for 2020, few change regions were confirmed as the requirement to confirm changes with 5 observations means that many changes are only confirmed once the following years' data (i.e., 2021) is available. Lowering the threshold to 3 observations increased the amount of change identified for 2020, which looks to be at a similar level as 2019. However, there was also an increase in the number of false positives. Therefore, the focus will be on reporting on the changes identified for 2019. The detected forest changes intend to provide an early indication of deforestation occurrences so that law enforcement officers, local communities, advocacy organisations, and other responders can take action including visiting the location in the field.

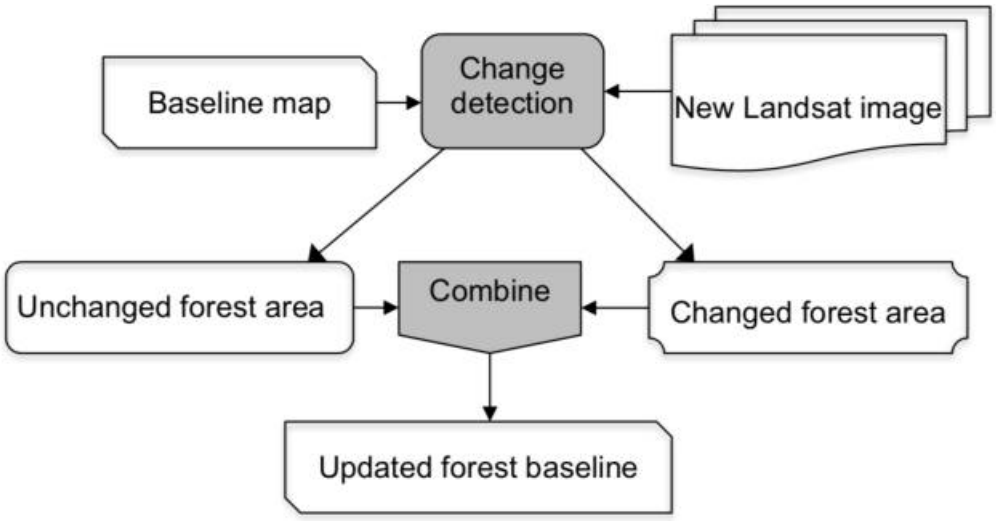

Figure 8.4: Flowchart for updating forest baseline following change detection analysis

8.2.4 Forest Change Accuracy Assessment

Assessing change detection accuracy is difficult as change is rare, with only a small percent of pixels changing within a given period (e.g., one year). Therefore, to assess the accuracy of the changes identified by this study, relatively small but intensively assessed plots were used. A single plot was defined as a 1×1 km area, corresponding to 1 km^2. The extent was observed as the most suitable trade-off, providing sufficient area for a representative assessment but being viable to interpret accuracy points intensively. A total of 16 sample plots (Figure 8.5) were selected in areas where changes were known to have occurred and stratified across the different forest types. For each 1×1 km plot, 1,000 randomly located points, with a minimum spacing of 30 m between points, were generated. The minimum distance constraint was designed to ensure a pixel was only assessed once. In total, 16,000 verification points were used for the accuracy assessment. The verification points were not stratified using the generated change layer to avoid bias in the location of the points, but the densely allocated points should enable the estimation of change omissions, a significant challenge when assessing the accuracy of a change product (Olofsson et al., 2020).

The evaluation of forest change was assessed using precision, recall, F1 score, user and producer accuracy, and overall accuracy metrics, which match binary classification and are widely applied in remote sensing classification methods (Pitkänen et al., 2020; Matton et al., 2015). Therefore, the evaluation focused on generating forest change information based on true positive, true negative, false positive, and false negative. The final forest loss accuracy assessment was compared (e.g., Galiatsatos et al., 2020) with available global forest change dataset from Hansen

et al. (2013) version 1.7 available online[4] and clipped to Tanzania's national boundary.

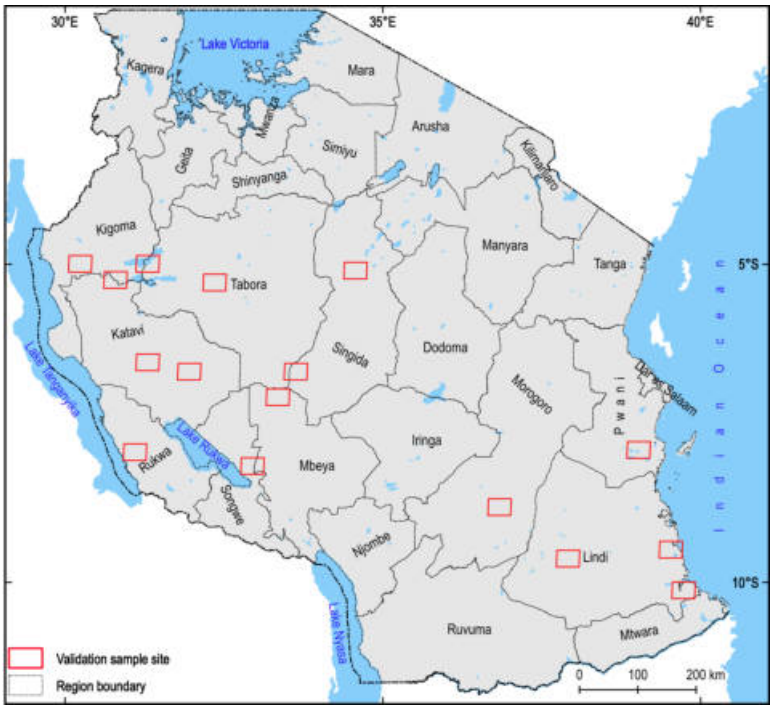

Figure 8.5: Distribution of sample accuracy assessment plots

8.2.4.1 Visual Validation of Forest Changes

The validation points were visually examined using the available Landsat 8 and PlanetScope images (3 m spatial resolution) for the presence of change using the Class Accuracy assessment tool in QGIS[5] (Bunting et al., 2018). The images were acquired in October or November between the two target years to minimise seasonal variation and temporally false changes (Table 4.1). For example, the validation was undertaken by observing the earlier image from the year 2018 and was confirmed using the later image of the year 2019, whether "real" or "false"

[4] http://earthenginepartners.appspot.com/science-2013-global-forest
[5] https://github.com/remotesensinginfo/classaccuracy

forest change. Utilising the images as the reference data to evaluate forest change result ensures more reliability than that applied to produce the information (Olofsson et al., 2014). The application of PlanetScope images (high spatial resolution) reduces uncertainty in evaluating detected forest loss results (Vargas et al., 2019).

8.3 Results

8.3.1 Forest Change Result

The accuracy assessment focused on the 2019 change product as this is the only complete year. As detailed, the 2018 change (Figure 8.6) contains the product of changes that occurred between 2013 and the end of 2018. While 2020 has not had sufficient observations to confirm the changes.

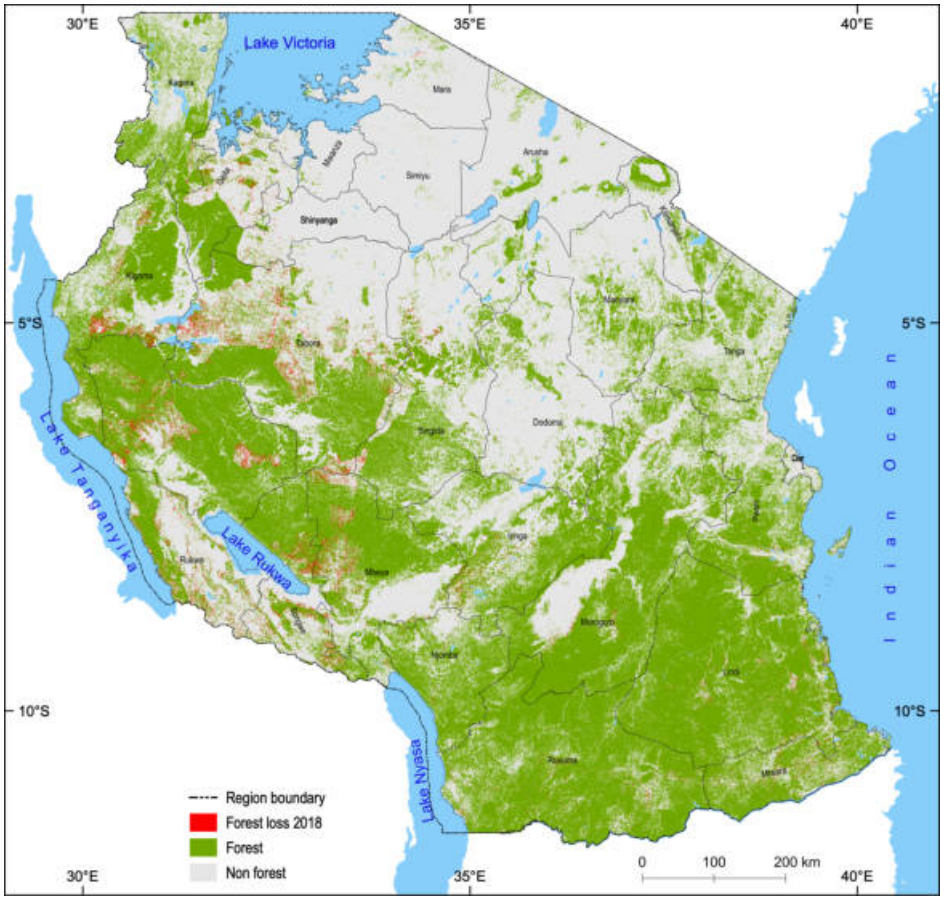

Figure 8.6: Forest change extent in Tanzania for the year 2018

The 2019 result demonstrates a countrywide wall-to-wall map of forest cover change over Tanzania (Figures 8.7–8.8 and Figure 8.9) adequately detected forest changes from the baseline map and could be used for reporting annual forest change statistics. The forest loss area estimates for 2019 from this study were compared with the global forest change analysis of Hansen et al. (2013) version 1.7, Table 8.1 and found to be comparable. A further comparison quantitative accuracy comparison is provided below.

Table 8.1: Forest loss area for the year 2019 (this study) compared with global forest cover loss from Hansen et al. (2013) version 1.7

Forest cover loss area (ha) and Percentage (%)				
Class	This study	%	Hansen et al. (2013)	%
Forest change	157,204	0.39	142,773	0.36

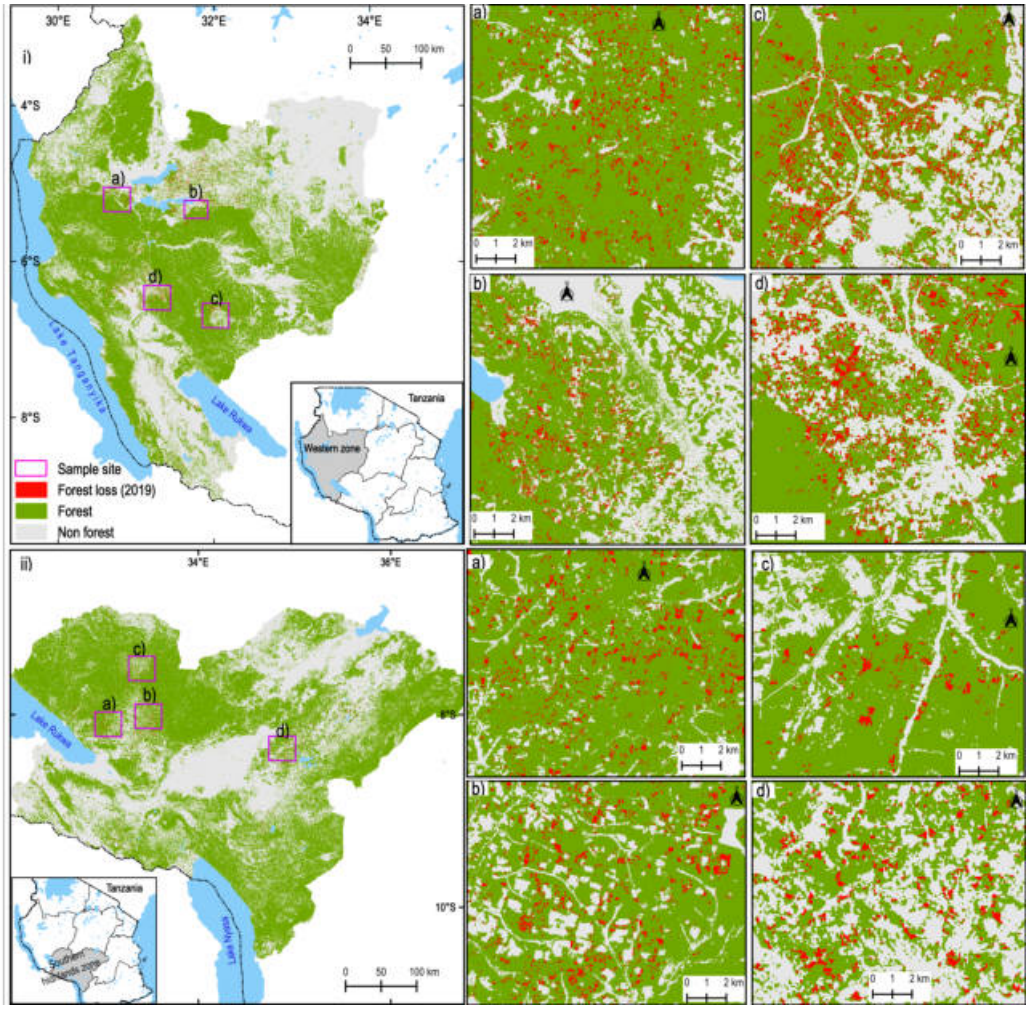

Figure 8.7: An example of forest cover loss area for 2019 from forest cover change analysis with detailed sample areas (a-d) as derived from Landsat 8. These areas are consistently experiencing increases in deforestation, and this information allows for rapid and consistent identification of priority forest areas in need of better protection, valuable insight for decision-makers, and law enforcement: i) Western and ii) Southern Highland of Tanzania

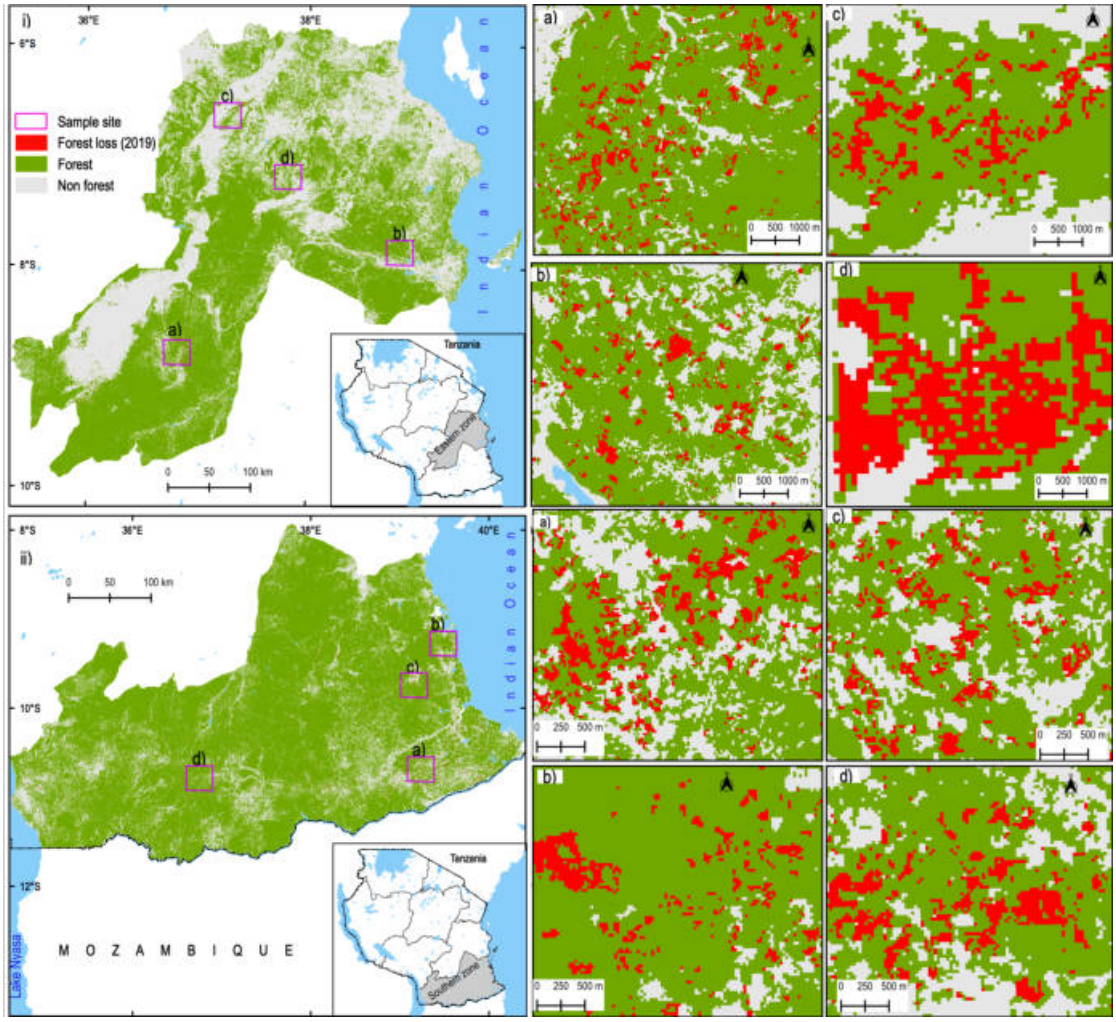

Figure 8.8: An example of forest cover loss area for 2019 from forest cover change analysis as derived from Landsat 8 with detailed sample areas (a-d) for i) Southern and ii) Eastern Tanzania

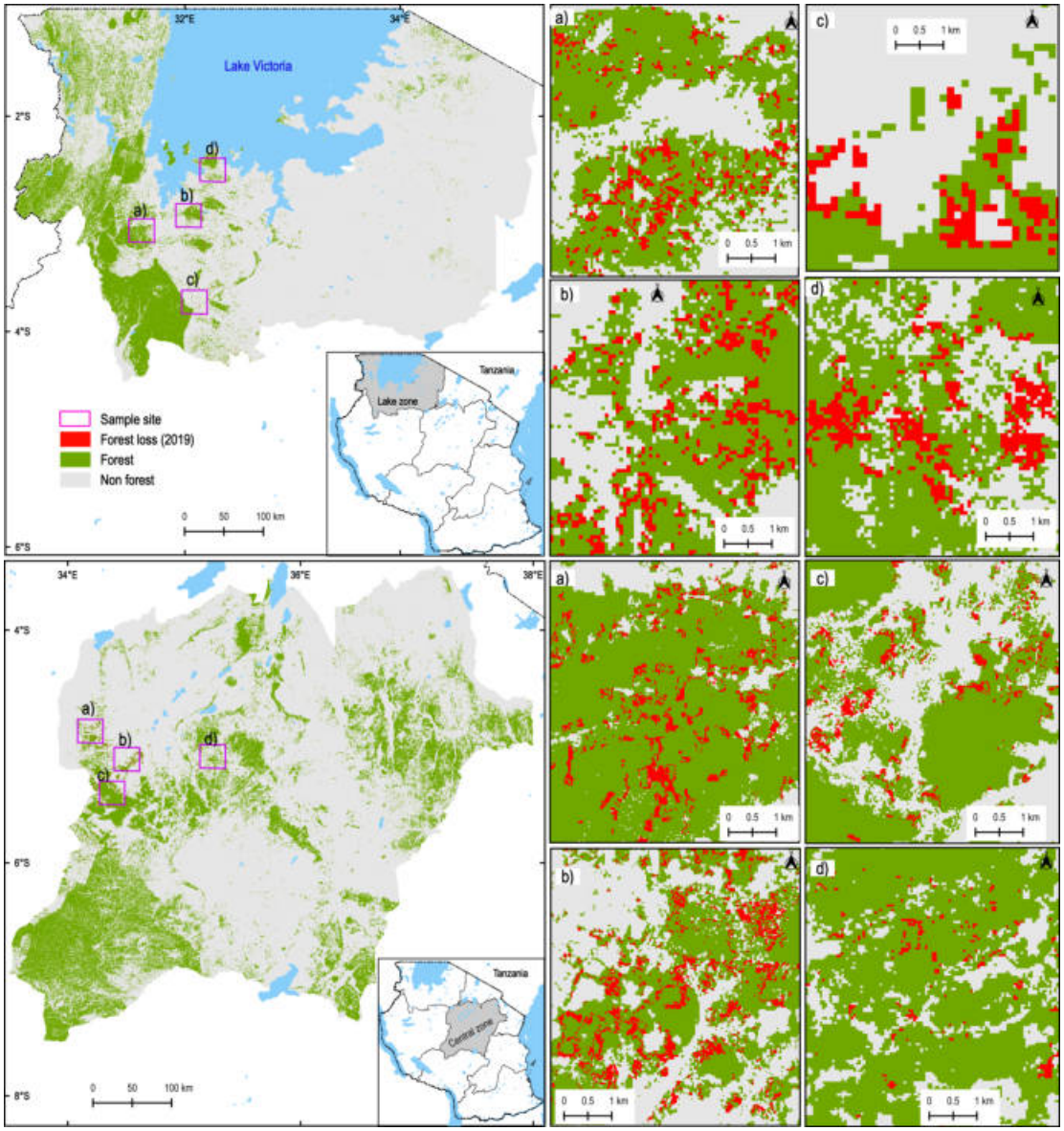

Figure 8.9: An example of forest cover loss area for 2019 from forest cover change analysis as derived from Landsat 8 with detailed sample areas (a-d) for i) Lake and ii) Central part of Tanzania

8.3.2 Accuracy Assessment

Table 8.2 summarises the accuracy assessment results for the changes identified in 2019. The accuracy was found to be good with an F1 score of 0.82 compared to the global forest change assessment of Hansen et al. (2013) with an F1 score of 0.45, highlighting that the Hansen et al. (2013) product is not capturing the full extent of forest change with Tanzania. The reasons for not picking up change to the same extent may be caused by the dissimilarity between datasets timing, including classification errors, and different treatment of mixed pixels due to phenological differences caused by image acquisition dates. For example, many canopy species in the woodlands lose their leaves during the dry season. Similarly, plantation harvesting and management as well as fire damage are interpreted as forest losses within the dataset, which is not the case in Tanzania.

For the no-change class, the accuracy was similar with an F1 score of 0.96 for this study and 0.89 for Hansen et al. (2013). It would be expected that the no-change results will be similar, with change only representing a few percent of the landscape. Therefore, the majority of the accuracy assessment points will be in no-change regions, and even significant errors within the change result would only result in small changes to the no-change class extent. This difference in the accuracy of the change product also demonstrates an improvement in the quality of forest change data available and highlights the importance of locally optimised analysis methods versus being reliant on global datasets.

Table 8.2: Model performance evaluation metrics for potential forest changes in 2019 at 95% confidence interval, compared to global forest change analysis version 1.7 of 2019 (Hansen et al., 2013)

Class	**Measure**	**This study**	**Hansen et al. (2013)**
Change	Producer accuracy (%)	96.13 ± 0.74	65.98 ± 2.04
No-change		92.74 ± 0.36	84.21 ± 0.33
Change	User accuracy (%)	71.42 ± 1.52	34.25± 1.59
No-change		99.22 ± 0.15	95.20 ± 0.37
Change	Precision	0.96	0.65
No-change		0.92	0.84
Change	Recall	0.71	0.34
No-change		0.99	0.95
Change	F1 score	0.82	0.45
No-change		0.96	0.89
	Overall accuracy (%)	93.28 ± 0.38	82.19 ± 0.59

Figure 8.10 illustrates an example of detected forest change by comparing two Landsat 8 images of 24/10/2018 (before) and 27/10/2019 (after) and a high-resolution image (PlanetScope), overlaid with a sample change area. It indicates the accuracy and capability of the model to detect forest loss.

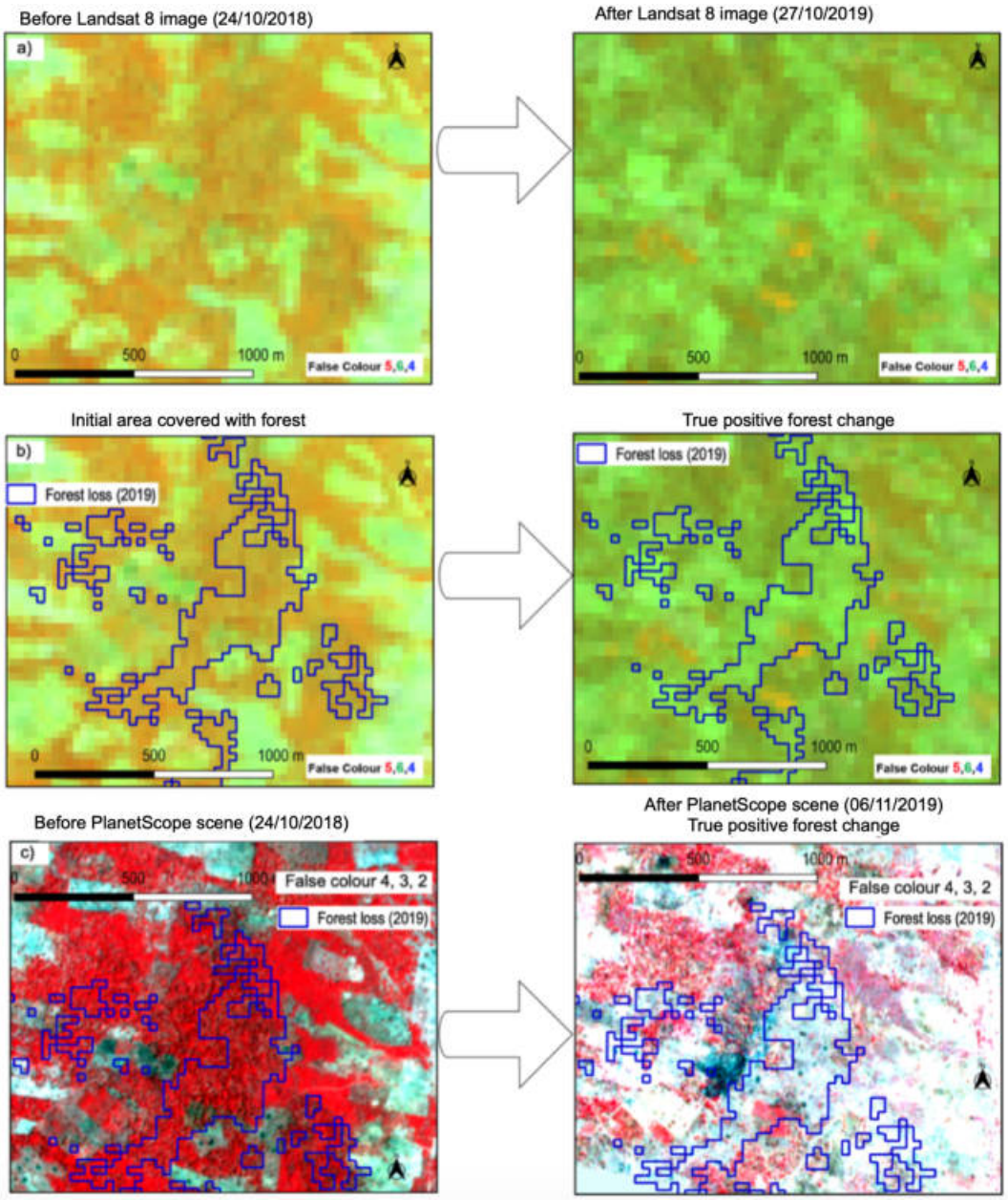

Figure 8.10: An example of forest loss for 2019 demonstrates that the model using Landsat 8 data captured the forest loss. The result was evaluated to a high-resolution image (PlanetScope image with a resolution of about 5 m) which indicated a similar forest loss over the two periods 24/10/2018 and 27/10/2019 for (a - b) Landsat 8 and c) PlanetScope image

8.3.2.1 Comparison with Hansen Product

Figure 8.11 demonstrates a detailed visualisation of the spatial distribution of forest loss comparing this study and to that of Hansen et al. (2013) for 2019. The changes identified by both products are correct (highlighted with a yellow circle), but Hansen et al. (2013) has underestimated the true area of change for this region.

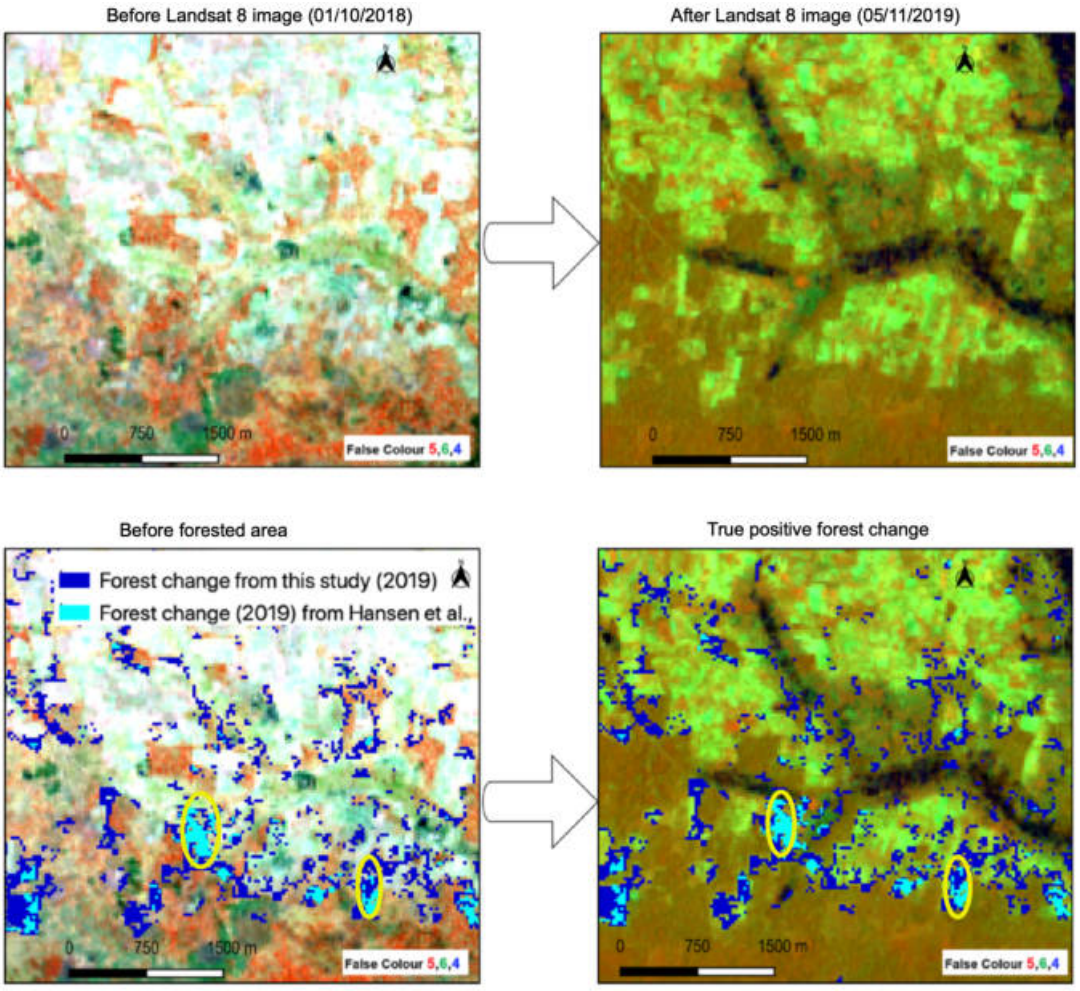

Figure 8.11: A detailed forest loss visual comparison with global forest change analysis from Hansen et al. (2013) version 1.7 for 2019 and overlap areas where both reported changes are highlighted (yellow circle).

8.3.2.2 False-Negative Forest Loss (omission error)

Despite the model attaining adequate forest loss detection, some false-negative forest loss also occurred (Figure 8.12). A false negative emerged when the model failed to identify an area of loss. Anomalies have been associated with pixel edge effects and seasonal fluctuations, particularly in semi-arid areas of the country and a small number of clear sky images. Similarly, inaccuracy has occurred in areas with low forest cover and forest changes in the form of numerous small-scale clearings.

However, these results highlight the fact that the system provides accurate detections with few false-negatives and can thus be used as an alert system (fast forest change detection from optical data) and for identifying losses of forest in Tanzania. These can then be used, for example, to compute national forest extent and change statistics.

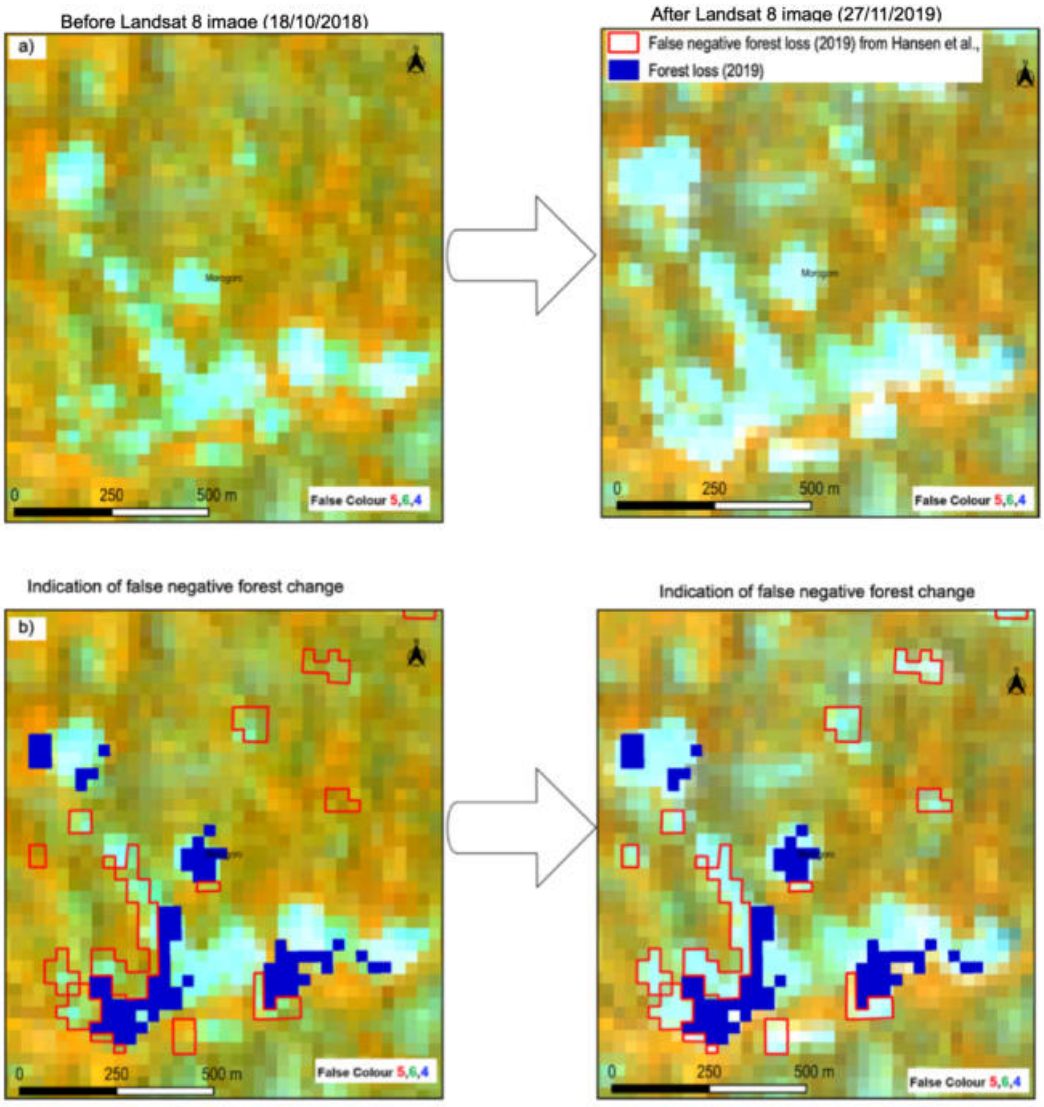

Figure 8.12: A detailed false-negative forest loss as compared to global forest change analysis (Hansen et al., 2013) version 1.7. This demonstrates forest areas that had forest loss but were not detected by the model

8.3.2.3 False-Positive Forest Loss (commission error)

The false-positive forest loss was also detected on the global dataset (Hansen et al., 2013) version 1.7 of 2019 in some areas that were not identified by this study. For

example, in forest nature reserves under category Ib (Wilderness Area) of the International Union for Conservation of Nature (IUCN) (Leberger et al., 2020) with importance biodiversity protection, and with no previous records related to anthropogenic disturbances (Figures 8.13–8.14).

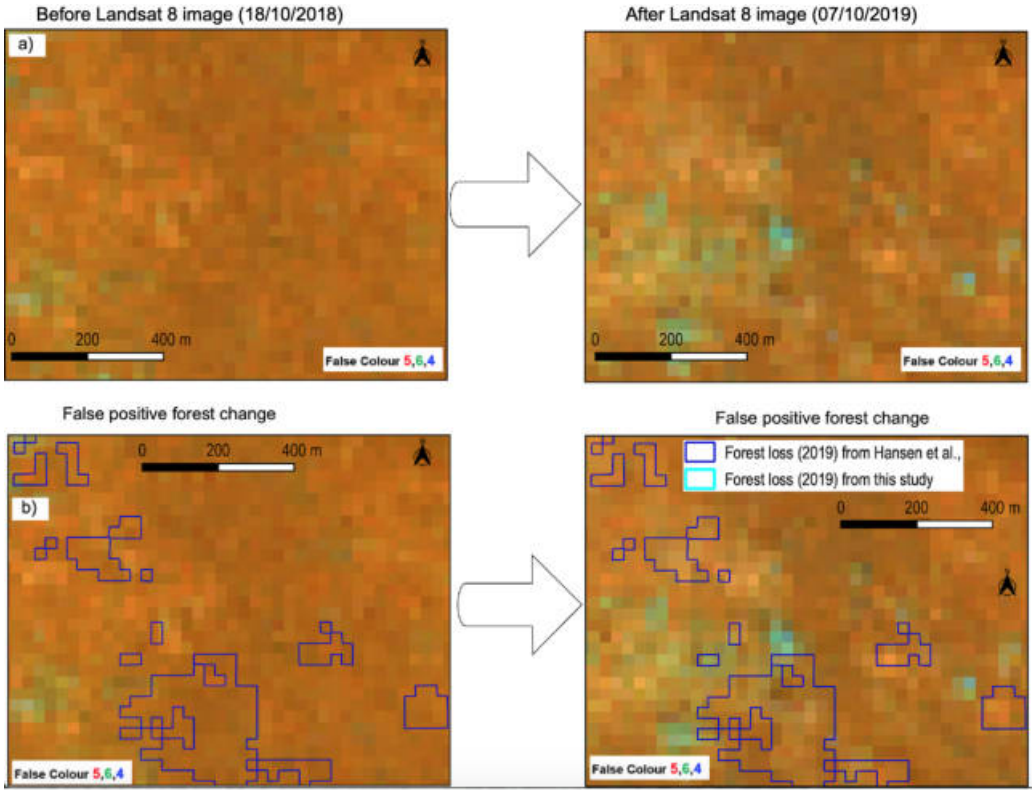

Figure 8.13: A detailed false-positive forest loss from global forest change analysis (Hansen et al., 2013) version 1.7 for 2019 as this study did not capture the false-positive change at Minziro Nature Forest Reserve. Forests in the nature reserve are reclaimed as deforestation occurs while the forest remains intact. Since it is a wet forest, these areas' signature constantly resembles that of the closed forest (lowland forest). As a result, when a pixel is continuously forested, the algorithm has trouble identifying a change from a forest to a non-forest. As a result, the algorithm becomes confused when detecting a transition from forest to non-forest when the pixel is forested throughout time.

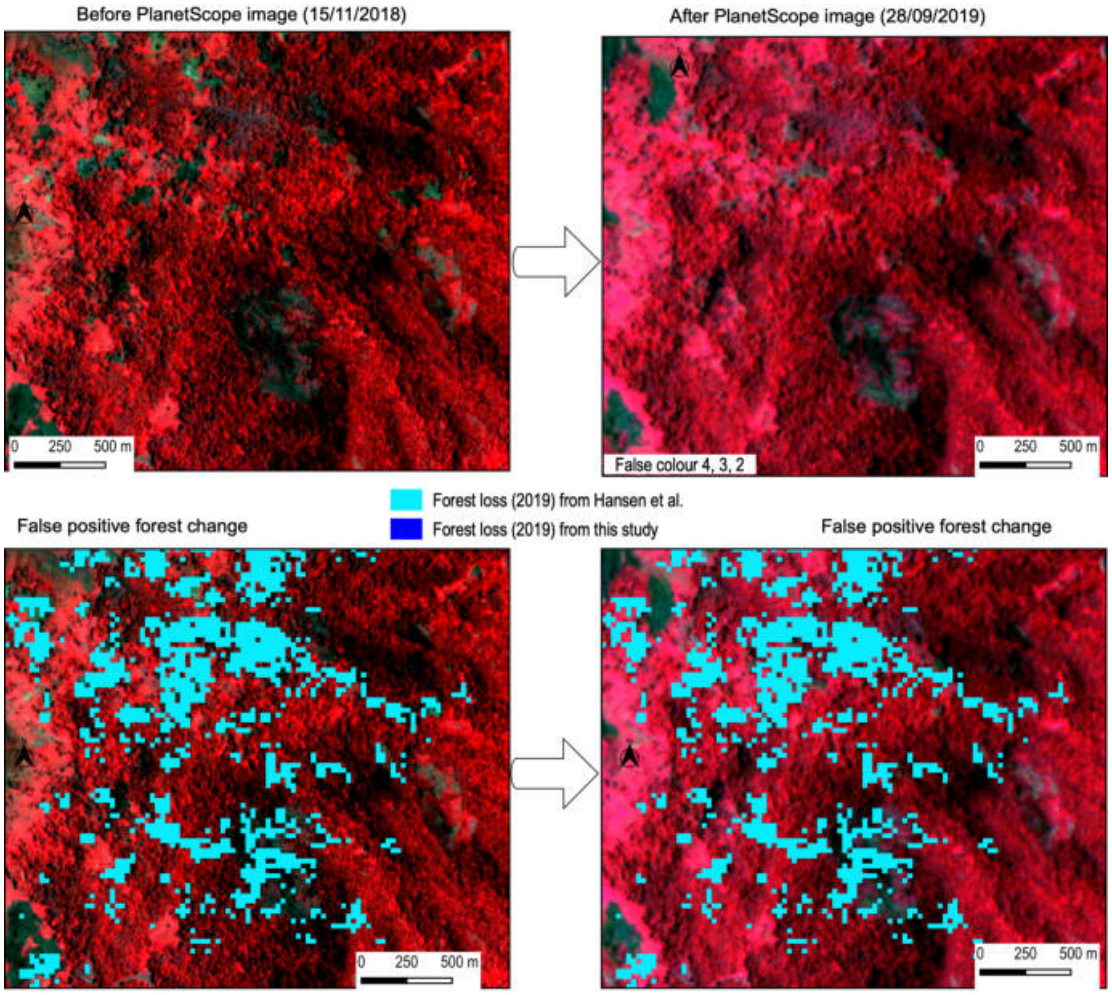

Figure 8.14: A detailed false-positive forest loss from global forest change analysis (Hansen et al., 2013) version 1.7 for 2019 as this study did not capture the false-positive change at Mkingu Nature Forest Reserve. Forests in the nature reserve are reclaimed as deforestation, while the forest is intact. The signature of these areas resembles that of the forest all the time as it is a mountainous forest (montane forest). In this way, the algorithm is confused in detecting a transition from forest to non-forest when the pixel is forested throughout time

8.3.3 Estimated Forest Change by Regions

The forest change results were also summarised at a localised level to indicate areas affected by deforestation (Table 8.3).

Table 8.3: Forest change extent summarised using a map by regions in Tanzania

	Area (ha), year		
Region	2018	2019	2020
Tabora	211,412	31,587	5,332
Katavi	120,629	23,171	2,030
Rukwa	74,957	13378	1,360
Mtwara	30,431	12,633	2,227
Mbeya	84,983	10,582	4,185
Lindi	35,004	10,223	780
Singida	32,096	10,175	4,268
Kigoma	76,750	8,926	893
Songwe	72,716	7,020	2,945
Iringa	22,470	6,033	664
Ruvuma	30,246	5,991	638
Morogoro	16,674	5,745	92
Geita	33,318	3,630	338
Pwani	8,120	1,769	57
Shinyanga	10,449	1,646	125
Njombe	5,529	1,384	111
Dodoma	5,233	759	1,054
Kagera	5,823	411	57
Mwanza	3,455	374	38
Kilimanjaro	27	28	-
Tanga	689	18	10
Mara	1,453	18	10
Simiyu	91	10	6
Manyara	456	9	3
Dar Es Salaam	10	2	-
Arusha	19	1	-

8.3.4 Change in Forest Types by Region

Changes can also be broken down by the forest types (Tables 8.4, 8.5 and 8.6). It can be seen that the majority of changes identified are within the open woodlands, primarily due to shifting cultivation. Closed woodlands and lowland forests have also witnessed significant change. However, it should also be noted that the volume of change within each type corresponds with the area of that type (i.e., Open woodland, Closed woodland, and lowland forest) are the 3 largest forest types by area in Tanzania.

Table 8.4: Forest types change by region

	Forest type change (area (ha))-2018						
Region	Montane	Lowland	Mangrove	Closed woodland	Open woodland	Plantation forest	Thicket
Tabora	-	-	-	406	199,969	-	1,122
Katavi		19	-	4,208	105,367	-	-
Mbeya	72	64	-	962	69,470	-	-
Songwe	57	15	-	845	67,283	-	-
Rukwa	21	14	-	3,699	66,912	-	-
Kigoma	-	85	-	6,613	61,048	-	-
Geita	-	5	-	593	32,686	-	-
Singida	-	-	-	280	27,460		3,274
Ruvuma	51	250		2,119	24,958	-	-
Iringa	-	250	-	239	19,998	-	-
Lindi	-	9,777	38	3,346	19,277	-	-
Mtwara	-	9,381		1,354	15,569	-	-
Shinyanga	-	-	-	82	10,316	-	2
Morogoro	39	3,106	-	4,490	6,848	-	-
Kagera	2	21	-	134	5,618	-	-
Dodoma	-	-	-	315	4,418	-	55
Njombe	40	276	-	142	4,371	-	-
Mwanza	-	491	-	215	2,646	-	-
Pwani	-	3,231	27	2,255	1,541	-	-
Manyara	-	-	-	10	336	-	-
Mara	-	161	-	1,041	221	-	-
Tanga	88	178	6	173	103	-	-
Simiyu				1	82	-	-
Kilimanjaro	-	-	-	2	23	-	-
Arusha	-	-	-	1	12	-	-
Dar Es Salaam	-	-		1	5	-	-

Table 8.5: Forest types change by region

Region	Forest type change (area (ha))-2019						
	Montane	Lowland	Mangrove	Closed woodland	Open woodland	Plantation forest	Thicket
Tabora	-	-	-	212	30,815	-	416
Katavi	-	2	-	687	21,256	-	-
Rukwa	8	2	-	1,765	11,225	-	-
Mbeya	8	10	-	267	9,860	-	-
Singida	-	-	-	40	7,677	-	2,441
Kigoma	11	20	-	1,003	7,432	-	-
Songwe	11	13	-	113	6,689	-	-
Iringa	5	11		131	5,382	-	-
Lindi	-	3,599	3	1,221	4,921	-	-
Mtwara	-	5,891	-	869	4,893	-	-
Ruvuma	7	154	-	843	4,766	-	-
Geita	-	1	-	106	3,519	-	-
Morogoro	13	1,116	-	2,582	1,669	-	-
Shinyanga	-	-	-	13	1,633	-	-
Njombe	9	151	-	53	709	-	-
Dodoma	-	-	-	83	630	-	16
Pwani	-	688	-	562	421	-	-
Kagera	-	1	-	18	390	-	-
Mwanza	-	81	-	48	239	-	-
Kilimanjaro	-	-	-	2	25	-	-
Simiyu	-	-	-	-	10	-	-
Tanga	3	7	-	5	8	-	-
Manyara	-	-	-	-	5	-	3
Mara	-	-	-	10	4	-	-
Dar Es Salaam	-	-	-	-	1	-	-
Arusha	-	-	-	-	-	-	-

Table 8.6: Forest types change by region

Region	Forest type change (area (ha))-2020						
	Montane	Lowland	Mangrove	Closed woodland	Open woodland	Plantation forest	Thicket
Tabora	-	-	-	84	4,936	-	291
Mbeya	1	1	-	176	3,943	-	-
Songwe	-	1	-	108	2,821	-	-
Singida			-	27	2,628	-	1,606
Katavi	-	1	-	156	1,819	-	-
Dodoma	-	-	-	17	985	-	16
Rukwa	2	1	-	492	848	-	-
Kigoma	-	4	-	172	695	-	-
Iringa	-	1	-	40	599	-	-
Ruvuma	1	15	-	137	477	-	-
Mtwara	-	1,504	-	176	442	-	-
Geita	-	-	-	23	314	-	-
Lindi	-	463	-	87	209	-	-
Shinyanga	-	-	-	2	122	-	-
Njombe	-	6	-	4	61	-	-
Kagera	-	1	-	5	51	-	-
Pwani	-	3	-	6	48	-	-
Morogoro	-	14	-	41	34	-	-
Mwanza	-	13	-	3	21	-	-
Tanga	-	3	-	3	21	-	-
Simiyu	-	-	-	-	6	-	-
Mara	-	2	-	4	3	-	-
Manyara	-	-			1	-	1
Arusha	-	-	-	-	-	-	-
Kilimanjaro							
Dar Es Salaam	-	-	-	-	-	-	-

8.3.5 Forest Cover Change in Protected Areas

Although forest loss is more pronounced outside the protected areas, the result also highlights forest loss is also occurring in protected areas (forest reserves and wildlife managed areas) (Table 8.7, 8.8 and 8.9). See Appendix 4 as Tables A.3, A.5, and A.6 for detailed forest change in the individual protected area category. These protected areas are designed to protect and support the country's biodiversity, and therefore changes within these areas are particularly significant. An example is shown in Figure 8.15, where deforestation in the protected area is occurring

due to encroachment at the boundaries, with changes occurring up to 500 m from the protected area boundary. This is particularly concerning as unchecked. These protected areas could witness further encroachment, increasing the vulnerability of these important habitats and ecosystems.

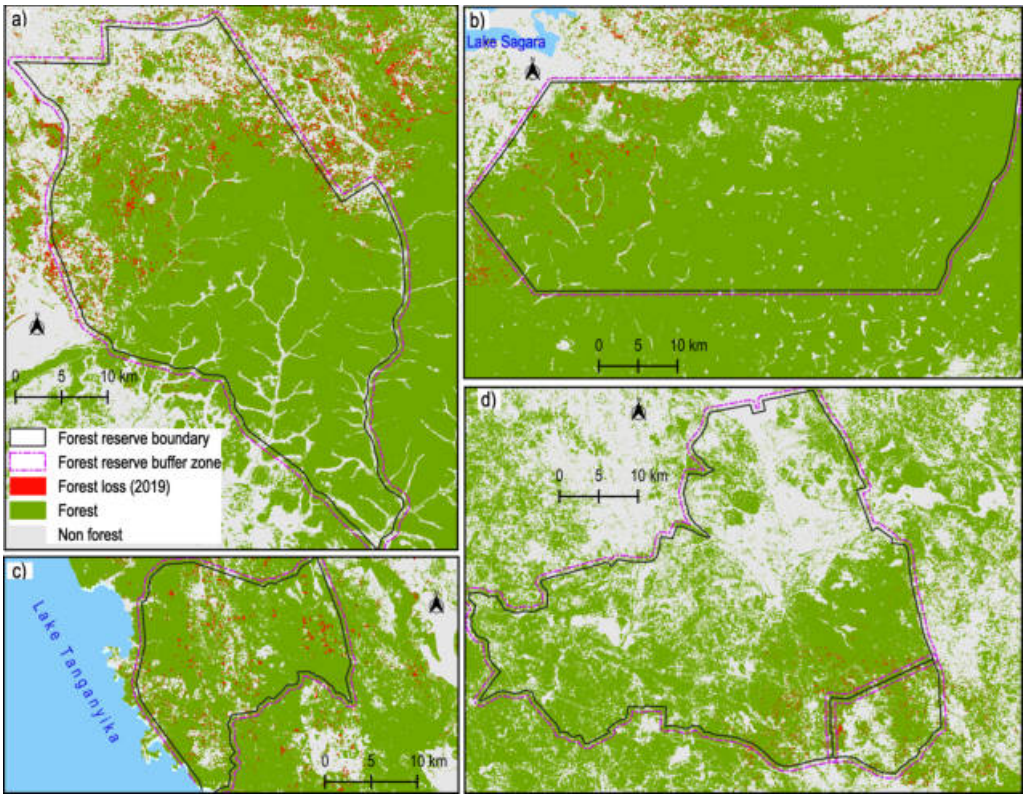

Figure 8.15: A sample of forest loss in protected areas on the western part of the country with a buffer of 500 m: a) Msaginia forest reserve, b) Ugalla North forest reserve, c) Loasi river forest reserve, d) Lugufu and Mkuti forest reserve

Table 8.7: Estimated forest cover change in protected areas

	Area (ha), year		
Category	2018	2019	2020
Forest reserve	126,925	24,869	3,600
Wildlife protected area	72,153	13,587	2,842

Table 8.8: Estimated forest type cover change in forest reserves

	Area (ha), year		
Forest type	2018	2019	2020
Montane	56	10	1
Lowland	1,793	352	31
Mangrove	49	3	-
Closed woodland	3,322	1,438	382
Open woodland	115,599	22,536	3,145
Thicket	48	38	
Plantation	-	-	-

Table 8.9: Estimated forest type cover change in wildlife areas

	Area (ha), year		
Forest type	2018	2019	2020
Montane	7	2	-
Lowland	593	191	1
Mangrove	-	-	-
Closed woodland	965	445	60
Open woodland	65,760	12,459	2,518
Thicket	404	236	-
Plantation	-	-	-

8.3.6 Updating Earlier Forest Baseline

The confirmed forest changes for 2018 and 2019 were used to update the forest baseline from Chapter 7 (Figure 7.10) to generate a country forest baseline for 2019 (Figure 8.16). Table 8.10 presents the comparison of forest loss from this study as compared to the global dataset of Hansen et al. (2013) version 1.7 over six years (2013 - 2019). It should be noted that these studies are not directly comparable for the period 2013 - 2019 as while the Hansen et al. (2013) product is producing

an annual change product for each year, this study is using a baseline forest mask which is the product of imagery from 2013 to 2018 and not a 2013 map of forest extent. Therefore, while the accuracy assessment of 2019 suggests that Hansen et al. (2013) is underestimating the true extent of change in Tanzania, this study has a lower value as it is against a different baseline, and only the 2019 annual change is directly comparable to the Hansen et al. (2013) product.

Table 8.11 summarises the updated baseline forest extent from the forest loss detected from the earlier baseline.

Table 8.10: Forest loss extent comparison with Hansen et al. (2013) version 1.7 for 2013 - 2019

	Forest cover loss area (km^2)	
Class	This study	Hansen et al. (2013)
Forest change	10,462.37	11,539.11

Table 8.11: Update of forest baseline extent from the detected forest loss for 2013 - 2019

	Forest area (km^2) for earlier baseline, updated baseline and Percentage (%)					
Class	Earlier baseline extent	%	Estimate forest loss	%	Updated baseline extent	%
Forest	407,976	45.76	10,462.37	2.56	397,514	43.20

Figure 8.16: Map showing areal proportional of the updated forest cover in Tanzania for 2019

8.4 Discussion

The wall-to-wall application of the XGBoost classification approach for mapping forest change at a national scale using Landsat 8 imagery was found to be successful with the areas of forest changes generally correctly identified with an accuracy of F1 score value of 0.82 (Figures 8.7–8.8 and Figure 8.9), compared to 0.45 for the change analysis from the global dataset of Hansen et al. (2013) version 1.7 for 2019

(Table 8.2). However, some false-positive errors (Figure 8.12) were associated with the savanna ecosystem's complex nature and low availability of Landsat cloud-free observations (Hansen et al., 2016).

The developed deforestation monitoring methodology aimed to support forest policy enforcement and carbon accounting in Tanzania by giving the most up-to-date deforestation alerts possible. For example, providing the ability to respond immediately to reduce or stop the newly-detected illegal deforestation situation from further expanding (Reiche et al., 2021). However, the monitoring system's application should be considered in the forest change scores selection to minimise false-positive detection. For early warning, a score value of 2 and visually checking the image once a change is identified is recommended for forest guardians working in areas of high importance, such as protected areas under pressure from deforestation. Additionally, ESA Sentinel-2 data should be integrated into the system, increasing the frequency of observations. The methodology should be directly transferable to the ESA Sentinel-2 data. However, for the annual reporting of forest loss for policy-makers, as presented in this chapter, a score of 5 has been demonstrated to produce reliable results which are fit for this purpose.

The result will support forest monitoring in policy formulation and implementation in protecting forests with better decision-making in government programs and other forest protection fiscal incentive projects (Neeff and Piazza, 2020). For reporting carbon, accounting requires estimation of activity data as an input for monitoring, reporting, and verification (MRV) (Olofsson et al., 2020), as needed for reducing emissions from deforestation and forest degradation (REDD+) (Krasovskii et al., 2018). Therefore, the proposed methodology is transparent and reproducible, enhancing the reliability and applicability based on machine learn-

ing with the application of an established forest baseline as a reference emissions level and assessing future emissions level (Romijn et al., 2012). A forest change was evaluated based on existing and incoming Landsat images. The developed methodology can be readily transferred to other local tropical regions in the sub-Saharan areas and beyond.

8.4.1 Forest Change Area Estimates

The forest change area estimates provide essential information to guide current and future conservation for sustainable forest management, especially in tropical Africa with high dependence on forest resources (Aleman et al., 2018). The result identified 157,204 ha of forest loss in Tanzania for 2019, presenting 0.39% loss of intact forest, close to the global forest change analysis of Hansen et al. (2013) (version 1.7), which mapped 142,773 ha in the same period. However, this study's forest change analysis presented a methodology that was optimised for Tanzania and therefore had a high degree of accuracy (Figures 8.13–8.14) and given that change is infrequent, even large changes in the accuracy of the change detection algorithm can result in relatively small changes in the area estimated. However, these relatively small geographic areas can be significant if found to occur in areas of importance (e.g., protected areas).

Therefore, it can be considered that global forest change datasets remain suitable for providing an indicative trend of forest loss at a national scale (Galiatsatos et al., 2020; Chen et al., 2020). However, this study's forest change area estimates provide an essential reference point in the region to which the Hansen et al. (2013) product can be compared as few countries have established a wall-to-wall forest

change map or methods for long-term national-scale forest monitoring.

8.4.2 Forest Management Outlook

The critical actions to prioritise climate change mitigation requires halting deforestation, enhancing forest restoration, and promoting sustainable forest management production (Mackey et al., 2020). Therefore, forest cover change mapping and monitoring information respond to a pressing need to support policy formulation and implementation of national and international commitments on forest protection and restoration (Bodart et al., 2013) whereby Tanzania is part of these obligations.

However, the situation is becoming critical, as highlighted by the forest change result of this study has demonstrated that deforestation in protected areas (Figure 8.15 and Tables A.3, A.5 and A.6) is still occurring, and these have been the dominant tools for conserving forests (Herrera et al., 2019) in Tanzania. This will impact biodiversity, as many of the protected areas preserve some of the region's last remnants of important tropical forests. Therefore, it provides a warning for enhancing protection and forest cover conservation for its biological resources.

If the situation remains unchecked, these protected areas will lose all of their protected statuses, leading to conversion to other land uses. Similarly, forest loss will increase the isolation (patches) of the protected areas (DeFries et al., 2005) impacting wildlife corridors (Ntongani et al., 2010). Figure 8.15 at Msaginia forest reserve supports wildlife movement between Katavi National Park and other protected areas, but the ongoing forest loss will limit this corridor. Moreover, the detected forest loss in the western part of the country around/near the river

and lake will disrupt water flow and increase soil erosion (Figure 8.15b and c). Therefore, ongoing deforestation will threaten the river Malagarasi that supports the Malagarasi-Muyovozi Ramsar site and increases siltation to Lake Tanganyika (Figure 8.15c), raising flood severity, which has already been happening in the country and disrupting livelihoods (Anande et al., 2019).

8.4.3 Updating Earlier Forest Baseline

The updated forest baseline extent from the detected forest changes increases the spatial accuracy of forest statistics, minimises the application of outdated datasets for policy-making (Bunting et al., 2018), and supports forest managers in forest monitoring and conservation plans (Koskikala et al., 2020). Therefore, the earlier baseline map with forest extent 407,976 km^2 (Table 7.4) was updated to 397,514 km^2 for 2019, showing a reduction of at least 2.6% (Table 8.11) of the forest cover in Tanzania over six years (2013 - 2019). The updated forest baseline presented is also consistent with national and international requirements for forest monitoring in terms of forest change trends over time.

8.4.4 Limitations

Apart from offering consistent and repeatable procedures for forest change detection, the method falls short by not providing the forest change direction “from” and “to” classes since the process focused only on two classes of change and no change. It implies that only primary vegetated (forest) and primary non-vegetated (non-forest) classes were considered during forest baseline establishment (Figure 7.1) with no detailed spatial information about other land covers and land use on the

thematic map. Similarly, persistent cloud cover remains a challenge along Tanzania's coastline, reducing clear-sky image availability.

8.5 Conclusions

The study demonstrated a thorough forest change, and the monitoring system method on a national scale is an essential component in policy-making. The results presented that monitoring efforts to overcome forest loss accounted for about 0.39% of intact forests in 2019 to help the country progress towards national sustainable development goals (Swamy et al., 2017; Neeff and Piazza, 2020). The developed forest monitoring system is intended to link forest conservation and protection policy-making to meet national forest data requirements but is also integrated into national institutions. However, this can be achieved holistically, intersectoral, interactive, and consistently with policies and national and local strategies. It should involve all stakeholders, promote secure land tenure, and integrate forest resource conservation and sustainable use.

Therefore, The mapping approach described in this study provided a highly accurate and effective means to monitor forest cover changes in regions prone to deforestation and degradation, with promise for application to improved monitoring of tropical and other forests in Tanzania. For instance, thickets have been identified as susceptible to deforestation. The government used this result to develop a thicket conservation mechanism by establishing a thicket reserve aimed at minimizing future loss of this critical vegetation through anthropogenic activities, such as agriculture and expansion of built-up areas. As a result, approximately 25,000 hectares of thickets were turned into a fully protected reserve.

Chapter 9

Discussion and Conclusions

This chapter revisits the thesis's main findings regarding the scientific questions established in Chapter 1 (Section 1.7) on the application of Earth Observation (EO) data on forest mapping and monitoring in Tanzania. The research project's general limitations are also addressed, and suggestions for further research and opportunities are provided.

9.1 Was the Aim Met?

The potential of remote sensing for tropical forest monitoring remains a vital tool as the loss of tropical forests is one of the world's most complex environmental problems (Lewis, 2006; Sayer, 1992). Timely tropical forest monitoring is required to provide information about forests' extent and changes over time, reducing data gaps and, consequently, supporting policy-making processes. It is necessary for forest conservation, management, responding to climate change, and supporting

sustainable development (Baumgartner, 2019). Therefore, this research aimed to create the basis for a long-term national forest monitoring system for Tanzania.

Additionally, the analysis focused on open-free software, freely available satellite data, and advanced remote sensing techniques to provide a cost-effective method of obtaining wall-to-wall information on the forest extent and associated changes in Tanzania. The aim was achieved by establishing four research questions in Section 1.7, and each question is addressed and presented through a series of chapters (Figure 9.1), ending in specific findings for each question. The overall aim has been achieved in that the components of a monitoring system for Tanzania have been demonstrated and these could be run as a national system for forest monitoring. However, as with all research, further improvements could also be made and a significant step in the understanding of the application of remote sensing over Tanzania's forests has also been achieved. A summary of the main research findings for each question is discussed below.

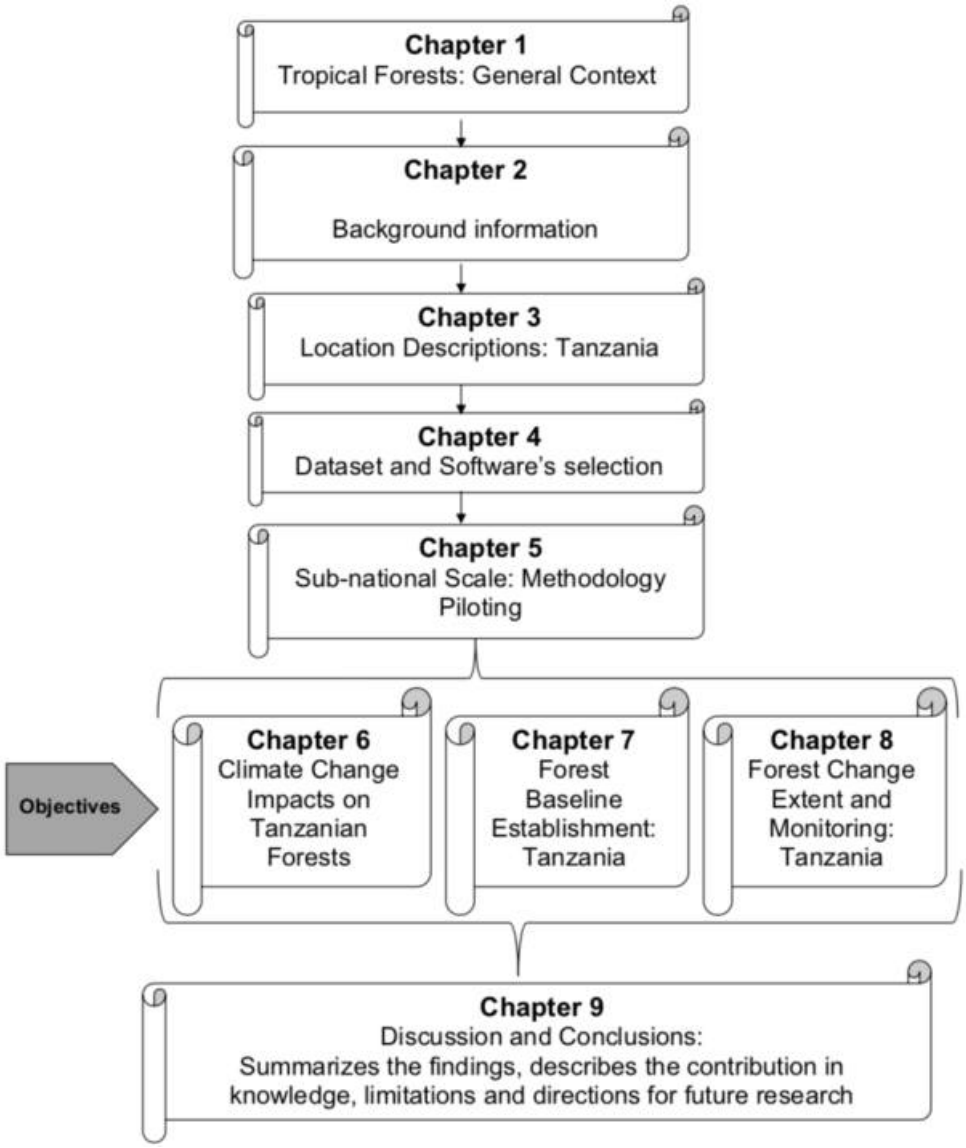

Figure 9.1: A conceptual plan of the structure of the thesis chapters

9.1.1 Forest Distribution and Impacts of Climate Change

The impact of climate change on forests in Tanzania was unknown or documented. Although the effects are already apparent and are anticipated to intensify in the

coming decades, through changes in temperature, precipitation, and indirectly via fire, pests, and pathogen pressure. A predicted change in climate is likely to induce changes in the distribution pattern of forests in Tanzania, causing changes in the environmental range of the different forest types, with a loss of habitat in some areas and an expanded range in others, depending on climatic preferences, tolerance limits and optimum for growth for each forest type. A Maximum Entropy model was used to predict different forest types' responses to climate change at a national scale using national forest inventory records and environmental data, as described in Chapter 6.

The results indicate that the climate changes are likely to be much more extreme in higher altitudes than in lower altitudes, and therefore the montane forests rich in biodiversity will be placed under more significant climatic stress with losses exceeding 40% even under the optimistic RCP4.5 scenario by 2055 than the other forest types. Likewise, climate change is predicted to threaten microhabitat forests (i.e., thickets), with losses exceeding 70% by 2085 (RCP8.5). Therefore, forest species with minimal distribution range will be at risk from changing conditions because there are no alternative sources for reinvasion with changing climate.

Tanzania is the world's tenth-largest country for the total number of endangered species on the IUCN Red List (Stévart et al., 2019). According to the 2021 classification, it is home to 1,422 critically endangered, endangered, and vulnerable species - the most endangered biodiversity of the African continent (Harfoot et al., 2021). Species face a variety of threats, including habitat loss and fragmentation, conflicts between humans and wildlife, hunting and other unsustainable natural resource management activities, poaching, and collecting for wildlife trade. Climate change is increasingly negatively affecting Tanzanian biodiversity.

The increase in temperature will probably lead to an expansion in sea volume and salinity conditions, causing mangrove forests to expand by more than 40% in both scenarios. It is a positive change for mangroves, providing a valuable economic resource for local communities and maintaining the seascape. Mangrove forests play an essential role in carbon storage (natural carbon sinks), capturing CO_2 from the atmosphere and storing it in their biomass than terrestrial trees. Therefore, sea level rise will result in increased flooding and potential redistribution of mangrove species and may replace part of the coastal forests of Tanzania adjacent to the mangrove forest which are characterised by a mosaic of vegetation types including evergreen forest, Brachystegia woodland, scrub forest, wooded grassland, and dry forest.

The predicted increase in temperature and reduced rainfall will increase further stress from a fire on savanna woodlands (miombo woodland), which represents essential ecological networks for wildlife ecosystems and can result in the permanent loss of suitable habitat or the creation of forests with a changed composition.

The replacement of forest with grassland is anticipated, causing a significant alteration of Tanzania's local climate. It will increase the fragmentation of the forested ecosystem, reducing corridors for wildlife and plant-pollinator movement, which may well contribute to the substantial extinction of important biodiversity. Human-wildlife conflict will intensify for the remaining suitable habitat for agriculture and grazing.

Therefore, the model predictions indicate that the rising temperature and decreased rainfall expected in the next 50 years could require an optimal management solution to increase ecological connectivity in current forest planning and management. Ecological connectivity should be maintained in habitats that are

predicted not to change and expand under future climate change by preserving native forests, and where possible, protecting the remaining forest areas from other anthropogenic disturbances. Improving ecological connectivity would significantly enhance sustainable forest management and improve forest projects and programs to reduce forest species turnover.

9.1.2 Current Forest Baseline for Tanzania

The future of the forests in Tanzania depends on conservation and sustainable harvesting that will minimise this precious resource's loss. The forest information is vital for developing practical, long-term plans to conserve and manage biodiversity, which requires understanding forest status, extent, location, type, and composition in Tanzania.

Therefore, the forest cover information for forests was generated as a baseline (reference level) representative of the extent (intact) of the forest area against forest cover change in Tanzania can be observed (Chapter 8). It focused on satellite data availability, the robustness of methods, and area coverage. Clouds have hindered the regular observations of EO data in generating forest information development over a large-scale (national level) (Mitchell et al., 2017). Consequently, a subset of a country (Rufiji basin) was used to experiment with the method, data availability, storage, and analysis (Chapter 5) which generated adequate forest extent with an accuracy of 93% enabled scale-up for national forest mapping (Chapter 7). Establishing forest baseline extent using EO data was achieved with an accuracy of 89.66% for forest/non-forest and bridges the information gap and knowledge concerning remote sensing in forest monitoring over a larger area (national level)

(Hościło and Lewandowska, 2019).

The analysis presented, estimated a forest area of 407,976 km^2 representing 45.76% of the country landmass (Table 7.4), compared to the previous national forest inventory (NAFORMA) conducted between May 2011 to June 2014 and released in 2015, estimated about 481,000 km^2 representing 54% of the total land area (MNRT, 2015). Arguably, the main observational gap between these analyses should not be considered forest loss in Tanzania, but due to different methodology and levels of accuracy, i.e., wall-to-wall mapping using EO data *viz.,* sample-based forest inventory plots with a relative sampling error of 8.89% on forests and woodlands (MNRT, 2015). The area of the forest is unevenly distributed over the country. Notably, the most forest-rich area includes the western part of the country covering extensive dry miombo woodlands stretching across Tabora, Katavi, Kigoma, and parts of Rukwa region (Figure 7.10). The next forested area is in the southeast part of the country with a mosaic of forest diversity (i.e., wet miombo woodlands, lowland and mangrove forest, upland forest zone). It spreads all over Pwani, Morogoro, Iringa, Njombe, Lindi, Mtwara, Ruvuma, Mbeya and Songwe regions (Table 7.5).

Overall, these areas occupy essential protected areas (Figure A.1) in the country and hence are the cornerstone of forest and biodiversity conservation in Tanzania. Therefore, increasing and maintaining well-connected systems of protected areas is a viable conservation strategy as a natural solution to global challenges, including climate change, deforestation or forest degradation. Accordingly, the result provides a consistent forest extent at a national level, whereby conservation policy actions can be planned.

9.1.3 Distribution of Forest Types in Tanzania

The forest type classification using the XGBoost classifier (Section 4.5.5) and the forest habitat suitability model (from Chapter 6) to characterise tropical forest distribution yielded an accuracy of 85%. The result provides an essential understanding of forest composition to develop sustainable forest management plans, as increasing human uses are anticipated to impact these ecosystems.

The largest forest type by area is open woodland, presenting 57% followed by closed woodland with 22%. Therefore, woodlands occupy around 79% of the forest types, spreading from the central to the western parts of the country and with a mosaic of lowland forests along the coast and southern areas of the country (Figure 7.16). The top three regions with extensive woodland areas include Lindi, Ruvuma, and Morogoro (Table 7.10). Providing forest-type information for protected areas (Table 7.11) is essential to safeguarding distinct species assemblages and national biodiversity.

Therefore, the utility of the classification result could support the estimation of forest structure in Tanzania which is a necessary first step toward quantifying above-ground biomass and developing a program for monitoring forest degradation. Forest structure is among the factors, that can largely influence forest productivity and carbon sequestration potential. Similarly, the classifications provide information about tree species distribution, with this informing forest management and potential impacts of climate change (e.g., John et al., 2020).

Therefore, timely and accurate forest-type mapping in Tanzania is imperative for forest management and monitoring necessary for conservation that advances the national forest monitoring system. Classifying forest-type distribution also

supports decision-makers by providing reliable information on the unique forest resources that play an essential role in the country's economy including benefits to many crucial sectors. For example, following their relative importance, montane forests occupying only 2.35% are vital for hydrological cycles supporting people's livelihood. While mangrove forests only occupy 0.19% of the national forest area but are important for coastal protection by creating a buffer zone, fisheries, and carbon storage.

The result will help the Tanzanian government develop forest-type conservation policies that may require different conservation states for different forest types that minimise overexploitation, especially on fragile sites. Similarly, the forest type map developed presents a baseline for evaluating future forest changes and carbon storage assessment (e.g., Suarez et al., 2021) and ecological systems for environmental management necessary for regional and international commitments of protecting forest habitats and the biodiversity therein.

9.1.4 Mapping Forest Change for Monitoring

This study focused on developing a national scale, automated, and systematic wall-to-wall forest cover change and monitoring system for Tanzania (Figure 8.1). Earth Observation (EO) datasets were used to characterise forest cover dynamics as advances in high-performance computing and machine learning classifier (XGBoost) supported the analysis at a national scale. The method discriminated forest change based on forest/non-forest baseline, masked to remove fires and plantations. An NDVI threshold was defined to identify potential change regions, and then the XGBoost forest/non-forest classifiers from Chapter 7 were applied to identify the

final scene-based change features. To identify 'True Change' a change had to be identified within 5 images. While the change analysis was applied to all Landsat-8 imagery from the beginning of 2018 to the end of 2020, the changes identified for 2018 were used to update the baseline forest/non-forest map to a discrete date (i.e., the end of 2018). While changes occurring in 2020 lacked sufficient observations to confirm them as changes and therefore the 2019 changes were the only confirmed annual changes (Figures 8.7–8.8 and Figure 8.9).

The need for more than 5 images was considered because an image is acquired every 16 days. Still, with the cloud cover, the number of available scenes is much lower, and therefore obtaining 5 observations of a change to confirm the change takes several months. Moreover, by only using images from May to November (avoiding images from the wet season), the maximum would be approximately 12 scenes during this period. If the change occurred in April or earlier, this will be captured in the following year. Probably only about 1 in 4 scenes could be useful, so for most areas, there might only be 4 observations in a year. Therefore, the following years' observations are needed to confirm the change.

The forest change analysis for the year 2019 achieved an accuracy of 82% compared to 45% from the global forest change analysis of Hansen et al. (2013) (version 1.7) (Table 8.2). Therefore, this study mapped a forest loss of 157,204 ha for 2019, amounting to 0.39% of the intact forest loss (Table 8.1) for the country. The monitoring system also updated the forest baseline map (Chapter 7). Therefore, the baseline map (forest mask) was updated from 407,976 km^2 to 397,514 km^2 by 2019, indicating a decrease of 2.56% of the forest cover in Tanzania compared to the baseline generated over the five years of 2013 – 2018.

Therefore, the developed methodology focused on supporting numerous national

and international forest programmes (Seidl et al., 2017; Romijn et al., 2012; Grainger, 2015; Bodart et al., 2013; Tobón et al., 2017; Swamy et al., 2017) on reducing forest loss and enhancing conservation and restoration. The result will help forest policy and regulation formulation at a national scale by developing a more comprehensive country framework for improving forest management. As deforestation is detected beyond general-use land into protected areas that typically have an explicit forest conservation status, indicating a threat to the forest ecosystem in Tanzania. Consequently, the forest monitoring system aims to enhance forest law enforcement and policy formulation in protecting forests with better decision-making.

9.2 Challenges and Limitations

For the first time, this study evaluated the potential of using freely available medium-resolution (30 m Landsat-8 Operational Land Imager) data for forest mapping and deforestation monitoring in Tanzania. However, there are some limitations and challenges that remain:

- Availability of Landsat cloud-free observations remains the major limitation of forest mapping and associated changes in Tanzania, particularly during the wet season. In particular, there are a lower number of cloud-free observations in the coastal and high-elevation areas of the Eastern Arc Mountains and Mt.Kilimanjaro. While a higher number of cloud-free observations extend from the central part, western and northern parts of the country. This necessitated generating a product using scenes across a broad period (2013 – 2018) to minimise the clouds and shadow problems but has also limited the period for which the change analysis could be demonstrated for.

- The methodology offers advanced opportunities for an in-depth reporting of forests and associated disturbances by utilising EO data in Tanzania. However, the lack of adequate ground truth data for accuracy assessment (e.g., Cohen et al., 2010) over a broad forest area coverage (national scale) and especially for the forest change analysis.
- The Landsat imagery was found to be limited in its ability to distinguish some vegetation classes (e.g., emergent marsh), due to the common heterogeneity and spectral similarity (mixed pixel problems) which create some challenges during forest classification and change analysis.
- The environmental variables used for the forest type habitat suitability analysis are only available at a resolution of 1 km and while this is relevant for assessing future climate scenarios, it was challenging to resample this to a 30 m resolution for inclusion in the forest type classification.

9.3 Contribution to the State of Knowledge

The research presents a unique approach to characterise forest extent and disturbance using Earth Observation data at a national scale. The research bridges the gap between complicated remote sensing practices accessing imagery and generating useful information relevant to the forest and other land managers and policymakers. The research also pioneered relating the forest-type distributions to the current climate and using this model for predicting future forest-type distribution for different climate scenarios. This highlights the risk to forest distributions and the knock-on effects on wildlife and biodiversity with an uncertain climate in

sub-Saharan Africa. Importantly for the resource-poor sub-Saharan Africa region of the globe, where data are scarce, this study has demonstrated what is possible for forest monitoring and incorporating climate change scenarios into land management and conservation planning using freely and openly available data and software. The methodology demonstrated in this study has the potential to be transferred directly to other areas of sub-Saharan Africa with only minimal extra training data to optimise the models. The methodology would be transferable to other regions of the world if sufficient reference data were available.

This study also adds several insights into the existing body of knowledge by presenting a robust, nationally consistent, and automated method for assessing forest extent and disturbances. It offers new opportunities to tackle the challenges associated with existing methods for generating forest information and monitoring deforestation at a national scale. The methodology was undertaken to derive more precise information about the forest extent and disturbance patterns in Tanzania than previous forest mapping products could offer due to their regional or global approaches. Hence, the methods and results presented illustrate Earth observation satellites' ability to extend wall-to-wall coverage (national scale) even with the challenges associated with high levels of cloud cover, adding immense value to the forest monitoring, reporting, and verification (MRV) system.

Specifically, the added contributions of this research to the body of scientific knowledge are:

- The first to demonstrate the potential impact of climate change on Tanzanian forests and woodlands. This is vital information for policy development and future conservation efforts.

- Production of the most reliable and up-to-date mapping of Tanzania's forests and woodlands, providing wall-to-wall coverage and forest-type distribution using a regionally applicable methodology.
- Demonstration of the application of forest habitat suitability models as input data to constrain the classification of forest types based on their adaptation and corresponding bioclimatic patterns, minimising misclassification. It improved the overall forest classification over a large area and a complex forest landscape.
- Provision of a methodology and demonstration for providing annual change information for Tanzania, which is more accurate than previously available datasets.
- Demonstration of a software system that can be freely used to provide a national monitoring system that automates the change analysis application, including EO data download and ARD production.

9.4 Contributions to Policy

Based on these findings, the implementation of a national forest mapping and monitoring system in Tanzania serves as a fundamental foundation for forest-related policies and laws, guidance, and review processes for enhancing forest-and-trees landscape management. Thereby guiding more effective decisions aimed at preventing all forms of forest loss arising from unplanned activities and mitigating climate change. It will improve forest management purposes by understanding forest status, its extent, and location based on consent amongst the general public,

and top-level decision-makers on the comprehensive direction and support among experts on forest ecosystem dynamics and harmonised with the legislation of other related sectors.

The forest monitoring system will assist law enforcement when urgent action is needed to stop the newly detected illegal deforestation case from expanding around the forest areas. It also forms a basis for forest management plans by forest managers whereby they need forest management inputs with extensive coverage across all the ecological zones to sustain forest production capacity. Similarly, forest cover monitoring information responds to a pressing need internationally in support of policy formulation and implementation. In particular, the UNFCCC process for the Reduction of Emissions from Deforestation and Forest Degradation (REDD+) (Romijn et al., 2012) and the protection of habitat for biodiversity conservation, as specified in the Convention on Biodiversity (CBD) Aichi Biodiversity Targets (especially Targets 5, 15, and 19) (O'Connor et al., 2015) of which Tanzania has been part of these commitments. Therefore, it is envisaged that attaining the 2030 agenda of the United Nations for Sustainable development goals (SDGs) 13 and 15 (Swamy et al., 2017) in developing countries like Tanzania will be pursued with effective national forest policies reversing current adverse trends in the loss of forest resources, consolidating the potential role of EO as a tool to support forest monitoring.

9.5 Direction for Future Research

Future work needs to investigate the utility of a larger number of image datasets from recent developments in satellite data provisions (Figure 1.3). Integrating

multi-sensor remote sensing data such as Sentinel-2A and Sentinel-2B data from the European Space Agency and increasing the number of observations and therefore reducing the period required to confirm a change. Similarly, the application of SAR which penetrates through clouds can supplement optical-based tropical forest monitoring systems. For example, long-wavelength L-band SAR data has been used to monitor tropical deforestation at larger scales (Shimada et al., 2014; Whittle et al., 2012). Also, Sentinel-1A and 1B C-band SAR satellites (Torres et al., 2012) overcome the problem of clouds to support tracking forest disturbances/deforestation of which its potential has yet utilised over a large scale.

Similarly, canopy height is a fundamental parameter for determining forest ecosystem functions such as biodiversity and above-ground biomass in Tanzania. The availability of Global Ecosystem Dynamic Investigation (GEDI), has provided sampled observations of the forest vertical structure at a near-global scale allowing for examining the vertical structure of vegetation spatially and temporally (Adrah et al., 2022). This will help better comprehend the variation in canopy height in tropical forests based on GEDI measurements, thereby supporting forest management practices, and monitoring forest response to climatic changes.

The ground validation data sets could be obtained through community-based monitoring (e.g., Pratihast et al., 2014; DeVries et al., 2016) in collecting more data from the forest with recent developments in the use of mobile apps. The local communities have regular access to forest areas, saving time and resources compared to surveys carried out by external experts. Therefore, enhancing the application of mobile data acquisition tools, such as Earth Track Wales[1] would support local communities' participation in forest monitoring. Hence, communities' effective

[1] https://wales.livingearth.online/data/ground-measurements/data-access/field-data/mobile-app/

engagement in the forest monitoring process may intensify the long-term sustainability of the REDD+ program in Tanzania.

Reducing highly mixed vegetated wetlands and other inundation areas (Figure 7.11) should explicitly be identified and mapped with tools like TropWet (Hardy et al., 2020) and masked to minimise mixed pixels with forest class.

Bibliography

Abdallah, J., Monela, G., 2007. Overview of Miombo woodlands in Tanzania. In: Proceedings of the First MITMIOMBO Project Workshop, Morogoro. pp. 6–12.

Achard, F., Beuchle, R., Mayaux, P., Stibig, H.-J., Bodart, C., Brink, A., Carboni, S., Desclée, B., Donnay, F., Eva, H. D., et al., 2014. Determination of tropical deforestation rates and related carbon losses from 1990 to 2010. Global change biology 20 (8), 2540–2554.

Achard, F., DeFries, R., Eva, H., Hansen, M., Mayaux, P., Stibig, H., 2007. Pan-tropical monitoring of deforestation. Environmental Research Letters 2 (4), 045022.

Achard, F., Eva, H. D., Stibig, H.-J., Mayaux, P., Gallego, J., Richards, T., Malingreau, J.-P., 2002. Determination of deforestation rates of the world's humid tropical forests. Science 297 (5583), 999–1002.

Achard, F., Stibig, H.-J., Eva, H. D., Lindquist, E. J., Bouvet, A., Arino, O., Mayaux, P., 2010. Estimating tropical deforestation from Earth observation data. Carbon Management 1 (2), 271–287.

Adrah, E., Wan Mohd Jaafar, W. S., Omar, H., Bajaj, S., Leite, R. V., Mazlan, S. M., Silva, C. A., Chel Gee Ooi, M., Mohd Said, M. N., Abdul Maulud, K. N., et al., 2022. Analyzing Canopy Height Patterns and Environmental Landscape Drivers in Tropical Forests Using NASA's GEDI Spaceborne LiDAR. Remote Sensing 14 (13), 3172.

Ahmad, A., Quegan, S., 2012. Analysis of maximum likelihood classification technique on Landsat 5 TM satellite data of tropical land covers. In: 2012 IEEE

International Conference on Control System, Computing and Engineering. pp. 280–285.

Aide, T. M., Clark, M. L., Grau, H. R., López-Carr, D., Levy, M. A., Redo, D., Bonilla-Moheno, M., Riner, G., Andrade-Núñez, M. J., Muñiz, M., 2013. Deforestation and Reforestation of L atin A merica and the C aribbean (2001–2010). Biotropica 45 (2), 262–271.

Ajonina, G., Diamé, A., Kairo, J., 2008. Current status and conservation of mangroves in Africa: An overview. World Rainforest Movement Bulletin 133.

Al Daoud, E., 2019. Comparison between XGBoost, LightGBM and CatBoost using a home credit dataset. International Journal of Computer and Information Engineering 13 (1), 6–10.

Aleman, J. C., Jarzyna, M. A., Staver, A. C., 2018. Forest extent and deforestation in tropical Africa since 1900. Nature ecology & evolution 2 (1), 26–33.

Alongi, D. M., 2008. Mangrove forests: resilience, protection from tsunamis, and responses to global climate change. Estuarine, Coastal and Shelf Science 76 (1), 1–13.

Alongi, D. M., 2012. Carbon sequestration in mangrove forests. Carbon management 3 (3), 313–322.

Alongi, D. M., 2015. The impact of climate change on mangrove forests. Current Climate Change Reports 1 (1), 30–39.

Alzubaidi, L., Zhang, J., Humaidi, A. J., Al-Dujaili, A., Duan, Y., Al-Shamma, O., Santamaría, J., Fadhel, M. A., Al-Amidie, M., Farhan, L., 2021. Review of deep learning: Concepts, CNN architectures, challenges, applications, future directions. Journal of big Data 8 (1), 1–74.

Anande, D. M., Luhunga, P. M., et al., 2019. Assessment of Socio-Economic Impacts of the December 2011 Flood Event in Dar es Salaam, Tanzania. Atmospheric and Climate Sciences 9 (03), 421.

Andersen, H.-E., Reutebuch, S. E., McGaughey, R. J., d'Oliveira, M. V., Keller, M., 2014. Monitoring selective logging in western Amazonia with repeat lidar flights. Remote Sensing of Environment 151, 157–165.

Anderson, K., Ryan, B., Sonntag, W., Kavvada, A., Friedl, L., 2017. Earth observation in service of the 2030 Agenda for Sustainable Development. Geo-spatial Information Science 20 (2), 77–96.

Antúnez, P., Hernández-Díaz, J. C., Wehenkel, C., Clark-Tapia, R., 2017. Generalized models: an application to identify environmental variables that significantly affect the abundance of three tree species. Forests 8 (3), 59.

Ardö, J., 2015. Comparison between remote sensing and a dynamic vegetation model for estimating terrestrial primary production of Africa. Carbon balance and management 10 (1), 8.

Arenas-Castro, S., Regos, A., Gonçalves, J. F., Alcaraz-Segura, D., Honrado, J., 2019. Remotely sensed variables of ecosystem functioning support robust predictions of abundance patterns for rare species. Remote Sensing 11 (18), 2086.

Baatuuwie, N., Van Leeuwen, L., 2011. Evaluation of three classifiers in mapping forest stand types using medium resolution imagery: a case study in the Offinso Forest District, Ghana. African Journal of Environmental Science and Technology 5 (1), 25–36.

Backéus, I., Pettersson, B., Strömquist, L., Ruffo, C., 2006. Tree communities and structural dynamics in miombo (Brachystegia–Julbernardia) woodland, Tanzania. Forest Ecology and Management 230 (1-3), 171–178.

Baloloy, A. B., Blanco, A. C., Candido, C. G., Argamosa, R. J. L., Dumalag, J. B. L. C., Dimapilis, L. L. C., Paringit, E. C., 2018. ESTIMATION OF MANGROVE FOREST ABOVEGROUND BIOMASS USING MULTISPECTRAL BANDS, VEGETATION INDICES AND BIOPHYSICAL VARIABLES DERIVED FROM OPTICAL SATELLITE IMAGERIES: RAPIDEYE, PLANETSCOPE AND SENTINEL-2. ISPRS Annals of Photogrammetry, Remote Sensing & Spatial Information Sciences 4 (3).

Barbier, E. B., Burgess, J. C., 2001. The economics of tropical deforestation. Journal of Economic Surveys 15 (3), 413–433.

Barmpoutis, P., Papaioannou, P., Dimitropoulos, K., Grammalidis, N., 2020. A

review on early forest fire detection systems using optical remote sensing. Sensors 20 (22), 6442.

Bartholome, E., Belward, A. S., 2005. GLC2000: a new approach to global land cover mapping from Earth observation data. International Journal of Remote Sensing 26 (9), 1959–1977.

Batjes, N. H., 2004. SOTER-based soil parameter estimates for Southern Africa (ver. 1.0). Tech. rep., ISRIC-World Soil Information.

Baumgartner, R. J., 2019. Sustainable development goals and the forest sector—A complex relationship. Forests 10 (2), 152.

Bazzaz, F., 1998. Tropical forests in a future climate: changes in biological diversity and impact on the global carbon cycle. In: Potential Impacts of Climate Change on Tropical Forest Ecosystems. Springer, pp. 177–196.

Belgiu, M., Drăguţ, L., 2016. Random forest in remote sensing: A review of applications and future directions. ISPRS Journal of Photogrammetry and Remote Sensing 114, 24–31.

Bellamy, C., Boughey, K., Hawkins, C., Reveley, S., Spake, R., Williams, C., Altringham, J., 2020. A sequential multi-level framework to improve habitat suitability modelling. Landscape Ecology, 1–20.

Benediktsson, J. A., Swain, P. H., Ersoy, O. K., 1990. Neural network approaches versus statistical methods in classification of multisource remote sensing data. IEEE Transactions on Geoscience and Remote Sensing.

Bergius, M., Benjaminsen, T. A., Maganga, F., Buhaug, H., 2020. Green economy, degradation narratives, and land-use conflicts in Tanzania. World Development 129, 104850.

Berninger, A., Lohberger, S., Stängel, M., Siegert, F., 2018. SAR-based estimation of above-ground biomass and its changes in tropical forests of Kalimantan using L-and C-band. Remote Sensing 10 (6), 831.

Bhavsar, D., Kumar, A., Roy, A., 2017. Applicability of NDVI temporal database for western Himalaya forest mapping using Fuzzy-based PCM classifier. European Journal of Remote Sensing 50 (1), 614–625.

Blaschke, T., 2010. Object based image analysis for remote sensing. ISPRS journal of photogrammetry and remote sensing 65 (1), 2–16.

Bodart, C., Brink, A. B., Donnay, F., Lupi, A., Mayaux, P., Achard, F., 2013. Continental estimates of forest cover and forest cover changes in the dry ecosystems of Africa between 1990 and 2000. Journal of biogeography 40 (6), 1036–1047.

Bodin, J., Badeau, V., Bruno, E., Cluzeau, C., Moisselin, J.-M., Walther, G.-R., Dupouey, J.-L., 2013. Shifts of forest species along an elevational gradient in Southeast France: climate change or stand maturation? Journal of Vegetation Science 24 (2), 269–283.

Bohak, C., Slemenik, M., Kordež, J., Marolt, M., 2020. Aerial LiDAR Data Augmentation for Direct Point-Cloud Visualisation. Sensors 20 (7), 2089.

Bonan, G. B., 2008. Forests and climate change: forcings, feedbacks, and the climate benefits of forests. science 320 (5882), 1444–1449.

Boria, R. A., Olson, L. E., Goodman, S. M., Anderson, R. P., 2014. Spatial filtering to reduce sampling bias can improve the performance of ecological niche models. Ecological modelling 275, 73–77.

Borlaf-Mena, I., Badea, O., Tanase, M. A., 2021. Assessing the Utility of Sentinel-1 Coherence Time Series for Temperate and Tropical Forest Mapping. Remote Sensing 13 (23), 4814.

Bosso, L., Di Febbraro, M., Cristinzio, G., Zoina, A., Russo, D., 2016. Shedding light on the effects of climate change on the potential distribution of Xylella fastidiosa in the Mediterranean basin. Biological Invasions 18 (6), 1759–1768.

Boughorbel, S., Jarray, F., El-Anbari, M., 2017. Optimal classifier for imbalanced data using Matthews Correlation Coefficient metric. PloS one 12 (6).

Bouvet, A., Mermoz, S., Ballère, M., Koleck, T., Le Toan, T., 2018. Use of the SAR shadowing effect for deforestation detection with Sentinel-1 time series. Remote Sensing 10 (8), 1250.

Bradshaw, C. J., Sodhi, N. S., Brook, B. W., 2009. Tropical turmoil: a biodiversity tragedy in progress. Frontiers in Ecology and the Environment 7 (2), 79–87.

Braunisch, V., Coppes, J., Arlettaz, R., Suchant, R., Schmid, H., Bollmann, K., 2013. Selecting from correlated climate variables: a major source of uncertainty for predicting species distributions under climate change. Ecography 36 (9), 971–983.

Breiman, L., 2001. Random forests. Machine learning 45 (1), 5–32.

Brink, A. B., Eva, H. D., 2009. Monitoring 25 years of land cover change dynamics in Africa: A sample based remote sensing approach. Applied Geography 29 (4), 501–512.

Brinkmann, K., Noromiarilanto, F., Ratovonamana, R. Y., Buerkert, A., 2014. Deforestation processes in south-western Madagascar over the past 40 years: what can we learn from settlement characteristics? Agriculture, Ecosystems & Environment 195, 231–243.

Britto Jr, A. S., Sabourin, R., Oliveira, L. E., 2014. Dynamic selection of classifiers—a comprehensive review. Pattern recognition 47 (11), 3665–3680.

Brockington, D., 2007. Forests, community conservation, and local government performance: The village forest reserves of Tanzania. Society and Natural Resources 20 (9), 835–848.

Broich, M., Hansen, M. C., Potapov, P., Adusei, B., Lindquist, E., Stehman, S. V., 2011. Time-series analysis of multi-resolution optical imagery for quantifying forest cover loss in Sumatra and Kalimantan, Indonesia. International Journal of Applied Earth Observation and Geoinformation 13 (2), 277–291.

Brolly, G., Király, G., Lehtomäki, M., Liang, X., 2021. Voxel-based automatic tree detection and parameter retrieval from terrestrial laser scans for plot-wise forest inventory. Remote Sensing 13 (4), 542.

Brovelli, M. A., Minghini, M., Moreno-Sanchez, R., Oliveira, R., 2017. Free and open source software for geospatial applications (FOSS4G) to support Future Earth. International Journal of Digital Earth 10 (4), 386–404.

Brown, H. C. P., Smit, B., Somorin, O. A., Sonwa, D. J., Nkem, J. N., 2014. Climate change and forest communities: prospects for building institutional adaptive capacity in the Congo Basin forests. Ambio 43 (6), 759–769.

Brownlee, J., 2018. XGBoost with Python. Machine Learning Mastery.

Brummitt, N. A., Bachman, S. P., Griffiths-Lee, J., Lutz, M., Moat, J. F., Farjon, A., Donaldson, J. S., Hilton-Taylor, C., Meagher, T. R., Albuquerque, S., et al., 2015. Green plants in the red: A baseline global assessment for the IUCN sampled Red List Index for plants. PloS one 10 (8).

Bruzzone, L., Prieto, D. F., 2002. An adaptive semiparametric and context-based approach to unsupervised change detection in multitemporal remote-sensing images. IEEE Transactions on image processing 11 (4), 452–466.

Bruzzone, L., Serpico, S. B., 1997. An iterative technique for the detection of land-cover transitions in multitemporal remote-sensing images. IEEE transactions on geoscience and remote sensing 35 (4), 858–867.

Bunting, P., 2017. Introduction to ARCSI for generating Analysis Ready Data (ARD).

Bunting, P., 2018. Earth Observation Data Downloader (EODataDown). Accessed on 21.02.2021.
URL https://eodatadown.remotesensing.info/

Bunting, P., Clewley, D., Lucas, R. M., Gillingham, S., 2014. The remote sensing and GIS software library (RSGISLib). Computers & geosciences 62, 216–226.

Bunting, P., Gillingham, S., 2013. The KEA image file format. Computers & geosciences 57, 54–58.

Bunting, P., Rosenqvist, A., Hilarides, L., Lucas, R. M., Thomas, N., Tadono, T., Worthington, T. A., Spalding, M., Murray, N. J., Rebelo, L.-M., 2022. Global Mangrove Extent Change 1996–2020: Global Mangrove Watch Version 3.0. Remote Sensing 14 (15), 3657.

Bunting, P., Rosenqvist, A., Lucas, R. M., Rebelo, L.-M., Hilarides, L., Thomas, N., Hardy, A., Itoh, T., Shimada, M., Finlayson, C. M., 2018. The global mangrove watch—a new 2010 global baseline of mangrove extent. Remote Sensing 10 (10), 1669.

Burgess, N., Hales, J., Underwood, E., Dinerstein, E., Olson, D., Itoua, I., Schip-

per, J., Ricketts, T., Newman, K., et al., 2004. Terrestrial ecoregions of Africa and Madagascar: a conservation assessment. Island Press.

Burgess, N. D., Bahane, B., Clairs, T., Danielsen, F., Dalsgaard, S., Funder, M., Hagelberg, N., Harrison, P., Haule, C., Kabalimu, K., et al., 2010. Getting ready for REDD+ in Tanzania: a case study of progress and challenges. Oryx 44 (3), 339–351.

Burgman, M. A., Fox, J. C., 2003. Bias in species range estimates from minimum convex polygons: implications for conservation and options for improved planning. Animal Conservation 6 (1), 19–28.

Burke, A., 2001. Classification and ordination of plant communities of the Naukluft Mountains, Namibia. Journal of Vegetation Science 12 (1), 53–60.

Busby, J. R., 1991. BIOCLIM: a bioclimate analysis and prediction system. In Margules, C. R. and Austin, M. P. (eds.), Nature Conservation: Cost Effective Biological Surveys and Data Analysis. CSIRO, Canberra, Australia.

Busch, J., Engelmann, J., 2015. The future of forests: emissions from tropical deforestation with and without a carbon price, 2016-2050. Center for Global Development Working Paper 22 (411).

Butt, N., Seabrook, L., Maron, M., Law, B. S., Dawson, T. P., Syktus, J., McAlpine, C. A., 2015. Cascading effects of climate extremes on vertebrate fauna through changes to low-latitude tree flowering and fruiting phenology. Global Change Biology 21 (9), 3267–3277.

Campbell, B., Angelsen, A., Cunningham, A., Katerere, Y., Sitoe, A., Wunder, S., 2007. Miombo woodlands–opportunities and barriers to sustainable forest management. CIFOR, Bogor, Indonesia http://www. cifor. cgiar. org/miombo/docs/Campbell_ BarriersandOpportunities. pdf (4th November 2008).

Campbell, B. M., et al., 1996. The Miombo in transition: woodlands and welfare in Africa. CIFOR.

Campbell, J. B., Wynne, R., 2007. Introduction to Remote Sensing. The Guilford Press. New York.

Carmona, P., Climent, F., Momparler, A., 2019. Predicting failure in the US banking sector: An extreme gradient boosting approach. International Review of Economics & Finance 61, 304–323.

Carpenter, G. A., Gjaja, M. N., Gopal, S., Woodcock, C. E., 1997. ART neural networks for remote sensing: vegetation classification from Landsat TM and terrain data. IEEE Transactions on Geoscience and Remote Sensing 35 (2), 308–325.

Castillo, M., Rivard, B., Sánchez-Azofeifa, A., Calvo-Alvarado, J., Dubayah, R., 2012. LIDAR remote sensing for secondary Tropical Dry Forest identification. Remote sensing of environment 121, 132–143.

Chakravarty, S., Pala, N. A., Tamang, B., Sarkar, B. C., Manohar, K. A., Rai, P., Puri, A., Shukla, G., et al., 2019. Ecosystem Services of Trees Outside Forest. In: Sustainable Agriculture, Forest and Environmental Management. pp. 327–352.

Chan, J. C.-W., Paelinckx, D., 2008. Evaluation of Random Forest and Adaboost tree-based ensemble classification and spectral band selection for ecotope mapping using airborne hyperspectral imagery. Remote Sensing of Environment 112 (6), 2999–3011.

Chen, H., Zeng, Z., Wu, J., Peng, L., Lakshmi, V., Yang, H., Liu, J., 2020. Large Uncertainty on Forest Area Change in the Early 21st Century among Widely Used Global Land Cover Datasets. Remote Sensing 12 (21), 3502.

Chen, J., Gong, P., He, C., Pu, R., Shi, P., 2003. Land-use/land-cover change detection using improved change-vector analysis. Photogrammetric Engineering & Remote Sensing 69 (4), 369–379.

Chen, M., Liu, Q., Chen, S., Liu, Y., Zhang, C.-H., Liu, R., 2019. XGBoost-based algorithm interpretation and application on post-fault transient stability status prediction of power system. IEEE Access 7, 13149–13158.

Chen, T., Guestrin, C., 2016. XGboost: A scalable tree boosting system. In: Proceedings of the 22nd acm sigkdd international conference on knowledge discovery and data mining. pp. 785–794.

Chen, T., He, T., 2022. Xgboost: eXtreme Gradient Boosting.

Chicco, D., Jurman, G., 2020. The advantages of the Matthews correlation coefficient (MCC) over F1 score and accuracy in binary classification evaluation. BMC genomics 21 (1), 6.

Chidumayo, E., 2001. Climate and phenology of savanna vegetation in southern Africa. Journal of Vegetation Science, 347–354.

Chidumayo, E., Okali, D., Kowero, G., Larwanou, M., 2011. Climate change and African forest and wildlife resources. African Forest Forum Nairobi.

Cho, M. A., Mathieu, R., Asner, G. P., Naidoo, L., van Aardt, J., Ramoelo, A., Debba, P., Wessels, K., Main, R., Smit, I. P., et al., 2012. Mapping tree species composition in South African savannas using an integrated airborne spectral and LiDAR system. Remote Sensing of Environment 125, 214–226.

Chorowicz, J., 2005. The east African rift system. Journal of African Earth Sciences 43 (1-3), 379–410.

Chutia, D., Bhattacharyya, D., Sarma, K. K., Kalita, R., Sudhakar, S., 2016. Hyperspectral remote sensing classifications: a perspective survey. Transactions in GIS 20 (4), 463–490.

Chuvieco, E., Martin, M. P., Palacios, A., 2002. Assessment of different spectral indices in the red-near-infrared spectral domain for burned land discrimination. International Journal of Remote Sensing 23 (23), 5103–5110.

Cihlar, J., Xiao, Q., Chen, J., Beaubien, J., Fung, K., Latifovic, R., 1998. Classification by progressive generalization: A new automated methodology for remote sensing multichannel data. International Journal of Remote Sensing 19 (14), 2685–2704.

Ciolli, M., Federici, B., Ferrando, I., Marzocchi, R., Sguerso, D., Tattoni, C., Vitti, A., Zatelli, P., 2017. FOSS tools and applications for education in geospatial sciences. ISPRS International Journal of Geo-Information 6 (7), 225.

Clark, J. S., Gelfand, A. E., Woodall, C. W., Zhu, K., 2014. More than the sum of the parts: forest climate response from joint species distribution models. Ecological Applications 24 (5), 990–999.

Clark, M. L., Roberts, D. A., Clark, D. B., 2005. Hyperspectral discrimination

of tropical rain forest tree species at leaf to crown scales. Remote sensing of environment 96 (3-4), 375–398.

Clewley, D., Bunting, P., Shepherd, J., Gillingham, S., Flood, N., Dymond, J., Lucas, R., Armston, J., Moghaddam, M., 2014. A python-based open source system for geographic object-based image analysis (GEOBIA) utilizing raster attribute tables. Remote Sensing 6 (7), 6111–6135.

Cohen, W. B., Yang, Z., Kennedy, R., 2010. Detecting trends in forest disturbance and recovery using yearly Landsat time series: 2. TimeSync—Tools for calibration and validation. Remote Sensing of Environment 114 (12), 2911–2924.

Congalton, R. G., 1991. A review of assessing the accuracy of classifications of remotely sensed data. Remote Sensing of Environment 37 (1), 35–46.

Congalton, R. G., Green, K., 2019. Assessing the accuracy of remotely sensed data: principles and practices. CRC press.

Connette, G., Oswald, P., Songer, M., Leimgruber, P., 2016. Mapping distinct forest types improves overall forest identification based on multi-spectral Landsat imagery for Myanmar's Tanintharyi Region. Remote Sensing 8 (11), 882.

Coppin, P., Jonckheere, I., Nackaerts, K., Muys, B., Lambin, E., 2004. Review Article Digital change detection methods in ecosystem monitoring: a review. International journal of remote sensing 25 (9), 1565–1596.

Coppin, P. R., Bauer, M. E., 1994. Processing of multitemporal Landsat TM imagery to optimize extraction of forest cover change features. IEEE Transactions on Geoscience and remote Sensing 32 (4), 918–927.

Coppin, P. R., Bauer, M. E., 1996. Digital change detection in forest ecosystems with remote sensing imagery. Remote sensing reviews 13 (3-4), 207–234.

Corlett, R. T., 2014. Tropical forests. e LS.

Cortijo, F., De La Blanca, N. P., 1997. A comparative study of some non-parametric spectral classifiers. Applications to problems with high-overlapping training sets. International Journal of Remote Sensing 18 (6), 1259–1275.

Costa, M. H., Foley, J. A., 2000. Combined effects of deforestation and doubled

atmospheric CO2 concentrations on the climate of Amazonia. Journal of Climate 13 (1), 18–34.

Craglia, M., de Bie, K., Jackson, D., Pesaresi, M., Remetey-Fülöpp, G., Wang, C., Annoni, A., Bian, L., Campbell, F., Ehlers, M., et al., 2012. Digital Earth 2020: towards the vision for the next decade. International Journal of Digital Earth 5 (1), 4–21.

Cramer, W., Bondeau, A., Schaphoff, S., Lucht, W., Smith, B., Sitch, S., 2004. Tropical forests and the global carbon cycle: impacts of atmospheric carbon dioxide, climate change and rate of deforestation. Philosophical Transactions of the Royal Society of London. Series B: Biological Sciences 359 (1443), 331–343.

Crase, B., Vesk, P. A., Liedloff, A., Wintle, B. A., 2015. Modelling both dominance and species distribution provides a more complete picture of changes to mangrove ecosystems under climate change. Global Change Biology 21 (8), 3005–3020.

Crouzeilles, R., Ferreira, M. S., Chazdon, R. L., Lindenmayer, D. B., Sansevero, J. B., Monteiro, L., Iribarrem, A., Latawiec, A. E., Strassburg, B. B., 2017. Ecological restoration success is higher for natural regeneration than for active restoration in tropical forests. Science Advances 3 (11), e1701345.

Crowley, M. A., Cardille, J. A., 2020. Remote sensing's recent and future contributions to landscape ecology. Current Landscape Ecology Reports 5 (3), 45–57.

Culas, R. J., 2007. Deforestation and the environmental Kuznets curve: An institutional perspective. Ecological Economics 61 (2-3), 429–437.

Cutler, D. R., Edwards Jr, T. C., Beard, K. H., Cutler, A., Hess, K. T., Gibson, J., Lawler, J. J., 2007. Random forests for classification in ecology. Ecology 88 (11), 2783–2792.

D'Amen, M., Rahbek, C., Zimmermann, N. E., Guisan, A., 2017. Spatial predictions at the community level: from current approaches to future frameworks. Biological Reviews 92 (1), 169–187.

Dargie, G. C., Lewis, S. L., Lawson, I. T., Mitchard, E. T., Page, S. E., Bocko,

Y. E., Ifo, S. A., 2017. Age, extent and carbon storage of the central Congo Basin peatland complex. Nature 542 (7639), 86–90.

David, R., Rosser, N. J., Donoghue, D. N., 2022. Remote sensing for monitoring tropical dryland forests: a review of current research, knowledge gaps and future directions for Southern Africa. Environmental Research Communications.

De Alban, J. D. T., Connette, G. M., Oswald, P., Webb, E. L., 2018. Combined Landsat and L-band SAR data improves land cover classification and change detection in dynamic tropical landscapes. Remote Sensing 10 (2), 306.

De Bem, P. P., de Carvalho Junior, O. A., Fontes Guimarães, R., Trancoso Gomes, R. A., 2020. Change detection of deforestation in the Brazilian Amazon using landsat data and convolutional neural networks. Remote Sensing 12 (6), 901.

De Grandi, G., Mayaux, P., Rauste, Y., Rosenqvist, A., Simard, M., Saatchi, S. S., 2000. The Global Rain Forest Mapping Project JERS-1 radar mosaic of tropical Africa: Development and product characterization aspects. IEEE Transactions on Geoscience and Remote Sensing 38 (5), 2218–2233.

de Klerk, H. M., Buchanan, G., 2017. Remote sensing training in African conservation. Remote Sensing in Ecology and Conservation 3 (1), 7–20.

De Wasseige, C., De Marcken, P., Bayol, N., Hiol Hiol, F., Mayaux, P., Desclée, B., Billand, A., Nasi, R., 2014. The forests of the Congo Basin: State of the Forest 2013. Publications office of the European Union.

Deb, J. C., Phinn, S., Butt, N., McAlpine, C. A., 2017. The impact of climate change on the distribution of two threatened Dipterocarp trees. Ecology and evolution 7 (7), 2238–2248.

Deepan, P., Sudha, L., 2020. Object classification of remote sensing image using deep convolutional neural network. In: The cognitive approach in cloud computing and internet of things technologies for surveillance tracking systems. pp. 107–120.

DeFries, R., Achard, F., Brown, S., Herold, M., Murdiyarso, D., Schlamadinger, B., de Souza Jr, C., 2007. Earth observations for estimating greenhouse gas

emissions from deforestation in developing countries. Environmental science & policy 10 (4), 385–394.

DeFries, R., Hansen, A., Newton, A. C., Hansen, M. C., 2005. Increasing isolation of protected areas in tropical forests over the past twenty years. Ecological applications 15 (1), 19–26.

DeFries, R. S., Houghton, R. A., Hansen, M. C., Field, C. B., Skole, D., Townshend, J., 2002. Carbon emissions from tropical deforestation and regrowth based on satellite observations for the 1980s and 1990s. Proceedings of the National Academy of Sciences 99 (22), 14256–14261.

Delgado-Aguilar, M., Fassnacht, F., Peralvo, M., Gross, C., Schmitt, C., 2017. Potential of TerraSAR-X and Sentinel 1 imagery to map deforested areas and derive degradation status in complex rain forests of Ecuador. International Forestry Review 19 (1), 102–118.

Delire, C., Ngomanda, A., Jolly, D., 2008. Possible impacts of 21st century climate on vegetation in Central and West Africa. Global and Planetary Change 64 (1-2), 3–15.

Desclée, B., Bogaert, P., Defourny, P., 2006. Forest change detection by statistical object-based method. Remote sensing of environment 102 (1-2), 1–11.

Deus, D., 2018. Assessment of Supervised Classifiers for Land Cover Categorization Based on Integration of ALOS PALSAR and Landsat Data. Advances in Remote Sensing 7 (2), 47–60.

Devaney, J., Barrett, B., Barrett, F., Redmond, J., OHalloran, J., 2015. Forest cover estimation in Ireland using radar remote sensing: a comparative analysis of forest cover assessment methodologies. Plos one 10 (8), e0133583.

DeVries, B., Pratihast, A. K., Verbesselt, J., Kooistra, L., Herold, M., 2016. Characterizing forest change using community-based monitoring data and Landsat time series. PloS one 11 (3), e0147121.

Dingle Robertson, L., King, D. J., 2011. Comparison of pixel-and object-based classification in land cover change mapping. International Journal of Remote Sensing 32 (6), 1505–1529.

Dong, J., Xiao, X., Sheldon, S., Biradar, C., Xie, G., 2012. Mapping tropical forests and rubber plantations in complex landscapes by integrating PALSAR and MODIS imagery. ISPRS Journal of Photogrammetry and Remote Sensing 74, 20–33.

Dormann, C. F., Elith, J., Bacher, S., Buchmann, C., Carl, G., Carré, G., Marquéz, J. R. G., Gruber, B., Lafourcade, B., Leitão, P. J., et al., 2012. Collinearity: a review of methods to deal with it and a simulation study evaluating their performance. Ecography 36 (1), 27–46.

Drusch, M., Del Bello, U., Carlier, S., Colin, O., Fernandez, V., Gascon, F., Hoersch, B., Isola, C., Laberinti, P., Martimort, P., et al., 2012. Sentinel-2: ESA's optical high-resolution mission for GMES operational services. Remote sensing of Environment 120, 25–36.

Dubayah, R. O., Drake, J. B., 2000. Lidar remote sensing for forestry. Journal of Forestry 98 (6), 44–46.

Dubeau, P., King, D. J., Unbushe, D. G., Rebelo, L.-M., 2017. Mapping the Dabus wetlands, Ethiopia, using random forest classification of Landsat, PALSAR and topographic data. Remote Sensing 9 (10), 1056.

Duvail, S., Mwakalinga, A., Eijkelenburg, A., Hamerlynck, O., Kindinda, K., Majule, A., 2014. Jointly thinking the post-dam future: exchange of local and scientific knowledge on the lakes of the Lower Rufiji, Tanzania. Hydrological Sciences Journal 59 (3-4), 713–730.

Duveiller, G., Defourny, P., Desclée, B., Mayaux, P., 2008. Deforestation in Central Africa: Estimates at regional, national and landscape levels by advanced processing of systematically-distributed Landsat extracts. Remote sensing of environment 112 (5), 1969–1981.

Dyderski, M. K., Paź, S., Frelich, L. E., Jagodziński, A. M., 2018. How much does climate change threaten European forest tree species distributions? Global change biology 24 (3), 1150–1163.

Edenius, L., Mikusiński, G., 2006. Utility of habitat suitability models as biodi-

versity assessment tools in forest management. Scandinavian Journal of Forest Research 21 (S7), 62–72.

Elith, J., H. Graham, C., P. Anderson, R., Dudík, M., Ferrier, S., Guisan, A., J. Hijmans, R., Huettmann, F., R. Leathwick, J., Lehmann, A., et al., 2006. Novel methods improve prediction of species' distributions from occurrence data. Ecography 29 (2), 129–151.

Elith, J., Leathwick, J., 2007. Predicting species distributions from museum and herbarium records using multiresponse models fitted with multivariate adaptive regression splines. Diversity and distributions 13 (3), 265–275.

Elith, J., Leathwick, J. R., Hastie, T., 2008. A working guide to boosted regression trees. Journal of Animal Ecology 77 (4), 802–813.

Elith, J., Phillips, S. J., Hastie, T., Dudík, M., Chee, Y. E., Yates, C. J., 2011. A statistical explanation of MaxEnt for ecologists. Diversity and distributions 17 (1), 43–57.

Encalada, A. C., Flecker, A. S., Poff, N. L., Suárez, E., Herrera-R, G. A., Ríos-Touma, B., Jumani, S., Larson, E. I., Anderson, E. P., 2019. A global perspective on tropical montane rivers. Science 365 (6458), 1124–1129.

Erinjery, J. J., Singh, M., Kent, R., 2018. Mapping and assessment of vegetation types in the tropical rainforests of the Western Ghats using multispectral Sentinel-2 and SAR Sentinel-1 satellite imagery. Remote Sensing of Environment 216, 345–354.

Eva, H., Brink, A., Simonetti, D., et al., 2006. Monitoring land cover dynamics in sub-Saharan Africa. Institute for Environmental and Sustainability, Tech. Rep. EUR 22498.

Fan, F., Wang, Y., Wang, Z., 2008. Temporal and spatial change detecting (1998–2003) and predicting of land use and land cover in Core corridor of Pearl River Delta (China) by using TM and ETM+ images. Environmental monitoring and assessment 137 (1-3), 127.

FAO, 2010. Global Forest Resources Assessment. Tech. Rep. 163, Rome, Italy.

FAO, 2016. State of the World's Forests 2016: Forests and agriculture: Land-use challenges and opportunities. FAO Report.

FAO, 2020. Global Forest Resources Assessment 2020: Main report. Rome. Tech. rep., FAO.

FAO and JRC, 2012. Global forest land-use change 1990–2005. FAO forestry paper 169.

FAO and JRC, 2014. Global Forest Land-Use Change 1990–2010. An update to FAO Forestry Paper (169).

Fearnside, P. M., 2000. Global warming and tropical land-use change: greenhouse gas emissions from biomass burning, decomposition and soils in forest conversion, shifting cultivation and secondary vegetation. Climatic change 46 (1-2), 115–158.

Fearnside, P. M., 2003. Deforestation control in Mato Grosso: a new model for slowing the loss of Brazil's Amazon forest. AMBIO: A Journal of the Human Environment 32 (5), 343–345.

Fensholt, R., Sandholt, I., Rasmussen, M. S., Stisen, S., Diouf, A., 2006. Evaluation of satellite based primary production modelling in the semi-arid Sahel. Remote Sensing of Environment 105 (3), 173–188.

Ferrier, S., Guisan, A., 2006. Spatial modelling of biodiversity at the community level. Journal of applied ecology 43 (3), 393–404.

Fick, S. E., Hijmans, R. J., 2017. WorldClim 2: new 1-km spatial resolution climate surfaces for global land areas. International journal of climatology 37 (12), 4302–4315.

Fielding, A. H., Bell, J. F., 1997. A review of methods for the assessment of prediction errors in conservation presence/absence models. Environmental conservation 24 (1), 38–49.

Fisher, R., 2012. Tropical forest monitoring, combining satellite and social data, to inform management and livelihood implications: Case studies from Indonesian West Timor. International journal of applied earth observation and geoinformation 16, 77–84.

Fjeldså, J., 1999. The impact of human forest disturbance on the endemic avifauna of the Udzungwa Mountains, Tanzania. Bird Conservation International 9 (1), 47–62.

Flood, N., Danaher, T., Gill, T., Gillingham, S., 2013. An operational scheme for deriving standardised surface reflectance from Landsat TM/ETM+ and SPOT HRG imagery for Eastern Australia. Remote Sensing 5 (1), 83–109.

Flores, S. E., Yool, S. R., 2007. Sensitivity of change vector analysis to land cover change in an arid ecosystem. International Journal of Remote Sensing 28 (5), 1069–1088.

Foga, S., Scaramuzza, P. L., Guo, S., Zhu, Z., Dilley Jr, R. D., Beckmann, T., Schmidt, G. L., Dwyer, J. L., Hughes, M. J., Laue, B., 2017. Cloud detection algorithm comparison and validation for operational Landsat data products. Remote sensing of environment 194, 379–390.

Fonseca, M. G., Alves, L. M., Aguiar, A. P. D., Arai, E., Anderson, L. O., Rosan, T. M., Shimabukuro, Y. E., de Aragão, L. E. O. e. C., 2019. Effects of climate and land-use change scenarios on fire probability during the 21st century in the Brazilian Amazon. Global change biology 25 (9), 2931–2946.

Foody, G., Hill, R., 1996. Classification of tropical forest classes from Landsat TM data. International journal of remote sensing 17 (12), 2353–2367.

Foody, G. M., 1995. Land cover classification by an artificial neural network with ancillary information. International Journal of Geographical Information Systems 9 (5), 527–542.

Foody, G. M., 2002. Status of land cover classification accuracy assessment. Remote sensing of environment 80 (1), 185–201.

Foody, G. M., Boyd, D. S., Cutler, M. E., 2003. Predictive relations of tropical forest biomass from Landsat TM data and their transferability between regions. Remote sensing of environment 85 (4), 463–474.

Foody, G. M., Cutler, M. E., 2006. Mapping the species richness and composition of tropical forests from remotely sensed data with neural networks. Ecological modelling 195 (1-2), 37–42.

Foody, G. M., Mathur, A., 2004. Toward intelligent training of supervised image classifications: directing training data acquisition for SVM classification. Remote Sensing of Environment 93 (1-2), 107–117.

Foody, G. M., Palubinskas, G., Lucas, R. M., Curran, P. J., Honzak, M., 1996. Identifying terrestrial carbon sinks: classification of successional stages in regenerating tropical forest from Landsat TM data. Remote Sensing of Environment 55 (3), 205–216.

Foster, P., 2001. The potential negative impacts of global climate change on tropical montane cloud forests. Earth-Science Reviews 55 (1-2), 73–106.

Franco-Lopez, H., Ek, A. R., Bauer, M. E., 2001. Estimation and mapping of forest stand density, volume, and cover type using the k-nearest neighbors method. Remote sensing of Environment 77 (3), 251–274.

Franklin, J., Serra-Diaz, J. M., Syphard, A. D., Regan, H. M., 2016. Global change and terrestrial plant community dynamics. Proceedings of the National Academy of Sciences 113 (14), 3725–3734.

Franklin, S., Wulder, M., 2002. Remote sensing methods in medium spatial resolution satellite data land cover classification of large areas. Progress in Physical Geography 26 (2), 173–205.

Franklin, S. E., 2001. Remote sensing for sustainable forest management. CRC press.

Frazier, A. E., Hemingway, B. L., 2021. A technical review of planet smallsat data: Practical considerations for processing and using planetscope imagery. Remote Sensing 13 (19), 3930.

Frost, P., Medina, E., Menaut, J., Solbrig, O., Swift, M., Walker, B., 1986. Responses of Savannas to Stress and Disturbance. Biology International, Special Issue 10. International Union of Biological Sciences, Paris.

Fuller, D. O., 2006. Tropical forest monitoring and remote sensing: A new era of transparency in forest governance? Singapore Journal of Tropical Geography 27 (1), 15–29.

Galiatsatos, N., Donoghue, D. N., Watt, P., Bholanath, P., Pickering, J., Hansen,

M. C., Mahmood, A. R., 2020. An assessment of global forest change datasets for national forest monitoring and reporting. Remote Sensing 12 (11), 1790.

García, M. L., Caselles, V., 1991. Mapping burns and natural reforestation using Thematic Mapper data. Geocarto International 6 (1), 31–37.

Gardner, T. A., Barlow, J., Chazdon, R., Ewers, R. M., Harvey, C. A., Peres, C. A., Sodhi, N. S., 2009. Prospects for tropical forest biodiversity in a human-modified world. Ecology letters 12 (6), 561–582.

Garreta, R., Moncecchi, G., 2013. Learning scikit-learn: machine learning in python.

Ge, S., Gu, H., Su, W., Rauste, Y., Praks, J., Antropov, O., 2022. Boreal Forest Height Mapping using Sentinel-1 Time Series and improved LSTM model. bioRxiv.

Geist, H. J., Lambin, E. F., 2002. Proximate Causes and Underlying Driving Forces of Tropical DeforestationTropical forests are disappearing as the result of many pressures, both local and regional, acting in various combinations in different geographical locations. BioScience 52 (2), 143–150.

Geurts, P., Ernst, D., Wehenkel, L., 2006. Extremely randomized trees. Machine learning 63 (1), 3–42.

Gibbs, H. K., Ruesch, A. S., Achard, F., Clayton, M. K., Holmgren, P., Ramankutty, N., Foley, J. A., 2010. Tropical forests were the primary sources of new agricultural land in the 1980s and 1990s. Proceedings of the National Academy of Sciences 107 (38), 16732–16737.

Gillingham, S., Flood, N., 2013. Raster I/O Simplification Python Library. URL https://bitbucket. org/chchrsc/rios/overview.

Girard, A., Schweiger, A. K., Carteron, A., Kalacska, M., Laliberté, E., 2020. Foliar spectra and traits of bog plants across nitrogen deposition gradients. Remote Sensing 12 (15), 2448.

Giuliani, G., Egger, E., Italiano, J., Poussin, C., Richard, J.-P., Chatenoux, B., 2020. Essential variables for environmental monitoring: what are the possible contributions of earth observation data cubes? Data 5 (4), 100.

Godoy, F. L., Tabor, K., Burgess, N. D., Mbilinyi, B. P., Kashaigili, J. J., Steininger, M. K., 2012. Deforestation and CO 2 emissions in coastal Tanzania from 1990 to 2007. Environmental Conservation 39 (1), 62–71.

Godoy, M. D., Lacerda, L. D. d., 2015. Mangroves response to climate change: a review of recent findings on mangrove extension and distribution. Anais da Academia Brasileira de Ciências 87 (2), 651–667.

Goetz, S. J., Baccini, A., Laporte, N. T., Johns, T., Walker, W., Kellndorfer, J., Houghton, R. A., Sun, M., 2009. Mapping and monitoring carbon stocks with satellite observations: a comparison of methods. Carbon balance and management 4 (1), 2.

Gomes, M. F., Maillard, P., Deng, H., 2018. Individual tree crown detection in submeter satellite imagery using Marked Point Processes and a geometrical-optical model. Remote Sensing of Environment 211, 184–195.

Gondo, P. C., 2012. A review of forest financing in Africa. Southern Alliance for Indigenous Resources (SAFIRE), Zimbabwe.

Govender, N., Trollope, W. S., Van Wilgen, B. W., 2006. The effect of fire season, fire frequency, rainfall and management on fire intensity in savanna vegetation in South Africa. Journal of Applied Ecology 43 (4), 748–758.

Grace, J., Mitchard, E., Gloor, E., 2014. Perturbations in the carbon budget of the tropics. Global Change Biology 20 (10), 3238 – 3255.

Grainger, A., 2015. Is land degradation neutrality feasible in dry areas? Journal of Arid Environments 112, 14–24.

Grantham, H., Duncan, A., Evans, T., Jones, K., Beyer, H., Schuster, R., Walston, J., Ray, J., Robinson, J., Callow, M., et al., 2020. Anthropogenic modification of forests means only 40% of remaining forests have high ecosystem integrity. Nature communications 11 (1), 1–10.

Green, J. M., Larrosa, C., Burgess, N. D., Balmford, A., Johnston, A., Mbilinyi, B. P., Platts, P. J., Coad, L., 2013. Deforestation in an African biodiversity hotspot: Extent, variation and the effectiveness of protected areas. Biological Conservation 164, 62–72.

Green Advocates International, Inc., 2014. Scoping Study of the Forestry Sector for the purpose of including the industry in Revenue Disclosure through the Tanzania Extractive Industries Transparency Initiative.

Grinand, C., Rakotomalala, F., Gond, V., Vaudry, R., Bernoux, M., Vieilledent, G., 2013. Estimating deforestation in tropical humid and dry forests in Madagascar from 2000 to 2010 using multi-date Landsat satellite images and the random forests classifier. Remote Sensing of Environment 139, 68–80.

Guild, L. S., Cohen, W. B., Kauffman, J. B., 2004. Detection of deforestation and land conversion in Rondonia, Brazil using change detection techniques. International Journal of Remote Sensing 25 (4), 731–750.

Guisan, A., Edwards Jr, T. C., Hastie, T., 2002. Generalized linear and generalized additive models in studies of species distributions: setting the scene. Ecological modelling 157 (2-3), 89–100.

Guisan, A., Thuiller, W., Zimmermann, N. E., 2017. Habitat suitability and distribution models: with applications in R. Cambridge University Press.

Guisan, A., Tingley, R., Baumgartner, J. B., Naujokaitis-Lewis, I., Sutcliffe, P. R., Tulloch, A. I., Regan, T. J., Brotons, L., McDonald-Madden, E., Mantyka-Pringle, C., et al., 2013. Predicting species distributions for conservation decisions. Ecology letters 16 (12), 1424–1435.

Guisan, A., Zimmermann, N. E., 2000. Predictive habitat distribution models in ecology. Ecological modelling 135 (2-3), 147–186.

Gupta, R., Sharma, L. K., 2019. The process-based forest growth model 3-PG for use in forest management: A review. Ecological Modelling 397, 55–73.

Guyana Forestry Commission and others, 2011. Guyana REDD+ Monitoring Reporfing and Verificafion System (MRVS) Interim Measures Report.

Haapanen, R., Ek, A. R., Bauer, M. E., Finley, A. O., 2004. Delineation of forest/nonforest land use classes using nearest neighbor methods. Remote Sensing of Environment 89 (3), 265–271.

Hanebuth, T. J., Kudrass, H. R., Linstädter, J., Islam, B., Zander, A. M., 2013. Rapid coastal subsidence in the central Ganges-Brahmaputra Delta

(Bangladesh) since the 17th century deduced from submerged salt-producing kilns. Geology 41 (9), 987–990.

Hanif, I., 2019. Implementing extreme gradient boosting (xgboost) classifier to improve customer churn prediction. In: ICSA 2019: Proceedings of the 1st International Conference on Statistics and Analytics, ICSA 2019, 2-3 August 2019, Bogor, Indonesia. p. 434.

Hannan, A., Anmala, J., 2021. Classification and Prediction of Fecal Coliform in Stream Waters Using Decision Trees (DTs) for Upper Green River Watershed, Kentucky, USA. Water 13 (19), 2790.

Hansen, M. C., Potapov, P. V., Goetz, S. J., Turubanova, S., Tyukavina, A., Krylov, A., Kommareddy, A., Egorov, A., 2016. Mapping tree height distributions in Sub-Saharan Africa using Landsat 7 and 8 data. Remote Sensing of Environment 185, 221–232.

Hansen, M. C., Potapov, P. V., Moore, R., Hancher, M., Turubanova, S. A., Tyukavina, A., Thau, D., Stehman, S., Goetz, S. J., Loveland, T. R., et al., 2013. High-resolution global maps of 21st-century forest cover change. science 342 (6160), 850–853.

Hansen, M. C., Roy, D. P., Lindquist, E., Adusei, B., Justice, C. O., Altstatt, A., 2008. A method for integrating MODIS and Landsat data for systematic monitoring of forest cover and change in the Congo Basin. Remote Sensing of Environment 112 (5), 2495–2513.

Hansen, M. C., Stehman, S. V., Potapov, P. V., 2010. Quantification of global gross forest cover loss. Proceedings of the National Academy of Sciences 107 (19), 8650–8655.

Hardy, A., Oakes, G., Ettritch, G., 2020. Tropical Wetland (TropWet) Mapping Tool: The Automatic Detection of Open and Vegetated Waterbodies in Google Earth Engine for Tropical Wetlands. Remote Sensing 12 (7), 1182.

Hardy, A. J., Gamarra, J. G., Cross, D. E., Macklin, M. G., Smith, M. W., Kihonda, J., Killeen, G. F., Ling'ala, G. N., Thomas, C. J., 2013. Habitat

hydrology and geomorphology control the distribution of malaria vector larvae in rural Africa. PLoS One 8 (12).

Harfoot, M. B., Johnston, A., Balmford, A., Burgess, N. D., Butchart, S. H., Dias, M. P., Hazin, C., Hilton-Taylor, C., Hoffmann, M., Isaac, N. J., et al., 2021. Using the IUCN Red List to map threats to terrestrial vertebrates at global scale. Nature ecology & evolution 5 (11), 1510–1519.

Harris, N., Brown, S., Hagen, S. C., Baccini, A., Houghton, R., 2012. Progress toward a consensus on carbon emissions from tropical deforestation. Policy Brief.

HDX, 2020. HOTOSM Tanzania Populated Places (OpenStreetMap Export). Accessed on 23.03.2020.
URL https://data.humdata.org/dataset/hotosm_tza_populated_places

Helmer, E. H., Brown, S., Cohen, W., 2000. Mapping montane tropical forest successional stage and land use with multi-date Landsat imagery. International Journal of Remote Sensing 21 (11), 2163–2183.

Hengl, T., Heuvelink, G. B., Kempen, B., Leenaars, J. G., Walsh, M. G., Shepherd, K. D., Sila, A., MacMillan, R. A., de Jesus, J. M., Tamene, L., et al., 2015. Mapping soil properties of Africa at 250 m resolution: Random forests significantly improve current predictions. PloS one 10 (6).

Herrera, D., Pfaff, A., Robalino, J., 2019. Impacts of protected areas vary with the level of government: Comparing avoided deforestation across agencies in the Brazilian Amazon. Proceedings of the National Academy of Sciences 116 (30), 14916–14925.

Herwindiati, D. E., Isa, S. M., et al., 2014. Robust discriminant analysis for classification of remote sensing data. In: 2014 International Conference on Advanced Computer Science and Information System. pp. 454–458.

Hijmans, R. J., Cameron, S. E., Parra, J. L., Jones, P. G., Jarvis, A., 2005. Very high resolution interpolated climate surfaces for global land areas. International Journal of Climatology: A Journal of the Royal Meteorological Society 25 (15), 1965–1978.

Hirschmugl, M., Deutscher, J., Sobe, C., Bouvet, A., Mermoz, S., Schardt, M.,

2020. Use of SAR and optical time series for tropical forest disturbance mapping. Remote Sensing 12 (4), 727.

Hofer, H., Hildebrandt, T. B., Goritz, F., East, M. L., Mpanduji, D. G., Hahn, R., Siege, L., Baldus, R. D., 2004. Distribution and movements of elephants and other wildlife in the Selous-Niassa wildlife corridor, Tanzania. Deutsche Gesellschaft für Technische Zusammenarbeit.

Hoffman, M., Koenig, K., Bunting, G., Costanza, J., Williams, K. J., 2016. Biodiversity Hotspots (version 2016.1), publisher = Zenodo, url = https://doi.org/10.5281/zenodo.3261807. Accessed on 10.02.2020.

Horning, N., Robinson, J. A., Sterling, E. J., Spector, S., Turner, W., 2010. Remote sensing for ecology and conservation: a handbook of techniques. Oxford University Press.

Hościło, A., Lewandowska, A., 2019. Mapping forest type and tree species on a regional scale using multi-temporal Sentinel-2 data. Remote Sensing 11 (8), 929.

Hosonuma, N., Herold, M., De Sy, V., De Fries, R. S., Brockhaus, M., Verchot, L., Angelsen, A., Romijn, E., 2012. An assessment of deforestation and forest degradation drivers in developing countries. Environmental Research Letters 7 (4), 044009.

Houghton, R., 2012. Carbon emissions and the drivers of deforestation and forest degradation in the tropics. Current Opinion in Environmental Sustainability 4 (6), 597–603.

Houghton, R., Byers, B., Nassikas, A. A., 2015. A role for tropical forests in stabilizing atmospheric CO2. Nature Climate Change 5 (12), 1022–1023.

Houghton, R. A., 2003a. Revised estimates of the annual net flux of carbon to the atmosphere from changes in land use and land management 1850–2000. Tellus B 55 (2), 378–390.

Houghton, R. A., 2003b. Why are estimates of the terrestrial carbon balance so different? Global change biology 9 (4), 500–509.

Huang, C., Davis, L., Townshend, J., 2002. An assessment of support vector

machines for land cover classification. International Journal of remote sensing 23 (4), 725–749.

Huang, C., Goward, S. N., Masek, J. G., Gao, F., Vermote, E. F., Thomas, N., Schleeweis, K., Kennedy, R. E., Zhu, Z., Eidenshink, J. C., et al., 2009. Development of time series stacks of Landsat images for reconstructing forest disturbance history. International Journal of Digital Earth 2 (3), 195–218.

Huang, C., Goward, S. N., Masek, J. G., Thomas, N., Zhu, Z., Vogelmann, J. E., 2010. An automated approach for reconstructing recent forest disturbance history using dense Landsat time series stacks. Remote Sensing of Environment 114 (1), 183–198.

Huang, H., Gong, P., Clinton, N., Hui, F., 2008. Reduction of atmospheric and topographic effect on Landsat TM data for forest classification. International Journal of Remote Sensing 29 (19), 5623–5642.

Hubert-Moy, L., Cotonnec, A., Le Du, L., Chardin, A., Pérez, P., 2001. A comparison of parametric classification procedures of remotely sensed data applied on different landscape units. Remote Sensing of Environment 75 (2), 174–187.

Hudak, A. T., Evans, J. S., Stuart Smith, A. M., 2009. LiDAR utility for natural resource managers. Remote Sensing 1 (4), 934–951.

Hudak, A. T., Lefsky, M. A., Cohen, W. B., Berterretche, M., 2002. Integration of lidar and Landsat ETM+ data for estimating and mapping forest canopy height. Remote sensing of Environment 82 (2-3), 397–416.

Huntingford, C., Zelazowski, P., Galbraith, D., Mercado, L. M., Sitch, S., Fisher, R., Lomas, M., Walker, A. P., Jones, C. D., Booth, B. B., et al., 2013. Simulated resilience of tropical rainforests to CO2-induced climate change. Nature Geoscience 6 (4), 268–273.

Huntley, B., 1982. Southern african savannas. In: Ecology of tropical savannas. Springer, pp. 101–119.

Hurtt, G. C., Chini, L. P., Frolking, S., Betts, R., Feddema, J., Fischer, G., Fisk, J., Hibbard, K., Houghton, R., Janetos, A., et al., 2011. Harmonization of land-use scenarios for the period 1500–2100: 600 years of global gridded annual land-

use transitions, wood harvest, and resulting secondary lands. Climatic change 109 (1-2), 117.

Hussain, M., Chen, D., Cheng, A., Wei, H., Stanley, D., 2013. Change detection from remotely sensed images: From pixel-based to object-based approaches. ISPRS Journal of photogrammetry and remote sensing 80, 91–106.

Ihlen, V., 2019. Landsat 8 (L8) data users handbook. Landsat Science Official Website.

Immitzer, M., Vuolo, F., Atzberger, C., 2016. First experience with Sentinel-2 data for crop and tree species classifications in central Europe. Remote sensing 8 (3), 166.

Ingram, J. C., Dawson, T. P., Whittaker, R. J., 2005. Mapping tropical forest structure in southeastern Madagascar using remote sensing and artificial neural networks. Remote Sensing of Environment 94 (4), 491–507.

International Renewable Energy Agency, 2017. Renewables Readiness Assessment of the United Republic of Tanzania . Tech. rep., Ministry of Energy and Minerals-Dar Es Salaam, Tanzania.

IPCC, 2014. Climate change 2014: impacts, adaptation, and vulnerability. Part A: global and sectoral aspects. Contribution of Working Group II to the Fifth Assessment Report of the Intergovernmental Panel on Climate Change.

Irons, J. R., Dwyer, J. L., Barsi, J. A., 2012. The next Landsat satellite: The Landsat data continuity mission. Remote Sensing of Environment 122, 11–21.

Jain, S., Sannigrahi, S., Sen, S., Bhatt, S., Chakraborti, S., Rahmat, S., 2020. Urban heat island intensity and its mitigation strategies in the fast-growing urban area. Journal of Urban Management 9 (1), 54–66.

Jensen, J. R., et al., 2005. Introductory digital image processing: a remote sensing perspective. No. 3678 J4/2005). Prentice-Hall Inc.

Jiang, F., Smith, A. R., Kutia, M., Wang, G., Liu, H., Sun, H., 2020. A modified KNN method for mapping the Leaf Area Index in arid and semi-arid areas of China. Remote Sensing 12 (11), 1884.

Jiménez-Alfaro, B., Suárez-Seoane, S., Chytrỳ, M., Hennekens, S. M., Willner, W., Hájek, M., Agrillo, E., Álvarez-Martínez, J. M., Bergamini, A., Brisse, H., et al., 2018. Modelling the distribution and compositional variation of plant communities at the continental scale. Diversity and Distributions 24 (7), 978–990.

Jin, C., Xiao, X., Merbold, L., Arneth, A., Veenendaal, E., Kutsch, W. L., 2013. Phenology and gross primary production of two dominant savanna woodland ecosystems in Southern Africa. Remote Sensing of Environment 135, 189–201.

Jin, S., Sader, S. A., 2005. Comparison of time series tasseled cap wetness and the normalized difference moisture index in detecting forest disturbances. Remote sensing of Environment 94 (3), 364–372.

John, E., Bunting, P., Hardy, A., Roberts, O., Giliba, R., Silayo, D. S., 2020. Modelling the impact of climate change on Tanzanian forests. Diversity and Distributions 26 (12), 1663–1686.

Johnson, R. D., Kasischke, E., 1998. Change vector analysis: A technique for the multispectral monitoring of land cover and condition. International Journal of Remote Sensing 19 (3), 411–426.

Jones, T., Bamford, A. J., Ferrol-Schulte, D., Hieronimo, P., McWilliam, N., Rovero, F., 2012. Vanishing wildlife corridors and options for restoration: a case study from Tanzania. Tropical Conservation Science 5 (4), 463–474.

Joshi, N., Baumann, M., Ehammer, A., Fensholt, R., Grogan, K., Hostert, P., Jepsen, M. R., Kuemmerle, T., Meyfroidt, P., Mitchard, E. T., et al., 2016. A review of the application of optical and radar remote sensing data fusion to land use mapping and monitoring. Remote Sensing 8 (1), 70.

Jozdani, S. E., Johnson, B. A., Chen, D., 2019. Comparing deep neural networks, ensemble classifiers, and support vector machine algorithms for object-based urban land use/land cover classification. Remote Sensing 11 (14), 1713.

Ju, J., Roy, D. P., 2008. The availability of cloud-free Landsat ETM+ data over the conterminous United States and globally. Remote Sensing of Environment 112 (3), 1196–1211.

Kääb, A., Altena, B., Mascaro, J., 2019. River-ice and water velocities using the Planet optical cubesat constellation. Hydrology and Earth System Sciences 23 (10), 4233–4247.

Kalluri, S., JáJá, J., Bader, D. A., Zhang, Z., Townshend, J., Fallah-Adl, H., 2000. High performance computing algorithms for land cover dynamics using remote sensing data. International Journal of Remote Sensing 21 (6-7), 1513–1536.

Kamavisdar, P., Saluja, S., Agrawal, S., 2013. A survey on image classification approaches and techniques. International Journal of Advanced Research in Computer and Communication Engineering 2 (1), 1005–1009.

Kamyo, T., Asanok, L., 2020. Modeling habitat suitability of Dipterocarpus alatus (Dipterocarpaceae) using maxent along the chao phraya river in central Thailand. Forest Science and Technology 16 (1), 1–7.

Karlson, M., Ostwald, M., Reese, H., Sanou, J., Tankoano, B., Mattsson, E., 2015. Mapping tree canopy cover and aboveground biomass in Sudano-Sahelian woodlands using Landsat 8 and random forest. Remote Sensing 7 (8), 10017–10041.

Kashaigili, J. J., Mdemu, M. V., Nduganda, A. R., Mbilinyi, B. P., 2013. Integrated assessment of forest cover change and above-ground carbon stock in Pugu and Kazimzubwi forest reserves, Tanzania. Advances in Remote Sensing.

Kaszta, Ż., Van De Kerchove, R., Ramoelo, A., Cho, M. A., Madonsela, S., Mathieu, R., Wolff, E., 2016. Seasonal separation of African savanna components using worldview-2 imagery: a comparison of pixel-and object-based approaches and selected classification algorithms. Remote Sensing 8 (9), 763.

Ke, G., Meng, Q., Finley, T., Wang, T., Chen, W., Ma, W., Ye, Q., Liu, T.-Y., 2017. Lightgbm: A highly efficient gradient boosting decision tree. In: Advances in neural information processing systems. pp. 3146–3154.

Keenan, R. J., Reams, G. A., Achard, F., de Freitas, J. V., Grainger, A., Lindquist, E., 2015. Dynamics of global forest area: Results from the FAO Global Forest Resources Assessment 2015. Forest Ecology and Management 352, 9–20.

Kennedy, R. E., Townsend, P. A., Gross, J. E., Cohen, W. B., Bolstad, P., Wang,

Y., Adams, P., 2009. Remote sensing change detection tools for natural resource managers: Understanding concepts and tradeoffs in the design of landscape monitoring projects. Remote sensing of environment 113 (7), 1382–1396.

Kent, R., Lindsell, J. A., Laurin, G. V., Valentini, R., Coomes, D. A., 2015. Airborne LiDAR detects selectively logged tropical forest even in an advanced stage of recovery. Remote Sensing 7 (7), 8348–8367.

Keramitsoglou, I., Sarimveis, H., Kiranoudis, C. T., Kontoes, C., Sifakis, N., Fitoka, E., 2006. The performance of pixel window algorithms in the classification of habitats using VHSR imagery. ISPRS Journal of Photogrammetry and Remote Sensing 60 (4), 225–238.

Kganyago, M., Mhangara, P., 2019. The Role of African Emerging Space Agencies in Earth Observation Capacity Building for Facilitating the Implementation and Monitoring of the African Development Agenda: The Case of African Earth Observation Program. ISPRS International Journal of Geo-Information 8 (7), 292.

Kim, D.-H., Sexton, J. O., Townshend, J. R., 2015. Accelerated deforestation in the humid tropics from the 1990s to the 2000s. Geophysical Research Letters 42 (9), 3495–3501.

Kimambo, N. E., Naughton-Treves, L., 2019. The Role of woodlots in forest regeneration outside protected areas: Lessons from Tanzania. Forests 10 (8), 621.

Kimball, K. D., Weihrauch, D. M., et al., 2000. Alpine vegetation communities and the alpine-treeline ecotone boundary in New England as biomonitors for climate change. In: USDA Forest Service Proceedings. Vol. 3. pp. 93–101.

Kimes, D., Nelson, R., Salas, W., Skole, D., 1999. Mapping secondary tropical forest and forest age from SPOT HRV data. International Journal of Remote Sensing 20 (18), 3625–3640.

Knorn, J., Rabe, A., Radeloff, V. C., Kuemmerle, T., Kozak, J., Hostert, P., 2009. Land cover mapping of large areas using chain classification of neighboring Landsat satellite images. Remote Sensing of Environment 113 (5), 957–964.

Koskikala, J., Kukkonen, M., Käyhkö, N., 2020. Mapping natural forest remnants

with multi-source and multi-temporal remote sensing data for more informed management of global biodiversity hotspots. Remote Sensing 12 (9), 1429.

Koukal, T., Suppan, F., Schneider, W., 2007. The impact of relative radiometric calibration on the accuracy of kNN-predictions of forest attributes. Remote Sensing of Environment 110 (4), 431–437.

Krasovskii, A., Maus, V., Yowargana, P., Pietsch, S., Rautiainen, M., et al., 2018. Monitoring deforestation in rainforests using satellite data: A pilot study from Kalimantan, Indonesia. Forests 9 (7), 389.

Kuching, S., 2007. The performance of maximum likelihood, spectral angle mapper, neural network and decision tree classifiers in hyperspectral image analysis. Journal of Computer Science 3 (6), 419–423.

Kumar, L., Sinha, P., Taylor, S., Alqurashi, A. F., 2015. Review of the use of remote sensing for biomass estimation to support renewable energy generation. Journal of Applied Remote Sensing 9 (1), 097696.

Lambin, E. F., Geist, H. J., Lepers, E., 2003. Dynamics of land-use and land-cover change in tropical regions. Annual review of environment and resources 28 (1), 205 – 241.

Landsberg, J., Waring, R., 1997. A generalised model of forest productivity using simplified concepts of radiation-use efficiency, carbon balance and partitioning. Forest ecology and management 95 (3), 209–228.

Lardeux, C., Frison, P.-L., Tison, C., Souyris, J.-C., Stoll, B., Fruneau, B., Rudant, J.-P., 2009. Support vector machine for multifrequency SAR polarimetric data classification. IEEE Transactions on Geoscience and Remote Sensing 47 (12), 4143–4152.

Laurin, G. V., Liesenberg, V., Chen, Q., Guerriero, L., Del Frate, F., Bartolini, A., Coomes, D., Wilebore, B., Lindsell, J., Valentini, R., 2013. Optical and SAR sensor synergies for forest and land cover mapping in a tropical site in West Africa. International Journal of Applied Earth Observation and Geoinformation 21, 7–16.

Laurin, G. V., Puletti, N., Hawthorne, W., Liesenberg, V., Corona, P., Papale,

D., Chen, Q., Valentini, R., 2016. Discrimination of tropical forest types, dominant species, and mapping of functional guilds by hyperspectral and simulated multispectral Sentinel-2 data. Remote Sensing of Environment 176, 163–176.

Lawrence, D., Vandecar, K., 2015. Effects of tropical deforestation on climate and agriculture. Nature climate change 5 (1), 27–36.

Le Quéré, C., Raupach, M. R., Canadell, J. G., Marland, G., Bopp, L., Ciais, P., Conway, T. J., Doney, S. C., Feely, R. A., Foster, P., et al., 2009. Trends in the sources and sinks of carbon dioxide. Nature geoscience 2 (12), 831–836.

Leberger, R., Rosa, I. M., Guerra, C. A., Wolf, F., Pereira, H. M., 2020. Global patterns of forest loss across IUCN categories of protected areas. Biological Conservation 241, 108299.

Lee, T. M., Jetz, W., 2008. Future battlegrounds for conservation under global change. Proceedings of the Royal Society B: Biological Sciences 275 (1640), 1261–1270.

Lefsky, M. A., Cohen, W. B., Hudak, A., Acker, S. A., Ohmann, J., 1999. Integration of lidar, Landsat ETM+ and forest inventory data for regional forest mapping. International Archives of Photogrammetry and Remote Sensing 32 (Part 3W14), 119–126.

Lek, S., Guégan, J.-F., 1999. Artificial neural networks as a tool in ecological modelling, an introduction. Ecological modelling 120 (2-3), 65–73.

Lemajic, S., Vajsová, B., Aastrand, P., 2018. New sensors benchmark report on PlanetScope: Geometric benchmarking test for Common Agricultural Policy (CAP) purposes. Tech. Rep. 29319, European Union, Luxembourg.

Lewis, S. L., 2006. Tropical forests and the changing earth system. Philosophical Transactions of the Royal Society B: Biological Sciences 361 (1465), 195–210.

Li, C., Wang, J., Hu, L., Yu, L., Clinton, N., Huang, H., Yang, J., Gong, P., 2014. A circa 2010 thirty meter resolution forest map for China. Remote Sensing 6 (6), 5325–5343.

Li, R., Fang, P., Xu, W., Wang, L., Ou, G., Zhang, W., Huang, X., 2022. Classi-

fying Forest Types over a Mountainous Area in Southwest China with Landsat Data Composites and Multiple Environmental Factors. Forests 13 (1), 135.

Li, Y., Li, C., Li, M., Liu, Z., 2019. Influence of variable selection and forest type on forest aboveground biomass estimation using machine learning algorithms. Forests 10 (12), 1073.

Li, Y., Li, M., Li, C., Liu, Z., 2020. Forest aboveground biomass estimation using Landsat 8 and Sentinel-1A data with machine learning algorithms. Scientific reports 10 (1), 1–12.

Ligate, E. J., Wu, C., Chen, C., 2019. Investigation of tropical coastal forest regeneration after farming and livestock grazing exclusion. Journal of Forestry Research 30 (5), 1873–1884.

Lillesand, T., Kiefer, R., Chipman, J., 2004. Remote sensing and image interpretation. Remote sensing and image interpretation (6).

Lillesand, T., Kiefer, R. W., Chipman, J., 2015. Remote sensing and image interpretation. John Wiley & Sons.

Lim, C.-H., Yoo, S., Choi, Y., Jeon, S. W., Son, Y., Lee, W.-K., 2018. Assessing climate change impact on forest habitat suitability and diversity in the Korean Peninsula. Forests 9 (5), 259.

Lim, K., Treitz, P., Wulder, M., St-Onge, B., Flood, M., 2003. LiDAR remote sensing of forest structure. Progress in physical geography 27 (1), 88–106.

Lima, T. A., Beuchle, R., Langner, A., Grecchi, R. C., Griess, V. C., Achard, F., 2019. Comparing Sentinel-2 MSI and Landsat 8 OLI imagery for monitoring selective logging in the Brazilian Amazon. Remote Sensing 11 (8), 961.

Lister, A. J., Andersen, H., Frescino, T., Gatziolis, D., Healey, S., Heath, L. S., Liknes, G. C., McRoberts, R., Moisen, G. G., Nelson, M., et al., 2020. Use of remote sensing data to improve the efficiency of national forest inventories: a case study from the United States national forest inventory. Forests 11 (12), 1364.

Longépé, N., Rakwatin, P., Isoguchi, O., Shimada, M., Uryu, Y., Yulianto, K., 2011. Assessment of ALOS PALSAR 50 m orthorectified FBD data for regional

land cover classification by support vector machines. IEEE Transactions on Geoscience and Remote Sensing 49 (6), 2135–2150.

Lopes, A., Touzi, R., Nezry, E., 1990. Adaptive speckle filters and scene heterogeneity. IEEE transactions on Geoscience and Remote Sensing 28 (6), 992–1000.

Lu, D., Chen, Q., Wang, G., Moran, E., Batistella, M., Zhang, M., Vaglio Laurin, G., Saah, D., 2012. Aboveground forest biomass estimation with Landsat and LiDAR data and uncertainty analysis of the estimates. International Journal of Forestry Research 2012.

Lu, D., Li, G., Moran, E., Kuang, W., 2014. A comparative analysis of approaches for successional vegetation classification in the Brazilian Amazon. GIScience & remote sensing 51 (6), 695–709.

Lu, D., Mausel, P., Brondizio, E., Moran, E., 2004. Change detection techniques. International journal of remote sensing 25 (12), 2365–2401.

Lu, D., Moran, E., Batistella, M., 2003. Linear mixture model applied to Amazonian vegetation classification. Remote sensing of environment 87 (4), 456–469.

Lu, D., Weng, Q., 2007. A survey of image classification methods and techniques for improving classification performance. International journal of Remote sensing 28 (5), 823–870.

Lucas, R., Bunting, P., Paterson, M., Chisholm, L., 2008. Classification of Australian forest communities using aerial photography, CASI and HyMap data. Remote Sensing of Environment 112 (5), 2088–2103.

Lunetta, R. S., Johnson, D. M., Lyon, J. G., Crotwell, J., 2004. Impacts of imagery temporal frequency on land-cover change detection monitoring. Remote Sensing of Environment 89 (4), 444–454.

Lunetta, R. S., Knight, J. F., Ediriwickrema, J., Lyon, J. G., Worthy, L. D., 2006. Land-cover change detection using multi-temporal MODIS NDVI data. Remote sensing of environment 105 (2), 142–154.

Lynch, J., Maslin, M., Balzter, H., Sweeting, M., 2013. Sustainability: Choose satellites to monitor deforestation. Nature 496 (7445), 293.

Mackey, B., Kormos, C. F., Keith, H., Moomaw, W. R., Houghton, R. A., Mittermeier, R. A., Hole, D., Hugh, S., 2020. Understanding the importance of primary tropical forest protection as a mitigation strategy. Mitigation and Adaptation Strategies for Global Change 25 (5), 763–787.

Macleod, R. D., Congalton, R. G., 1998. A quantitative comparison of change-detection algorithms for monitoring eelgrass from remotely sensed data. Photogrammetric engineering and remote sensing 64 (3), 207–216.

Maghsoudi, Y., Collins, M. J., Leckie, D., 2012. Speckle reduction for the forest mapping analysis of multi-temporal Radarsat-1 images. International journal of remote sensing 33 (5), 1349–1359.

Maharaj, S. S., New, M., 2013. Modelling individual and collective species responses to climate change within Small Island States. Biological conservation 167, 283–291.

Mai, L., Park, M., 2016. A comparison of clustering algorithms for botnet detection based on network flow. In: Ubiquitous and Future Networks (ICUFN), 2016 Eighth International Conference on. pp. 667–669.

Makundi, W., Okiting'ati, A., 1995. Carbon flows and economic evaluation of mitigation options in Tanzania's forest sector. Biomass and Bioenergy 8 (5), 381–393.

Malhi, Y., Adu-Bredu, S., Asare, R. A., Lewis, S. L., Mayaux, P., 2013. African rainforests: past, present and future. Philosophical Transactions of the Royal Society B: Biological Sciences 368 (1625), 20120312.

Malhi, Y., Gardner, T. A., Goldsmith, G. R., Silman, M. R., Zelazowski, P., 2014. Tropical forests in the anthropocene. Annual Review of Environment and Resources 39.

Malhi, Y., Roberts, J. T., Betts, R. A., Killeen, T. J., Li, W., Nobre, C. A., 2008. Climate change, deforestation, and the fate of the Amazon. science 319 (5860), 169–172.

Malimbwi, R., Eid, T., Chamshama, S., 2016. Allometric tree biomass and volume models in Tanzania.

Malmer, A., 2007. General ecological features of miombo woodlands and considerations for utilization and management. In: MITMIOMBO–Management of Indigenous Tree Species for Ecosystem Restoration and Wood Production in Semi-Arid Miombo Woodlands in Eastern Africa. Proceedings of the First MITMIOMBO Project Workshop held in Morogoro, Tanzania. Citeseer, pp. 6–12.

Manaf, S., Mustapha, N., Sulaiman, M., Husin, N., Shafri, H., Razali, M., 2018. Hybridization of SLIC and Extra Tree for Object Based Image Analysis in Extracting Shoreline from Medium Resolution Satellite Images. Int. J. Intell. Eng. Syst 11, 62–72.

Marchant, R., 2010. Understanding complexity in savannas: climate, biodiversity and people. Current Opinion in Environmental Sustainability 2 (1-2), 101–108.

Marée, R., Geurts, P., Wehenkel, L., 2007. Random subwindows and extremely randomized trees for image classification in cell biology. BMC Cell Biology 8 (1), 1–12.

Marée, R., Wehenkel, L., Geurts, P., 2013. Extremely randomized trees and random subwindows for image classification, annotation, and retrieval. In: Decision Forests for Computer Vision and Medical Image Analysis. pp. 125–141.

Markham, A., 1998. Potential Impacts of Climate Change on Tropical Forest Ecosystems. Climatic Change 39 (2-3), 141–143.

Marselis, S. M., Tang, H., Armston, J. D., Calders, K., Labrière, N., Dubayah, R., 2018. Distinguishing vegetation types with airborne waveform lidar data in a tropical forest-savanna mosaic: A case study in Lopé National Park, Gabon. Remote Sensing of Environment 216, 626–634.

Mas, J.-F., 1999. Monitoring land-cover changes: a comparison of change detection techniques. International journal of remote sensing 20 (1), 139–152.

Mas, J. F., Flores, J. J., 2008. The application of artificial neural networks to the analysis of remotely sensed data. International Journal of Remote Sensing 29 (3), 617–663.

Matton, N., Canto, G. S., Waldner, F., Valero, S., Morin, D., Inglada, J., Arias, M., Bontemps, S., Koetz, B., Defourny, P., 2015. An automated method for annual

cropland mapping along the season for various globally-distributed agrosystems using high spatial and temporal resolution time series. Remote Sensing 7 (10), 13208–13232.

Mayaux, P., Bartholomé, E., Fritz, S., Belward, A., 2004. A new land-cover map of Africa for the year 2000. Journal of Biogeography 31 (6), 861–877.

Mayaux, P., Holmgren, P., Achard, F., Eva, H., Stibig, H.-J., Branthomme, A., 2005. Tropical forest cover change in the 1990s and options for future monitoring. Philosophical Transactions of the Royal Society B: Biological Sciences 360 (1454), 373 – 384.

Mayes, M. T., Mustard, J. F., Melillo, J. M., 2015. Forest cover change in Miombo Woodlands: modeling land cover of African dry tropical forests with linear spectral mixture analysis. Remote sensing of environment 165, 203–215.

McCarty, D. A., Kim, H. W., Lee, H. K., 2020. Evaluation of light gradient boosted machine learning technique in large scale land use and land cover classification. Environments 7 (10), 84.

McLeod, E., Salm, R. V., et al., 2006. Managing mangroves for resilience to climate change. Vol. 64.

McRoberts, R. E., Tomppo, E. O., 2007. Remote sensing support for national forest inventories. Remote sensing of environment 110 (4), 412–419.

Means, J. E., Acker, S. A., Harding, D. J., Blair, J. B., Lefsky, M. A., Cohen, W. B., Harmon, M. E., McKee, W. A., 1999. Use of large-footprint scanning airborne lidar to estimate forest stand characteristics in the Western Cascades of Oregon. Remote sensing of environment 67 (3), 298–308.

Medley, K. E., . H. F. M. R., 1996. Riverine forests. In T. R. McClanahan and T. P. Young (Eds.). East African ecosystems and their conservation. Oxford University Press, New York, USA.

Mellor, A., Haywood, A., Stone, C., Jones, S., 2013. The performance of random forests in an operational setting for large area sclerophyll forest classification. Remote Sensing 5 (6), 2838–2856.

Merow, C., Smith, M. J., Silander Jr, J. A., 2013. A practical guide to MaxEnt

for modeling species' distributions: what it does, and why inputs and settings matter. Ecography 36 (10), 1058–1069.

Meyer, W. B., Turner, B. L., 1992. Human population growth and global land-use/cover change. Annual review of ecology and systematics 23 (1), 39–61.

Mills, A. J., Vyver, M. V. d., Gordon, I. J., Patwardhan, A., Marais, C., Blignaut, J., Sigwela, A., Kgope, B., 2015. Prescribing innovation within a large-scale restoration programme in degraded subtropical thicket in South Africa. Forests 6 (11), 4328–4348.

Minu, S., Shetty, A., 2015. A comparative study of image change detection algorithms in MATLAB. Aquatic procedia 4, 1366–1373.

Minunno, F., Peltoniemi, M., Härkönen, S., Kalliokoski, T., Makinen, H., Mäkelä, A., 2019. Bayesian calibration of a carbon balance model PREBAS using data from permanent growth experiments and national forest inventory. Forest ecology and management 440, 208–257.

Mitchard, E., Saatchi, S., White, L., Abernethy, K., Jeffery, K., Lewis, S., Collins, M., Lefsky, M., Leal, M., Woodhouse, I., et al., 2011. Mapping tropical forest biomass with radar and spaceborne LiDAR: overcoming problems of high biomass and persistent cloud. Biogeosciences Discussions 8 (4).

Mitchard, E. T., 2018. The tropical forest carbon cycle and climate change. Nature 559 (7715), 527–534.

Mitchard, E. T., Flintrop, C. M., 2013. Woody encroachment and forest degradation in sub-Saharan Africa's woodlands and savannas 1982–2006. Philosophical Transactions of the Royal Society B: Biological Sciences 368 (1625), 20120406.

Mitchell, A. L., Rosenqvist, A., Mora, B., 2017. Current remote sensing approaches to monitoring forest degradation in support of countries measurement, reporting and verification (MRV) systems for REDD+. Carbon Balance and Management 12 (1), 9.

Mitchell, R., Frank, E., 2017. Accelerating the XGBoost algorithm using GPU computing. PeerJ Computer Science 3, e127.

Miyoshi, G. T., Arruda, M. d. S., Osco, L. P., Marcato Junior, J., Gonçalves,

D. N., Imai, N. N., Tommaselli, A. M. G., Honkavaara, E., Gonçalves, W. N., 2020. A novel deep learning method to identify single tree species in UAV-based hyperspectral images. Remote Sensing 12 (8), 1294.

Mlingano Agricultural Research Institute, 2006. Soils of Tanzania and their potential for agriculture development.

MNRT, 2015. National Forest Resources Monitoring and Assessment (NAFORMA) main results, Dar Es Salaam, Tanzania. Tech. rep., Tanzania Forest Services (TFS) Agency.

Moncrieff, G., Scheiter, S., Slingsby, J., Higgins, S., 2015. Understanding global change impacts on South African biomes using Dynamic Vegetation Models. South African Journal of Botany 101, 16–23.

Montagnini, F., Jordan, C. F., et al., 2005. Tropical forest ecology: the basis for conservation and management. Springer Science & Business Media.

Moore, P. D., 2008. Tropical forests. Infobase Publishing.

Moss, R. H., Edmonds, J. A., Hibbard, K. A., Manning, M. R., Rose, S. K., Van Vuuren, D. P., Carter, T. R., Emori, S., Kainuma, M., Kram, T., et al., 2010. The next generation of scenarios for climate change research and assessment. Nature 463 (7282), 747–756.

Mountrakis, G., Im, J., Ogole, C., 2011. Support vector machines in remote sensing: A review. ISPRS Journal of Photogrammetry and Remote Sensing 66 (3), 247–259.

Mugasha, A., 1996. Silviculture in the tropical natural forests with special reference to tanzania, a compendium. Faculty of Forestry, 98–115.

Mugasha, A., Chamshama, S., Gerald, V., 2004. Indicators and tools for restoration and sustainable management of forests in east Africa. State of Forests and Forestry Research in Tanzania paper 3, 66.

Müller, C., Waha, K., Bondeau, A., Heinke, J., 2014. Hotspots of climate change impacts in sub-Saharan Africa and implications for adaptation and development. Global change biology 20 (8), 2505–2517.

Mustalahti, I., Bolin, A., Boyd, E., Paavola, J., 2012. Can REDD+ reconcile local priorities and needs with global mitigation benefits? Lessons from Angai Forest, Tanzania. Ecology and Society 17 (1).

Mwalyosi, R. B., 1990. Resource potentials of the Rufiji River basin, Tanzania. Ambio, 16–20.

Mwampamba, T. H., Schwartz, M. W., 2011. The effects of cultivation history on forest recovery in fallows in the Eastern Arc Mountain, Tanzania. Forest Ecology and Management 261 (6), 1042–1052.

Myers, N., 1993. Tropical forests: the main deforestation fronts. Environmental conservation 20 (1), 9–16.

Myers, N., Mittermeier, R. A., Mittermeier, C. G., Da Fonseca, G. A., Kent, J., 2000. Biodiversity hotspots for conservation priorities. Nature 403 (6772), 853.

Myroniuk, V., Kutia, M., J Sarkissian, A., Bilous, A., Liu, S., 2020. Regional-Scale Forest Mapping over Fragmented Landscapes Using Global Forest Products and Landsat Time Series Classification. Remote Sensing 12 (1), 187.

Nackaerts, K., Vaesen, K., Muys, B., Coppin, P., 2005. Comparative performance of a modified change vector analysis in forest change detection. International Journal of Remote Sensing 26 (5), 839–852.

Næsset, E., Ørka, H. O., Solberg, S., Bollandsås, O. M., Hansen, E. H., Mauya, E., Zahabu, E., Malimbwi, R., Chamuya, N., Olsson, H., et al., 2016. Mapping and estimating forest area and aboveground biomass in miombo woodlands in Tanzania using data from airborne laser scanning, TanDEM-X, RapidEye, and global forest maps: A comparison of estimated precision. Remote Sensing of Environment 175, 282–300.

Nair, C., Tieguhong, J., 2004. African forests and forestry: An overview. A report prepared for the project. Lessons Learnt on Sustainable Forest Management in Africa. Royal Swedish Academy of Sciences, African Forest Research Network (AFORNET) and FAO.

National Bureau of Statistics, 2017. National Environmental Statistics Report, (NESR, 2017). National Bureau of Statistics (NBS).

Neeff, T., Piazza, M., 2020. How countries link forest monitoring into policy-making. Forest Policy and Economics 118, 102248.

Negassa, M. D., Mallie, D. T., Gemeda, D. O., 2020. Forest cover change detection using Geographic Information Systems and remote sensing techniques: a spatio-temporal study on Komto Protected forest priority area, East Wollega Zone, Ethiopia. Environmental Systems Research 9 (1), 1–14.

Nelson, P. R., Maguire, A. J., Pierrat, Z., Orcutt, E. L., Yang, D., Serbin, S., Frost, G. V., Macander, M. J., Magney, T. S., Thompson, D. R., et al., 2022. Remote sensing of tundra ecosystems using high spectral resolution reflectance: opportunities and challenges. Journal of Geophysical Research: Biogeosciences 127 (2), e2021JG006697.

Nepstad, D., Carvalho, G., Barros, A. C., Alencar, A., Capobianco, J. P., Bishop, J., Moutinho, P., Lefebvre, P., Silva Jr, U. L., Prins, E., 2001. Road paving, fire regime feedbacks, and the future of Amazon forests. Forest ecology and management 154 (3), 395–407.

Newmark, W. D., 2006. A 16-year study of forest disturbance and understory bird community structure and composition in Tanzania. Conservation Biology 20 (1), 122–134.

Nobre, C. A., Sampaio, G., Borma, L. S., Castilla-Rubio, J. C., Silva, J. S., Cardoso, M., 2016. Land-use and climate change risks in the Amazon and the need of a novel sustainable development paradigm. Proceedings of the National Academy of Sciences 113 (39), 10759–10768.

Nobre, C. A., Sellers, P. J., Shukla, J., 1991. Amazonian deforestation and regional climate change. Journal of climate 4 (10), 957–988.

Ntongani, W. A., Munishi, P. K., Mbilinyi, B. P., 2010. Land use changes and conservation threats in the eastern Selous–Niassa wildlife corridor, Nachingwea, Tanzania. African journal of ecology 48 (4), 880–887.

Ochieng, C. A., 2002. Research masterplan for the Rufiji floodplain and delta 2003–2013. Rufiji Environment Management Project Technical Report 28.

O'Connor, B., Secades, C., Penner, J., Sonnenschein, R., Skidmore, A., Burgess,

N. D., Hutton, J. M., 2015. Earth observation as a tool for tracking progress towards the Aichi Biodiversity Targets. Remote sensing in ecology and conservation 1 (1), 19–28.

Olander, L. P., Gibbs, H. K., Steininger, M., Swenson, J. J., Murray, B. C., 2008. Reference scenarios for deforestation and forest degradation in support of REDD: a review of data and methods. Environmental Research Letters 3 (2), 025011.

Olivier, P. I., van Aarde, R. J., Lombard, A. T., 2013. The use of habitat suitability models and species–area relationships to predict extinction debts in coastal forests, South Africa. Diversity and distributions 19 (11), 1353–1365.

Olofsson, P., Arévalo, P., Espejo, A. B., Green, C., Lindquist, E., McRoberts, R. E., Sanz, M. J., 2020. Mitigating the effects of omission errors on area and area change estimates. Remote Sensing of Environment 236, 111492.

Olofsson, P., Foody, G. M., Herold, M., Stehman, S. V., Woodcock, C. E., Wulder, M. A., 2014. Good practices for estimating area and assessing accuracy of land change. Remote Sensing of Environment 148, 42–57.

Olofsson, P., Foody, G. M., Stehman, S. V., Woodcock, C. E., 2013. Making better use of accuracy data in land change studies: Estimating accuracy and area and quantifying uncertainty using stratified estimation. Remote Sensing of Environment 129, 122–131.

Olson, J., Moore, N., Andresen, J., Alagarswamy, G., 2015. Analysis of the Impact of Climate Change on Crop and Water Availability, and Consideration of Potential Adaptation Practices for the Rufiji River Basin, Tanzania. Tech. rep.

Olthof, I., King, D. J., Lautenschlager, R., 2004. Mapping deciduous forest ice storm damage using Landsat and environmental data. Remote Sensing of Environment 89 (4), 484–496.

Omer, G., Mutanga, O., Abdel-Rahman, E. M., Adam, E., 2015. Performance of support vector machines and artificial neural network for mapping endangered tree species using WorldView-2 data in Dukuduku forest, South Africa. IEEE Journal of Selected Topics in Applied Earth Observations and Remote Sensing 8 (10), 4825–4840.

Osorio, J. A., Wingfield, M. J., Roux, J., 2016. A review of factors associated with decline and death of mangroves, with particular reference to fungal pathogens. South African Journal of Botany 103, 295–301.

Pacifici, M., Foden, W. B., Visconti, P., Watson, J. E., Butchart, S. H., Kovacs, K. M., Scheffers, B. R., Hole, D. G., Martin, T. G., Akçakaya, H. R., et al., 2015. Assessing species vulnerability to climate change. Nature climate change 5 (3), 215–224.

Pal, M., 2005. Random forest classifier for remote sensing classification. International Journal of Remote Sensing 26 (1), 217–222.

Palo, M., 1999. No end to deforestation? In: World forests, society and environment. Springer, pp. 65–77.

Pandit, M., Sodhi, N. S., Koh, L. P., Bhaskar, A., Brook, B. W., 2007. Unreported yet massive deforestation driving loss of endemic biodiversity in Indian Himalaya. Biodiversity and Conservation 16 (1), 153–163.

Paola, J. D., Schowengerdt, R. A., 1995. A detailed comparison of backpropagation neural network and maximum-likelihood classifiers for urban land use classification. IEEE Transactions on Geoscience and remote sensing 33 (4), 981–996.

Patenaude, G., Milne, R., Dawson, T. P., 2005. Synthesis of remote sensing approaches for forest carbon estimation: reporting to the Kyoto Protocol. Environmental Science & Policy 8 (2), 161–178.

Pedregosa, F., Varoquaux, G., Gramfort, A., Michel, V., Thirion, B., Grisel, O., Blondel, M., Prettenhofer, P., Weiss, R., Dubourg, V., et al., 2011. Scikit-learn: Machine learning in Python. Journal of machine learning research 12 (Oct), 2825–2830.

Pelletier, C., Valero, S., Inglada, J., Champion, N., Dedieu, G., 2016. Assessing the robustness of Random Forests to map land cover with high resolution satellite image time series over large areas. Remote Sensing of Environment 187, 156–168.

Pelletier, J., Goetz, S. J., 2015. Baseline data on forest loss and associated uncertainty: advances in national forest monitoring. Environmental Research Letters 10 (2), 021001.

Pettorelli, N., Laurance, W. F., O'Brien, T. G., Wegmann, M., Nagendra, H., Turner, W., 2014. Satellite remote sensing for applied ecologists: opportunities and challenges. Journal of Applied Ecology 51 (4), 839–848.

Pfeifer, M., Burgess, N. D., Swetnam, R. D., Platts, P. J., Willcock, S., Marchant, R., 2012. Protected areas: mixed success in conserving East Africa's evergreen forests. PloS one 7 (6), e39337.

Phillips, S. J., Anderson, R. P., Dudík, M., Schapire, R. E., Blair, M. E., 2017. Opening the black box: An open-source release of Maxent. Ecography 40 (7), 887–893.

Phillips, S. J., Anderson, R. P., Schapire, R. E., 2006. Maximum entropy modeling of species geographic distributions. Ecological modelling 190 (3-4), 231–259.

Phillips, S. J., Dudík, M., Schapire, R. E., 2004. A maximum entropy approach to species distribution modeling. In: Proceedings of the twenty-first international conference on Machine learning. p. 83.

Phillips, S. J., et al., 2005. A brief tutorial on Maxent. AT&T Research 190 (4), 231–259.

Pienaar, B., Thompson, D. I., Erasmus, B. F., Hill, T. R., Witkowski, E. T., 2015. Evidence for climate-induced range shift in Brachystegia (miombo) woodland. South African Journal of Science 111 (7-8), 1–9.

Pitkänen, T. P., Sirro, L., Häme, L., Häme, T., Törmä, M., Kangas, A., 2020. Errors related to the automatized satellite-based change detection of boreal forests in Finland. International Journal of Applied Earth Observation and Geoinformation 86, 102011.

Planet Team, 2017. Planet Application Program Interface. Accessed on 15.01.2020. URL `https://api.planet.com`

Platts, P. J., Omeny, P. A., Marchant, R., 2015. Africlim: high-resolution climate projections for ecological applications in a frica. African Journal of Ecology 53 (1), 103–108.

Pontius Jr, R. G., Millones, M., 2011. Death to kappa: birth of quantity dis-

agreement and allocation disagreement for accuracy assessment. International Journal of Remote Sensing 32 (15), 4407–4429.

Potapov, P. V., Turubanova, S. A., Hansen, M. C., Adusei, B., Broich, M., Altstatt, A., Mane, L., Justice, C. O., 2012. Quantifying forest cover loss in Democratic Republic of the Congo, 2000–2010, with Landsat ETM+ data. Remote Sensing of Environment 122, 106–116.

Pouteau, R., Stoll, B., 2012. SVM selective fusion (SELF) for multi-source classification of structurally complex tropical rainforest. IEEE Journal of Selected Topics in Applied Earth Observations and Remote Sensing 5 (4), 1203–1212.

Pratihast, A. K., DeVries, B., Avitabile, V., De Bruin, S., Kooistra, L., Tekle, M., Herold, M., 2014. Combining satellite data and community-based observations for forest monitoring. Forests 5 (10), 2464–2489.

Putzenlechner, B., Marzahn, P., Koal, P., Sánchez-Azofeifa, A., 2022. Fractional Vegetation Cover Derived from UAV and Sentinel-2 Imagery as a Proxy for In Situ FAPAR in a Dense Mixed-Coniferous Forest? Remote Sensing 14 (2), 380.

Qi, X., Zhang, C., Wang, K., 2019. Comparing remote sensing methods for monitoring karst rocky desertification at sub-pixel scales in a highly heterogeneous karst region. Scientific reports 9 (1), 1–12.

Qian, Y., Zhou, W., Yan, J., Li, W., Han, L., 2015. Comparing machine learning classifiers for object-based land cover classification using very high resolution imagery. Remote Sensing 7 (1), 153–168.

Quegan, S., Yu, J. J., 2001. Filtering of multichannel SAR images. IEEE Transactions on Geoscience and Remote Sensing 39 (11), 2373–2379.

Rahman, S., Irfan, M., Raza, M., Moyeezullah Ghori, K., Yaqoob, S., Awais, M., 2020. Performance analysis of boosting classifiers in recognizing activities of daily living. International Journal of Environmental Research and Public Health 17 (3), 1082.

Ray, R., Jana, T. K., 2017. Carbon sequestration by mangrove forest: one approach for managing carbon dioxide emission from coal-based power plant. Atmospheric Environment 171, 149–154.

Reiche, J., Lucas, R., Mitchell, A. L., Verbesselt, J., Hoekman, D. H., Haarpaintner, J., Kellndorfer, J. M., Rosenqvist, A., Lehmann, E. A., Woodcock, C. E., et al., 2016. Combining satellite data for better tropical forest monitoring. Nature Climate Change 6, 120–122.

Reiche, J., Mullissa, A., Slagter, B., Gou, Y., Tsendbazar, N.-E., Odongo-Braun, C., Vollrath, A., Weisse, M. J., Stolle, F., Pickens, A., et al., 2021. Forest disturbance alerts for the Congo Basin using Sentinel-1. Environmental Research Letters 16 (2), 024005.

Reiche, J., Souza, C. M., Hoekman, D. H., Verbesselt, J., Persaud, H., Herold, M., 2013. Feature level fusion of multi-temporal ALOS PALSAR and Landsat data for mapping and monitoring of tropical deforestation and forest degradation. IEEE Journal of Selected Topics in Applied Earth Observations and Remote Sensing 6 (5), 2159–2173.

Renner, I. W., Warton, D. I., 2013. Equivalence of MAXENT and Poisson point process models for species distribution modeling in ecology. Biometrics 69 (1), 274–281.

Reynolds, J., Wesson, K., Desbiez, A. L., Ochoa-Quintero, J. M., Leimgruber, P., 2016. Using remote sensing and random forest to assess the conservation status of critical Cerrado habitats in Mato Grosso do Sul, Brazil. Land 5 (2), 12.

Riahi, K., Rao, S., Krey, V., Cho, C., Chirkov, V., Fischer, G., Kindermann, G., Nakicenovic, N., Rafaj, P., 2011. RCP 8.5—A scenario of comparatively high greenhouse gas emissions. Climatic change 109 (1-2), 33.

Riggio, J., Jacobson, A. P., Hijmans, R. J., Caro, T., 2019. How effective are the protected areas of East Africa? Global ecology and conservation 17, e00573.

Riley, S. J., DeGloria, S. D., Elliot, R., 1999. Index that quantifies topographic heterogeneity. Intermountain Journal of sciences 5 (1-4), 23–27.

Ripple, W. J., Newsome, T. M., Wolf, C., Dirzo, R., Everatt, K. T., Galetti, M., Hayward, M. W., Kerley, G. I., Levi, T., Lindsey, P. A., et al., 2015. Collapse of the world's largest herbivores. Science advances 1 (4), e1400103.

Roberts, O., Bunting, P., Hardy, A., McInerney, D., 2020. Sensitivity Analysis of

the DART Model for Forest Mensuration with Airborne Laser Scanning. Remote Sensing 12 (2), 247.

Roberts, P., 2019. Tropical forests in prehistory, history, and modernity. Oxford University Press.

Roberts, P., Hunt, C., Arroyo-Kalin, M., Evans, D., Boivin, N., 2017. The deep human prehistory of global tropical forests and its relevance for modern conservation. Nature Plants 3 (8), 1–9.

Robertson, H. G., 2002. Comparison of leaf litter ant communities in woodlands, lowland forests and montane forests of north-eastern Tanzania. Biodiversity & Conservation 11 (9), 1637–1652.

Rodriguez-Galiano, V. F., Ghimire, B., Rogan, J., Chica-Olmo, M., Rigol-Sanchez, J. P., 2012. An assessment of the effectiveness of a random forest classifier for land-cover classification. ISPRS Journal of Photogrammetry and Remote Sensing 67, 93–104.

Rogan, J., Franklin, J., Stow, D., Miller, J., Woodcock, C., Roberts, D., 2008. Mapping land-cover modifications over large areas: A comparison of machine learning algorithms. Remote Sensing of Environment 112 (5), 2272–2283.

Rogelj, J., Shindell, D., Jiang, K., Fifita, S., Forster, P., Ginzburg, V., Handa, C., Kheshgi, H., Kobayashi, S., Kriegler, E., et al., 2018. Global Warming of 1.5° C. An IPCC Special Report on the impacts of global warming of 1.5° C above pre-industrial levels and related global greenhouse gas emission pathways, in the context of strengthening the global response to the threat of climate change, sustainable development, and efforts to eradicate poverty. Sustainable Development, and Efforts to Eradicate Poverty, V. Masson-Delmotte et al., Eds.(Cambridge University Press, Cambridge, UK).

Romijn, E., Herold, M., Kooistra, L., Murdiyarso, D., Verchot, L., 2012. Assessing capacities of non-Annex I countries for national forest monitoring in the context of REDD+. Environmental Science & Policy 19, 33–48.

Romijn, E., Lantican, C. B., Herold, M., Lindquist, E., Ochieng, R., Wijaya, A., Murdiyarso, D., Verchot, L., 2015. Assessing change in national forest moni-

toring capacities of 99 tropical countries. Forest Ecology and Management 352, 109–123.

Rondinini, C., Stuart, S., Boitani, L., 2005. Habitat suitability models and the shortfall in conservation planning for African vertebrates. Conservation Biology 19 (5), 1488–1497.

Rosa, I., Rentsch, D., Hopcraft, J. G. C., 2018. Evaluating forest protection strategies: A comparison of land-use systems to preventing forest loss in Tanzania. Sustainability 10 (12), 4476.

Rosa, I. M., Smith, M. J., Wearn, O. R., Purves, D., Ewers, R. M., 2016. The environmental legacy of modern tropical deforestation. Current Biology 26 (16), 2161–2166.

Rose, P. M., Kennard, M. J., Moffatt, D. B., Sheldon, F., Butler, G. L., 2016. Testing three species distribution modelling strategies to define fish assemblage reference conditions for stream bioassessment and related applications. PLoS One 11 (1).

Rosenqvist, A., Shimada, M., Chapman, B., Freeman, A., De Grandi, G., Saatchi, S., Rauste, Y., 2000. The global rain forest mapping project-a review. International Journal of Remote Sensing 21 (6-7), 1375–1387.

Rovero, F., Struhsaker, T. T., Marshall, A. R., Rinne, T. A., Pedersen, U. B., Butynski, T. M., Ehardt, C. L., Mtui, A. S., 2006. Abundance of diurnal primates in Mwanihana forest, Udzungwa Mountains, Tanzania. International Journal of Primatology 27 (3), 675–697.

Roy, D. P., Wulder, M. A., Loveland, T. R., Woodcock, C., Allen, R. G., Anderson, M. C., Helder, D., Irons, J. R., Johnson, D. M., Kennedy, R., et al., 2014. Landsat-8: Science and product vision for terrestrial global change research. Remote sensing of Environment 145, 154–172.

Sahoo, G., Kumar, Y., 2012. Analysis of parametric & non parametric classifiers for classification technique using WEKA. International Journal of Information Technology and Computer Science (IJITCS) 4 (7), 43.

Samanta, A., Knyazikhin, Y., Xu, L., Dickinson, R. E., Fu, R., Costa, M. H.,

Saatchi, S. S., Nemani, R. R., Myneni, R. B., 2012. Seasonal changes in leaf area of Amazon forests from leaf flushing and abscission. Journal of Geophysical Research: Biogeosciences 117 (G1).

Sangeda, A., Maleko, D., 2018. Regeneration effectiveness post tree harvesting in natural Miombo woodlands. Tanzania. J Plant Sci Agric Res 2 (1), 10.

Santoro, M., Kirches, G., Wevers, J., Boettcher, M., Brockmann, C., Lamarche, C., Defourny, P., 2017. Land Cover CCI: Product User Guide Version 2.0. Accessed on 13.02.2020.

Santos, J. R., Freitas, C. C., Araujo, L. S., Dutra, L. V., Mura, J. C., Gama, F. F., Soler, L. S., Sant'Anna, S. J., 2003. Airborne P-band SAR applied to the aboveground biomass studies in the Brazilian tropical rainforest. Remote Sensing of Environment 87 (4), 482–493.

Sarker, I. H., 2021. Machine learning: Algorithms, real-world applications and research directions. SN Computer Science 2 (3), 1–21.

Sayer, J., 1992. The conservation atlas of tropical forests: Africa. Springer.

Sayer, J., Sheil, D., Galloway, G., Riggs, R. A., Mewett, G., MacDicken, K. G., Arts, B., Boedhihartono, A. K., Langston, J., Edwards, D. P., 2019. SDG 15: life on land–The Central role of forests in sustainable development. Sustainable development goals: their impacts on forests and people. Cambridge University Press, Cambridge.

Scholes, R., Archer, S., 1997. Tree-grass interactions in savannas. Annual review of Ecology and Systematics 28 (1), 517–544.

Scholes, R. J., Frost, P. G., Tian, Y., 2004. Canopy structure in savannas along a moisture gradient on kalahari sands. Global Change Biology 10 (3), 292–302.

Schowengerdt, R. A., 2006. Remote sensing: models and methods for image processing. Elsevier.

Schuster, C., Förster, M., Kleinschmit, B., 2012. Testing the red edge channel for improving land-use classifications based on high-resolution multi-spectral satellite data. International Journal of Remote Sensing 33 (17), 5583–5599.

Sculley, D., 2010. Web-scale k-means clustering. In: Proceedings of the 19th international conference on World wide web. pp. 1177–1178.

Segal, M. R., 2004. Machine learning benchmarks and random forest regression. Bioinformatics and Molecular Biostatistics.

Seidl, R., Thom, D., Kautz, M., Martin-Benito, D., Peltoniemi, M., Vacchiano, G., Wild, J., Ascoli, D., Petr, M., Honkaniemi, J., et al., 2017. Forest disturbances under climate change. Nature climate change 7 (6), 395–402.

Serdeczny, O., Adams, S., Baarsch, F., Coumou, D., Robinson, A., Hare, W., Schaeffer, M., Perrette, M., Reinhardt, J., 2017. Climate change impacts in Sub-Saharan Africa: from physical changes to their social repercussions. Regional Environmental Change 17 (6), 1585–1600.

Sesnie, S. E., Finegan, B., Gessler, P. E., Thessler, S., Ramos Bendana, Z., Smith, A. M., 2010. The multispectral separability of Costa Rican rainforest types with support vector machines and Random Forest decision trees. International Journal of Remote Sensing 31 (11), 2885–2909.

Shapiro, A. C., Trettin, C. C., Küchly, H., Alavinapanah, S., Bandeira, S., 2015. The mangroves of the Zambezi Delta: increase in extent observed via satellite from 1994 to 2013. Remote Sensing 7 (12), 16504–16518.

Sharam, G., Sinclair, A., Turkington, R., 2006. Establishment of Broad-leaved Thickets in Serengeti, Tanzania: The Influence of Fire, Browsers, Grass Competition, and Elephants 1. Biotropica 38 (5), 599–605.

Shepherd, J., Dymond, J., 2003. Correcting satellite imagery for the variance of reflectance and illumination with topography. International Journal of Remote Sensing 24 (17), 3503–3514.

Shepherd, J. D., Bunting, P., Dymond, J. R., 2019. Operational large-scale segmentation of imagery based on iterative elimination. Remote Sensing 11 (6), 658.

Sherman, G. E., Sutton, T., Blazek, R., Luthman, L., 2004. Quantum GIS User Guide.

Shi, X., Cheng, Y., Xue, D., 2019. Classification Algorithm of Urban Point Cloud

Data based on LightGBM. In: IOP Conference Series: Materials Science and Engineering. Vol. 631. p. 052041.

Shimada, M., Itoh, T., Motooka, T., Watanabe, M., Shiraishi, T., Thapa, R., Lucas, R., 2014. New global forest/non-forest maps from ALOS PALSAR data (2007–2010). Remote Sensing of environment 155, 13–31.

Shimizu, K., Ota, T., Mizoue, N., 2019. Detecting Forest Changes Using Dense Landsat 8 and Sentinel-1 Time Series Data in Tropical Seasonal Forests. Remote Sensing 11 (16), 1899.

Siegert, F., Ruecker, G., Hinrichs, A., Hoffmann, A., 2001. Increased damage from fires in logged forests during droughts caused by El Nino. Nature 414 (6862), 437–440.

Silva, P., Santos, J., Shimabukuro, Y., Souza, P., Graça, P., 2003. Change vector analysis technique to monitor selective logging activities in Amazon. In: IGARSS 2003. 2003 IEEE International Geoscience and Remote Sensing Symposium. Proceedings (IEEE Cat. No. 03CH37477). Vol. 4. pp. 2580–2582.

Singh, A., 1989. Review article digital change detection techniques using remotely-sensed data. International journal of remote sensing 10 (6), 989–1003.

Sitch, S., Friedlingstein, P., Gruber, N., Jones, S. D., Murray-Tortarolo, G., Ahlström, A., Doney, S. C., Graven, H., Heinze, C., Huntingford, C., et al., 2015. Recent trends and drivers of regional sources and sinks of carbon dioxide. Biogeosciences 12 (3), 653–679.

Sivanpillai, R., Smith, C. T., Srinivasan, R., Messina, M. G., Wu, X. B., 2005. Estimating regional forest cover in east Texas using Enhanced Thematic Mapper (ETM+) data. Forest Ecology and Management 218 (1-3), 342–352.

Skarpe, C., 1992. Dynamics of savanna ecosystems. Journal of vegetation Science 3 (3), 293–300.

Sofaer, H. R., Hoeting, J. A., Jarnevich, C. S., 2019. The area under the precision-recall curve as a performance metric for rare binary events. Methods in Ecology and Evolution 10 (4), 565–577.

Soh, M. C., Mitchell, N. J., Ridley, A. R., Butler, C. W., Puan, C. L., Peh, K. S.-

H., 2019. Impacts of habitat degradation on tropical montane biodiversity and ecosystem services: a systematic map for identifying future research priorities. Frontiers in Forests and Global Change 2.

Sowmya, D., Deepa Shenoy, P., Venugopal, K., 2017. Remote sensing satellite image processing techniques for image classification: a comprehensive survey. International Journal of Computer Applications 161 (11), 24–37.

Spiers, J. A., Oatham, M. P., Rostant, L. V., Farrell, A. D., 2018. Applying species distribution modelling to improving conservation based decisions: a gap analysis of Trinidad and Tobago's endemic vascular plants. Biodiversity and conservation 27 (11), 2931–2949.

Spinoni, J., Vogt, J., Naumann, G., Carrao, H., Barbosa, P., 2015. Towards identifying areas at climatological risk of desertification using the Köppen–Geiger classification and FAO aridity index. International Journal of Climatology 35 (9), 2210–2222.

Stehman, S. V., Czaplewski, R. L., 1998. Design and analysis for thematic map accuracy assessment: fundamental principles. Remote sensing of environment 64 (3), 331–344.

Stévart, T., Dauby, G., Lowry, P., Blach-Overgaard, A., Droissart, V., Harris, D., Mackinder, B. A., Schatz, G., Sonké, B., Sosef, M. S., et al., 2019. A third of the tropical African flora is potentially threatened with extinction. Science advances 5 (11), eaax9444.

Storch, F., Dormann, C. F., Bauhus, J., 2018. Quantifying forest structural diversity based on large-scale inventory data: a new approach to support biodiversity monitoring. Forest Ecosystems 5 (1), 34.

Su, L., Huang, Y., Chopping, M., Rango, A., Martonchik, J., 2009. An empirical study on the utility of BRDF model parameters and topographic parameters for mapping vegetation in a semi-arid region with MISR imagery. International Journal of Remote Sensing 30 (13), 3463–3483.

Suarez, D. R., Rozendaal, D. M., De Sy, V., Gibbs, D. A., Harris, N., Sexton, J. O., Feng, M., Channan, S., Zahabu, E., Pekkarinen, A., et al., 2021. Variation in

aboveground biomass in forests and woodlands in Tanzania along gradients in environmental conditions and human use. Environmental Research Letters.

Sun, L., Mi, X., Wei, J., Wang, J., Tian, X., Yu, H., Gan, P., 2017. A cloud detection algorithm-generating method for remote sensing data at visible to short-wave infrared wavelengths. ISPRS journal of photogrammetry and remote sensing 124, 70–88.

Swamy, L., Drazen, E., Johnson, W. R., Bukoski, J. J., 2017. The future of tropical forests under the United Nations Sustainable Development Goals. Journal of Sustainable Forestry 37 (2), 221–256.

Szuster, B. W., Chen, Q., Borger, M., 2011. A comparison of classification techniques to support land cover and land use analysis in tropical coastal zones. Applied Geography 31 (2), 525–532.

Tejaswi, G., 2007. Manual on Deforestation, Degradation, And Fragmentation Using Remote Sensing And GIS. Strengthening Monitoring, Assessment and Reporting on Sustainable Forest Management. Forest Deparment, Food and Agriculture Organization of the United Nations.

Tewkesbury, A. P., Comber, A. J., Tate, N. J., Lamb, A., Fisher, P. F., 2015. A critical synthesis of remotely sensed optical image change detection techniques. Remote Sensing of Environment 160, 1–14.

Thanh Noi, P., Kappas, M., 2018. Comparison of random forest, k-nearest neighbor, and support vector machine classifiers for land cover classification using Sentinel-2 imagery. Sensors 18 (1), 18.

Théau, J., 2022. Change detection. In: Springer Handbook of Geographic Information. pp. 151–159.

Thessler, S., Sesnie, S., Bendaña, Z. S. R., Ruokolainen, K., Tomppo, E., Finegan, B., 2008. Using k-nn and discriminant analyses to classify rain forest types in a Landsat TM image over northern Costa Rica. Remote Sensing of Environment 112 (5), 2485–2494.

Thomas, N., Bunting, P., Lucas, R., Hardy, A., Rosenqvist, A., Fatoyinbo, T.,

2018. Mapping mangrove extent and change: a globally applicable approach. Remote Sensing 10 (9), 1466.

Thomas, S. C., Baltzer, J. L., 2001. Tropical forests. e LS.

Thomson, A. M., Calvin, K. V., Chini, L. P., Hurtt, G., Edmonds, J. A., Bond-Lamberty, B., Frolking, S., Wise, M. A., Janetos, A. C., 2010. Climate mitigation and the future of tropical landscapes. Proceedings of the National Academy of Sciences 107 (46), 19633–19638.

Title, P. O., Bemmels, J. B., 2017. ENVIREM: an expanded set of bioclimatic and topographic variables increases flexibility and improves performance of ecological niche modeling. Ecography 41 (2), 291–307.

Tobón, W., Urquiza-Haas, T., Koleff, P., Schröter, M., Ortega-Álvarez, R., Campo, J., Lindig-Cisneros, R., Sarukhán, J., Bonn, A., 2017. Restoration planning to guide Aichi targets in a megadiverse country. Conservation Biology 31 (5), 1086–1097.

Tomppo, E., Halme, M., 2004. Using coarse scale forest variables as ancillary information and weighting of variables in k-NN estimation: a genetic algorithm approach. Remote Sensing of Environment 92 (1), 1–20.

Tomppo, E., Malimbwi, R., Katila, M., Mäkisara, K., Henttonen, H. M., Chamuya, N., Zahabu, E., Otieno, J., 2014. A sampling design for a large area forest inventory: case Tanzania. Canadian Journal of Forest Research 44 (8), 931–948.

Tong, X., Tian, F., Brandt, M., Liu, Y., Zhang, W., Fensholt, R., 2019. Trends of land surface phenology derived from passive microwave and optical remote sensing systems and associated drivers across the dry tropics 1992–2012. Remote Sensing of Environment 232, 111307.

Torello-Raventos, M., Feldpausch, T. R., Veenendaal, E., Schrodt, F., Saiz, G., Domingues, T. F., Djagbletey, G., Ford, A., Kemp, J., Marimon, B. S., et al., 2013. On the delineation of tropical vegetation types with an emphasis on forest/savanna transitions. Plant Ecology & Diversity 6 (1), 101 – 137.

Torres, R., Snoeij, P., Geudtner, D., Bibby, D., Davidson, M., Attema, E., Potin,

P., Rommen, B., Floury, N., Brown, M., et al., 2012. GMES Sentinel-1 mission. Remote Sensing of Environment 120, 9–24.

Tottrup, C., 2004. Improving tropical forest mapping using multi-date Landsat TM data and pre-classification image smoothing. International Journal of remote sensing 25 (4), 717–730.

Tu, Y.-H., Johansen, K., Aragon, B., El Hajj, M. M., McCabe, M. F., 2022. The radiometric accuracy of the 8-band multi-spectral surface reflectance from the planet SuperDove constellation. International Journal of Applied Earth Observation and Geoinformation 114, 103035.

Tucker, C. J., Townshend, J. R., 2000. Strategies for monitoring tropical deforestation using satellite data. International Journal of Remote Sensing 21 (6-7), 1461–1471.

United Nations, 2019. World urbanization prospects 2018: highlights (ST/ESA/SER. A/421).

URT, 1998. National Forest Policy. Forestry and Beekeeping, Ministry of Natural Resources and Toursim.

URT, 2001. National forest programme in tanzania 2001–2010.

URT, 2014a. Fifth National Report on the Implementation of the Convention on Biological Diversity. Tech. Rep. 9987-8990-5-6, Vice President's Office, Division of Environment.

URT, 2014b. Second National Communication to the United Nations Framework Convention on Climate Change. Tech. rep., Vice President's Office, Division of Environment.

URT, 2017. Tanzania's Forest Reference Emission level submission to the UNFCCC. United Republic of Tanzania.

URT, 2018. National Population Projections. Tech. rep., National Bureau of Statistics, Ministry of Finance and Planning-Dar Es Salaam and Ministry of Finance and Planning Zanzibar.

Ustuner, M., Balik Sanli, F., 2019. Polarimetric Target Decompositions and Light

Gradient Boosting Machine for Crop Classification: A Comparative Evaluation. ISPRS International Journal of Geo-Information 8 (2), 97.

Valavi, R., Elith, J., Lahoz-Monfort, J. J., Guillera-Arroita, G., 2020. Modelling species presence-only data with random forests. bioRxiv.

Van Vuuren, D. P., Edmonds, J., Kainuma, M., Riahi, K., Thomson, A., Hibbard, K., Hurtt, G. C., Kram, T., Krey, V., Lamarque, J.-F., et al., 2011a. The representative concentration pathways: an overview. Climatic change 109 (1), 5–31.

Van Vuuren, D. P., Edmonds, J., Kainuma, M., Riahi, K., Thomson, A., Hibbard, K., Hurtt, G. C., Kram, T., Krey, V., Lamarque, J.-F., et al., 2011b. The representative concentration pathways: an overview. Climatic change 109 (1-2), 5.

Vargas, C., Montalban, J., Leon, A. A., 2019. Early warning tropical forest loss alerts in Peru using Landsat. Environmental Research Communications 1 (12), 121002.

Veloz, S. D., 2009. Spatially autocorrelated sampling falsely inflates measures of accuracy for presence-only niche models. Journal of Biogeography 36 (12), 2290–2299.

Venter, Z., Cramer, M., Hawkins, H.-J., 2018. Drivers of woody plant encroachment over Africa. Nature communications 9 (1), 1–7.

Verdone, M., Seidl, A., 2017. Time, space, place, and the Bonn Challenge global forest restoration target. Restoration Ecology 25 (6), 903–911.

Verhegghen, A., Kuzelova, K., Syrris, V., Eva, H., Achard, F., 2022. Mapping Canopy Cover in African Dry Forests from the Combined Use of Sentinel-1 and Sentinel-2 Data: Application to Tanzania for the Year 2018. Remote Sensing 14 (6), 1522.

Vermote, E. F., Tanré, D., Deuze, J. L., Herman, M., Morcette, J.-J., 1997. Second simulation of the satellite signal in the solar spectrum, 6S: An overview. IEEE transactions on geoscience and remote sensing 35 (3), 675–686.

Vesa, L., Malimbwi, R., Tomppo, E., Zahabu, E., Maliondo, S., Chamuya, N.,

Maliondo, S., Nsokko, E., Otieno, J., Dalsgaard, S., 2010. A national forestry resources monitoring and assessment of Tanzania (NAFORMA). FAO.

Vieira, I. C. G., de Almeida, A. S., Davidson, E. A., Stone, T. A., de Carvalho, C. J. R., Guerrero, J. B., 2003. Classifying successional forests using Landsat spectral properties and ecological characteristics in eastern Amazonia. Remote Sensing of Environment 87 (4), 470–481.

Waldeland, A. U., Trier, Ø. D., Salberg, A.-B., 2022. Forest mapping and monitoring in Africa using Sentinel-2 data and deep learning. International Journal of Applied Earth Observation and Geoinformation 111, 102840.

Walker, K. L., 2016. Seasonal mixing in forest-cover maps for humid tropics and impact of fluctuations in spectral properties of low vegetation. Remote Sensing of Environment 179, 79–88.

Walter, V., 2004. Object-based classification of remote sensing data for change detection. ISPRS Journal of photogrammetry and remote sensing 58 (3-4), 225–238.

Wang, H., Zhao, Y., Pu, R., Zhang, Z., 2015. Mapping Robinia pseudoacacia forest health conditions by using combined spectral, spatial, and textural information extracted from IKONOS imagery and random forest classifier. remote Sensing 7 (7), 9020–9044.

Wang, Q., Zhang, C., Atkinson, P. M., 2020. Sub-pixel mapping with point constraints. Remote Sensing of Environment 244, 111817.

Wang, Y., Tobey, J., Bonynge, G., Nugranad, J., Makota, V., Ngusaru, A., Traber, M., 2005. Involving geospatial information in the analysis of land-cover change along the Tanzania coast. Coastal Management 33 (1), 87–99.

Wang, Y., Weinacker, H., Koch, B., 2008. A lidar point cloud based procedure for vertical canopy structure analysis and 3D single tree modelling in forest. Sensors 8 (6), 3938–3951.

Warren, D. L., Seifert, S. N., 2011. Ecological niche modeling in Maxent: the importance of model complexity and the performance of model selection criteria. Ecological applications 21 (2), 335–342.

Waske, B., Braun, M., 2009. Classifier ensembles for land cover mapping using multitemporal SAR imagery. ISPRS Journal of Photogrammetry and Remote Sensing 64 (5), 450–457.

Watling, J. I., Brandt, L. A., Mazzotti, F. J., Romañach, S. S., 2013. Use and interpretation of climate envelope models: a practical guide. University of Florida, Gainesville, FL, 43.

Wessels, K. J., Van den Bergh, F., Roy, D. P., Salmon, B. P., Steenkamp, K. C., MacAlister, B., Swanepoel, D., Jewitt, D., 2016. Rapid land cover map updates using change detection and robust random forest classifiers. Remote sensing 8 (11), 888.

White, F., 1983. The vegetation of Africa: a descriptive memoir to accompany the UNESCO/AETFAT/UNSO vegetation map of Africa by F White. Natural Resources Research Report XX, UNESCO, Paris, France, 1876–1895.

White, J. C., Hermosilla, T., Wulder, M. A., Coops, N. C., 2022. Mapping, validating, and interpreting spatio-temporal trends in post-disturbance forest recovery. Remote Sensing of Environment 271, 112904.

White, J. D., Scott, N. A., Hirsch, A. I., Running, S. W., 2006. 3-PG productivity modeling of regenerating Amazon forests: climate sensitivity and comparison with MODIS-derived NPP. Earth Interactions 10 (8), 1–26.

Whittle, M., Quegan, S., Uryu, Y., Stüewe, M., Yulianto, K., 2012. Detection of tropical deforestation using ALOS-PALSAR: A Sumatran case study. Remote Sensing of Environment 124, 83–98.

Williams, H. W., Cross, D. E., Crump, H. L., Drost, C. J., Thomas, C. J., 2015. Climate suitability for European ticks: assessing species distribution models against null models and projection under AR5 climate. Parasites & vectors 8 (1), 440.

Willis, K., Bennett, K. D., Burrough, S., Macias-Fauria, M., Tovar, C., 2013. Determining the response of African biota to climate change: using the past to model the future. Philosophical Transactions of the Royal Society B: Biological Sciences 368 (1625), 20120491.

Wilson, R. T., 2013. Py6S: A Python interface to the 6S radiative transfer model. Comput. Geosci. 51 (2), 166.

Wise, M., Calvin, K., Thomson, A., Clarke, L., Bond-Lamberty, B., Sands, R., Smith, S. J., Janetos, A., Edmonds, J., 2009. Implications of limiting CO2 concentrations for land use and energy. Science 324 (5931), 1183–1186.

Witten, I. H., Frank, E., Hall, M. A., Pal, C. J., 2016. Data Mining: Practical machine learning tools and techniques. Morgan Kaufmann.

World Bank, 2019. Tanzania: Country Environmental Analysis – Environmental Trends and Threats, and Pathways to Improved Sustainability. Tech. rep., Washington, DC.

World Bank Group and others, 2019. Climate Change Knowledge Portal. Accessed on 25.02.2020.
URL https://climateknowledgeportal.worldbank.org/country/tanzania-united-republic/impacts-agriculture

Wright, S. J., Muller-Landau, H. C., 2006. The Future of Tropical Forest Species 1. Biotropica: The Journal of Biology and Conservation 38 (3), 287–301.

Wu, S., Wang, J., Yan, Z., Song, G., Chen, Y., Ma, Q., Deng, M., Wu, Y., Zhao, Y., Guo, Z., et al., 2021. Monitoring tree-crown scale autumn leaf phenology in a temperate forest with an integration of PlanetScope and drone remote sensing observations. ISPRS Journal of Photogrammetry and Remote Sensing 171, 36–48.

Ygorra, B., Frappart, F., Wigneron, J.-P., Moisy, C., Catry, T., Baup, F., Hamunyela, E., Riazanoff, S., 2021. Monitoring loss of tropical forest cover from Sentinel-1 time-series: A CuSum-based approach. International Journal of Applied Earth Observation and Geoinformation 103, 102532.

Yildirim, N., Ansal, H., 2011. Foresighting FLOSS (free/libre/open source software) from a developing country perspective: The case of Turkey. Technovation 31 (12), 666–678.

You, H., Tian, S., Yu, L., Lv, Y., 2019. Pixel-level remote sensing image recogni-

tion based on bidirectional word vectors. IEEE Transactions on Geoscience and Remote Sensing 58 (2), 1281–1293.

Yu, L., Gong, P., 2012. Google Earth as a virtual globe tool for Earth science applications at the global scale: progress and perspectives. International Journal of Remote Sensing 33 (12), 3966–3986.

Zagajewski, B., Kluczek, M., Raczko, E., Njegovec, A., Dabija, A., Kycko, M., 2021. Comparison of random forest, support vector machines, and neural networks for post-disaster forest species mapping of the Krkonoše/Karkonosze transboundary biosphere reserve. Remote Sensing 13 (13), 2581.

Zanchetta, A., Bitelli, G., 2017. A combined change detection procedure to study desertification using opensource tools. Open Geospatial Data, Software and Standards 2 (1), 1–12.

Zanchetta, A., Bitelli, G., Karnieli, A., 2015. Tasselled Cap transform for change detection in the drylands: findings for SPOT and Landsat satellites with FOSS tools. In: Third International Conference on Remote Sensing and Geoinformation of the Environment (RSCy2015). Vol. 9535. pp. 330–338.

Zhan, X., Defries, R., Townshend, J., Dimiceli, C., Hansen, M., Huang, C., Sohlberg, R., 2000. The 250 m global land cover change product from the Moderate Resolution Imaging Spectroradiometer of NASA's Earth Observing System. International Journal of Remote Sensing 21 (6-7), 1433–1460.

Zhang, H., Eziz, A., Xiao, J., Tao, S., Wang, S., Tang, Z., Zhu, J., Fang, J., 2019. High-Resolution Vegetation Mapping Using eXtreme Gradient Boosting Based on Extensive Features. Remote Sensing 11 (12), 1505.

Zhang, K., Sun, L., Tao, J., 2020. Impact of Climate Change on the Distribution of Euscaphis japonica (Staphyleaceae) Trees. Forests 11 (5), 525.

Zhao, J., Wang, Y., Zhang, H., 2011. Automated batch processing of mass remote sensing and geospatial data to meet the needs of end users. In: 2011 IEEE International Geoscience and Remote Sensing Symposium. pp. 3464–3467.

Zhu, Z., Wang, S., Woodcock, C. E., 2015. Improvement and expansion of the

Fmask algorithm: Cloud, cloud shadow, and snow detection for Landsats 4–7, 8, and Sentinel 2 images. Remote Sensing of Environment 159, 269–277.

Zhu, Z., Woodcock, C. E., 2012. Object-based cloud and cloud shadow detection in Landsat imagery. Remote sensing of environment 118, 83–94.

Zhuravleva, I., Turubanova, S., Potapov, P., Hansen, M., Tyukavina, A., Minnemeyer, S., Laporte, N., Goetz, S., Verbelen, F., Thies, C., 2013. Satellite-based primary forest degradation assessment in the Democratic Republic of the Congo, 2000–2010. Environmental Research Letters 8 (2), 024034.

Zimmermann, J.-B., Jullien, N., 2007. Free/Libre/Open Source Software (FLOSS): lessons for intellectual property rights management in a knowledge-based economy. The Icfai Journal of Cyber Law 6 (3), 19–36.

Appendix A

A.1 Soil groups in Tanzania

A.2 Correlation matrix between environmental predictors

Table A.1: Summary of dominant soil groups in Tanzania (Batjes, 2004)

Code	Major soil group	Descriptions
1	Acrisols	Strongly weathered acid soils, with low base saturation
2	Andosols	Black soils of volcanic landscapes, rich in organic matters
3	Arenosols	Sandy soils with limited soil development, under scattered (mostly grassy) vegetation to very old plateaus of light forest
4	Cambisols	Weakly to moderately developed soil soils occurring from seal level to the highlands and under all kind of vegetation (savanna woodland and forests)
5	Chernozems	Black soil rich in organic matter, occurring in flat to undulating plains with forest and tall grass vegetation
6	Ferralsols	Deep, strongly weathered, physically stable but chemically depleted
7	Fluvisols	Associated with important river plains, periodically flooded areas
8	Gleysols	Temporary or permanent wetness near soil surface, support swamp forests or permanent grass cover
9	Histosols	Peat and muck soils with incompletely decomposed plant remains
10	Leptosols	Shallow soils over hard rock/gravel, at medium to high altitude landscapes, suitable for forestry and nature conservation
11	Lixisols	Strongly weathered and leached, finely textured materials support natural savanna or open woodland vegetation
12	Luvisols	Common in flat or gently sloping land with unconsolidated alluvial, colluvial, aeolian deposits in cooler environments and young surface
13	Nitisols	Deep, red, well-drained tropical soils with a clayey, well defined nut-shaped peds with shiny surface. Found in level to highland under tropical rain forest or savanna vegetation
14	Phaeozems	Dark soils, rich in organic matter. Occur on flat to undulating land in a warm to cool (tropical highland). Support natural vegetation with tall grass steppe and or/forest
15	Planosols	Clayey alluvial and colluvial deposits and support light forest or grass vegetation
16	Regosols	Contain gravelly lateritic materials (murrum) with low suitability for plant growth
17	Solonchanks	Occur in seasonally or permanently water logged areas with grasses and /or halophytic herbs
18	Solonetz	Associated with flat lands in a hot climate, dry summers, coastal deposit. Contain a high proportional of sodium ions
19	Vertisols	Contain sediments with a high proportion of smectite clay, high swelling and shrinking of results in deep cracks during dry season. Climax vegetation is savanna, natural grass and / or woodland
20	Water body	-

Table A.2: Correlation matrix between environmental predictors

and variables with high correlation are shown with r > 0.7 or < -0.7 in **bold** at a significance level of .01 (see Table 2 for the details of abbreviations)

	Tri	TopoWet	Elv	ThermicitI	Bio1	PET	PETWetQ	PETWarmQ	PETseason	Mi	Bio14	Bio13	Bio12	ST	Soilwat
Tri	1														
TopoWet	**-0.795**	1													
Elv	0.325	-0.423	1												
ThermicitI	-0.441	0.572	**-0.862**	1											
Bio1	-0.426	0.553	-0.205	0.473	1										
PET	-0.324	0.422	-0.046	0.401	0.38	1									
PETWetQ	-0.282	0.333	0.005	0.298	0.289	**0.896**	1								
PETWarmQ	-0.257	0.317	-0.007	0.297	0.28	**0.916**	**0.853**	1							
PETseason	0.115	-0.16	-0.222	-0.041	0.009	**-0.74**	0.058	0.2116	1						
Mi	0.235	-0.304	-0.124	-0.073	-0.061	-0.31	-0.43	-0.627	0.013	1					
Bio14	0.101	-0.049	-0.336	0.138	0.151	-0.163	-0.333	-0.172	0.209	0.249	1				
Bio13	0.152	-0.205	-0.208	0.075	0.092	-0.522	-0.55	-0.409	0.157	0.007	0.201	1			
Bio12	0.177	-0.234	-0.18	0.052	0.059	-0.545	-0.618	-0.477	-0.021	0.073	0.249	0.025	1		
ST	0.325	-0.347	0.482	-0.409	-0.414	-0.001	0.008	0.010	-0.111	-0.023	-0.115	-0.051	-0.035	1	
Soilwat	0.198	-0.22	0.258	-0.237	-0.243	-0.135	-0.17	-0.11	-0.117	**0.709**	-0.049	0.196	0.259	0.154	1

A.3 Forest extent in the protected area

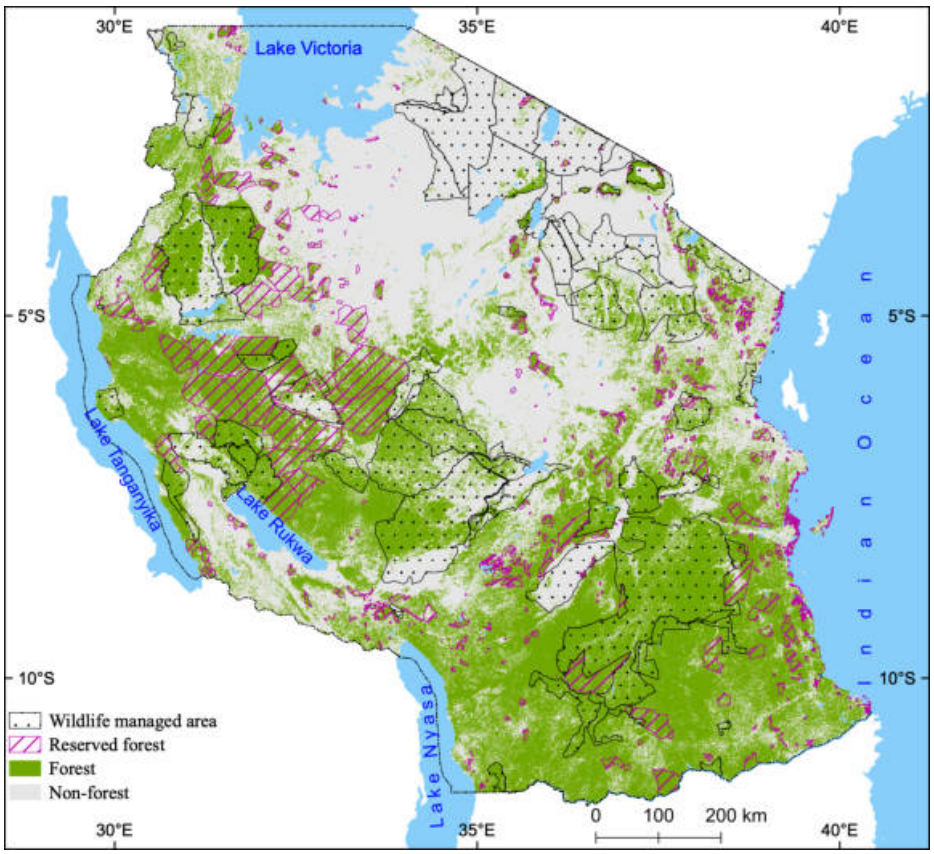

Figure A.1: Relationship of the protected area and forest extent

A.4 Forest extent and changes in protected areas

Table A.3: A summary of forest types extent in the forest nature reserves, under category Ib (Wilderness Area) of the International Union for Conservation of Nature (IUCN)

	Forest type (ha)							
Name	Baseline	Montane	Lowland	Closed Woodland	Open Woodland	Plantation	Thicket	Mangrove
Itulu Hill	323,641	-	-	4,427	319,100	-	115	
Kilombero	124,754	51,944	56,367	13,041	3,357	15	-	-
Mwambesi	107,484	-	556	39,624	67,303	-	-	-
Kalambo River	34,853	-	-	28,075	6,779	-	-	-
Uzungwa Scarp	34,470	26,975	6,871	439	42	143	-	-
Uluguru	22,147	20,453	1,283	245	79	87	-	-
Mkingu	20,831	16,970	2,725	556	570	-	-	-
Minziro	20,598	11	19,601	705	280	-	-	-
Mount Rungwe	13,586	11,162	349	146	411	1,518	-	-
Chome	13,125	10,722	1,527	125	176	574	-	-
Pindiro	11,934	-	10,489	607	838	-	-	-
Rondo	11,602	-	11,210	262	107	24	-	-
Magamba	9,150	7,330	1,108	222	118	373	-	-
Amani	7,749	7,423	221	40	7	60	-	-
Nilo	5,193	5,141	30	11	2	8	-	-
Mount Hanang	4,967	3,479	396	523	569	-	-	-
Magombera	2,067	-	1,525	512	31	-	-	-
Pugu	1,442	-	1,434	6	3	-	-	-

Table A.4: An overview of forest extent and change (ha) in the nature reserve

	Forest extent				**Forest change**		
Name	Baseline	2018	2019	2020	2018	2019	2020
Itulu Hill	323,641	323,508	323,497	323,494	133	11	3
Kilombero	124,754	124,752	124,750	124,750	2	2	-
Mwambesi	107,484	107,480	107,480	107,480	4	-	-
Kalambo River	34,853	34,433	34,321	34,284	420	113	37
Uzungwa Scarp	34,470	34,470	34,468	34,468	-	2	-
Uluguru	22,147	22,147	22,147	22,147	-	-	-

Mkingu	20,831	20,831	20,831	20,831	-	-	-
Minziro	20,598	20,598	20,598	20,598	3	-	-
Mount Rungwe	13,586	13,586	13,586	13,586	-	-	-
Chome	13,125	13,125	13,125	13,125	-	-	-
Pindiro	11,934	11,924	11,921	11,921	10	3	-
Rondo	11,602	11,602	11,602	11,602	-	-	-
Magamba	9,150	9,150	9,150	9,150	-	-	-
Amani	7,749	7,749	7,749	7,749	-	-	-
Nilo	5,193	5,193	5,193	5,193	-	-	-
Mount Hanang	4,967	4,967	4,967	4,967	-	-	-
Magombera	2,067	2,067	2,067	2,067	-	-	-
Pugu	1,442	1,442	1,442	1,442	-	-	-

Table A.5: Forest reserves: Forest extent and change (ha)

		Forest extent				**Forest change**		
No.	Name	Baseline	2018	2019	2020	2018	2019	2020
1	Nyahua Mbuga	465,749	457,836	456,243	455,500	10,553	1,672	751
2	Mpanda North East	413,574	405,815	403,433	403,373	11,039	2,849	65
3	Inyonga	403,348	392,905	392,017	391,573	10,475	890	443
4	Ugalla River	317,781	317,669	317,612	317,607	112	57	5
5	Mpanda Line	301,505	294,850	292,031	291,611	7,249	2,882	422
6	North East Undendeule	263,787	263,787	263,787	263,787	-	-	-
7	Lukwati	195,324	195,324	195,324	195,324	-	-	-
8	Rukwa	163,155	159,886	159,800	159,707	3,269	87	92
9	Muhuwesi	153,359	152,839	152,784	152,783	547	56	1
10	Ugalla North	151,379	150,040	149,117	148,855	1,362	934	261
11	Lungonya	136,651	136,590	136,569	136,569	99	24	-
12	Muipa	114,665	114,665	114,665	114665	-	-	-
13	Biharamulo	94,049	90,187	89,754	89,696	4,953	488	61
14	Wala River	91,449	91,240	91,238	91,238	270	2	-
15	Ruiga River	89,400	89,276	89,243	89,239	123	33	4
16	Nyera/Kiperere	82,763	82,754	82,751	82,751	9	3	-
17	Igombe River	75,484	62,183	61,200	60,934	13,300	983	266
18	Ruhoi River	71,295	70,818	70,660	70,660	609	168	-

19	Coastal mangrove	70,155	70,083	70,076	70076	103	8	-
20	Mulele Hills	68,054	63,799	61,754	61,700	4,382	2,080	55
21	Ukanga	63,946	63,809	63,782	63,781	147	30	2
22	North Makere	62,782	61,848	61,577	61,534	1,008	273	43
23	Mkuti	60,958	55,703	55,194	55,133	5,296	5,11	61
24	Mtarure	55,451	55,447	55,446	55,446	11	2	-
25	Mkulazi	50,116	50,088	50,087	50,088	28	-	-
26	Makere South	44,165	42,551	42,330	42,319	1,911	238	11
27	Ngarama North	42,940	42,881	42,875	42,875	62	5	-
28	Sasawara	39,198	39,174	39,172	39,172	32	2	-
29	Lohombero/Luwengu	39,169	39,076	39,025	39,025	104	51	-
30	Mamboto	38,064	38,058	38,058	38,058	6	-	-
31	Malehi	37,627	37,594	37,589	37,589	40	5	
32	Mbagala	32,038	31,9723	31,946	31,946	108	33	-
33	Geita	31,994	29,526	29,108	29,077	3,118	452	33
34	Ukwiva	30,122	30,122	30,122	30,122	-	-	-
35	Ushetu Ubagwe	29,897	29,885	29,882	29,882	12	3	-
36	Songa	29,074	29,039	29,034	29,034	36	5	-
37	Nou	29,059	29,059	29,059	29,059	-	-	-
38	Uyui-Kigwa	29,033	26,431	26,423	26,414	3,689	9	9
39	Loasi river	28,408	26,642	25,691	25,427	2,439	1,039	271
40	Nyantakara	25,368	25,358	25,357	25,358	17	1	-
41	Ruvu South	22,173	22173	22173	22173	-	-	-
42	Chinene West	22,039	22,034	22,033	22,033	13	2	-
43	Nampekeso	21,820	21,814	21,812	21,812	7	2	-
44	Livingstone	21,786	21,788	21,785	21,785	5	-	-
45	Karitu	21,286	19,799	19,707	19,620	1,487	92	87
46	Lionja	20,846	20,843	20,843	20,843	5	-	-
47	Ruamagazi	19,196	15,114	14,557	14,483	4,849	569	75
48	Chenene East	17,936	17,862	17,848	17,847	96	15	1
49	Unyambiu North	17,570	17,536	17,535	17,534	50	1	1
50	Kisinga Lugaro	17,216	17,216	17,216	17,216	-	-	-
51	Rungo	16,999	16,981	16,975	16,975	23	8	-
52	Mgololo	16,588	16,588	16,588	16,588	1	-	-
53	Ngindo	16,393	16,393	16,393	16,393	-	-	-
54	Matapwa	15,785	15,607	15,584	15,584	183	23	-
55	Uvinza	15,672	15,643	15,638	15,638	38	5	-

56	Mufindi Scarp	15,255	15,255	15,255	15,255	-	-	-
57	Goweko	15,209	13,453	13,424	13,414	2,196	32	11
58	Uzigua	14,948	14,948	14,948	14,948	-	-	-
59	Nyaganje	14,615	14,613	14,611	14,611	3	1	-
60	Kichi Hills	14,581	14,581	14,581	14,581	-	-	-
61	Runzewe	13,929	13,419	13,296	13,269	697	133	28
62	Nguru North	11,479	11,479	11,479	11,479	-	-	-
63	Ilomero Hill	11,056	10,368	10,301	10,274	693	68	27
64	Chimala Scarp	10,961	10,883	10,878	10,877	123	5	1
65	Isalala	10,762	10,583	10,577	10,576	216	7	-
66	Urumwa	9,893	9,839	9,836	9,835	54	3	-
67	Lyambo Hill	9,764	9,313	8,986	8,966	451	327	19
68	Maisome	9,419	8,649	8,527	8,513	770	123	13
69	Chumwa Range	9,264	9,259	9,259	9,259	11	-	-
70	Poroto Ridge	8,977	8,977	8,977	8,977	-	-	-
71	Kipengere Range	8,687	8,671	8,670	8,670	22	1	-
72	Pala Mountains	8,444	8,444	8,444	8,444	-	-	-
73	Mitundumbea	8,388	8,353	8,352	8,352	44	2	-
74	Image	8,012	8,012	8,012	8,012	-	-	-
75	North Mamiwa Kisara	7,916	7,916	7,916	7,916	-	-	-
76	Matogoro East	7,624	7,619	7,618	7,618	6	1	-
77	Pagale	7,405	7,405	7,405	7,405	-	-	-
78	Ivuna North	6,479	6,357	6,356	6,359	175	1	-
79	Kanga	6,353	6,353	6,353	6,353	-	-	-
80	Salanga	6,302	6,302	6,302	6,302	-	-	-
81	Ilunde	6,035	5,979	5,965	5,955	70	15	10
82	Lugufu	5,984	3,180	2,926	2,903	2,955	264	24
83	Monduli	5,878	5,878	5,878	5,878	-	-	-
84	Mamiwa Kisara South	5,628	5,628	5,628	5,628	-	-	-
85	Mbogwe Bukombe	5,591	5,572	5,569	5569	31	3	-
86	Mienze	5,450	4,987	4,844	4,832	620	150	12
87	Mangalisa	5,274	5,274	5,274	5,274	-	-	-
88	Mlali	5,001	5,000	4,999	4,999	2	-	1
89	Tambulu	4,972	4,972	4,972	4,972	-	-	-
90	Ndechela	4,968	4,966	4,966	4,966	2	-	-
91	Bereku	4,863	4,862	4,862	4,862	-	-	-
92	Mlola	4,819	4,710	4,705	4,705	117	5	-

93	Loliondo II		4,774	4,774	4,774	4,774	-	-	-
94	Kungwe Bay		4,737	4,560	4,545	4,543	226	15	3
95	Kitonbeine		4,620	4,620	4,620	4,620	-	-	-
96	Namakutwa/Namade		4,495	4,493	4,493	4,493	3	-	-
97	Ufiome		4,431	4,431	4,431	4,431	-	-	-
98	Ngogwa Busangi		4,316	4,025	3,963	3,961	385	67	3
99	Nandembo		4,167	4,166	4,166	4,166	2	-	-
100	Essimingor		4,130	4,130	4,130	4,130	-	-	-
101	Mdando		4,124	4,124	4,124	4,124	-	-	-
102	Katundu		4,093	4,047	3,976	3,976	62	79	-
103	Mafwomero		3,987	3,987	3,987	3,987	-	-	-
104	Mkusu		3,926	3,926	3,926	3,926	-	-	-
105	Changandu		3,826	3,826	3,826	3,826	-	-	-
106	Umalila		3,777	3,710	3,705	3,704	81	5	1
107	Dabaga New		3,731	3,730	3,730	3,730	1	-	-
108	Mtanza		3,721	3,704	3,696	3,696	23	9	-
109	Kitope Hill		3,692	3,692	3,692	3,692	-	-	-
110	Kiwengoma		3,618	3,618	3,617	3,617	-	1	-
111	Makonde Scarp II		3,504	3,372	3,314	3,303	190	68	12
112	Igombe Dam		3,499	3,485	3,485	3,485	14	-	-
113	Nyumburuni		3,495	3,291	3,269	3,269	230	23	-
114	Kikuru		3,479	3,479	3,479	3,479	-	-	-
115	Baga I (Mzinga)		3,456	3,456	3,456	3,456	-	-	-
116	Mafi Hill		3,441	3,441	3,441	3,441	-	-	-
117	Mkungwe		3,326	3,324	3,324	3,324	2	-	-
118	Gulosilo		3,305	3,305	3,305	3,305	-	-	-
119	Hassama Hill		3,281	3,281	3,281	3,281	-	-	-
120	Ruvu		3,271	3,270	3,270	3,270	1	-	-
121	Derema		3,256	3,256	3,256	3,256	-	-	-
122	Kitapilimwa		3,170	3,170	3,170	3,170	-	-	-
123	Makonde Scarp I		3,081	3,027	2,991	2,989	70	42	3
124	Ndimba		3,004	3,004	3,004	3,004	-	-	-
125	Mtai		3,001	2,998	2,998	2,998	4	-	-
126	Chambogo		2,893	2,893	2,893	2,893	-	-	-
127	Mamboto		2,764	2,762	2,761	2,761	2	1	-
128	Kabulo		2,763	2,762	2,760	2,760	2	2	-
129	Mtita		2,763	2,763	2,763	2,763	-	-	-

130 Tongomba New	2,742	2,739	2,739	2,739	5	-	-
131 Gwami	2,720	2,720	2,720	2,720	-	-	-
132 Kipembawe	2,690	2,435	2,338	2,235	282	97	104
133 Kitulanghalo	2,651	2,651	2,651	2,651	-	-	-
134 Msumbugwe	2,593	2,593	2,593	2,593	-	-	-
135 Kilindi	2,586	2,586	2,586	2,586	-	-	-
136 Kigogo	2,577	2,577	2,577	2,577	-	-	-
137 Ruande	2,570	1,977	1,932	1,924	610	45	8
138 Mpunze	2,567	2,547	2,543	2,542	20	4	-
139 Mkuli Extension	2,232	2,232	2,232	2,232	-	-	-
140 Rupiage	2,227	2,226	2,226	2,226	1	-	-
141 Mtunguru	2,225	2,225	2,225	2,225	-	-	-
142 Kwizu	2,209	2,209	2,209	2,209	-	-	-
143 Ruawa	2,188	2,085	2,078	2,077	106	8	1
144 Ngulakula	2,139	2,139	2,139	2,139	-	-	-
145 Loliondo I	2,130	2,130	2,130	2,130	-	-	-
146 Lwenza	2,124	2,094	2,092	2,092	44	3	-
147 Isabe	2,121	2,121	2,121	2,121	-	-	-
148 Ndumbi Valley	2,090	2,085	2,085	2,085	6	-	-
149 Kwasumba	2,055	2,055	2,055	2,055	-	-	-
150 Bombo West	1,940	1,936	1,936	1,936	6	-	-
151 Kazimzumbwi	1,887	1,887	1,887	1,887	-	-	-
152 Kome	1,874	1,874	1,874	1,874	-	-	-
153 Kome Island	1,809	1,809	1,809	1,809	-	-	-
154 Ngogwa	1,807	1,524	1,522	1,521	422	2	1
155 Bondo	1,710	1,710	1,710	1,710	-	-	-
156 North Makere	1,705	1,660	1,656	1,655	44	4	1
157 Uyovu	1,703	1,372	1,351	1,349	504	24	2
158 Mbinga Kimaji / Kimate	1,698	1,697	1,697	1,697	1	-	-
159 Ndukunduku	1,697	1,691	1,691	1,691	5	-	-
160 Ilamba	1,681	1,479	1,468	1,463	266	12	6
161 Masagati	1,639	1,639	1,639	1,639	-	-	-
162 Ukune	1,638	1,454	1,418	1,412	184	36	6
163 Chilangala	1,634	1,629	1,625	1,625	7	4	1
164 Longido	1,620	1,620	1,620	1,620	-	-	-
165 Nagaga	1,602	1,602	1,601	1,601	1	1	-
166 Mohoro	1,535	1,468	1,468	1,468	87	-	-

167	Ivuna South	1,459	1,456	1,456	1,456	6	-	-
168	South Gendagenda	1,441	1,441	1,441	1,441	-	-	-
169	Nambinga	1,439	1,430	1,430	1,430	14	-	-
170	Lupa North	1,436	1,354	1,352	1,352	116	3	1
171	Kisima Gonja	1,428	1,428	1,428	1,428	-	-	-
172	Ndekemai	1,405	1,405	1,405	1,405	-	-	-
173	Mkangala	1,382	1,374	1,373	1,373	8	-	-
174	Mbagala	32,038	31,9723	31,946	31,946	108	33	-
175	Vikindu	1,375	1,375	1,375	1,375	-	-	-
176	Manga	1,356	1,355	1,355	1,355	1	-	-
176	Mramba	1,307	1,307	1,307	1,307	-	-	-
177	Sengoma	1,294	1,292	1,292	1,292	2	-	-
178	Namikupa	1,292	1,264	1,254	1,251	45	14	3
179	Vumari	1,280	1,280	1,280	1,280	-	-	-
180	Kiverenge	1,279	1,279	1,279	1,279	-	-	-
181	Ihanga	1,248	1,238	1,238	1,238	11	-	-
182	Kwamgumi	1,232	1,231	1,231	1,231	2	-	-
183	Gelai	1,231	1,231	1,231	1,231	-	-	-
184	Liteho	1,229	1,214	1,209	1,208	15	5	2
185	Nandimba	1,211	1,199	1,197	1,197	15	2	-
186	Masanganya	1,100	1,100	1,100	1,100	-	-	-
187	Sima	1,099	1,074	1,072	1,072	26	2	-
188	Kiranzi Kitunguu	1,068	1,068	1,068	1,068	-	-	-
189	Matogoro West	1,067	1,067	1,067	1,067	-	-	-
190	Mtandi	1,067	1,063	1,063	1,063	5	1	-
191	Kwani	1,064	1,064	1,064	1,064	-	-	-
192	Mgambo	1,063	1,062	1,062	1,062	2	-	-
193	Sali	1,045	1,045	1,045	1,045	-	-	-
194	Ngwasi	1,037	1,037	1,037	1,037	-	-	-
195	Mahuta	1,021	948	938	932	105	11	6
196	Litipo	1,021	1,021	1,021	1,021	-	-	-
197	Bamba Ridge	1,017	1,017	1,017	1,017	-	-	-
198	Milindo	1,005	1,004	1,004	1,004	1	-	-
199	Kalangai	997	885	878	878	158	7	-
200	Irangi Escarpment	996	996	996	996	-	-	-
201	Mpara	992	992	992	992	-	-	-
202	Wotta	981	981	981	981	-	-	-

203 Irungu	970	968	968	968	9	-	-
204 Balangai West	958	958	958	958	-	-	-
205 Kwamrimba	933	932	932	932	1	-	-
206 Bombo East I	932	890	889	875	49	1	16
207 Ndasha Hill	930	929	929	929	-	-	-
208 Pumula	914	914	914	914	-	-	-
209 Kambai	892	892	892	892	-	-	-
210 Semdoe/Msige	874	873	872	872	2	-	-
211 Magoroto	867	867	867	867	-	-	-
212 Ukamba	854	823	816	816	31	7	-
213 Iyonda	826	826	826	826	-	-	-
214 Kikoka	817	817	817	817	-	-	-
215 Mwenga	811	811	811	811	-	-	-
216 Ilongafipa	798	798	798	798	-	-	-
217 Sawago	791	791	791	791	1	-	-
218 Chitoa	786	786	786	786	-	-	
219 Liwili/Kiteza/Lwekea	763	763	763	763	-	-	-
220 Ndolwa	742	742	742	742	-	-	-
221 Chitoa	740	735	732	732	5	3	-
222 Kipo	735	728	719	719	13	11	-
223 Dindili	696	696	696	696	-	-	-
224 Mswima	685	685	685	685	-	-	-
225 Kyosa	676	676	676	676	-	-	
226 Nguru ya Ndege	660	660	660	660	-	-	
227 Ikwamba	655	655	655	655	-	-	
228 Lusungulu	655	655	655	655	-	-	
229 Sisu	654	654	654	654	-	-	
230 Mkundi	645	645	645	645	1	-	-
231 Kitara Ridge	628	628	628	628	-	-	-
232 Magambazi	627	627	627	627	-	-	-
233 Talagwe	590	590	590	590	-	-	-
234 Kindoroko	580	580	580	580	-	-	-
235 Mvuha	561	561	561	561	-	-	-
236 Kyejo	561	561	561	561	-	-	-
237 Tongwe	552	552	552	552	-	-	-
238 Mfumbia	551	551	551	551	-	-	-
239 Kingoma	537	537	537	537	-	-	-

240 Makonde Scarp III	530	486	473	470	62	15	3
241 Masukulu	518	518	518	518	-	-	-
242 Ziwani	509	508	507	507	1	1	-
243 Mtama	506	462	457	457	52	5	-
244 Haraa	499	499	499	499	-	-	-
245 Mlinga	497	497	497	497	-	-	-
246 Rau	492	492	492	492	-	-	-
247 Ntazu	483	483	483	483	-	-	-
248 Kalambo falls	477	477	477	477	-	-	-
249 Chala Hills	460	408	396	395	51	12	1
250 Simbo-Bagamoyo	456	456	456	456	-	-	-
251 Kiranga Hengae	441	441	441	441	-	-	-
252 Mhulu	433	433	433	433	-	-	-
253 Chamanyani	428	428	428	428	-	-	-
254 Iditima	428	426	426	426	3	-	-
255 Minja	422	422	422	422	-	-	-
256 Njogi	421	421	421	421	-	-	-
257 Kimboza	399	398	398	398	-	-	-
258 Irenga	396	396	396	396	2	-	-
259 Mhalo	392	392	392	392	-	-	-
260 Handeni Hill	365	365	365	365	-	-	-
261 Burko	357	357	357	357	-	-	-
262 Mselezi	352	351	350	350	2	1	-
263 Pongwe	344	344	344	344	-	-	-
264 Mamani	334	334	334	334	-	-	-
265 Nagaliendele	331	328	328	328	4	-	-
266 Rudewa South	310	310	310	310	-	-	-
267 Bagai	305	305	305	305	-	-	-
268 Mbwegere	300	300	300	300	-	-	-
269 Ihoho	298	298	298	298	4	-	-
270 Kamwalla II	296	296	296	296	-	-	-
271 Negoma	295	295	295	295	-	-	-
272 Ijogo	292	292	292	292	-	-	1
273 Mkongo	292	292	292	292	-	-	-
274 Idewa	290	290	290	290	-	-	-
275 Chuvwi	284	283	283	283	2	-	-
276 Mahenge Scarp	283	283	283	283	-	-	-

277 Irunda	278	278	278	278	-	-	-
278 Mahezangulu	276	276	276	276	-	-	-
279 Ikuru	268	266	265	265	3	-	-
280 Kwangola	267	267	267	267	-	-	-
281 Mindu	255	255	255	255	-	-	-
282 Mtumbi	252	252	252	252	-	-	-
283 Simbo	242	237	237	237	7	-	-
284 Puge North	232	231	231	231	1	-	-
285 Shinkurufumi	229	229	229	229	-	-	-
286 Kyanyari	223	223	223	223	-	-	-
287 Kikongoloi	221	221	221	221	-	-	-
288 Vigoregore	220	177	161	161	45	15	-
289 Gumbiro	217	217	217	217	-	-	-
290 Vugiri	211	211	211	211	-	-	-
291 Irunga	206	206	206	206	1	-	-
292 Pangawe East	196	194	194	194	2	-	-
293 Mwantini Hill	194	158	158	158	62	-	-
294 Kiamawe	192	192	192	192	-	-	-
295 Kurwirwi	191	191	191	191	-	-	-
296 Mrema Kingarussina	188	186	186	186	2	-	-
297 Ngalijembe	186	186	186	186	-	-	-
298 Kitweli	185	185	185	185	-	-	-
299 Uponera	181	181	181	181	-	-	-
300 Kabingo	175	175	175	175	-	-	-
301 Kasanga	170	170	170	170	-	-	-
302 Lukoka Hill	169	169	169	169	-	-	-
303 Mninga	159	159	159	159	-	-	-
304 Mamboto	158	158	158	158	-	-	-
305 Kwamarukanga	149	149	149	149	-	-	-
306 Mlungui	148	148	148	148	-	-	-
307 Mkewe	147	145	145	145	5	-	-
308 Usindikwe	143	141	141	141	4	-	-
309 Mamboya	142	142	142	142	-	-	-
310 Marenda	137	137	137	137	-	-	-
311 Bombo East II	132	132	132	132	1	-	-
312 Kihiriri	129	129	129	129	-	-	-
313 Bulongwa Madehani	126	121	120	120	6	1	-

314 Mzogoti	125	125	125	125	-	-	-
315 Manka	122	122	122	122	-	-	-
316 Myoe	116	116	116	116	-	-	-
317 Kamwalla I	114	114	114	114	-	-	-
318 Long'isont	114	114	114	114	-	-	-
319 Mafleta	108	108	108	108	-	-	-
320 Litoni	107	107	107	107	-	-	-
321 Kibao	103	103	103	103	-	-	-
322 Kiriguru	103	103	103	103	-	-	-
323 Kabungu	102	63	49	49	62	16	-
324 Kambona	91	89	89	89	3	1	-
325 Igoma Logala	86	86	86	86	-	-	-
326 Isililo	86	86	86	86	-	-	-
327 Sasajila	85	85	85	85	-	-	-
328 Gonja	83	83	83	83	-	-	-
329 Mpagalalu	82	82	82	82	-	-	-
330 Ikonde	80	80	80	80	-	-	-
331 Garafuno	80	80	80	80	-	-	-
332 Rushwezi	77	77	77	77	-	-	-
333 Idunda	76	76	76	76	-	-	-
334 Ngukumo	75	75	75	74	-	-	-
335 Mwanhala	74	74	72	72	2	1	1
336 Kitulio	73	73	73	73	-	-	-
337 Ito	71	70	70	70	1	-	-
338 Mkigagi	69	69	69	69	-	-	-
339 Kankoma	63	63	63	63	-	-	-
340 Mfulikilo	63	63	63	63	-	-	-
341 Kitivo North	61	61	61	61	-	-	-
342 Fonera	59	58	58	58	1	-	-
343 Mpala	59	59	59	59	-	-	-
344 Chongweni	57	57	57	57	-	-	-
345 Nguluka	56	56	56	56	-	-	-
346 Malenga	54	53	53	53	5	-	-
347 Kwekanda	52	52	52	52	-	-	-
348 Ndugumia	51	51	51	51	-	-	-
349 Msingeho Hill	49	49	49	49	-	-	-
350 Mabundi Mtwange	49	49	49	49	-	-	-

351 Puge South	48	47	47	47	1	-	-
352 Mkoro	48	48	48	48	-	-	-
353 Mamboto	48	48	48	48	-	-	-
354 Jasini	47	47	47	47	-	-	-
355 Ilonganjaula	43	43	43	43	-	-	-
356 Sakila	43	43	43	43	-	-	-
357 Mafifi	41	41	41	41	-	-	-
358 Kantale	39	39	39	39	-	-	-
359 Kisiwani	37	37	37	37	-	-	-
360 Kitivo South	35	35	35	35	-	-	-
361 Mamboto	35	35	35	35	-	-	-
362 Kigongkwe	34	33	32	32	3	-	-
363 Idamba	33	33	33	33	-	-	-
364 Ligamba	32	32	32	32	-	-	-
365 Igwata	28	28	28	28	-	-	-
366 Maganda	25	25	25	25	-	-	-
367 Hebangwe	24	24	24	24	-	-	-
368 Kihanga	24	24	24	24	-	-	-
369 Nindo	24	21	21	21	11	-	-
370 Lake Duluti	22	22	22	22	-	-	-
371 Hupanga	21	21	21	21	-	-	-
372 Nyandira	21	21	21	21	-	-	-
373 Kyarano	19	19	19	19	-	-	-
374 Mzashai	19	19	19	19	-	-	-
375 Shambalai	19	19	19	19	-	-	-
376 Milawilila	18	18	18	18	-	-	-
377 Pangawe West	17	17	17	17	-	-	-
378 Mohoro River	17	17	17	17	1	-	-
379 Manongho Hill	17	15	15	15	3	-	-
380 Kiav Island	17	17	17	17	-	-	-
381 Kibwezi	16	16	16	16	-	-	-
382 Nyandiduma	15	15	15	15	-	-	-
383 Mangala	15	15	15	15	-	-	-
384 Mbuga ya Goima	15	14	13	13	4	1	-
385 Kilengwe	14	14	14	14	-	1	-
386 Disalasala	13	13	13	13	-	-	-
387 Kiamawe	8	8	8	8	-	-	-

388 Vigoza	7	7	7	7	-	-	-
389 Zinge	6	6	6	6	-	-	-
390 Kwembago	5	5	5	5	-	-	-
391 Mkangala	3	3	3	3	-	-	-
392 Kahe II	3	3	3	3	-	-	-
393 Koko Hill	3	3	3	3	-	-	-
394 Mbeya fuel	2	2	2	2	-	-	-
395 Bassi	2	2	2	2	-	-	-
396 Kagongho	2	2	2	2	-	-	-
397 Kahe I	1	1	1	1	-	-	-
388 Mombo	1	1	1	1	-	-	-
399 Kingongoro	1	1	1	1	-	-	-
400 Bunduki 3	-	-	-	-	-	-	-
401 Kiutu	-	-	-	-	-	-	-
402 Mbogo	-	-	-	-	-	-	-
403 Chemi chemi	-	-	-	-	-	-	-
404 Dodoma Reservoir	-	-	-	-	-	-	-
405 Ibondo	-	-	-	-	-	-	-
406 Igwata	-	-	-	-	-	-	-
407 Kakora	-	-	-	-	-	-	-
408 Kileo East	-	-	-	-	-	-	-
409 Konga	-	-	-	-	-	-	-
410 Lubaga	-	-	-	-	-	-	-
411 Mwakulu	-	-	-	-	-	-	-
412 Mwatunge Hill	-	-	-	-	-	-	-
413 Sayaka	-	-	-	-	-	-	-

Table A.6: Wildlife Protected Areas: Forest extent and change (ha)

			Forest extent				**Forest change**		
Name	Designation		Baseline	2018	2019	2020	2018	2019	2020
Ruaha	National Park		937,210	937,020	936,911	936,851	367	125	64
Kigosi	National Park		641,746	641,631	641,622	641,622	132	9	-
Mikumi	National Park		249,875	249,833	249,825	249,825	47	8	-
Katavi	National Park		178,691	178,658	178,631	178,637	41	22	2

Udzungwa Mountains	National Park	169,365	169,346	169,346	169,346	20	-	-
Mkomazi	National Park	108,802	108,800	108,800	108,800	3	-	-
Mahale	National Park	105,917	105,812	105,806	105,805	152	7	1
Kilimanjaro	National Park	90,384	90,384	90,384	90,384	-	-	-
Ugalla	National Park	86,370	86,370	86,370	86,370	-	-	-
Burigi-Chato	National Park	78,982	78,982	78,982	78,982	-	-	-
Lake Manyara	National Park	25,695	25,695	25,695	25,695	-	-	-
Arusha	National Park	24,002	24,002	24,002	24,002	-	-	-
Rumanyika	National Park	20,732	20,732	20,732	20,732	-	-	-
Rubondo	National Park	19,194	19,194	19,194	19,194	-	-	-
Tarangire	National Park	8,951	8,951	8,951	8,951	-	-	-
Ibanda	National Park	4,265	4,265	4,265	4,265	-	-	-
Serengeti	National Park	3,631	3,623	3,622	3,621	8	1	-
Gombe	National Park	3,052	3,052	3,052	3,052	-	-	-
Kitulo Plateau	National Park	2,243	2,243	2,243	2,243	-	-	-
Ngorongoro	Conservation Area	91,061	91,061	91,061	91,061	-	-	-
Selous	Game Reserve	3,103,500	3,103,453	3,103,442	3,103,366	56	11	76
Moyowosi	Game Reserve	688,689	688,511	688,491	688,491	209	21	-
Rungwa	Game Reserve	607,792	605,064	604,885	604,782	3,280	189	105
Rukwa	Game Reserve	354,163	354,138	354,137	354,137	25	1	-
Kizigo	Game Reserve	350,513	350,445	350,430	350,418	80	16	13
Muhezi	Game Reserve	197,649	196,813	196,627	196,506	1,289	215	133
Lwafi-Nkamba	Game reserve	166,958	165,774	165,459	165,445	1,494	343	14
Piti O.A.(E)	Game reserve	164,176	154,417	153,895	153,588	11,344	530	308
Limparamba	Game Reserve	56,254	56,195	56,173	56,172	102	25	-
Lukwika-Lumesule	Game Reserve	38,690	38,672	38,670	38,670	27	2	-
Swangaswanga	Game Reserve	24,280	24,278	24,278	24,278	2	-	-
Msanjesi	Game Reserve	14,768	14,693	14,686	14,686	78	7	-
Kimisi	Game Reserve	9,131	9,131	9,131	9,131	-	-	-
Mkungunero	Game Reserve	5,962	5,962	5,962	5,962	-	-	-
Maswa	Game Reserve	3,695	3,695	3,695	3,695	1	-	-
Pande	Game Reserve	1,218	1,218	1,218	1,218	-	-	-
Ikorongo	Game Reserve	260	260	260	260	-	-	-
Grumeti	Game Reserve	142	140	140	140	2	-	-
Lunda-Mkwabi	Game Controlled Area	209,350	208,495	208,388	208,269	934	108	128
Mlele	Game controlled area	202,283	199,936	198,907	198,790	2,346	1,029	117
Kitwai	Game controlled area	148,525	148,524	148,524	148,524	-	-	-

Mlele	Game controlled area	119,158	119,158	119,158	119,158	-	-	-
Gombe	Game controlled area	98,897	67,068	58,638	57,764	32,965	8,517	878
Wembere	Game controlled area	88,436	83,334	81,921	81,051	7,790	1,535	911
Handeni	Game controlled area	78,605	78,602	78,595	78,595	3	7	-
Kilombero	Game controlled area	51,127	50,369	50,027	50,027	1,561	465	-
Lunda Nkwambi	Game controlled area	48,000	47,954	47,951	47,929	47	2	22
Loliondo	Game controlled area	38,729	38,719	38,719	38,719	12	-	-
Ruvu Masai	Game controlled area	28,274	28,274	28,274	28,274	-	-	-
Lake Natron	Game controlled area	20,154	20,152	20,152	20,152	3	-	-
Simanjiro	Game controlled area	12,338	12,338	12,338	12,338	-	-	-
Landanai	Game controlled area	3,485	3,485	3,485	3,485	-	-	-
Mlela	Game Controlled Area	2,626	2,626	2,626	2,626	-	-	-
Lolkisale	Game controlled area	2,622	2,622	2,622	2,622	-	-	-
Mto wa Mbu	Game controlled area	562	562	562	562	-	-	-
Mlele	Game controlled area	263	263	263	263	-	-	-
Liwale	Wildlife management area	338,274	338,250	338,246	338,246	26	4	-
Mbarang'andu	Wildlife management area	263,151	263,035	263,017	263,016	190	21	1
Ipole	Wildlife management area	185,162	180,804	180,737	180,706	6,167	71	31
Makame	Wildlife management area	184,947	184,919	184,919	184,919	31	-	-
Pawaga-Idodi	Wildlife management area	125,050	124,995	124,990	124,980	58	5	11
Wami Mbiki	Wildlife management area	122,960	122,960	122,959	122,959	2	1	-
Tunduru	Wildlife management area	119,051	118,792	118,737	118,729	322	57	9
Uyumbu	Wildlife management area	79,031	78,839	78,775	78,757	193	64	17
Ngarambe-Tapika	Wildlife management area	69,334	69,305	69,295	69,295	65	12	-
Ukutu	Wildlife management area	62,213	61,637	61,495	61,495	592	146	-
Enduimet	Wildlife management area	1,473	1,473	1,473	1,473	-	-	-
Burunge	Wildlife management area	1,208	1,202	1,202	1,202	9	-	-
Ikona	Wildlife management area	727	727	727	727	1	-	-